

Alma Mater Studiorum – Università di Bologna

DOTTORATO DI RICERCA IN

CHIMICA

Ciclo XVIII

Settore Concorsuale di afferenza: 03/A1

Settore Scientifico disciplinare: CHIM/12

**THE INFLUENCE OF THE ENVIRONMENT ON THE
ATMOSPHERIC CORROSION OF WEATHERING STEEL:
FIELD AND LABORATORY STUDIES**

Presentata da: SIMONA RAFFO

**Coordinatore Dottorato
PROF. ALDO RODA**

**Relatore
DOTT.ssa ELENA BERNARDI**

**Correlatore
PROF. IVANO VASSURA**

Esame finale anno 2016

Table of Contents

Chapter 1. Abstract.....	1
Chapter 2. Environment and Corrosion	4
2.1 Corrosion process: general definition	4
2.2 Morphology of corrosion attack.....	5
2.3 Electrochemical nature of corrosion	6
2.4 Atmospheric corrosion.....	11
2.4.1 Temperature and Relative Humidity	13
2.4.2 The composition of atmosphere	13
2.4.3 Corrosivity of atmospheres	19
Chapter 3. Steel in Art and Architecture.....	22
3.1 Steel.....	22
3.2 Corrosion of steel	26
3.2.1 Methods for preventing steel corrosion.....	28
3.2.2 Weathering steel.....	32
Chapter 4. Metals and the Environment	49
4.1 Metals in the Environment.....	50
4.2 Bioavailability and mobility of metals.....	52
4.3 Environmental behavior and potential toxicity of WS alloying elements	53
4.3.1 Chromium.....	54
4.3.2 Copper	55
4.3.3 Iron	56
4.3.4 Manganese.....	57
4.3.5 Nickel	58
Chapter 5. Materials and Methods	59

5.1	Working Plan	61
5.2	Description of materials	62
5.2.1	Weathering steel: Cor-Ten A	62
5.3	Environmental Exposure	64
5.3.1	Exposure site and conditions	64
5.3.2	Experimental procedure	66
5.4	Artificial Ageing Test	67
5.4.1	Immersion/emersion Test (Cebelcor)	68
5.5	Analytical Techniques	71
5.5.1	Atomic Absorption Spectroscopy (AAS)	71
5.5.1.1	General principles	71
5.5.1.2	Instrumentation	72
5.5.1.3	Operating conditions	79
5.5.2	Ion Chromatography (IC)	81
5.5.2.1	General principle and instrumentation	81
5.5.2.2	Operating Conditions	82
5.5.3	Scanning Electron Microscopy (SEM)	83
5.5.3.1	General principles	83
5.5.3.2	Instrumentation	84
5.5.4	Energy Dispersive X-ray Spectroscopy (EDS)	89
5.5.5	Raman Spectroscopy	89
5.5.6	X-ray Diffraction (XRD)	92
5.5.7	Open Circuit Potential (OCP)	95
5.5.8	Mass Loss Determination	96
5.6	Data processing	97
5.6.1	Multivariate data analysis	97
5.6.1.1	Principal component analysis (PCA)	99
5.6.1.2	Three-way principal component analysis (3W-PCA)	100

Chapter 6. Results.....	102
6.1 Microstructure of CorTen A	102
6.2 Environmental Exposure.....	103
6.2.1 Characterization of the exposure site	103
6.2.2 Characterization of corrosion products	111
6.2.2.1 Mass variation	111
6.2.2.2 Patina composition	113
6.2.3 Metal dissolution	129
6.2.4 Multivariate data analysis.....	139
6.3 Accelerated ageing test (Cebelcor)	146
6.3.1 General consideration on patinas	146
6.3.2 Open Circuit Potential (OCP)	150
6.3.3 Mass loss determination	153
6.3.4 Characterization of corrosion products	155
6.3.5 Metal analysis.....	162
6.3.6 Multivariate data analysis.....	169
Chapter 7. Discussion of results	173
7.1 Influence of the geometry of exposure	173
7.2 Influence of surface finish.....	176
7.3 Atmospheric factors affecting corrosion and metal dissolution.....	177
7.4 Influence of saline compounds on corrosion	182
Chapter 8. Conclusions	189
References	192
Figure Captions	207
Table Captions	215

APPENDIX A – Atmospheric corrosion of Bronze	218
A1. Indroduction	218
A1.1 Bronzes	219
A1.2 Gilded Bronzes.....	221
A1.3 Methods for preventing bronze corrosion	222
A2. Experimental	223
A3. Results	224
A4. Conclusion	228
APPENDIX B – Papers and Contributions	229

Chapter 1

Introduction

Weathering steel (WS) describes a class of material, namely high-strength low alloy steel, that presents higher corrosion resistance and enhanced mechanical properties than traditional carbon steel when exposed to medium-aggressive environments (i.e. rural, urban and light industrial).

Actually, the specific chemical composition of this material, including low percentage ($< 1\%$) of elements such as Cu, Cr, Ni, Mn, P, promotes the creation of an adherent passivation layer, which opposes the entry of corrosive species and protects the material from further corrosion.

The process of passivation of weathering steel is accompanied by a peculiar change of color, which gradually alters from basic metal gray to brownish tone. These aesthetic characteristics make WS a "living" material, thus aesthetically and conceptually appreciated by artists and architects.

Resistance to atmospheric corrosion and aesthetical appearance allowed WS to assume an increasing role in architectural, artistic and infrastructural applications. Since its first commercialization in 1933 to date, weathering steel structures, including bridges and facades cladding, architectural ornaments and sound-adsorbing panels alongside highways, have been increasing exponentially and even now weathering steel is among the most popular and esteemed materials for street furniture and outdoor applications.

However, depending on the exposure environment and conditions, the evolution and the composition of the passivation layer can strongly change, due to several factors, such as geometry,

inclination and orientation of exposure, temperature, relative humidity, winds, precipitations and presence and amount of atmospheric pollutants.

The exposure to corrosive atmospheres, such as those found at marine sites, where high amounts of chloride ions inhibit the creation of efficient passivation layers, and in industrial and traffic-congested urban areas, characterized by other aggressive species such as NO_x , SO_x and particulate matter (PM), destabilizes the patina and reduces corrosion resistance, leading WS to be more susceptible to corrosion and wash-out processes. Consequently, WS releases a certain quantity of alloying metals that could disperse in surrounding areas (soil or water) or accumulate near the structures.

Therefore, beside producing significant economic impact, reduced aesthetic appeal or structural damages, the decrease in passivation properties of patina formed on WS could also cause environmental concerns; in fact, depending on their chemical form, mobility and bioavailability, some of the elements present in the alloy and washed out could represent a hazard to the environment and to living organisms, because of their persistence and their potential chronic toxicity.

In this work, the issue of corrosion of weathering steel was addressed not only in terms of composition and morphology of corrosion product layer; in fact, an innovative perspective was applied, that is the study and quantification of corrosion-induced metal release and the identification of main environmental factors affecting this process, in order to give an evaluation of patina stability from a different point of view and to assess the suitability of this material for specific outdoor applications.

Moreover, as several artists and architects during the last decades, both for aesthetical or time saving reasons, have resorted to procedures of patination of WS surfaces, an evaluation of the corrosion behavior of both bare and artificially-rusted surfaces is needed.

The investigation on atmospheric corrosion of weathering steel was performed by means of natural field exposure and accelerated ageing tests.

The first part of the work was focused on the evaluation of atmospheric corrosion of a commercial WS, named Cor-Ten A, after natural exposure to the marine-urban atmosphere of Rimini, with the purpose of assessing the effects of a critical environmental condition, different exposure geometry and surface finishes on the development and the stabilization of the protective layer and on metal release during first years of exposure, the most critical phase with regards to environmental impact; only alloying metals released in dissolved, thus mobile and soon bioavailable, form are considered, while metals released as non-soluble species are not included in this study.

In the second part of the work, performed at Centro Nacional de Investigaciones Metalúrgicas - Consejo Superior de Investigaciones Científicas (CENIM - CSIC) in Madrid, the influence of main ionic components of particulate matter on Cor-Ten corrosion was studied through the application of a specific accelerated ageing test (CEBELCOR test).

Patina composition and morphology and metal release during both tests were determined and results were treated by means of multivariate data analysis, to extract relevant information from the large number of analytical and environmental data.

This work allowed to give a more complete and comprehensive characterization of the environmental behavior of weathering steel and to point out interesting conclusion on the main environmental aspects affecting outdoor corrosion of this material.

Chapter 2

Environment and corrosion

2.1 Corrosion process: general definition

Corrosion of materials is a natural process, well known since ancient times, that received several definitions over time.

Among them, according to the DIN EN ISO Standard 8044, corrosion is defined as all the interactions occurring between material and its surroundings which produce a spontaneous decay in its chemical-physical properties and a consequent functional impairment.

When the material is a metal, the process of corrosion is also described as anti-metallurgy, because it promotes the tendency of the metal to return in its natural oxidized and thermodynamically more stable state, from which it was initially extracted [1].

Nowadays, the topic of material corrosion has been receiving large scientific interest and increasing demand of deep knowledge, both for technical reasons, such as the evaluation of the performances of new materials in ever-changing atmosphere, and for economic reasons [2]. Suffice to say that the natural decay of these materials not only provides structural damages and, thus, direct costs, such as the simple replacement of failed assets, but it is also connected to a series of management and maintenance costs, loss of earning and so on.

In a 2-year study entitled “Corrosion costs and preventive strategies in the United States” conducted by CC Technologies Laboratories, the annual direct costs of corrosion were estimated at about \$276 billion [3]; further studies conducted in China, Japan, Venezuela, Australia and UK

[4], [5], estimated even greater annual economic impacts, so much so that in 2009 the World Corrosion Organization (WCO) estimated that worldwide corrosion costs exceed 1,8 trillion dollars per year [6], that corresponds approximately to the 4-5% of Gross Domestic Product (GDP) for industrialized countries.

These numbers make it clear the importance of applying correct corrosion prevention strategies, which start from preliminary tests on materials up to the continuous monitoring of exposed facilities.

Obviously, in order to better manage both prevention and maintenance programs, a deep knowledge of the chemistry and the morphology of corrosion process is needed.

2.2 Morphology of corrosion attack

One of the main classifications of the corrosive phenomenon concerns the morphology of the corrosion attack, which is closely related to the intrinsic characteristics of the medium in which corrosion occurs.

The corrosion process is, thus, classified [7] as:

- ✓ Uniform corrosion, occurring on the entire surface at nearly the same rate. It is the most common form of corrosion and although it is the responsible for a great loss of material, it is not particularly dangerous because of its predictability [2].
- ✓ Pitting corrosion, that is local corrosion resulting in corroded cavities expanding from the surface to the inside of the material. It is usually connected to the presence of corrosive species, such as halides or sulfates; it is a very dangerous form of corrosion because it progresses in autocatalytic way and causes very deep damages to the material [2].
- ✓ Crevice corrosion, local corrosion occurring in proximity of a crevice area.

- ✓ Contact corrosion or galvanic corrosion, occurring at contact surfaces of different metals.
- ✓ Intergranular corrosion, occurring in proximity of the grain boundaries of a metal.

2.3 Electrochemical nature of corrosion

Another classification, based on the nature of the corrosion process, distinguishes between

- ✓ Dry corrosion
- ✓ Wet corrosion

Dry or chemical corrosion is the oxidation process occurring when metal is in contact with gaseous atmospheric agents in the absence of water; usually this process proceeds with an appreciable rate only at high temperature and for this reason it is also named 'hot (high-temperature) corrosion'.

Dry corrosion is driven by a chemical mechanism and is, thus, subjected to the laws of chemical thermodynamics and kinetics in the gaseous phase [8].

Wet corrosion, instead, occurs when the metallic material is placed in an environment containing water; in this case the mechanism that regulates the process is electrochemical.

In almost all natural cases, corrosion phenomena are electrochemical processes and represent the result of an oxidation reaction and a reduction reaction, as in the case of galvanic cells.

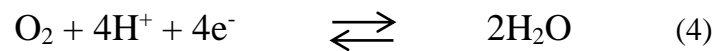
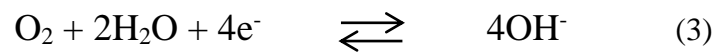
The oxidation reaction, or anodic reaction, causes the oxidation of the metal and the consequent release of electrons in the metallic phase.



The reduction reaction, or cathodic reaction, captures the available electrons to reduce one or more species present in the environment. In the case of corrosion in acidic solutions the cathodic reaction is the reduction of the hydrogen ion according to the reaction



In natural environments, however, the main cathodic reaction is the reduction of oxygen dissolved in the electrolyte solution, according to the reactions,



that show reductions in a neutral / alkaline and acid environment, respectively.

The total reaction resulting from anodic and cathodic semi-reactions describes the corrosion process (Fig. 1), which leads to the formation of corrosion products at metal / electrolyte interface.

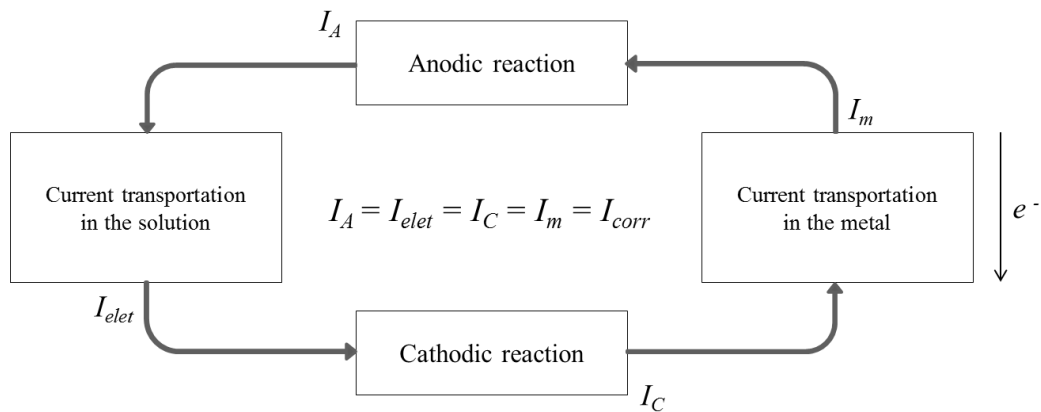


Fig. 1: Scheme of the electrochemical mechanism of corrosion [1]

Beside the main process, other redox reactions may occur at rust/media interface, when corrosion products get in contact with atmospheric compounds, leading to the formation of secondary corrosion products (oxides, hydroxides, hydrates, alkali salts, etc).

In order to assess the trend of metallic species to corrode, evaluation on both thermodynamic and kinetic aspects has to be made; in fact, the thermodynamics specifies if the corrosion reaction is energetically allowed and proceeds spontaneously; on the contrary, the study of kinetic factors indicates the speed of the process and may provide useful guidance for prevention and maintenance procedures [1], [9].

Take, therefore, the reactions of oxidation and reduction that characterize the corrosion process (eq. 1-4); to assess the spontaneity of corrosion, it is necessary to consider Gibbs free energy associated to it and defined as

$$\Delta G = \Delta G_0 + RT \cdot \ln \frac{a_P}{a_R} \quad (5)$$

where ΔG is the free energy change, ΔG_0 is the energy change in standard conditions, R is the universal gas constant, T is the temperature and a_P and a_R are the activities of products and reactants of the reaction.

A negative free energy change ($\Delta G < 0$) indicates that the reaction proceeds spontaneously; on the contrary, a positive free energy change ($\Delta G > 0$) excludes the possibility that the reaction is produced unless external energy is supplied.

By comparing the system to a short-circuit galvanic cell [10], the change in Gibbs free energy can be expressed as

$$\Delta G = -n \cdot F \cdot E_{\text{Rev}} \quad (6)$$

where n is the number of electrons, F is the Faraday constant and E_{rev} is the reversible potential, that represents the driving force of the process and is defined as the difference between cathodic and anodic potential, according to

$$E_{\text{Rev}} = E_{\text{Rev},C} - E_{\text{Rev},A} \quad (7)$$

For the reaction to be spontaneous ($\Delta G < 0$), cathodic potential must be greater than anodic potential.

Considering a generic corrosion process, $\Delta G < 0$ corresponds to the condition of activity of the corroding material; on the contrary, $\Delta G = 0$ or $\Delta G > 0$ suggest the condition of equilibrium and immunity, respectively. Finally, there is also the possibility that the corrosion process is favored thermodynamically ($\Delta G < 0$), but with very slow reaction rate; in this case, metal exhibits passivation (section 3.2.1) of its surface [8].

However, the factors described above, including the decrease in free energy, constitute a necessary but not sufficient condition for the corrosion process to occur.

In fact, the intervention of other factors, such as the presence of impurities in the metallic material, the formation of passivation film, changes in the electrolyte composition of the medium, and so on, may slow down or alter the kinetics of the process, reducing the possibility to predict the evolution of corrosion behavior solely on the basis of thermodynamic knowledge.

To deepen the kinetic aspect [1], [8], [9], [11], consider a metal or an alloy placed in contact with electrolytic medium and think that $\Delta G < 0$ is associated to the resulting corrosion reaction; in these conditions, a flow of electrons from the anode to the cathode is established: the charge produced by the process of metal oxidation will be consumed in the cathodic reaction and at any time

$$I_A = - I_C = I_{\text{corr}} \quad (8)$$

(I_A = anodic current; I_C = cathodic current; I_{corr} = corrosion current), resulting in equalization of E_A and E_C in E_{CORR} , the corrosion potential [1], [9], [11], [12].

Even though E_{corr} , representing the potential in the steady state, gives much information about the corroding system, it does not provide any kinetic information; to extrapolate the corrosion rate of the process, an external current is applied and the change in potential is measured. This process is called polarization and the deviation of the potential from the equilibrium value is defined overpotential η

$$\eta = |E - E_{eq}| \quad (9)$$

The total overpotential, which represents the dissipative term spent during the process, is the sum of overpotentials associated with each stage of the reaction mechanism (diffusion of reactants from bulk to metal surface, dissociation or adsorption reactions of reagents, charge transfer, etc.) [1], [13].

Overpotentials can be grouped into three main categories:

- ✓ Activation or charge transfer overpotential, connected to all processes that involve the transfer of charge; it is analogous to the activation energy barrier of chemical reactions. The general expression that connects current density and overpotential for a reaction controlled by charge transfer is the Butler-Volmer equation

$$i = i_0 \left[e^{\frac{(1-\beta)z \cdot F \cdot \eta}{RT}} - e^{-\frac{\beta \cdot z \cdot F \cdot \eta}{RT}} \right] \quad (10)$$

where η is the overpotential, i_0 is the exchange current density, F is the Faraday constant, z is the number of electrons and β is the charge transfer coefficient, i.e. a measure of symmetry of the energy barrier of redox reaction; in this equation the exponential terms represent the anodic and cathodic charge transfer coefficient, respectively. In the event that

the activation overpotential of the reaction is relatively high (usually $|\eta| > 50$ mV), the equation (10) can be simplified into the Tafel equation

$$\eta = a \pm b \cdot \log(i) \quad (11)$$

that links overpotential η to the exchange current i linearly.

- ✓ Concentration of mass transfer overpotential. This term is associated with the variation in reactants availability at the metal / electrolyte interface. In natural environments, the main cathodic reaction is the reduction of oxygen dissolved in the electrolyte solution. As the reaction proceeds, O_2 present at the interface is used up; its concentration decreases and, therefore, it must be replaced by other molecules. However, being a neutral molecule, its transfer is subjected to diffusion phenomena exclusively, which limit the speed of the process. As a consequence, concentration overvoltage helps to increase the speed of the diffusion process.
- ✓ Ohmic overpotential, connected to the formation of a film on metal surface, which limits the conductivity of the material.

2.4 Atmospheric corrosion

Atmospheric corrosion is a particular kind of electrochemical corrosion occurring in atmosphere, where several factors, such as temperature, humidity, environment contaminants and pollutants can affect the rate and the extent of the process [11], [14].

First of all, for the corrosion process to take place, the vital factor is the presence of a thin electrolyte film on the surface of the material [9]; the process of consumption-renovation of the film, which mainly depends on temperature and relative humidity represents one of the most important variable affecting the corrosion rate [2], [15].

Beside this, also the composition of the electrolyte film, clearly connected to the composition of the atmosphere of exposure, assumes a critical role in the definition and study of the corrosion mechanism.

Atmospheric corrosion generally consists of three main steps, the initial, the intermediate and the final stages [14]:

- ✓ When the metal is exposed, it instantly reacts with water vapor, in molecular or dissociated form, creating an hydroxylated surface. Metal-hydroxyl groups continue to attract and adsorb other water molecule creating a thin liquid layer; water molecules in the layer are disposed with high degree of order near the substrate, while are randomly oriented moving away from the surface.

Then, the electrochemical reactions take place: the anodic reaction corresponding to the metal dissolution and the cathodic reaction corresponding to the reduction of oxygen.

- ✓ During the intermediate step, atmospheric contaminants, such as sulfur dioxide (SO_2), carbon dioxide (CO_2), nitrogen dioxide (NO_2), hydrogen sulfide (H_2S) and aerosol particles ($(\text{NH}_4)_2\text{SO}_4$, NaCl) deposit and dissolve in the liquid layer, through dry or wet deposition, altering the chemistry of the film and promoting metal dissolution (see section 2.4.2 for a detailed explanation on the action of main contaminants).

After dissolution, metal ions can coordinate with a series of counter-ions present in the layer, following Lewis acid-base concept, and precipitate into small nuclei.

- ✓ With the passing of time, the number of nuclei increases up to completely cover the surface; at this point further corrosion requires that electrolyte and dissolved species must reach the uncorroded surface.

However, the presence and the amount of a great variety of contaminants and pollutants, together with the action of environmental factors, make this topic very complex to face; so it could be very useful to deepen each contribution of these factors on atmospheric corrosion.

2.4.1 Temperature and Relative Humidity

Temperature may act in different ways on corrosion: on the one hand, the increase in temperature corresponds to an increase in the kinetic of electrochemical reaction; on the other hand, instead, it causes evaporation of the electrolyte, thus reducing the solubility of oxygen and the rate of reaction [16].

Another important factor affecting the electrolyte, particularly its thickness, and, as a consequence, the corrosion process is relative humidity (RH); to reach the adequate thickness a critical humidity value, which depends on both the nature of metal and the composition of exposure environment, must be passed [1], [14].

However, if the film thickness is too high, diffusion of oxygen is reduced and the rate of corrosion decreases. According to experimental observation, the thickness connected to the higher corrosion is assumed at about 150 μm [11].

For convenience, let us thus introduce the Time of Wetness (TOW), a parameter widely used in corrosive studies, which estimates the period of time during which the material surface is exposed to certain atmospheric conditions that permit the creation of the electrolyte film, generally regarded as corresponding to temperature above 0 °C and RH above 80% [17].

2.4.2 The composition of atmosphere

Chemical-physical properties of the electrolyte obviously depends on its composition, especially in relation to the presence and the amount of compounds that can act as corrosive agents. In turn, the composition of liquid layer depends on the environment in which the material is exposed.

To properly study the atmospheric corrosion process is thus necessary to start from the average composition of the atmosphere (Table 1) and consider the possible sources of contamination/pollution.

Table 1: Average composition of atmosphere (dry air) [18]

Constituent	Chemical symbol	Mole percent
Nitrogen	N ₂	78.08 %
Oxygen	O ₂	20.95 %
Argon	Ar	0.93 %
Carbon dioxide	CO ₂	0.040 %
Neon	Ne	0.0018 %
Helium	He	0.0005 %
Methane	CH ₄	0.00017 %
Krypton	Kr	0.00011 %
Hydrogen	H ₂	0.00005 %
Nitrous oxide	N ₂ O	0.00003 %
Xenon	Xe	0.000009 %
Ozone *	O ₃	Trace to 0.0008 %
* Low concentrations in troposphere: ozone maximum in the 30-to-40 km regime of the equatorial region		

Among the main components of troposphere (N₂, O₂ and rare gasses), only O₂ plays an active role in atmospheric corrosion; other compounds affecting the process are H₂O, with a concentration ranging from 100 ppm to 10000 ppm, that represents the electrolyte and CO₂, which has a concentration of about 400 ppm and is high soluble in water, that contributes to the acidification of the liquid layer, forming carbonate ions [14], [16].

Environmental contaminants may be originated from natural sources, as in the case of sea spray, volcanic eruption or erosion and dust resuspension, or anthropogenic sources, such as industrial emissions or vehicular traffic. Further reactions of these primary contaminants give rise to the development of secondary contaminants.

All these species may act on the material through direct or indirect mechanism; in the first case, these substances, once deposited on the surface through dry (~ 70%) or wet (~ 30%) deposition [1], may produce an increase in the conductivity, favor the formation of the electrolyte or locally lower the pH, enhancing the metal dissolution process [2].

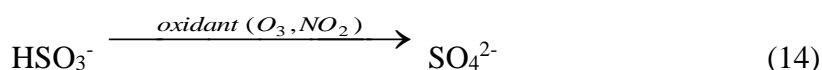
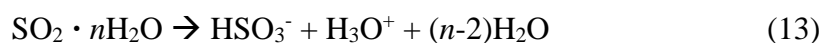
On the other hand, other species may act in indirect way, being precursors of secondary phenomena, as in the case of acid rains, or conducting other corrosive agents on the material, as in the case of particulate matter.

The atmospheric contaminants and the reactions in which they are involved that could mainly affect the corrosion of metallic material are quickly described here below.

2.4.2.1 Sulfur dioxide (SO₂)

Sulfur dioxide (SO₂) has always been considered as the most aggressive gaseous species for metallic material exposed to atmosphere [13]. It is formed by anthropogenic sources, mainly coal and oil combustion or industry emissions.

In the aqueous phase [13], [14], SO₂ oxidizes into the sulfate ion according to



In the gas phase [13], [14], instead, it reacts with the hydroxyl radical to form sulfuric acid:





Sulfur-containing compounds may interact with metallic materials exposed in atmosphere through dry or wet deposition. Dry deposition is the main form in which SO_2 reach the material, where it is adsorbed; this kind of deposition mainly occurs in industrial and urban environments where the concentration of SO_2 is greater, especially during winter: values of $100 \mu\text{g}/\text{m}^3$ are enough to produce a significant increase in corrosion rate or to cause degradation of protective coatings [1].

On the other hand, sulfate ions that reach the corroding surface through wet deposition may cause the reduction of critical RH value, enhancing water condensation and accelerating corrosion [16].

2.4.2.2 Nitrogen oxides

NO_2 and NO have anthropogenic origin and are formed during high-temperature combustion processes such as in power plants or vehicles.

NO , produced in higher amounts, converts into NO_2 [16] through oxidative reaction



or radical reaction (favored reaction)



Then, NO_2 can be further oxidized to form nitric acid according to (20)



Nitrogen oxides, together with sulfur oxides, represent the main responsible of acid rain phenomenon, that is the deposition producing the acidification of the substrate [13], [14], [16].

Corrosion and particularly electrochemical corrosion strongly depends on the pH of the medium and generally acidic environments appear more corrosive than alkaline or neutral environments.

2.4.2.3 Chloride

Chloride ion is one of the most aggressive corrosive species in atmosphere. The main source of Cl^- is marine spray, but it can also derive from human activities (road deicers, coal burning, incinerators, and so on) [2]. The maximum concentration, corresponding to the worst corrosive damages, is found in coastal areas.

Generally, the first step of chloride attack consists in the absorption on the substrate surface: Cl^- competes with OH^- (see section 2.4) to bond the metal surface, especially if it presents some irregularities or damages in the oxide layer [9].

Then, the oxidative anodic reaction causes the formation of soluble transient compounds, that could be easily dissolved in the solution, making the film locally thinner [13].

This is the starting point for *pitting* corrosion, one of the most dangerous form of corrosion [9].

The damaged areas, known as cavities or pits, behave as nuclei for the propagation of the process; in the cavity, the metal dissolution causes hydrolysis according to



and, consequently, the acidification of solution and the diffusion of other Cl^- ions in the cavity to balance the positive charge.

The corrosion products deriving from this anodic reaction are quite unstable and highly soluble; as this reaction is in competition with the formation of more stable compounds, it is clear that Cl^- ions also interfere with the process of repassivation of damaged films.

Outside the pit, instead, the reduction of O₂ produces an increase in pH value and in film passivity [2], [13].

An autocatalytic process is now occurring, with penetration rate and deep (up to 1 mm/year [1]) that increase with time.

2.4.2.4 Particulate matter

Particulate matter (PM) is a complex mixture of small particle and liquid droplets. It consists of a very large number of components, including metals, organic compounds, acids, salts, soil particles [19].

Beside the well-known hazard for human health, these particles may also have negative effects on the corrosion of metallic material. In this regard, PM action obviously depends on the concentration, but also on the composition, which reflects the environment where they formed [14].

Particulate matter can be emitted from natural and anthropogenic sources (fires, vehicular traffic, plant emission) but it can also arise from secondary reaction of emitted gasses in atmosphere. Nowadays it is considered as one of the most dangerous pollutants [16].

PM can act on materials through direct or indirect mechanism; in the first case, PM constituents, such as NaCl or (NH₄)₂SO₄, adsorb on the surface, dissolve in the liquid layer and affect the corrosion process (see section 2.4.2.3 for the mechanism).

On the other hand, particulate may act indirectly, promoting the adsorption of corrosive gasses, such as SO₂, from the atmosphere or carrying on the surface metals, which can give galvanic corrosion [14], [16].

2.4.2.5 Other compounds

Hydrogen sulfide (H₂S) [14] has both natural (volcanic emissions) and anthropogenic (industry and plant emissions) origin. It is slightly soluble in water and dissolves according to



with HS⁻ behaving as the corrosive agent.

Moreover, it can also react with OH⁻ to form SO₂ again, according to



Ammonia (NH₃) [16] is produced both by natural and anthropogenic processes and is the only common basic gaseous compound. It is highly soluble in water where it is in equilibrium with the ammonium cation NH₄⁺, allowing the local increase in pH



Moreover, NH₃ also acts in atmospheric corrosion by neutralizing aggressive acidifying ions (for instance, by forming ammonium sulfates such as NH₄HSO₄ and (NH₄)₃H(SO₄)₂).

2.4.3 Corrosivity of atmospheres

As described in previous sections, corrosion behavior of a material exposed to the environment strongly depends on several atmospheric factors; for this reason, a good knowledge of the atmosphere of exposure corresponds to easier understanding of corrosion mechanism.

Generally, exposure environments are divided into four categories [17]:

- ✓ Rural, that is unpolluted or slightly polluted atmosphere.
- ✓ Urban, where pollution is mainly due to vehicular traffic and domestic heating.
- ✓ Industrial, characterized by medium/high pollution grade, due to the presence of industries.
- ✓ Marine, corresponding to coastal areas that, due to the presence of corrosive species such as chlorides and sulphates (see section 2.4.2), prove to be very aggressive for metallic materials.

Considering the most significant atmospheric factors and contaminants characterizing those environments and influencing corrosion, corrosivity levels have been assigned to each listed class and summarized in the International Standard ISO 9223.

Classifications based on Cl^- and SO_2 depositions and TOW and the deriving corrosivity categories are presented in Table 2 and Table 3 [17].

Table 2: Corrosivity levels based on Cl^- and SO_2 depositions and TOW values

Time of wetness h/a	Level	Deposition rate of Cl^- $\text{mg}/(\text{m}^2 \cdot \text{d})$	Level	Deposition rate of SO_2 $\text{mg}/(\text{m}^2 \cdot \text{d})$	Level
$\tau \leq 10$	τ_1	$S_d \leq 3$	S_0	$P_d \leq 4$	P_0
$10 < \tau \leq 250$	τ_2	$3 < S_d \leq 60$	S_1	$4 < P_d \leq 24$	P_1
$250 < \tau \leq 2500$	τ_3	$60 < S_d \leq 300$	S_2	$24 < P_d \leq 80$	P_2
$2500 < \tau \leq 5500$	τ_4	$300 < S_d \leq 1500$	S_3	$80 < P_d \leq 200$	P_3
$5500 < \tau$	τ_5				

Table 3: Corrosion rates for the first year of exposure of carbon steel for the different corrosivity categories

Corrosivity Category	Carbon steel corrosion rate <i>g/(m² · a)</i> <i>μm/a</i>
C1	$r_{\text{corr}} \leq 10$ $r_{\text{corr}} \leq 1.3$
C2	$10 < r_{\text{corr}} \leq 200$ $1.3 < r_{\text{corr}} \leq 25$
C3	$200 < r_{\text{corr}} \leq 400$ $25 < r_{\text{corr}} \leq 50$
C4	$400 < r_{\text{corr}} \leq 650$ $50 < r_{\text{corr}} \leq 80$
C5	$650 < r_{\text{corr}} \leq 1500$ $80 < r_{\text{corr}} \leq 200$
CX	$1500 < r_{\text{corr}} \leq 5500$ $200 < r_{\text{corr}} \leq 700$

Chapter 3

Steel in Art and Architecture

3.1 Steel

Steels are alloys consisting of iron and carbon, with other alloying elements in lower percentages. Thanks to their properties, such as resistance, ductility, versatility, tensile strength and so on, steels are commonly used in several indoor and outdoor applications.

Chemical-physical features of steels primary depends on the composition of the alloy, with the amount of carbon being one of the main factor in defining the mechanical properties of material.

Going into more details, steel appears as a solid interstitial solution, where iron behaves as the solvent and carbon is the solute [20].

At atmospheric pressure, iron exists in three different allotropic forms:

- ✓ α iron, that presents body-centered cubic (BCC) structure and is stable up to 912 °C;
- ✓ γ iron, having face-centered cubic (CFC) structure and is stable between 912 and 1394 °C;
- ✓ δ iron, presenting body-centered cubic (BCC) structure and is stable between 1394 and 1536 °C.

Each of these allotropic forms can combine with carbon to give different interstitial solutions [21]:

- ✓ α ferrite and δ ferrite are interstitial solid solutions where carbon is solubilized into α or δ iron BCC structure, depending on the temperature of formation.

As the inclusion of carbon atoms causes great distortion in the crystal lattice, both structures can contain only small percentage of carbon, up to 0.02% and 0.09% respectively.

- ✓ *Austenite* is the interstitial solution where carbon is included into FCC structure of γ iron. In contrast with what happens to ferrite, the solubility of carbon in the γ lattice is relatively high, reaching values of 2.1% by weight; this is due to the greater stability that characterizes this structure.
- ✓ *Cementite* is an interstitial compound consisting of ~ 93.3% by weight of Fe and ~ 6.7% by weight of C. It is an iron carbide with formula Fe_3C and presents an orthorhombic structure. Fe_3C is metastable and tends to decompose in ferrite or austenite and graphite according to



The main phases and transformation are illustrated in the iron-carbon phase diagram (Fig. 2).

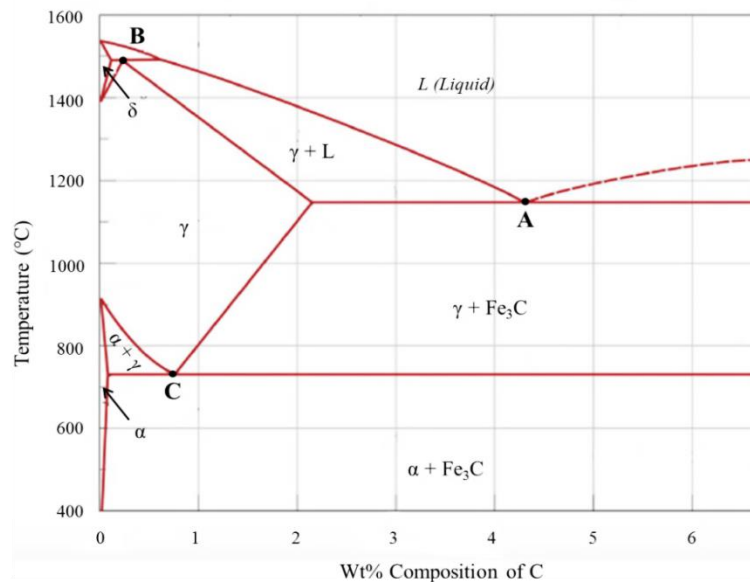


Fig. 2: Iron-carbon equilibrium phase diagram

The carbon percentage in steel ranges from 0.002% to 2.1%; alloys with a carbon content higher than 2.1% are called cast iron and will not be considered here.

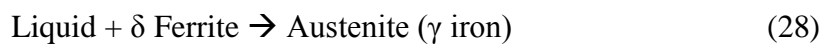
The diagram exhibits three critical points corresponding to phase transformations occurring at invariable conditions [21]:

- ✓ Eutectic transformation, A ($T = 1148\text{ °C}$ and 4.3% by weight of carbon)

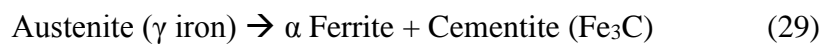


The resulting products constitute a compound called Ledeburite.

- ✓ Peritectic transformation, B ($T = 1495\text{ °C}$ and 0.17% by weight of carbon)



- ✓ Eutectoid transformation, C ($T = 723\text{ °C}$ and 0.8% by weight of carbon)



The resulting agglomerate is called Pearlite, whose structure is characterized by the alternation of thin plates of ferrite and cementite.

Even though not included in phase diagram, other compounds, such as *bainite*, *martensite* and *pearlite*, may characterize the composition of steel [21].

Bainite [20] is a solid structure that forms when austenite is cooled rapidly, giving rise to nuclei of ferrite and needle-shaped iron carbide. Generally two kind of bainite (upper and lower bainite) can be observed, but only lower bainite presents good mechanical properties, due to the particular structure consisting of thin plates of ferrite containing very fine rods or blades of carbide.

Martensite [22], instead, is a metastable compound; it forms when austenite is cooled at higher rates. The body-centered tetragonal (BCT) lattice of ferrite, supersaturated with carbon, appears tensionated and spontaneously rearrange into a body-centered cubic structure, a more stable configuration, by shear transformation, that is cooperative small displacements of all atoms in the structure (because diffusion processes are forbidden by low temperature).

Finally, pearlite is a characteristic structure of Fe-C alloys, consisting of ferrite and cementite, that forms when austenite is cooled below $T = 723 \text{ }^\circ\text{C}$.

Pearlite structure is characterized by the alternation of thin plates of ferrite and cementite; at first, nucleation of ferrite crystal starts on the austenitic grain boundaries; carbon present in the grain is pushed away and accumulate in the surroundings, where nuclei of cementite starts to grow [21].

Under certain operative conditions, globular pearlite may form: it presents a stable configuration, due to the reduction in surface energy compared to "classic" lamellar configuration. It is obtained by means of spheroidization annealing, a particular heat treatment of steel which involves heating about 30 hours at a temperature close to $723 \text{ }^\circ\text{C}$. Such a treatment increases the toughness and ductility of steel [23].

The amount of carbon, as stated before, affects the crystalline structure, which is connected to the chemical-physical properties of the material.

According to carbon percentage in the alloy, steels can be divided into [21]:

- ✓ Mild steel, or Low-carbon steel, which contains approximately 0.05-0.25% of carbon. This composition makes the alloy very malleable and ductile and, thus, suitable for the application as structural material.
- ✓ Medium carbon steel, containing 0.25-0.6% of carbon, represents a good combination of ductility and strength, especially after heat treatments.
- ✓ Hard steel, or High-carbon steel, contains from 0.6 to 1.0% of carbon of the overall weight. Steels of this group are the hardest within the three categories, but their ductility is quite low.

Chemical-physical properties of steel also depends on the nature and the amount of other elements in the alloy. Metals, such as manganese, nickel, chromium, vanadium, tungsten, molybdenum and

so on, are usually added to the alloy to obtain desired technological or mechanical properties: for instance, it is well known that manganese and nickel increases the tensile strength and vanadium the hardness of the alloy [9].

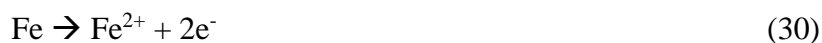
According to the total amount of alloying elements, another classification of steels is obtained [24]:

- ✓ Unalloyed steel, in which the percentages of alloying elements do not overcome the values specified in UNI EN 10020 (for example, 0.5% of Si, 0.25% of Cu, 0.8% of Mn);
- ✓ Low alloy steel, in which at least one metal overcomes the specified values and all the element are lower than 5% by weight.
- ✓ High alloy steel, in which at least one metal is higher than UNI EN values and is present in percentage greater than 5%.

3.2 Corrosion of steel

As other metallic materials, steels exposed to the atmosphere suffer the spontaneous process of corrosion. As stated in section 2.4, atmospheric corrosion only occur in the presence of an aqueous electrolyte film on the surface of the material.

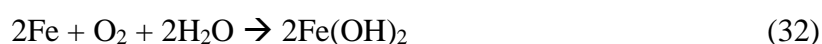
The anodic reaction consists in the oxidative dissolution of iron



And the main cathodic reaction is the reduction of atmospheric oxygen



To give the following total redox reaction



In atmospheric conditions, the sequential cycles of wetting and drying of steel surface produces periodical changes in corrosion potential. For this reason, it is evident that in atmospheric conditions, the process of formation of corrosion products is rather complicated and, generally, is characterized by three stages [14], [25], [26]:

- ✓ *Wetting of the dry surface.* When a thin aqueous film starts to form on steel, the dissolution of iron is balanced by the reduction of ferric compound (FeOOH), according to (eq. 29) and (32)



In this stage, the reduction of FeOOH proceeds faster than other cathodic reaction, mainly because of the poor amount of dissolved oxygen in the thin aqueous layer.

- ✓ *Wet surface.* When all reducible FeOOH is consumed, the oxygen reaction becomes the main cathodic reaction, according to (eq. 30). During this phase, the corrosion rate is quite low because it is limited by the O₂ diffusion rate.
- ✓ *Drying of the surface.* During the third phase, the liquid layer becomes thinner and the diffusion rate of oxygen increases; this produces an increase in corrosion rate, as well.

The higher amount of dissolved oxygen allows the reoxidation of Fe²⁺ formed during the first step; the reactions occurring in this step are:



This is the step during which the corrosion rate is higher. When the surface is wet again, the process restarts.

Ferrous oxides and hydroxides form and cover the surface, giving it the typical brownish-red texture of rust. The layer of corrosion products formed on the material is flaky and weakly attached to the surface and does not give any protection to the fresh metal, which continues to be corroded as long as it is exposed.

3.2.1 Methods for preventing steel corrosion

As stated before (see section 1), the corrosion of metallic materials not only causes structural damages, but it also produces huge economic costs, due to rehabilitation and maintenance work.

Several methods for preventing corrosion have been developed and are now usually adopted; they can basically be divided into three main classes:

- ✓ *Use of coatings.* The use of coatings is one of the most common techniques for corrosion prevention; coatings can be classified in two groups, metallic coatings and non-metallic (organic or inorganic) coatings. In all cases, they act as a physical barrier against corrosion, reducing the supply of water, oxygen or other atmospheric compounds to the substrate [9].

The effectiveness of surface coatings is connected to uniformity, porosity and thickness of the film, as well as to the ability to adhere to underlying metal or alloy [15].

Probably, the most common technique for corrosion control involves the use of metallic coatings, which offer protection through both barrier effect and electrochemical reaction (cathodic protection).

That is the case of hot-dip galvanizing, a process in which iron or steel are immersed in molten zinc; once deposited on the alloy and exposed to the atmosphere, zinc serves as a sacrificial anode and corrodes, forming a thick and protective zinc oxide film [1], [9].

- ✓ *Use of inhibitors.* Corrosion inhibitors are usually classified according to their action on metallic surface and are known as anodic, cathodic or mixed inhibitors [2].

Anodic inhibitors are compounds that can reduce the rate of the anodic metal dissolution by forming insoluble compounds or preventing absorption of aggressive ion (see section 2.4.2). They act via competitive absorption on the metallic surface. Chromates (CrO_4^{2-}) and nitrites (NO_2^-) have always been the best anodic inhibitors, but their use is now limited due to toxicity. Nowadays, molybdates (MoO_4^{2-}) represent a good alternative, leading to the formation of insulating ferric-molybdate complexes which cover and protect the surface [9].

Cathodic inhibitors are compounds able to reduce the rate of cathodic reaction; they form precipitates at the cathodic sites, thus limiting the entry of oxidizing substances. Zinc and magnesium salts, phosphates, bicarbonates and oxygen scavengers are the most widely used cathodic inhibitors.

Mixed inhibitors are compound that retard both anodic and cathodic reactions simultaneously.

- ✓ *Alloying.* Alloying process for corrosion control is one of the main developments in metallurgy in the last centuries. Beside modifying chemical-physical properties (see section 3), the addition of small percentage of specific elements in steel composition allows to improve corrosion resistance of the material even if exposed to quite aggressive environments, through the creation of protective and passive layer of corrosion products.

A new concept is now being introduced, the passivity of metallic materials. Passivity is the property of metals and alloys of forming a corrosion product film that protects the material from further corrosion [13], [15].

Polarization curve of passivating material, obtained by applying growing potential scan and recording density current variations, exhibits the typical shape of Fig. 3.

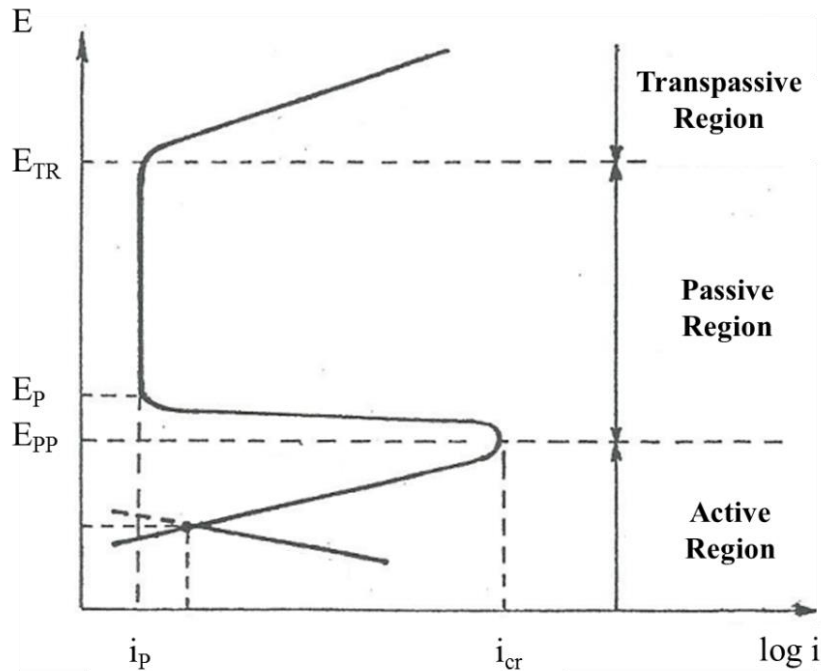


Fig. 3: Anodic polarization curve of passivating material [27]

At the beginning, alloy is active and corrodes, up to the primary passive potential, E_{PP} , where the current density reaches the maximum value (critical current density, i_{cr}); then, with increasing applied potential, the protective film starts to form. However, the real passive region begins at more positive potential, the passive potential E_P . In the passive region, ranging from passive potential E_P to transpassive potential E_{TR} , current density and corrosion rate drastically decrease. With sufficient potential increase a current growth is measured again, indicating transpassivity.

Not all passive films exhibit the same protective ability; in fact, it depends on several factors, such as homogeneity, thickness, compactness, porosity, conductivity of the layer formed. In turn, these features are connected to the composition of the material and the environment where it is exposed [28].

Then, it is clear that, by modifying alloy composition, resistance to atmospheric corrosion can be improved.

First hypotheses about the possibility of increasing corrosion resistance of steel using alloying elements in the composition date back to the first decades of 1800: among others, in 1827 Karl Karsten showed that the addition of only 0,29% of Cu to steel improved the corrosion resistance in H₂SO₄ solution of about 6 times; obviously, first remarks on this subject were mainly based on visual evaluations or mass loss analysis, without any knowledge of the specific action of alloying elements [29]. Then, it was not until XX century that first outdoor exposure of alloying steel were performed. The industrial development and the consequent increase in environment aggressivity, in fact, increased the interest of manufacturing and researchers in formulating new alloys with enhanced performances. In 1907, William et al. analyzed the environmental behavior of carbon steel and steels containing different amount of Cu (from 0.2% to 0.4% by weight) and confirmed the higher corrosion resistance of copper-steels [1].

In 1910, those results were further confirmed by Buck et al.: they exposed steel with 0.07% of copper in three environments of different corrosivities (rural, industrial and marine) and observed a higher resistance to corrosion (~ 1.5–2%) than CS [30]. As a result, in 1911 first structural steels with copper were commercialized in the United States. From that moment on, researchers were prompted to investigate the possible effects of adding other elements to the alloy to further improve its environmental performances.

This was the idea behind the formulation of high-strength low-alloy (HSLA) steel, a class of materials characterized by greater resistance to corrosion than carbon steel, thanks to the addition of metals showing passive ability, such as copper, silicon, nickel, chromium and phosphorus.

Among them, weathering steel (WS) represents a subset of steels characterized by interesting mechanical properties and good resistance to atmospheric corrosion, together with appreciated aesthetical features; this allowed it to be widely used for outdoor applications.

Weathering steel is the subject of this study and will be extensively described in this chapter.

3.2.2 Weathering steel

3.2.2.1 General remarks

Weathering steel (WS) is a steel belonging to the class of HSLA materials. It was first presented on the market in 1933 by US Steel Corporation, under the brand name of Cor-Ten, which reflected the two main properties that differentiated it from carbon steel: on the one hand the higher corrosion resistance (Cor), due to the addition of specific passive metals in its composition and, on the other hand, the improved mechanical properties, i.e. tensile strength (Ten) [30].

The advantages connected to the use of WS mainly concern technical and economic aspects; in fact, the superior mechanical properties compared to plain carbon steel allow to obtain significant reductions in thickness and weight of steel sheets, producing benefits with regards to the amount of necessary material and to safety concerns. Moreover, the improved corrosion resistance allows to use raw material without the need of additional coatings or regular maintenance.

The performances of Cor-Ten steel are connected to the creation of a compact and adherent passive layer of corrosion products, mainly oxides and hydroxides, on metallic surface, that protects the material from further corrosion.

In order to deal with several applicative requirements, Cor-Ten steel was, and is even now, commercialized in different variants, each characterized by a specific composition. Obviously, early versions of Cor-Ten steel, which were based on Fe-Cu-Cr-P systems [30], have been subjected to several developments in order to improve performances in environment with different aggressivity. Nowadays, three main types of Cor-Ten steel are available on the market [31].

- ✓ Cor-Ten A: it is commonly named ‘phosphorus Cor-Ten’, even though the amount of P in the alloy has been considerably reduced compared to the first commercialized formulations. Its composition (Table 4) lends it excellent corrosion resistance, about five-to-eight times higher than carbon steel. It is usually employed in architectural applications.
- ✓ Cor-Ten B: this product, unlike Cor-Ten A, exhibits not only good corrosion resistance (about four times higher than carbon steel) but also excellent mechanical properties, which make it highly recommended for structural applications. The main compositional difference consists in the amounts of P, V and Mn (see Table 4).
- ✓ Cor-Ten C: it has been introduced on the market only recently. While maintaining high corrosion resistance (comparable to Cor-Ten B), it also exhibits higher mechanical resistance which makes it suitable for the application in severely stressed structures.

Table 4: Elemental composition (% by weight) of commercial Cor-Ten

	C	Mn	P	S	Si	Cu	Cr	V
Cor-Ten A	≤ 0.12	0.20–0.50	0.07–0.15	≤ 0.035	0.25–0.75	0.25–0.55	0.30–1.25	≤ 0.65
Cor-Ten B	0.10–0.19	0.90–1.25	≤ 0.025	≤ 0.035	0.15–0.30	0.25–0.40	0.40–0.65	0.02–0.10
Cor-Ten C	0.12–0.19	0.90–1.35	≤ 0.025	≤ 0.035	0.15–0.30	0.25–0.40	0.40–0.70	0.04–0.10

Another classification of weathering steel is supplied by The American Society for Testing and Materials (ASTM), which has defined a series of standardized compositions of steels, characterized by different mechanical and resistance properties which are connected to different percentages of alloying element in the alloy [32]–[36].

The improved corrosion resistance of weathering steel compared to carbon steel appear clear in all types of atmosphere, as shown in Fig. 4; the differences in the corrosion rate, relatively limited in the case of exposure in rural environment, gradually become more pronounced when the material is exposed to more aggressive atmospheres.

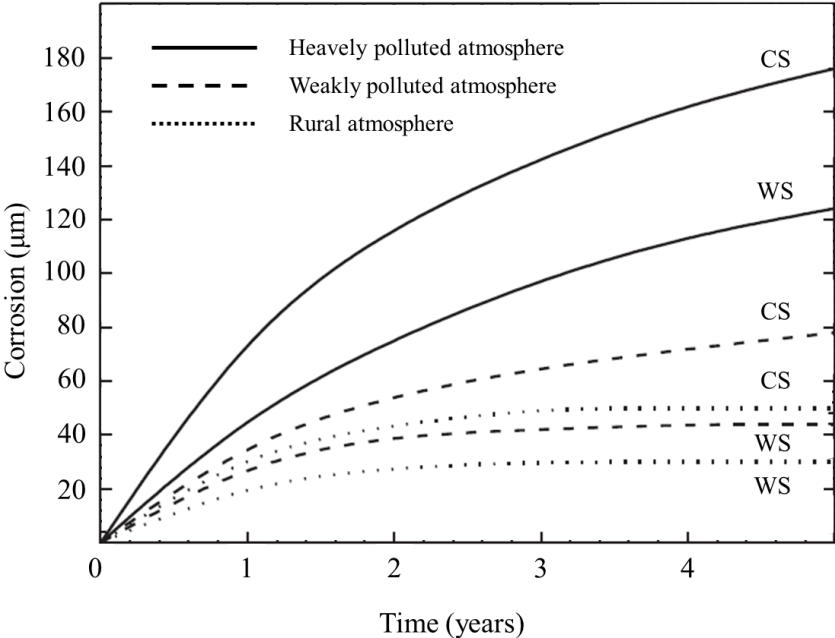


Fig. 4: Corrosion trends vs exposure time for weathering steels (WS) and carbon steel (CS) exposed in rural atmosphere and polluted areas [30]

Despite WS was initially designed as a less expensive and better performing alternative to structural carbon steel, with the passing of time, its peculiar aesthetical features stimulated the interest of architects and artists all around the world.

The passive layer forming on the material after atmospheric exposure shows unique chromatic features, which depend on the composition of the alloy, the environment and, especially, the time of exposure: as time goes on, in fact, the alloy changes its color, passing from yellowish to dark-brown (Fig. 5) and proving to be a living material.

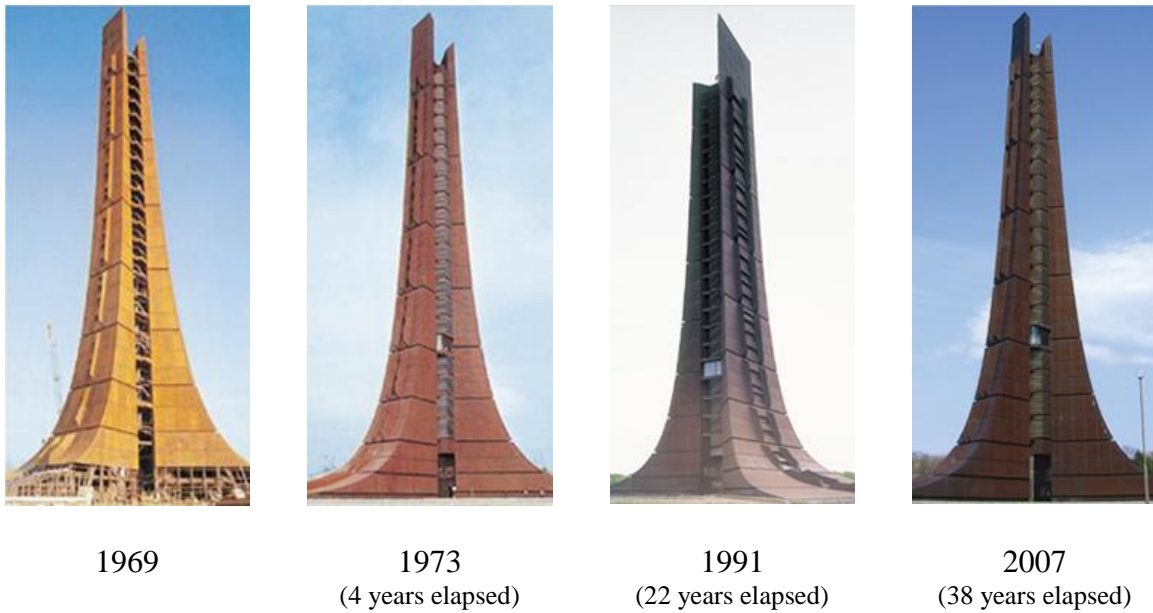


Fig. 5: Hokkaido 100 years memorial tower, Sapporo [37]

3.2.2.2 Mechanism of patina formation

The distinctive feature of WS lies in the surface patina that offers a unique appearance and protection to the material. Let's go then to analyze the conditions and the mechanism of formation of this particular layer.

It is well known that the proper formation of protective patinas requires several factors to take place [30]:

- ✓ Regular and continuous cycles of wet and dry periods, with rainwater polishing the surface and fast dry action, promote the formation of adherent and dense passive layers.
- ✓ No water stagnation on surfaces, that means that cavities or interstices should be avoided, because they could act as starting points for atmospheric corrosion, due to too long TOW.
- ✓ Photo-catalytic action of solar radiation
- ✓ Low amounts of corrosive species that, as stated, may promote the formation of unstable corrosion product, creating less protective patinas.

Similarly to what happens for carbon steel, patina formed on WS includes oxides, hydroxides and magnetite (Fe_3O_4), with the relative amount of each compounds depending on the environment and the time of exposure.

The protective ability of weathering steel is connected to the features of this patina, which consists of two overlapping layers, a loose and porous outer layer of lepidocrocite ($\gamma\text{-FeOOH}$) and a compact and adherent inner layer of goethite ($\alpha\text{-FeOOH}$) [38]–[40].

Lepidocrocite (Fig. 6a) forms during the first stage of environmental exposure (approximately several months - a few years); with the passing of time, mechanisms of dissolution-precipitation of $\gamma\text{-FeOOH}$ (see section 3.2) cause the creation of an amorphous intermediate (Fig. 6b), identified as amorphous ferric oxy-hydroxide (or feroxyhyte), that slowly (years) transforms to goethite (Fig. 6c), electrochemically and thermodynamically more stable [38], [39], [41].

In this process, Cu and P are supposed to promote and catalyze the formation of amorphous matter, thus enhancing stability and compactness of patina.

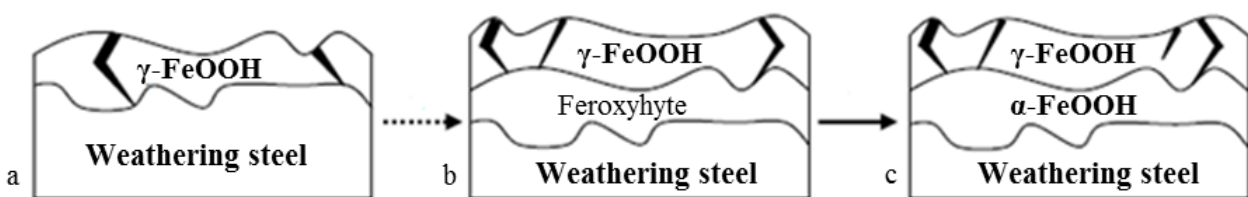


Fig. 6: Mechanism of formation of the passive layer on weathering steel [42]

A better understanding about the process of stabilization of the passive layer is given by the pioneering work of Kimura et al. [40], [43], which studied the nanostructured morphology of the rust formed on WS and proposed the new concept of 'Fe(O,OH)₆ network': according to this study, octahedral Fe(O,OH)₆ unit nuclei corresponding to the γ -FeOOH phase form in the first step of corrosion and then combine with each other during the wetting/drying cycles to form a network.

As the exposure time increases, the initial arrangement of octahedral units in the γ -FeOOH phase becomes more ordered and α -FeOOH, consisting of the alternation of double chains of octahedral units of Fe(O,OH)₆ and double chains of vacant sites, is obtained in the inner layer.

To explain the active role of alloying elements, especially Cr, in enhancing the corrosion resistance of WS, Yamashita et al. [44] suggested that Cr resulting from the alloy coordinates with O₂⁻ to form [CrO₂]⁻ and fills these vacant sites; this causes the distortion of the network and the creation of ultrafine crystals of Cr-goethite with a mean particle size of 12 nm [45]. The formation of this Cr-goethite complex gives greater density and compactness and increases the cationic selectivity of the inner layer of patina [46], [47], which thus becomes a barrier that opposes the entry of corrosive substances [44].

Clearly, the transformation of lepidocrocite into more stable goethite, not only depends on time, but also on the atmosphere of exposure; thus, α/γ ratio may represent an index describing the rate of the corrosion process: the greater this value becomes, the slower the corrosion process goes on. So, Kamimura et al. [48] investigated the relation between the relative amounts of γ -FeOOH and α -FeOOH and corrosion rate and proposed to use α/γ ratio, defined as PAI (Protective Ability Index), to estimate the protectiveness of the rust formed on WS.

However, the composition of the passive layer and its protective ability together with the stabilization rate are strongly affected by exposure environments and conditions.

The presence of atmospheric pollutants may modify the behavior of WS and inhibit patina stabilization process. This is the case of SO₂, that above a critic threshold value of ~ 20 mg/m²-d, typical of urban and industrialized areas, causes an increase of corrosion rate [30], [49].

In marine environment, where the amount of corrosive species, especially chlorides, is relatively high, the protective patina does not develop at all. In this cases, in fact, besides lepidocrocite and goethite, the typical corrosion product formed is akaganeite (β-FeOOH).

Akaganeite consists of tetragonal unit cells that organize into a hollandite structure containing tunnels, that are stabilized by the entrance of Cl⁻ ions [50]. With the increase of chloride concentration in the exposure atmosphere, the relative amount of akaganeite in the patina naturally becomes greater [51].

An interesting behavior is that pointed out by Wang et al. [52], that presented the results of an exposure at Qinghai salt lake: the analysis of the composition of the rust layer throughout the duration of the exposure showed that the main constituents were altered from initial β-FeOOH and γ-FeOOH (in 6 months), via β-FeOOH and magnetite (18 months) to magnesoferrite and iowaite (30 months). Both β-FeOOH and iowaite (Mg₄Fe(OH)₈OCl·xH₂O) showed anion-selectivity properties and may act as chloride reserve or chloride channel, producing a ionic flow toward the inner part of the patina and accelerating the corrosion of the alloy [39].

After several exposure tests in marine environments, Kamimura integrated its definition of PAI (Protective Ability Index), by adding an alternative value, α/γ^* (α -FeOOH / [γ -FeOOH + β -FeOOH + Fe₃O₄]), that takes into account the different composition of patinas formed in chlorine-rich environments [48].

Differences in patina composition due to the features of the exposure environment reflect on the rate and the extent of the corrosion phenomenon.

Some examples of corrosion trends of WS exposed in different environments, reported by Morcillo et al. [30] (Fig. 7 and Fig. 8), show that corrosion rate grows when moving from rural atmospheres, where the patinas generally take ~ 6-8 years to stabilize, to industrial and marine atmospheres, where, in some cases, the stabilization of corrosion rate does not occur at all [30].

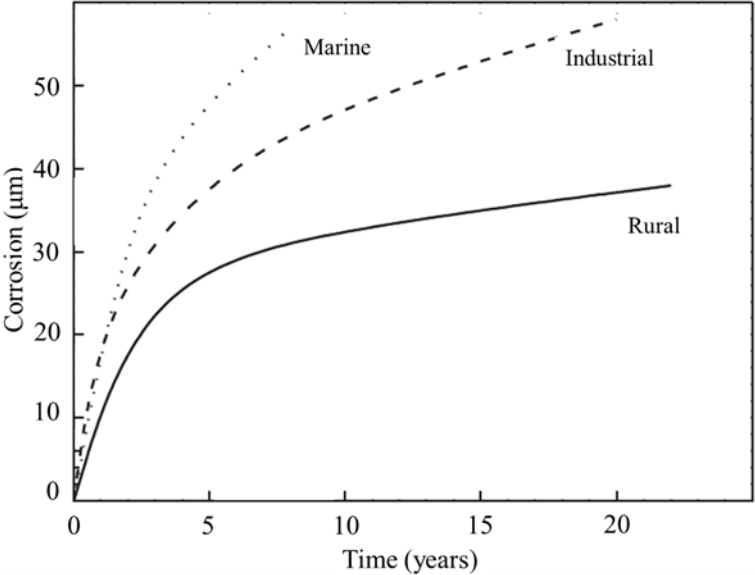


Fig. 7: Corrosion trends vs exposure time for weathering steels (Cor-Ten A) exposed in rural, industrial and marine atmospheres [30].

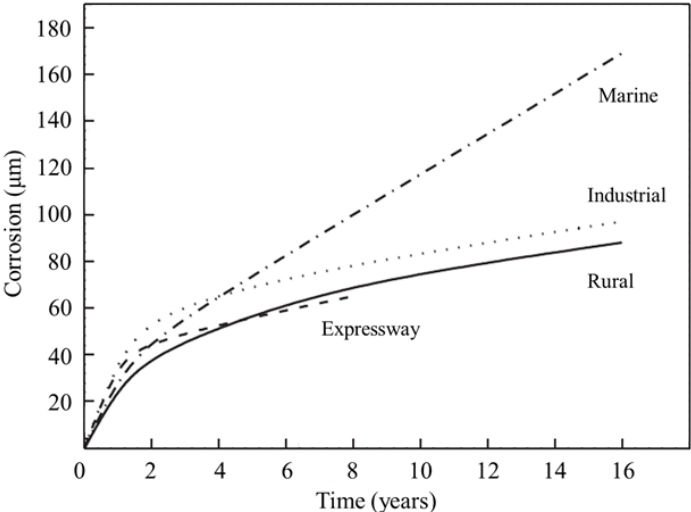


Fig. 8: Corrosion trends vs exposure time for weathering steels (Cor-Ten B) exposed in rural, industrial and marine atmospheres [30].

3.2.2.3 Role of alloying elements

Since the distribution of first weathering steels, researchers and industries have focused their interest on studying the effects that each alloying element may have on atmospheric corrosion resistance.

Copper, chromium and nickel were defined as the most abundant alloying elements in steel that present an active role in preventing corrosion (C is not considered as an alloying element) [42]. So, let's briefly analyze their action.

Copper was the first alloying element tested and added to steel composition (see section 3.2.2.1), leading to the development of weathering steels. In areas with high amount of SO₂, it is supposed to promote corrosion resistance through the formation of insoluble hydrosulphates. Apart from reducing the aggressivity of SO₂, these compounds, accumulating in pores and in the inner part of the rust layer, promote the densification of patina and oppose the entry of other corrosive species [39].

Chromium, as well known, affects the resistance to atmospheric corrosion of WS taking an active role in the process of transformation and stabilization of inner part of corrosion layer (section 3.2.2.2). Several works in literature [53]–[55] demonstrated the increase in corrosion resistance due to the presence of Cr in alloy composition.

Nickel, initially added in order to minimize embrittlement of alloy during processing, later proved to be one of the elements responsible of corrosion resistance, especially in marine environments. Similarly to copper, Cr forms insoluble oxy-hydroxides, that act as nucleation sites for Fe(O,OH)₆ units and promote the formation of very fine nano-networks [56]. The deriving rust, more dense and compact, also presents enhanced cation selectivity and thus act like a barrier against major anionic aggressive species [57].

3.2.2.4 Weathering steel in art and architecture

The peculiar aesthetic features together with mechanical properties and resistance to atmospheric corrosion led Cor-Ten steel to be esteemed all over the world and selected for a wide number of artistic, architectural and infrastructural applications. The Cor-Ten ability to change its appearance over time and to integrate itself completely within different landscapes have crowned it as the ultimate 'living material'. The warm, welcoming colors that assumes with the passage of time led Cor-Ten to be widely used in construction or modernization of buildings and in urban regeneration works.



Fig. 9: Old Flour Store, Tallin [58] © Martin Siplane



Fig. 10: Museum of Montegudo, Bolivia [59] ©David Frutos



Fig. 11: Caixa Forum, Madrid (Spain) [60] ©Pierre Engel



Fig. 12: House in Nieuw Leyden, Netherlands [61] © Boris Zeisser



Fig. 13: Museum of Tadeusz Kantor and Cricoteka, Kraków, Poland [62] © Wojciech Kryński

The changing nature of the material in relation with the time and place of exposure makes it unique, especially for artists; many world-renowned sculptors have thus embraced, in the course of their career, Cor-Ten steel both for its aesthetical features and for its conceptual value.

Among them, Mauro Staccioli is one of the contemporary artists who has been able to better exploit the potential of the material for art installations. Its Cor-Ten structures have simple geometric shapes, which can enclose the surrounding landscape and create timeless images.



Fig. 14: Piazza Duomo '08, Mauro Staccioli, Racconigi (CN) [63] © Enzo Isaia



Fig. 15: Cerchio Imperfetto, Mauro Staccioli, Parco Archeologico Scolacium (CZ) [64] © Marco Gronchi



Fig. 16: Da sinistra a destra, Mauro Staccioli, Parco Archeologico Scolacium (CZ) [65] ©
Cultura Italia

Another artist who chose the cardboard as the main material in his works is Richard Serra; with its installations alternating concave and convex surfaces, he has been able to create vital and interactive structures to generate a flow that involves and disorient the spectator.



Fig. 17: Vortex, Richard Serra, Modern Art Museum of Fort Worth, Texas, USA [66] © Dallas
Photoworks



Fig. 18: Te Tuhirangi Contour, Richard Serra, Gibbs Farm, New Zeland [67] © Gibbs Farm

2013



Fig. 19: Blade Runners, Richard Serra, Florida, USA [68] © Martina Muller

Among the main exponents of contemporary environmental sculpture is Bernar Venet (Fig. 20, Fig. 21 and Fig. 22), who, thanks to more or less random arrangement of arched or angular structures, creates a perfect frame for the surrounding landscape, depicting the fine balance between man and the environment.



Fig. 20: Bernar Venet, 219.5° Arc x 28, 2011. Temporary exhibition along the Hong Kong bay, November 2015 – February 2016 [69]



Fig. 21: Bernar Venet, Three indeterminate lines. Permanent exhibition at Frederik Meijer Gardens & Sculpture Park, Michigan [70]



Fig. 22: Bernar Venet, 85.8° Arc x 16, 2011. Temporary exhibition at Place d'Armes in Versailles, June 2011 – November 2011 [71]

Beside architectural and artistic works, Cor-Ten steel is often used in infrastructural application (bridges, viaducts, guardrail, sound-adsorbing panels, and so on), due to its good mechanical properties and high resistance to atmospheric corrosion.



Fig. 23: Footbridge in Granollers (Spain) [72] © Xavier Font



Fig. 24: Restoration of a Middle Ages bridge in Sant Celoni (Spain) [72] © Xavier Font

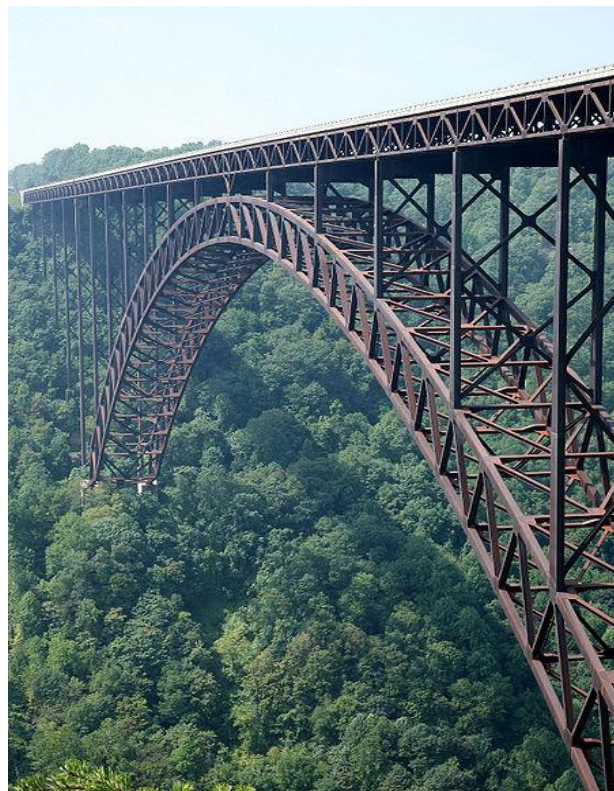


Fig. 25: New River Gorge Bridge (USA) [73] © N. Mueller

Chapter 4

Metals and the Environment

The biosphere [74], [75] is defined as the global ecological system including lithosphere, hydrosphere, geosphere and atmosphere, that, by interacting with each other, are able to support life. The biosphere can be considered as a 'thin' layer (~ 20 km) on the Earth's surface. Depending on the type of interactions occurring between different ecosystems, several and characteristic living beings are created that are connected with environmental conditions. Equilibria established in the biosphere are the result of complex evolutionary processes due to environmental and climatic changes that occurred over time.

However, the increase in population and the intensive exploitation of territories have caused further environmental changes, interfering with these balances. This fact led to the definition of anthroposphere (or technosphere), that is that portion of the environment that has been modified by human activities.

Pollution is the clearest proof of human intervention on the environment and metals represent some of the most persistent and dangerous pollutants [76], [77]. In fact, unlike organic pollutants, that may undergo changes and degradation processes in the environment, metals exhibit great tendency to accumulate.

Both natural (volcanic eruptions, natural weathering of rocks, forest fires and biogenic processes) and anthropogenic (industrial activities, mining, vehicular traffic) sources introduced metals into the biosphere [78]. All environmental compartments are affected by metal input, including the air,

during combustion or extracting processes, or surface waters, via runoff occurring during storage or transport of material, or soil, due to agricultural activities [79].

The continuous introduction and persistence of metals in the environment may therefore lead to potential risk situations for both ecosystems and living beings.

4.1 Metals in the Environment

Metals are natural components of the biosphere and are generally divided into non-essential elements (such as Hg, Cd and Pb) and essential elements (Cu, Mn, Fe, Zn, Se, Co); the latter, also known as micronutrients, are required in low concentrations for plant growth and animal and human health, taking an active role in physiological and metabolic processes [80].

Despite that, if present in higher amounts, essential metals may represent a risk to ecosystems and human livings, causing a wide range of adverse effects.

The case of manganese represents a clarifying example. Mn is essential for the human body where it acts as enzyme activator or constituent: for instance, manganese activates pyruvate carboxylase, the enzyme involved in the process of gluconeogenesis, and is a cofactor of superoxide-dismutase, antioxidant enzyme involved in the processes of free-radical protection [81].

On the other hand, however, excessive exposure to manganese can cause motor and neurological disorders, known under the name of manganism, as well as liver diseases [77].

The tendency of metals to accumulate in the environment or in living organisms (*bio-accumulation*) makes it clear the need for extensive studies on the processes of accumulation and action of metals in all compartments of the biosphere.

With the development of industrialization and technology and the consequent problem of increasing pollution, metal contamination of waters and soils created collective concern, not only with regards to human health but also to the sustainability of ecosystems.

Metals in the hydrosphere are mainly concentrated in superficial films and sediments and represent an hazard for aquatic biota that, through an uptake process, may give rise to biomagnification and bioaccumulation phenomena [82].

The hydrosphere, including oceans, seas, glaciers, ground waters, contains metals in dissolved or particulate state; then, dissolved metals may exist as free hydrated ions or as complex ions chelated with organic or inorganic ligands [83]. The form in which they are present, chemical-physical properties and mobility in the hydrosphere, that are connected to their potential toxicity, depend on several factors, such as pH, redox potential, ionic strength, dissolved oxygen, water hardness, and so on [77].

The geosphere can present metal contamination both for direct release (industrial plants, mining, fertilizers, etc.) and for interaction with other ecosystems: in fact, both the atmospheric depositions and the contact with polluted waters can modify the amount of metals in soils. Obviously, the processes of adsorption of contaminants depends on soil composition, grain size and permeability [77].

Metals may exist in soil solutions as free cations or oxyanions or as organic or inorganic complexes and in soil solid phase as adsorbed or complexed particles. They exhibit different properties and reactivity according to the chemical form: free ions are immediately available to be caught by organisms or plants or to be exchanged with other ecosystems; on the other hand, metals adsorbed on solid-phase components appear temporarily not available and metals included in mineral structure are not available at all and may be released only after its consumption [78].

Lastly, the main carrier for metal transport and introduction in soils and surface waters is the atmosphere. Metals are released in the atmosphere by natural sources, such as volcanic eruption, soil suspension, and human activities, that nowadays represent the dominant source. They are mainly present in the particulate phase and, according to their chemical-physical features, may be subjected to short- or long-range transportation until they settle on soils or waters through dry or wet depositions [84].

4.2 Bioavailability and mobility of metals

According to what said in the previous section, contamination by metal cannot be evaluated solely by the total concentration of metal in a selected environmental compartment [80]; on the contrary, the potential toxicity of each element is connected to the concepts of speciation, bioavailability and mobility. To better understand the topic, here below are the definitions of these concepts, according to which:

- ✓ Chemical Species: specific form of an element defined as to isotopic composition, electronic or oxidation state and/or complex or molecular structure [85].
- ✓ Speciation: distribution of an element amongst defined chemical species in a system [86].
- ✓ Bioavailability: the fraction of the total concentration of contaminants that is potentially available for plant or organism uptake [78].

Mobility, bioavailability and, thus, toxicity of an element are linked to its speciation, namely the form in which it is present in nature.

As stated before (section 4), the different environmental compartments include metals in several forms, such as free or complexed ions, organic and inorganic complexes, adsorbed particles and precipitates. Since the environment represents a complex and dynamic system, chemical speciation

of an element in contact with it may vary several times [87], due to acid-base reactions, redox reactions, dissolution-precipitation processes, complexation or ion-exchange reactions, sorption-desorption equilibrium [78].

In turn, all the chemical-physical factors affecting those processes are considered very important in controlling metal activity and mobility. The main parameters [88] can be divided in two groups:

- ✓ Local environmental conditions, such as pH, redox potential, ionic strength;
- ✓ Features of the medium, such as oxidizing or reducing character, main constituents, presence of reactive species (i.e. ligands or colloidal materials [89]), porosity, and so on.

4.3 Environmental behavior and potential toxicity of WS alloying elements

When weathering steel is exposed to the environment, the presence of corrosive species (see sections 2.4.1 and 2.4.2) may result in the formation of instable, soluble or not completely adherent corrosion products, that do not ensure the passivation (section 3.2.1) of material.

In these conditions, phenomena of corrosion product detachment or surface washout by rainfall may occur, causing the dispersion of iron and other alloying elements in the environment.

Some of these metals may accumulate in soils or be transferred to aquatic systems, thus representing a potential risk for ecosystems and living beings.

In the next few sections, main WS alloying metals and their potential toxicity are reviewed.

4.3.1 Chromium

Chromium is a metallic element, naturally-occurring in rocks, soils, plants and animals, as Cr(0), Cr(III) or Cr(VI) [90].

It is commonly used in alloyed steel and pigment production or for wood conservation. It can be released in the environment as a result of industrial processes or burning of natural gas or coal [91].

The solubility, environmental mobility and toxicity of chromium depends on its oxidation state: Cr(III) compounds are generally soluble in water at low pH and are not toxic; on the contrary, Cr(VI) compounds, totally derived from anthropogenic sources, are much more toxic (~ 100-1000 times) than trivalent compounds [92].

To understand the possible impact on the environment, it is very useful to analyze the complex chemistry of this element.

Cr(III) is the most stable form in nature and creates a very large variety of compounds, including oxides, halides and sulfides, or complexes. An important environmental process for the transport of Cr in waters and soils involves the formation of very stable complexes with humic substances; in fact, according to their solubility, the mobility of Cr(III) can substantially change [91].

Under oxidizing conditions, Cr(III) may oxidize to Cr(VI), forming CrO_4^{2-} (chromate) and HCrO_4^- (dichromate); in this form chromium is more soluble and mobile and may lead to phytotoxicity phenomena, that produce several problems in plant growth [92].

Beside this, chromium compounds may also represent a risk for animal and human health. Although Cr(III) is an essential nutrient for living beings, exposure to high levels of this element may cause adverse effects, such as chronic respiratory problems.

Cr(VI) compounds, instead, may negatively affect human and animal health even in small amounts; they are more soluble and bioavailable than Cr(III) compounds and can easily enter cellular membranes. The uptake or the prolonged exposure to hexavalent chromium cause skin and respiratory irritation, up to ulceration and stomach and lung cancer. In 1990, the IARC (International Agency for Research on Cancer) recognized Cr(VI) as carcinogenic to humans (Group 1) [93].

Moreover, although Cr(VI) is unreactive towards DNA, the reduction of Cr(VI) to Cr(III) occurring into cellular membranes under physiological conditions results in the formation of radicalic species that may lead to alterations and mutations of chromosomes and DNA lesions [93].

4.3.2 Copper

Copper is a common element in the environment; it is present in rocks, sediments, waters and, in a limited manner, in air. It derives from natural (volcanoes, forest fires) and anthropogenic sources (industries, mining, fossil fuel combustion, agriculture).

In the atmosphere copper is present as particulate matter, that can be subjected to different removal processes (i.e., bulk, dry or wet depositions) and transferred to soil or water ecosystems.

In soil solutions, copper is mainly present as Cu(II) and forms hydroxide, carbonate, and sulfate complexes; depending on soil pH, some species will dominate on the others: in acidic soil solutions, copper sulphates are the main species present; on the other hand, the increase in pH values favors the formation of carbonates or hydroxides [91].

In organic soils, Cu strongly binds organic materials, such as humic or fulvic acids, forming very stable complexes that drastically reduce copper mobility and bioavailability.

As for soils, in aquatic systems, copper is mainly present as Cu(II) and forms hydroxides and carbonates; moreover, it easily forms chelates with a large variety of ligands, that affect its bioavailability and mobility. The stability of these chelates is affected by pH, ionic strength and presence of competing ions. In water solutions, small amounts of free ions can also be found, that may represent a risk for some fish, invertebrates or microorganism, even at low concentrations.

Copper(II) is an essential nutrient for almost all living beings and takes part to a series of biochemical and metabolic processes; it is actively involved in the normal functioning of more than 30 enzymes in human body [94].

However, the inhalation or the long-term exposure to copper may cause irritation to eyes and respiratory apparatus and headaches; moreover, one of the most documented adverse effect is gastrointestinal distress, including stomach cramps, nausea and vomiting.

Finally, in the early 2000s, it was proved that the simultaneous presence of copper ions in drinking water and high-cholesterol diet may promote an Alzheimer-like disease in rabbits [95].

4.3.3 Iron

Iron is an essential element in most biological systems and represents the most abundant trace mineral in the body.

In the environment, it is present in two oxidation states, Fe(II) and Fe(III), mainly as iron oxides. In soils, it forms stable chelates with organic matter, producing nutrients for plants, that need iron for photosynthesis, respiration and nitrogen fixation; however, high amounts of Fe²⁺ may catalyze excessive production of reactive oxygen species, that could result very toxic for the plant [92].

When it enters the animal or human body, iron is included in fundamental proteins, such as hemoglobin, myoglobin, ferritin and transferrin, or enzymes, such as peroxidase or cytochrome-c.

The exposure and the intake of large amount of iron lead to the saturation of iron-binding proteins and, as a consequence, free iron ions begin to circulate in the organism and penetrate liver, heart or brain cells, causing several damages to cellular compartments.

The most dangerous effects of iron excess are those on the cardiovascular system, but hepatic disorders may also manifest [96].

4.3.4 Manganese

Manganese is widely distributed in soils, waters, sediments, rocks and air, as Mn(II), Mn(III) and Mn(IV). In the atmosphere it is present as particulate matter, whose deposition is the dominant source of manganese in surface waters. In soils, manganese is present as Mn²⁺ free ion (acidic soil), as oxide (neutral and basic soils) or included in complexes (organic soils) [97].

Both in aquatic and terrestrial ecosystems, Mn speciation is governed by temperature, pH, redox potential, O₂ availability and dissolved organic matter.

Manganese is an essential nutrient for plants, animals and humans; being both a constituent and a catalyst of several proteins and enzymes, such as superoxide dismutase, pyruvate carboxylase and arginase, Mn take an active role in important biochemical processes (i.e. photosynthesis, proteoglycan biosynthesis, antioxidative action).

However, high amounts of Mn in soils may cause accumulation in plants with consequent toxicity. Symptoms of excessive manganese supply first affect the old parts of the plant, that turn brown because of MnO₂ deposits, and, in the case of high toxicity, also the younger areas, with a reduction of chlorophyll content and the inhibition of plant growth.

In humans, adverse effects due to manganese are mainly connected to prolonged exposures or accidental intake. The central nervous system is the critical target for Mn toxicity; symptoms of

Mn intoxication include headache, emotional liability, hallucinations, speech disorder, up to chronic, irreversible neurological and motor disorders [92].

4.3.5 Nickel

Nickel is emitted in the environment by natural (volcanoes emission, weathering of rocks, wind-blown dust) and anthropogenic (combustion of fossil fuels, industrial processes) sources. It is mainly present as Ni(II) and forms a wide variety of compounds such as oxides, hydroxides, halides, sulfates, chromates and so on [92].

In natural ecosystems, nickel compounds are generally insoluble at pH values > 6.5 , but the occurrence of acid rain tends to mobilize Ni, leading to increased uptake and potential risk for plants, animals and humans.

Nickel is an essential element for plants, being a constituent of several enzymes, among which urease, a nickel-dependent metalloenzyme responsible for the hydrolysis of urea to form ammonia and carbon dioxide [98].

Although it plays an important role in several metabolic processes, Ni excess may cause toxicity in plants, with adverse effects including necrosis of leaves, retardation of germination and inhibition of growth [99].

In humans, contact with nickel and its alloy may cause dermatitis, while the oral intake can produce allergic reactions and irritation to respiratory system [92].

The most alarming risk associated with nickel compounds is their carcinogenic effect on lung and nasal cavities, so that, in 1990, the IARC (International Agency for Research on Cancer) recognized Ni compounds as carcinogenic to humans (Group 1) and metallic Ni as possibly carcinogenic to humans (Group 2B) [93].

Chapter 5

Materials and methods

During the PhD project the corrosion behaviour of weathering steel has been analysed by means of field and laboratory tests, with the aim of assessing the influence of a series of environmental parameters on the process of formation and stabilization of passivation patinas and on the process of metal release. Field exposure and laboratory tests allow to obtain complementary information about a phenomenon: in fact, on the one hand, field tests, despite the time required to collect significant data is generally in the order of years, allow to consider and study the synergic action of environmental parameters and atmospheric pollutants on WS corrosion, a condition that would be difficult to faithfully reproduce during laboratory tests. On the other hand, simulated ageing tests in controlled conditions offer the possibility to isolate specific phenomena and to obtain, in relatively short times, valuable information for the comprehensive explanation of the process.

The environmental exposure involved three different WS finishes, bare, pre-patinated and pre-patinated/waxed, which are commonly commercialized and used for outdoor application, even in aggressive environments. Moreover, considering the structural complexity of several WS installations, the influence of two exposure geometries (sheltered and unsheltered) on the corrosion of material has been also investigated.

The evolution and the stability of patinas formed on WS samples were monitored by means of the evaluation of mass variation and periodical surface investigation (SEM/EDS, sections 5.5.3 and 5.5.4; Raman Spectroscopy, section 5.5.5).

During the whole period of exposure (4 years), rainwater impinging each unsheltered specimen was monthly collected and metals and ions in runoff waters were analysed (AAS, section 5.5.1; Ion Chromatography, section 5.5.2); in order to quantify corrosion induced metal runoff in the freely dissolved fraction, that is the most mobile and bioavailable fraction from an environmental point of view, the collected solutions were filtered (0.45 μm) to remove metals released in particulate form [100].

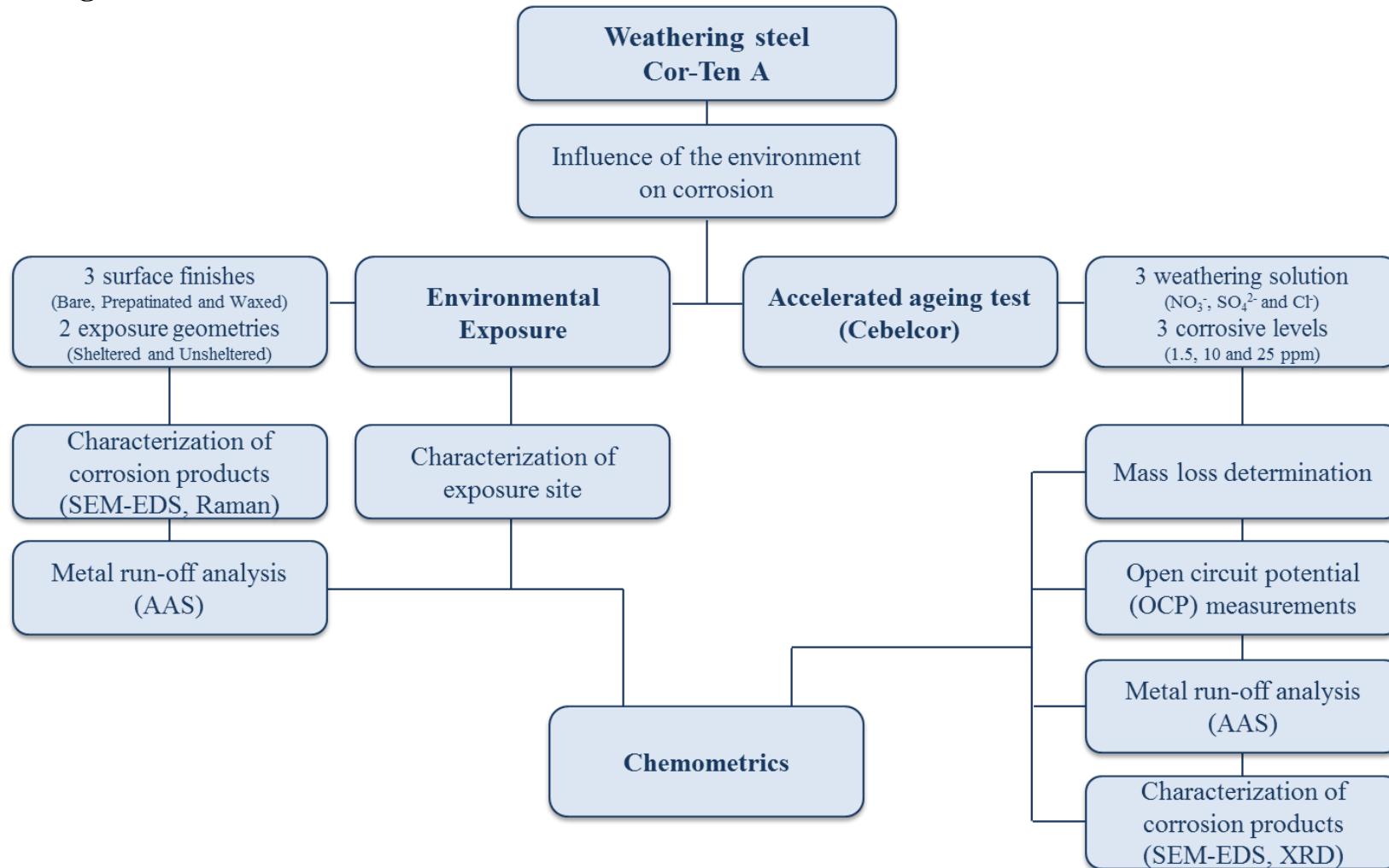
Hourly and daily environmental data, including temperature, solar radiation, relative humidity, wind direction and speed and air pollutant concentration were constantly monitored.

All data resulted from these numerous investigations were treated by means of univariate (Pearson's Coefficient) and multivariate (2Way- and 3Way- Principal Component Analysis) techniques to extrapolate the maximum information and to better explain the corrosive trend of WS in relation to the several environmental factors involved and the different surface finishes considered.

Simultaneously, accelerated ageing tests allowed to consider a more specific aspect of the atmospheric corrosion of WS, that is the interaction of the material with some of the most corrosive agents present in the atmosphere; particularly, an immersion / emersion test (Cebelcor test, section 5.4.1) was carefully planned and performed to study the action that different concentrations of the three main saline components of particulate matter and atmospheric depositions (chlorides, sulphates and nitrates) may have on the process of patina formation and stabilization and on metal release of bare WS.

Also in this case, several information were obtained, including mass loss determination (section 5.5.8) and open circuit potential (OCP) data (section 5.5.7), compositional and morphological (SEM/EDS, section 5.5.3 and 5.5.4; XRD, section 5.5.6) characterization of patina formed and quantification of metals released in dissolved and particulate form (AAS, section 5.5.1).

5.1 Working Plan



5.2 Description of materials

5.2.1 Weathering steel: Cor-Ten A

The material examined in this work is a commercial weathering steel, known as Cor-Ten A, provided by a local supplier. The nominal composition of the material is shown in Table 5.

Table 5: Alloy composition (weight %) determined on CorTen A sample by Optical Emission Spectroscopy.

Element	C	Si	Mn	P	S	Cr	Ni	Cu	Fe
Weight %	0,085	0,44	0,38	0,091	0,022	0,80	0,17	0,30	~ 97,71

Going into more details, for the environmental exposure three different kinds of surface finishes of commercial Cor-Ten (Fig. 26) were considered:

- ✓ Bare Cor-Ten (BA)
- ✓ Pre-patinated Cor-Ten (PA)
- ✓ Pre-patinated and waxed Cor-Ten (PWA)

The pre-patination procedure of materials, carried out by the supplier, consists in a controlled and accelerated oxidation treatment and a subsequent passivation, generally performed using aqueous solution containing HCl (about 10% by volume), evenly spread over the alloy surface.

After that, a beeswax coating may be applied on the pre-patinated surface to obtain a new finish characterized by a darker tonality.

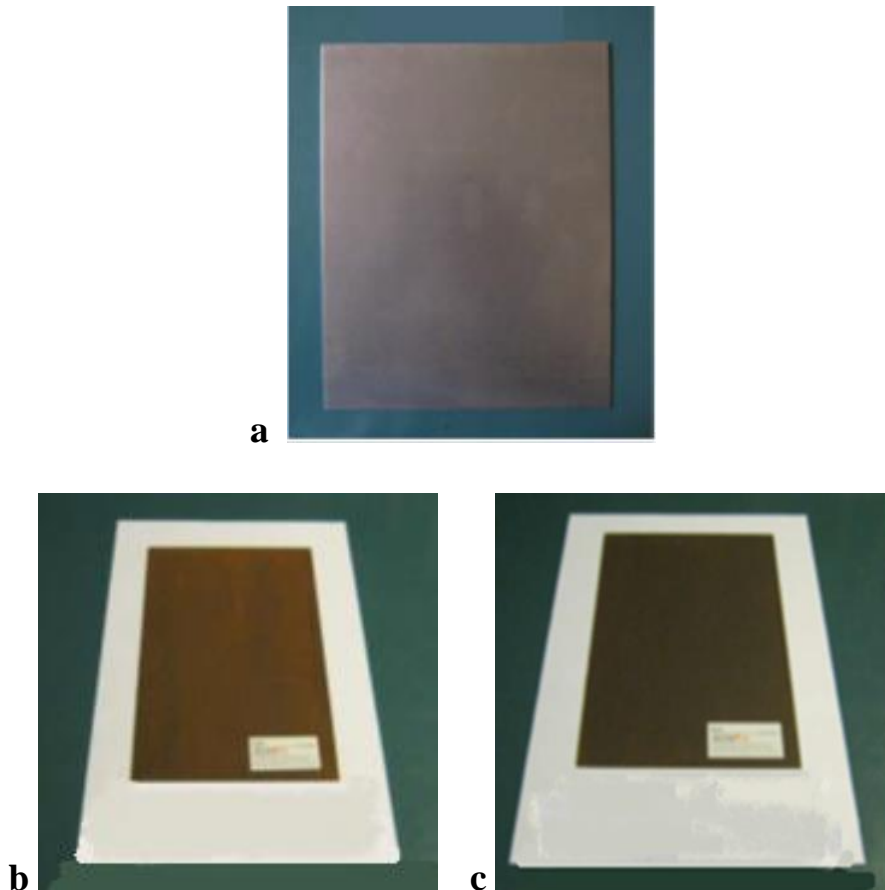


Fig. 26: Commercial sample of a) bare, b) pre-patinated and c) pre-patinated/waxed CorTen A

Before the environmental exposure, both pre-patinated and waxed specimens were not subjected to any other preparation procedure; on the other hand, bare samples were degreased with acetone, washed with water and dried.

For accelerated ageing tests, instead, only bare material was considered.

The WS sheet (thickness = 2 mm) provided were cut to give 5 x 5 cm specimens.

The microstructure of WS was observed through a Nikon EPIP- HOT 300 polarized light microscope both in the longitudinal and transversal sections.

To do this, two Cor-Ten samples with approximate area of 1x1 cm² were obtained by means of a Buehler IsoMet[®] Low Speed Saw equipped with a diamond cut-off wheel (Mod. 13 Struers); the cut samples were incorporated into epoxy resin and, after 24h-drying, polished on SiC abrasive papers (240, 600, 1200, 2000 grit) and lapping pastes (3 μm and 1 μm) to obtain a mirrored surface. Immediately before the microscopic observation, samples are immersed into a 2% Nital solution (HHNO₃ 2% – EtOH 98%) for 30-40 seconds. This chemical etching allows to highlight the crystal structure (ferritic grain) of the material as a result of a selective corrosion of surface areas with greater energy, such as grain edges. Results are shown in section 6.

5.3 Environmental Exposure

5.3.1 Exposure site and conditions

According to what said in section 2.4, the features of the environment of exposure strongly affect the performances of WS. So, aiming at evaluating the behavior of the material in a stressful condition, the urban-coastal site of Rimini (Italy) was chosen (Fig. 27).



Fig. 27: Site of exposure (Rimini, Italy) [101]

According to ISO 8565:2011 [102] and ISO 9226:2012 [103], Cor-Ten A specimens were mounted on Teflon holders and exposed facing south, with an inclination of 45° from the horizontal. The

test site was located on the roof of a building, closed to the city center, at about 1.5 km from the Adriatic Sea coastal line.

In addition to the study of the influence of different surface finishes on the corrosion behavior, evaluations on the effect of the exposure geometry were also carried out by exposing the specimens in both sheltered (Fig. 28) and unsheltered (Fig. 29) conditions.

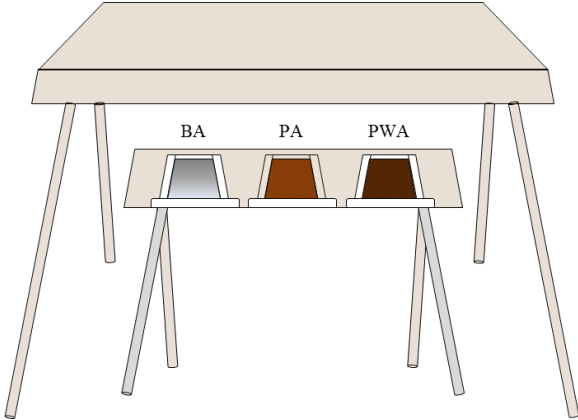


Fig. 28: Scheme of Bare (BA), Pre-patinated (PA) and Pre-patinated/Waxed (PWA) Cor-Ten A specimens exposed in sheltered conditions

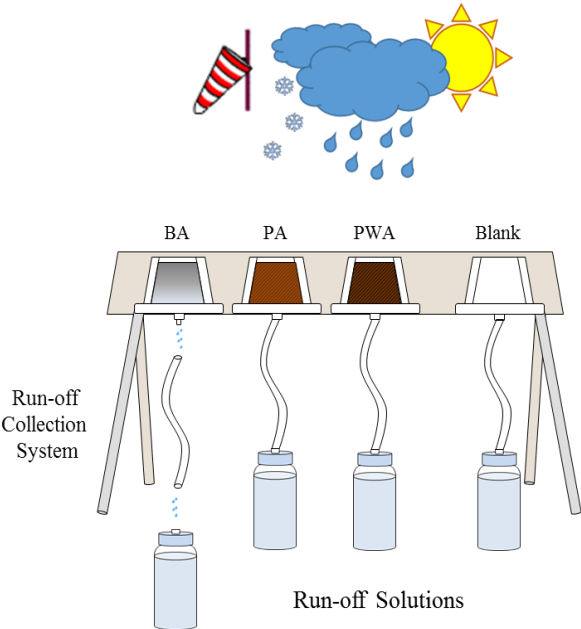


Fig. 29: Scheme of Bare (BA), Pre-patinated (PA) and Pre-patinated/Waxed (PWA) Cor-Ten A specimens exposed in unsheltered conditions

The exposure started during the spring of 2011 and lasted for four years, during which the environmental impact of the material with regards to the corrosion-induced metal release was evaluated.

The environmental parameters describing the exposure environment (section 6.2.1), including temperature, relative humidity, wind direction and speed and main pollutants (NO, NO₂, O₃, PM₁₀, PM_{2.5}) concentration, were recorded at a monitoring station placed at about 1 km from the test site and provided by the Regional Agency for Environmental Protection (ARPA) of Emilia Romagna. SO₂ is no longer monitored in Rimini since 2008 because, in previous years, it always showed concentrations well below the Italian law limits; specifically, from 2004 to 2007, the SO₂ annual average was equal to 2 µg/m³ (typical of rural environments, according to ISO 9223:2012) [104].

5.3.2 Experimental procedure

Three samples of commercial Cor-Ten A for each surface finish (see section 5.2.1) were exposed, both in sheltered and unsheltered conditions.

Before the exposure, bare sample were polished with acetone and distilled water; pre-treated sample, instead, were exposed as supplied (see section 5.2.1). All the specimens were labeled, protected on their back side with transparent acrylic varnish and weighed on analytical balance (sensitivity of 0.1 mg).

According to ISO 17752:2012 [105], runoff waters from unsheltered specimens were periodically (about once a month) sampled in HDPE vessels and transferred to the laboratory, where the total volume of each collected solution was measured. Then, a representative aliquot of each solution was filtered (cellulose acetate membrane, 0.45 µm pore-size) and analyzed by Ion Chromatography (IC) for ion determination; the remaining solution was subjected to pH determination, filtration,

acidification with HNO₃ until pH < 2, to dissolve potential metal complexes from the container walls, and analysis in Atomic Absorption Spectroscopy (AAS) for the determination of alloying metals released. Specifically, the filtration procedure on 0.45 µm membrane filters allows to separate metals released in the dissolved form from those released in the particulate fraction and, in the case of environmental exposure, only the dissolved fraction has been considered.

In order to evaluate background concentrations at the test site, rainwater impinging only Teflon holders was collected in triplicate. Blank solutions underwent to the same procedure described above.

During each sampling, all the exposed specimens were removed and, after stabilization at room temperature, weighed to determine mass variations.

Before and periodically after the exposure, one of the three specimen for each finish and condition was subjected to surface investigations (see section 5.5.3, section 5.5.4, section 5.5.5).

5.4 Artificial Ageing Test

Artificial ageing tests represent a group of laboratory tests aimed at reproducing the effect of one or more factors on the degradation process of a material under controlled condition. They were developed to support natural ageing tests (i.e. environmental exposure) and overcome their non-practical long exposure requirements, in order to obtain information about the performances of materials in shorter time.

5.4.1 Immersion/emersion Test (Cebelcor)

Immersion/emersion test is a typical laboratory test usually performed to speed up the normal aging process of metallic materials and to study their corrosion behaviour. By alternating cycle of wet and dry periods, this test simulates the exposure of the selected material to stagnant conditions, that is to say when it is not directly subjected to the action of pouring rain. In this way it is possible to create and constantly analyse during the test artificial corrosion patinas under controlled laboratory conditions (i.e. temperature, time of wetness, composition of weathering solution, etc.).

In this work, a particular kind of alternating emersion test, the CEBELCOR technique, developed in 1960s at the Belgian Center for Corrosion Study, was used.

The automatic equipment used for this test was designed by the CAPA group of Madrid, where I spent a 4-month period under the supervision of Prof. Manuel Morcillo Linares, and consists of a metal bar where the samples to be aged are fixed through a threaded rod of stainless steel, protected by a polypropylene tube (Fig. 30); this arrangement allows to follow the evolution of the open circuit corrosion potential for the entire duration of the test.

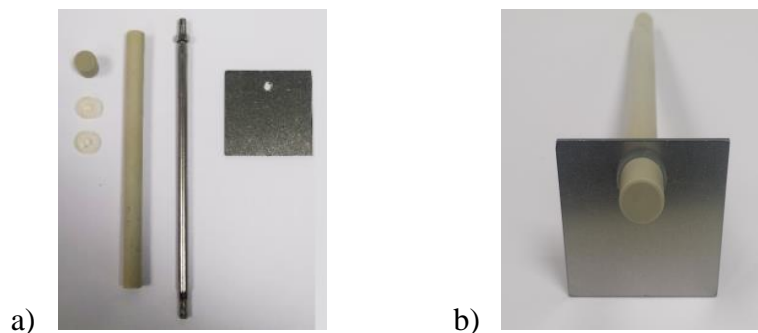


Fig. 30: Assembling of WS specimens

At pre-set times, the bar is rotated so as to alternately expose samples to the position of immersion (Fig. 31a) and to that of emersion (Fig. 31b). During the wet period, metallic specimens are submerged into a weathering solution with known composition and concentration, placed in a glass

container; during the dry period, instead, samples are exposed to 100 W infrared lamps, supplying a temperature of 50 °C on the specimen surface, thus accelerating the drying process.

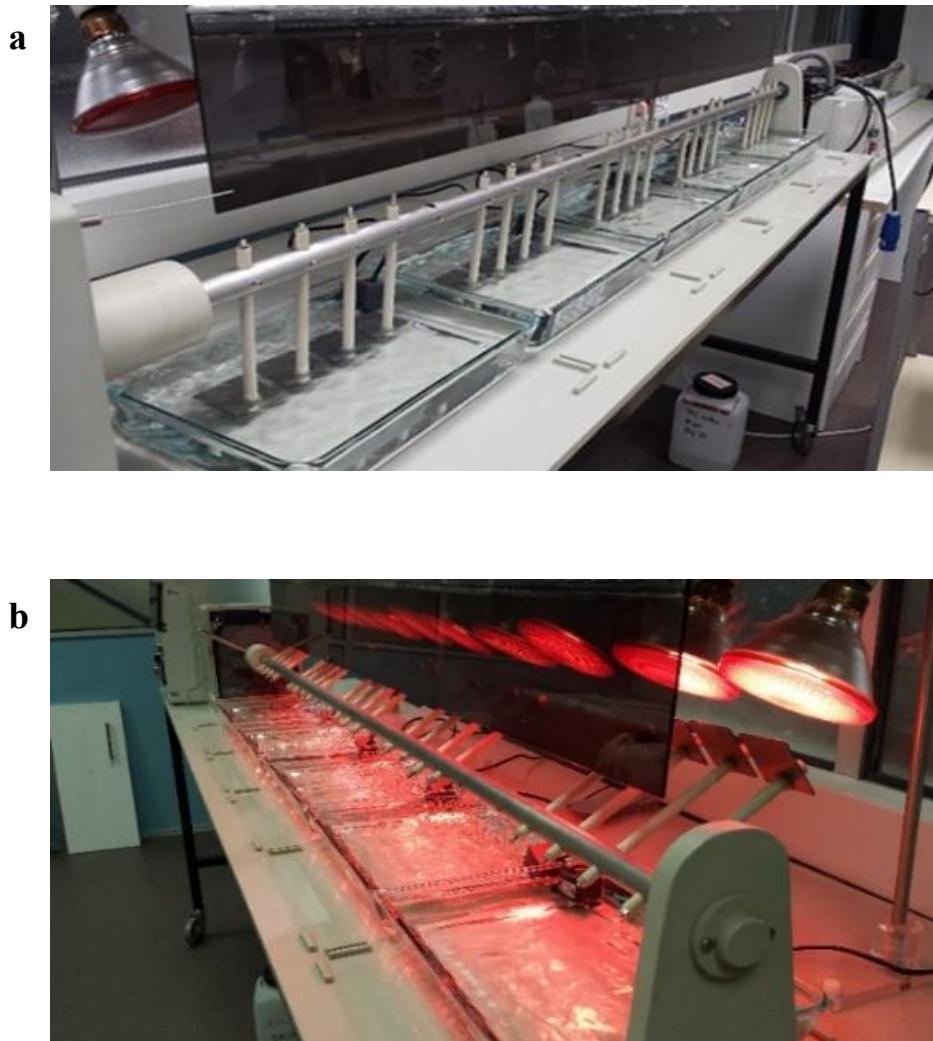


Fig. 31: CEBELCOR chamber in the wet (a) and dry (b) positions

To make sure that weathering solution was well aerated and therefore to reproduce as closely as possible what happens in the environment, water pumps with flow rate of 300 L/h were placed in each container.

In this work, the overall duration of the test was 24 days, alternating 12 minutes of immersion and 42 minutes of emersion. The weathering solutions were weekly renewed.

The Cebelcor test was performed to evaluate the effect of the main saline constituents of particulate matter (Cl^- , NO_3^- and SO_4^{2-}) on weathering steel corrosion; for this purpose, three concentrations for each PM component were selected in order to simulate the exposure to both mild and quite aggressive environments, according to mean values of these ions in bulk deposition found in literature [106]–[113]. The weathering solution chosen are listed in Table 6. After being cleaned with universal solvent and weighed (0.1 mg of sensitivity), four 5x5 cm WS samples were tested for each solution.

Table 6: Weathering solution for the Cebelcor ageing test

<i>Solution</i>	Cl^-			NO_3^-			SO_4^{2-}		
<i>Concentration (ppm)</i>	1,5	10	25	1,5	10	25	1,5	10	25

After 6, 12, 18 and 24 days of test, aliquots of each weathering solution, before and after filtration (0.45 μm) were sampled and the main elements of the alloy (Cr, Cu, Fe, Ni, Mn) were analysed (section 6.3.5.1).

Moreover, two of the four specimens for each solution were removed after 12 and 24 days: one of them was subjected to pickling (section 6.3.3), according to ISO 8407 [114], the other was employed for patina characterization (section 6.3.4).

Pickling solutions were analysed (section 6.3.5.2) for the determination of metals present as adherent rust (AR).

The evolution of open circuit corrosion potential was daily monitored (section 6.3.2).

The overall Cebelcor working plan is summarized in Fig. 32.

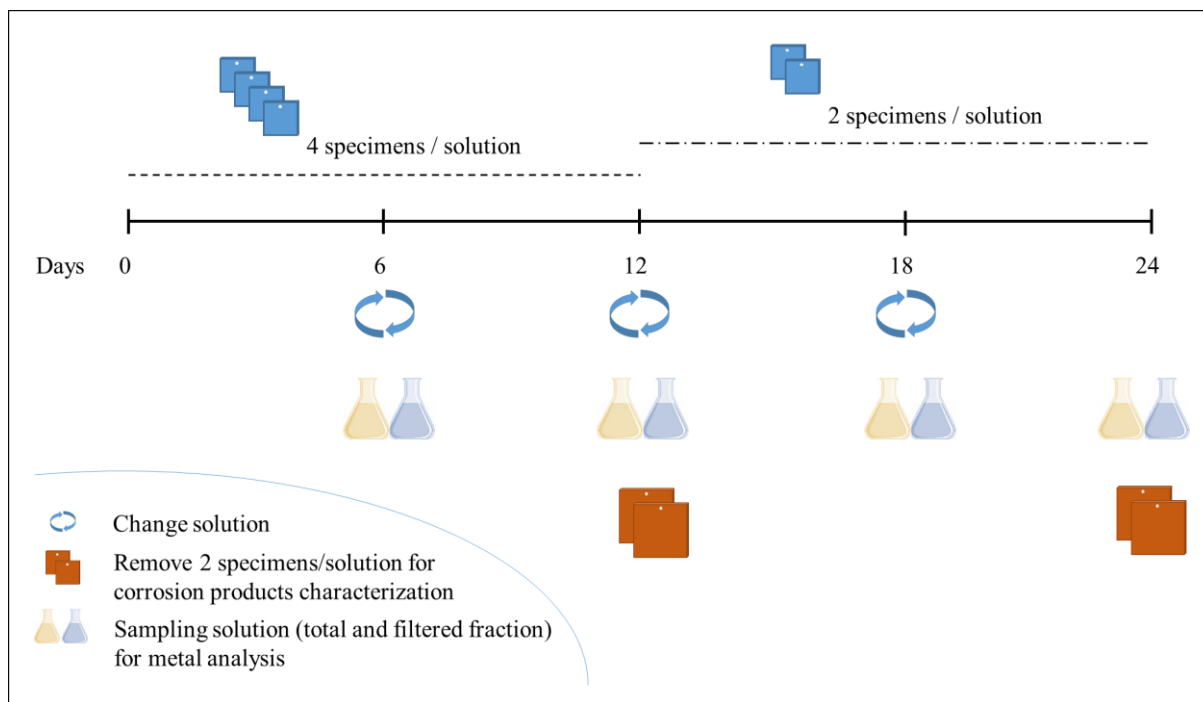


Fig. 32: Working plan for Cebelcor test

5.5 Analytical Techniques

As mentioned at the beginning of this chapter, the study of the corrosion behavior of weathering steel required the application of several analytical techniques for a complete morphological and compositional characterization of patinas and the quantification of corrosion induced metal release. So, in the following sections, the main analytical techniques used and the operative conditions applied are briefly described.

5.5.1 Atomic Absorption Spectroscopy (AAS)

5.5.1.1 General principles

Atomic Absorption Spectroscopy (AAS) is an analytical technique for the qualitative and quantitative determination of chemical elements in several matrices. The chemical-physical

principle supporting this technique is the property of atoms of absorbing light with specific wavelength, characteristic for each element.

In fact, when an appropriate energy irradiates an atom, one or more electrons in the outer shell are promoted to an orbital with higher energy, promoting its transition from the fundamental configuration to the excited state, energetically less stable.

Since atomic energy levels are quantized, atomic electron transitions are quantized too and are characteristic for each element. The absorption spectrum of each elements consists of a series of lines, called resonance lines, at specific wavelengths, each corresponding to an energetic transition; the identification of these specific wavelengths allows identifying the element. On the other hand, the amount of absorbed radiation is proportional to the number of atoms undergoing the transition, so it allows the element quantification. The experimental quantity describing the absorption process is Absorbance, defined as

$$A = \log (I_0 / I) \quad (35)$$

where I_0 and I represent the intensities of radiation before and after the interaction with vaporized sample, respectively. Absorbance is related to the concentration of analyte by means of a 'Lambert-Beer' type law

$$A = x \cdot b \cdot N \quad (36)$$

with x corresponding to the spectral absorption coefficient ($L \text{ mol}^{-1} \text{ cm}^{-1}$), b is the optical path length (cm) and N the total number of free atoms (mol L^{-1}).

5.5.1.2 Instrumentation

In order to identify and quantify an element with Atomic Absorption Spectroscopy, atomization of sample is necessary; after that, electromagnetic radiation with a specific wavelength hit the sample. The outgoing radiation is thus collimated by means of a monochromator and send to detector.

Let's deeply analyse now the operation of each part of the equipment.



Fig. 33: PinAAcle 900T Atomic Absorption Spectrometer (Perkin Elmer)

As already stated, atomic absorption spectrometer consists of five main units:

- ✓ Radiation source
- ✓ Background correction system
- ✓ Sample atomizer
- ✓ Optical devices and monochromator
- ✓ Detector

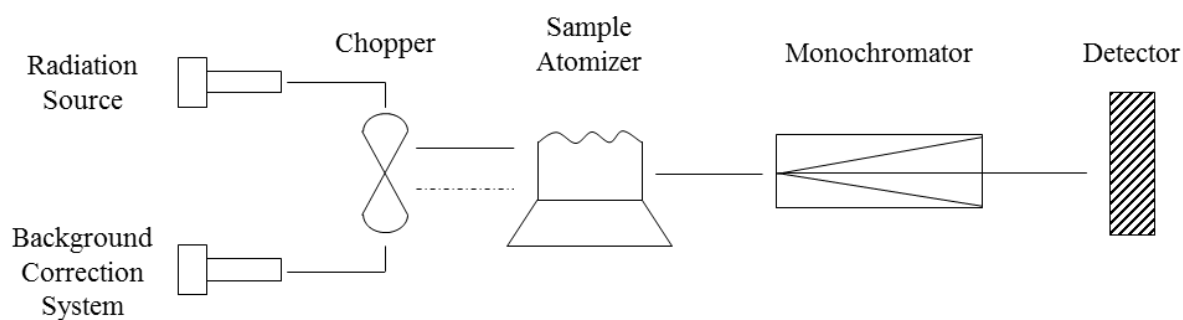


Fig. 34: Scheme of Atomic Absorption Spectrometer

Radiation source

According to what said at the beginning of this paragraph, atomic absorption studies need a radiation source that is able to emit the spectrum of the element to analyse, in order to obtain the desired spectral resolution.

Among these ‘line-sources’, Hollow Cathode Lamp and Electrodeless Discharge Lamp are the most common.

Hollow Cathode Lamp

Hollow cathode lamp consists of a glass cylinder, filled with low pressure of inert gas (commonly Ar), where a little plate of the element to be analysed is positioned (Fig. 35). By applying a difference of electric potential between anode and cathode, gas atoms are partially ionized; positive ions are accelerated by the electric field and collide with the cathode, causing the ejection of surface metal atoms (*sputtering*). These atoms, excited by additional collisions with gas molecules, tend to return to the ground state by emitting radiation with the wavelength that is characteristic of the element.

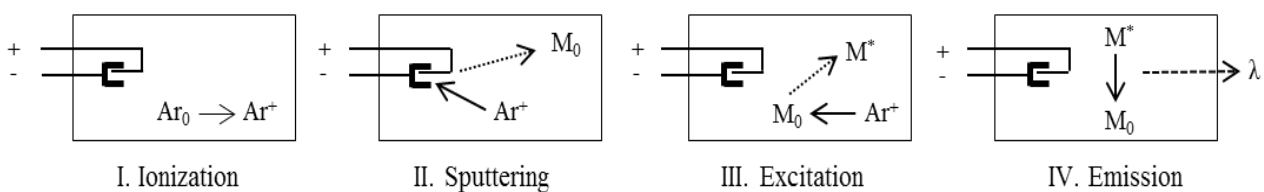


Fig. 35: Hollow Cathode Lamp emission process

Electrodeless Discharge Lamp

A suitable alternative to HCL is Electrodeless Discharge Lamp, which consists of a ceramic tube containing low pressure Ar. Inside, a quartz bulb containing the element to be analysed, surrounded by a radiofrequencies generator, is positioned. The energy due to the electric field vaporizes the element and excites atoms that emit their characteristic spectrum to return in the ground state.

Background correction system

One of the most common methods for the correction of background signal in atomic absorption contemplates the use of a continuum source of radiation, such a deuterium lamp that emits from 190 to 320 nm. A chopper, constantly spinning, sends to atomizer alternating pulses of radiation from deuterium lamp and HCL or EDL lamp. When the beam from the 'line-source' passes, the total absorbance (Analyte + Background) is measured; while, when the radiation of the continuum source passes through the vaporized sample, it provides an estimate of the background absorbance. Subtracting the background signal from the total absorption gives the corrected absorption arising only from the analyte.

An alternative to deuterium lamp background correction involves the application of the Zeeman effect, which consists in the splitting of atomic spectral lines in the presence of a magnetic field. With the magnet off, the total absorbance at the analytical λ is measured; when the magnet is on, the analyte absorption line is split into three components, the π component at the analytical λ and two σ components negatively and positively shifted around the analytical λ . Considering that these components are differently polarized with respect to the magnetic field (π polarizes parallel and σ polarize perpendicular to the magnetic field), a polarizer in the optical system can easily remove the π component of the radiation, so that only the background absorbance is measured. Finally, the

atomic absorbance can be calculated by subtracting the background absorbance measurement from the total absorbance value.

Sample atomizer

Two systems are commonly used to atomize samples, Electrothermal and Flame atomizers.

Electrothermal Atomizer

Electrothermal systems use graphite furnace for the atomization of samples; the furnace is a cylindrical graphite tube equipped with a platform and an injection hole; a known amount of the sample is deposited on this platform and subjected to a thermal program, generally consisting of four steps:

- Drying, during which the solvent evaporates
- Incineration, that allows the removal of volatile organic matter eventually present in the sample through its conversion into H₂O and CO₂
- Atomization, when temperature rapidly increases to vaporize and atomize the analytes; during this step, the reading of absorbance is performed.
- Cleaning, in order to prepare the tube for the next sample.

During the entire cycle the graphite furnace is continuously flushed with an inert gas (Argon) to prevent its early deterioration.

This technique is generally used for determination of analytes in the ng L⁻¹ - μg L⁻¹ range.

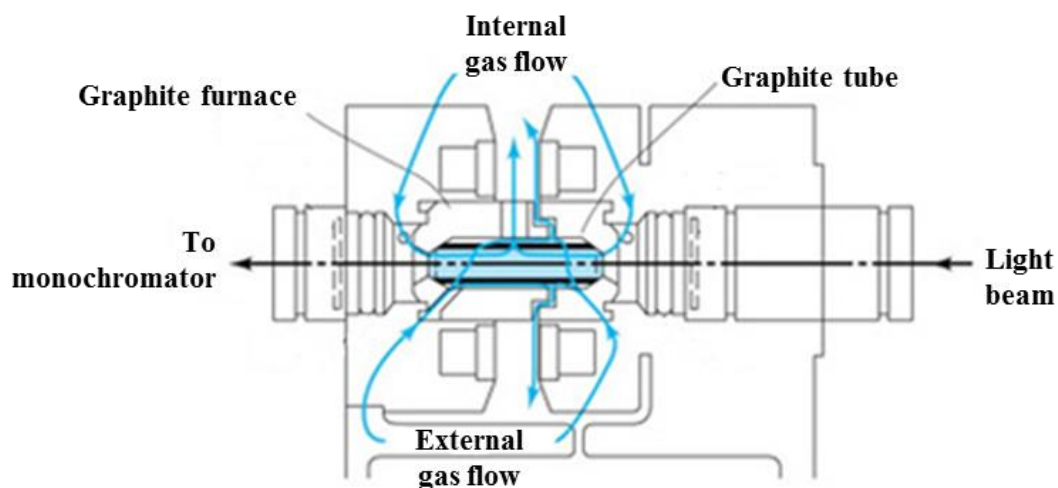


Fig. 36: Scheme of an electrothermal atomizer [115]

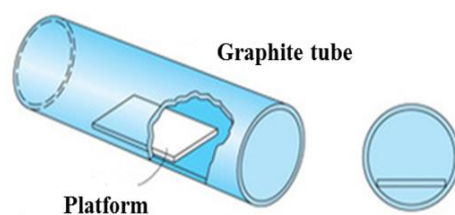


Fig. 37: Representation of graphite tube with platform [115]

Flame Atomizer

In flame atomization, the sample is aspirated by a pneumatic nebulizer and converted in aerosol; then, the smallest droplets of the nebulized sample pass through a mixing chamber where a combination of fuel and oxidant gases (generally air/acetylene, flame temperature $\sim 2300\text{ }^{\circ}\text{C}$) flows. The sample is then transferred, through the burner head, to the laminar flame. In the first part of the flame (primary combustion zone), desolvation of analyte occurs; then, the molecular aerosol formed passes in the second combustion zone, the hottest one, and is vaporized and atomized.

The radiation generated by the lamp crosses the entire length of the laminar flame, passes through the atomic cloud in the second combustion area and then continues to the monochromator.

This technique is generally used for determination of analytes in the mg L^{-1} range.

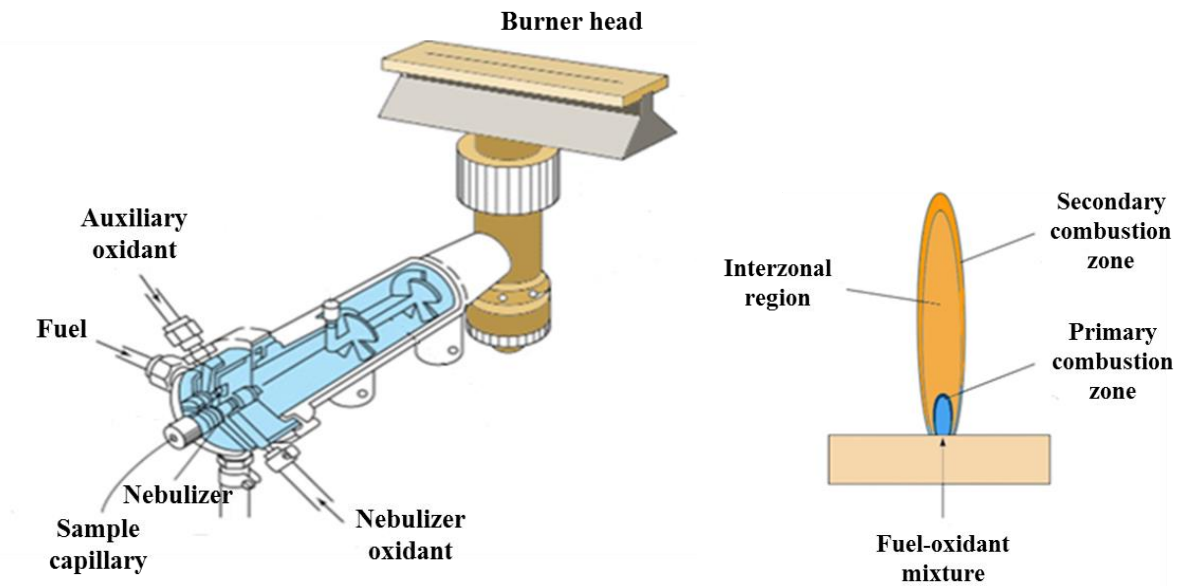


Fig. 38: Laminar flow burner head (left) and flame regions (right) [115]

Optical devices and monochromator

Once the radiation passes through the sample in the atomizer, a system of lenses guides it to a monochromator, whose function is to isolate only the spectral line of the desired analyte.

Monochromator comprises an entrance slit, a dispersion device (in AAS dispersion grating are commonly used) and an exit slit.

Detector

The radiation selected by the monochromator is directed to a detector. In AAS, photomultiplier (PM) tube is the most common detector used, mainly due to its high sensitivity; PM converts light

signal into an electrical signal and then, thanks to a series of dynodes, amplifies it to a useful level by emission of secondary electrons (photoelectric effect).

All secondary electrons emitted by the last dynode, which are proportional to the initial light signal, are collected on the anode, so that the electric signal can be converted to a voltage and measured.

5.5.1.3 Operating conditions

A Perkin Elmer AAnalyst 400 and a Perkin Elmer PinnAAcle900z Atomic Absorption Spectrometers with electro-thermal atomizer were used for metal (Cu, Cr, Fe, Mn and Ni) determination.

The instrumental condition, the graphite furnace temperature programs and the limits of quantifications for each metal are listed in the tables here below (the performances of the two instruments are comparable, so, for brevity, only information referring to AAnalyst 400 are reported in tables below). Limits of Determination (LoD) were determined as the metal concentrations corresponding to 3 times the standard deviation of 20 replicates of a blank solution.

Table 7: Operating conditions for Cr.

Analyte	Step	Temp °C	Ramp time (sec)	Hold time (sec)	Internal gas flow (mL/min)	Gas Type	Wavelength (nm)	Silt (nm)	LoD (µg/L)
Cr	1	100	1	30	250	Argon	357,9	0,7	0,2
	2	130	15	40	250	Argon	357,9		
	3	800	10	10	250	Argon	357,9		
	4	2300	0	5	-	-	357,9		
	5	2450	1	3	250	Argon	357,9		

Table 8: Operating conditions for Cu.

Analyte	Step	Temp °C	Ramp time (sec)	Hold time (sec)	Internal gas flow (mL/min)	Gas Type	Wavelength (nm)	Silt (nm)	LoD (µg/L)
Cu	1	100	1	30	250	Argon	324,7	0,7	0,3
	2	130	15	40	250	Argon	324,7		
	3	600	10	20	250	Argon	324,7		
	4	2000	0	5	-	-	324,7		
	5	2450	1	3	250	Argon	324,7		

Table 9: Operating conditions for Fe.

Analyte	Step	Temp °C	Ramp time (sec)	Hold time (sec)	Internal gas flow (mL/min)	Gas Type	Wavelength (nm)	Silt (nm)	LoD (µg/L)
Fe	1	100	5	20	250	Argon	248,3	1,8	0,8
	2	140	15	15	250	Argon	248,3		
	3	1400	10	20	250	Argon	248,3		
	4	2400	0	5	-	-	248,3		
	5	2600	1	3	250	Argon	248,3		

Table 10: Operating conditions for Mn.

Analyte	Step	Temp °C	Ramp time (sec)	Hold time (sec)	Internal gas flow (mL/min)	Gas Type	Wavelength (nm)	Silt (nm)	LoD (µg/L)
Mn	1	100	1	30	250	Argon	279,5	0,2	0,2
	2	130	15	40	250	Argon	279,5		
	3	600	10	20	250	Argon	279,5		
	4	1900	0	5	-	-	279,5		
	5	2450	1	3	250	Argon	279,5		

Table 11: Operating conditions for Ni.

Analyte	Step	Temp °C	Ramp time (sec)	Hold time (sec)	Internal gas flow (mL/min)	Gas Type	Wavelength (nm)	Silt (nm)	LoD (µg/L)
Ni	1	100	1	30	250	Argon	232,0	0,2	0,6
	2	130	15	40	250	Argon	232,0		
	3	600	10	20	250	Argon	232,0		
	4	2300	0	5	-	-	232,0		
	5	2450	1	3	250	Argon	232,0		

5.5.2 Ion Chromatography (IC)

5.5.2.1 General principle and instrumentation

Ion chromatography (IC) is an analytical technique for the determination and quantification of ionic compounds, generally in aqueous phase. The leading principle on which IC is based is ion-exchange: once introduced into a column anionic or cationic species are separated and analysed according to their higher or lower affinity with a stationary phase, consisting of ion-exchange resins.

IC is further subdivided into Cation Exchange Chromatography (CEC) and Anion Exchange Chromatography (AEC), used for the determination of cations and anions, thanks to sample interactions with stationary phases displaying negatively and positively charged functional groups, respectively.

Ion-chromatography equipment (Fig. 39) consists of:

- ✓ Pump for the introduction of the mobile phase (eluent) in the column
- ✓ Sample injection system, generally a multiport valve (loop), used to introduce an exact volume of sample connected to the eluent tubing
- ✓ Guard column, to protect the separation column from contamination
- ✓ Separation column, in which the separation process occurs; as said before, positively charged stationary phases are used for anions separation and, on the contrary, negatively charged stationary phases for cations determination.
- ✓ Suppressor, a supplementary column placed after the separation column in AEC with the function of decreasing the background conductivity of the eluent and optimizing the signal-to-noise ratio.
- ✓ Detector, usually conductivity or UV/Vis detectors.

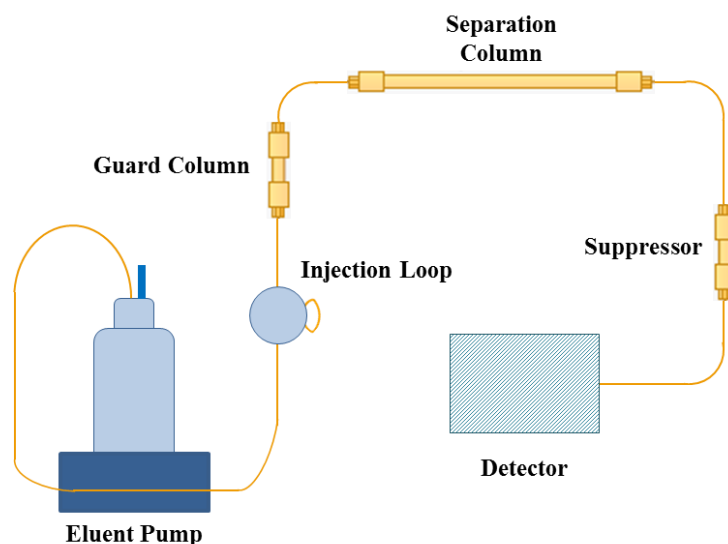


Fig. 39: Ion-chromatography equipment for anion determination; the equipment for cation quantification does not include the suppressor.

5.5.2.2 Operating Conditions

In this work a Metrohm 761 Compact IC equipped with a conductivity detector was used for the analysis of water soluble ions.

Cations (NH_4^+ , Na^+ , Ca^{2+} , Mg^{2+} , K^+) were separated on a Metrosep C2/150 column (150 x 4 mm) with an eluent phase of tartaric acid 1 mM and dipicolinic acid 4 mM, at a flow rate of 1.5 mL min^{-1} . Anions (Cl^- , NO_2^- , NO_3^- , SO_4^{2-}) were separated on a Metrosep A sup 4 column (250 x 4 mm), followed by a suppressor, with an eluent phase of Na_2CO_3 1.8 mM, NaHCO_3 1.7 mM and acetone 2%, at a flow rate of 1.5 mL min^{-1} .

Ion concentrations were determined by external standard method using stock standard solutions.

Limits of Quantification (LoQ) for the investigated ions are listed in Table 12.

Table 12: Limits of quantification (LoQ) for soluble ions.

Cations	LdQ (mg/L)	Anions	LdQ (mg/L)
Ca ²⁺	0.05	Cl ⁻	0.08
K ⁺	0.05	NO ₂ ⁻	0.01
Mg ²⁺	0.05	NO ₃ ⁻	0.1
Na ⁺	0.02	SO ₄ ²⁻	0.1
NH ₄ ⁺	0.02		

5.5.3 Scanning Electron Microscopy (SEM)

5.5.3.1 General principles

Scanning Electron Microscopy (SEM) is a powerful analytical technique for the acquisition of morphological and compositional information about a sample, thanks to the interaction between an electron beam and its surface.

By moving the electron beam throughout the surface and recording the various signals produced by electron-atom interactions, it is possible to obtain an high-resolution image of the sample and to extract several kinds of information about it.

In order to understand which kind of information we can obtain by means of SEM, it is necessary to explain the possible interaction between electrons and sample surface.

Electrons deriving from an electron gun are focused on the surface and interact with the atoms of the sample within an interaction volume, whose depth depends on the energy of the beam and the composition of the material tested.

This interaction produces both elastic and inelastic scattering. In the first case the electron beam is deflected without significant loss of energy; if it is deflected out of the sample, then the electron is called a backscattered electron (BSE). In the second case, instead, the beam transfers a certain

amount of energy to the atom it's interacting with, producing an expulsion of an electron as a secondary electron (SE).

Beside them, a multitude of other signal are generated (X-ray, Auger electron, Cathodoluminescence), but BSE and SE are the most common signal used in this technique.

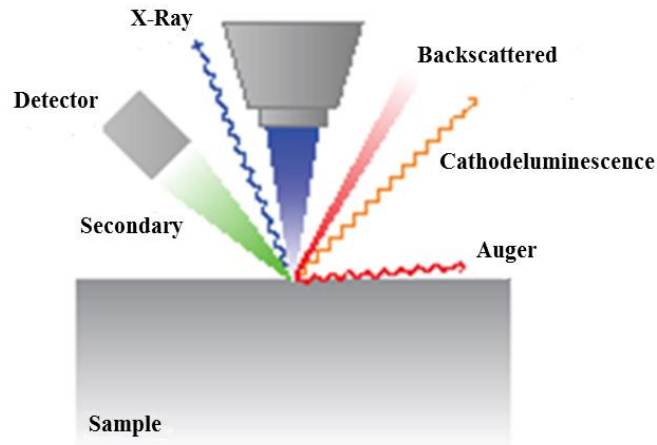


Fig. 40: Kinds of signal produced in SEM [116]

5.5.3.2 Instrumentation

A scanning electron microscope (Fig. 41) generally consists of

- ✓ Electron column
- ✓ Specimen stage
- ✓ Detectors
- ✓ Vacuum chamber

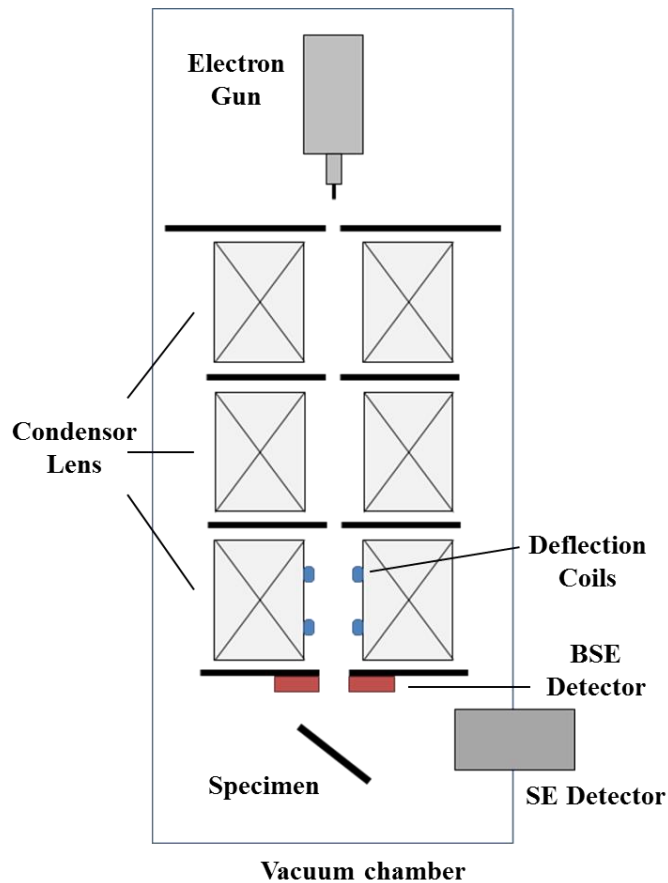


Fig. 41: Diagram of scanning electron microscope

In the following sub-sections each of these components will be briefly presented.

Electron column and specimen holder

The electron column is the part of SEM equipment where the electron beam is generated. A thermal or field-emission electron gun is positioned on the top of the column.

In thermal emission, a filament, usually tungsten or LaB₆ filament, is heated at high temperature so that electrons can escape from its surface (thermoionic emission). Setting the proper temperature is a critical point: in fact, excessively high temperature could lead to a significant decrease in the filament life; on the other hand, too low temperature may result in unstable beam current and poor image.

In field emission, instead, a strong difference of potential between the filament (cathode) and an underlying anode allows the electrons to be pulled off; in this way, the beam generated results smaller in diameter, producing a better resolution and the filament life is longer. However, the use of field emission guns entails more drastic operating conditions (i.e. higher vacuum, approximately 10^{-7} Torr).

After being generated, the divergent electron beam is adjusted and collimated by means of a series of magnetic lenses and apertures; then, in the last part of the column, it passes through pairs of deflection coils that deflect the beam in the x and y directions, allowing the scan of the desired area of the sample. The final aperture below the coils determines the spot size of the beam, affecting the resolution and the depth of field [117].

The sample is placed on a specimen mobile holder, just at the end of the electron column; if it is not conductive, a metal coating has to be applied.

Detectors

When the electron beam collides with the sample, several signals are produced. Detectors for the capture of these signals are placed just beside the electron column (see Fig. 41). As stated before, Secondary Electrons (SE) and Back Scattered Electrons (BSE) are the most useful signals in SEM, giving information about the topography and the composition of sample surface.

SE are collected by the Everhart–Thornley (ET) detector, BSE by a solid state detector. Let's briefly examine the operating principles of these detectors.

The ET detector is basically made of a scintillator and a photomultiplier; a Faraday cage surrounding the scintillator is biased with a low positively voltage to attract only secondary

electrons (energy < 50 eV). An higher voltage (10-12 kV) applied to the scintillator make the SE to be sufficiently accelerated to convert into photons; through a quartz light pipe, photons are conducted to a photomultiplier tube, that converts the amplified light signals back into electrons, finally manipulated to give an usable image.

BSE are collected by a solid state detector. Unlike in the case of the ET detector, a positive bias is not applied to attract electrons in the detector; otherwise, a Faraday cage is negatively biased so that SE are repelled and only BSE, keeping the energy of the incident beam unaltered, could reach the detector to form the backscattered image. However, as BSE are not attracted to the detector anymore, only those travelling with the right path might actually be collected; to overcome this problem and maximize the collection, BSE detector with a 'donut-type' arrangement is positioned above the sample holder, coaxial with the incident beam. When BSE passes through the detector, it converts the energy of the detected electron into a proportional electric signal.

Beside the topographic information, BSE analysis tells us something about the chemical composition of the material: in fact, the increase in the element atomic number corresponds to an increase in the number of positive charges on the nucleus and, as a consequence, of backscattered electrons. Results are visualized as a black and white image, where each shade of grey depends on the chemical composition.

Vacuum system

To ensure its smooth functioning, the SEM system has to be kept under high vacuum conditions, at least 10^{-3} Pa. The reasons for this are mainly two:

- at the high temperatures reached during the production of the electron beam ($\sim 2700 - 2800$ K), the filament would oxidize and burn out in the presence of air at atmospheric pressure;

- the presence of vacuum increases the mean free path of primary electrons and helps to minimize the probabilities of collisions between the electrons and the residual air molecules.

However, in some cases, high-vacuum mode is not the better option. In fact, for the analysis of wet or non-conducting samples, environmental SEM (ESEM) was developed; by means of some instrumental modifications, this technique allows to apply the same advantages of conventional SEM analysis to a broader range of samples (plastics, ceramic materials, corroded metals) without the need for prior preparation.

ESEM equipment, operating in variable pressure (VP) mode, consists of two areas, an electron gun under high vacuum conditions to prevent the filament deterioration or beam deflection and a specimen chamber sustaining an higher pressure environment; the two areas are connected by an intermediate cavity where a pressure gradient is present.

The phases of production and the focusing of the electron beam are remain approximately the same; what changes is the system of SE detection. The standard ET detector is replaced by the Robinson detector, which is based on the ionization of environmental gas present in the chamber.

Secondary electrons produced by the beam-specimen interaction are accelerated by a positive bias and collide with the gas molecules, producing new electrons that reach the detector and are further amplified for the creation of the scanned image.

In this study, morphological and elemental analysis of exposed surfaces and cross-sections were performed through Scanning Electron Microscopy in Extended Pressure mode (SEM, Zeiss EVO 50 EP) coupled with Dispersive Energy Spectroscopy (EDS, Oxford INCA 350).

5.5.4 Energy Dispersive X-ray Spectroscopy (EDS)

Energy dispersive X-ray spectroscopy (EDS) is an analytical technique for the determination of the elemental composition of points or areas of sample surfaces; it is based on the collection and analysis of x-ray radiation emitted by a material when it is subjected to an electron bombardment [118].

EDS system includes a x-ray detector (generally made of Si-Li crystals), a liquid nitrogen dewar for cooling and a software for collecting and analyzing energy spectra.

EDS is usually coupled with scanning electron microscopy; in this configuration, a microprobe placed in the specimen chamber of SEM equipment collects x-ray radiation produced by the interaction between the primary electron beam and the sample. X-ray photons reach the solid state detector, causes ionization and produces an electrical charge bias; this process enables to convert x-ray energy into voltage signals of proportional size. The software finally collects the signals and creates a x-ray counts vs energy bi-dimensional plot, in which each peak corresponds to an element in the sample.

5.5.5 Raman Spectroscopy

Raman spectroscopy is an analytical technique used for material identification. Being designed to study of vibrational states of molecules, it allows to obtain a real fingerprint of the examined material.

Raman spectroscopy is based on the phenomenon of inelastic diffusion of light. When radiation interacts with a molecule, absorption or diffusion can occur; among the diffused portion, the majority of radiation is elastically diffused (Rayleigh scatter), that is scattered photons keep the energy of incident beam unchanged. A small fraction of the incident radiation (approximately 1 in

10^7 photons), instead, is inelastically scattered, with diffused photons showing a higher or lower frequency (*shift*) than incident radiation. This phenomenon is known as Raman effect.

Particularly, the decrease in frequencies is called Stokes shift and occurs when a molecule in its fundamental state is excited to an upper virtual level and then emits a photon at lower energy (Fig. 42). The increase in frequencies is known as Anti-Stokes shift and occurs when molecules in excited vibrational states are further excited to a virtual level and then decay to the fundamental state, with the emission of higher-energy photons.

As molecules are almost completely in the ground state at room temperature, there is much lower probability that an incident photon will be Anti-Stokes scattered; for this reason, Raman measurements are performed considering only the Stokes shifted radiation.

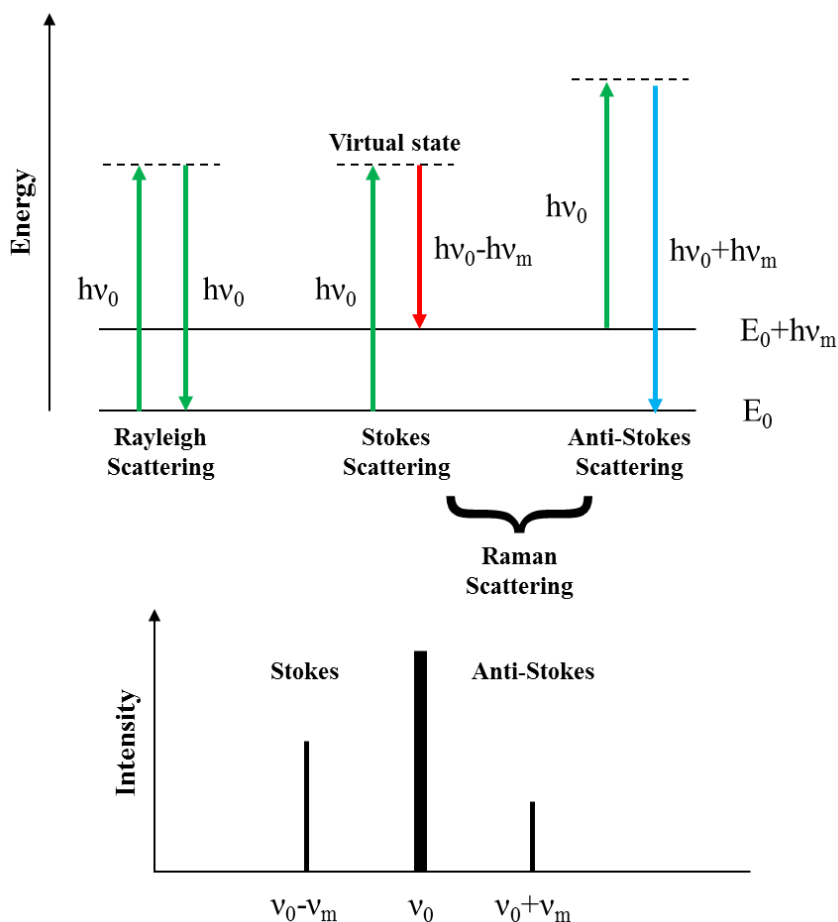


Fig. 42: Scheme of radiation scattering and Raman spectrum.

The difference in the energy of incident and inelastically diffused radiation corresponds to vibrational levels of the investigated molecule, so by analyzing the Raman shift of spectral stripes it is possible to obtain information about the molecular structure and intermolecular interaction [119].

The main components of a Raman Spectrometer (Fig. 43) are:

- ✓ Excitation source
- ✓ Sampling apparatus
- ✓ Monochromator or Interferometer
- ✓ Detector

In Raman spectroscopy, a laser is commonly used as excitation source because it provides a stable, coherent and intense beam of monochromatic radiation and ensures a useful amount of Raman scatter. The incident radiation enters in the sampling device, generally a fiber-optic probe, and passes through a narrow band-pass filter; after that, a series of lenses focalize the laser beam on the sample. After interacting with the sample, the scattered radiation passes through a notch filter to isolate the weak Raman signal from the more intense Rayleigh scatter and other background signal and, thanks to a 180° backscattering geometry, is collected along the same optical path as the incoming laser. At the end, a grating monochromator disperses the Raman scattered light over a detector, for example a CCD array, which converts the electromagnetic radiation into an electric signal. The result is given as an intensity vs wavelength shift plot.

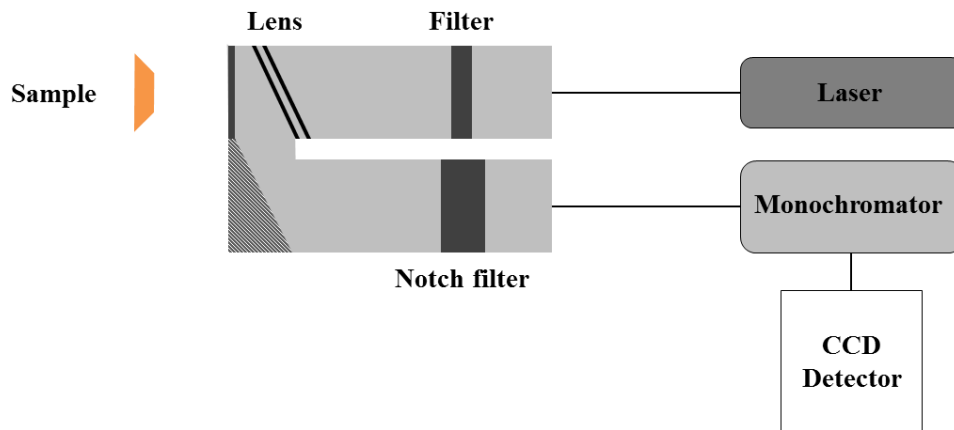


Fig. 43: Scheme of a Raman equipment

For this work, a Renishaw Raman InVia microprobe coupled with a Leica DMLM microscope and equipped with a CCD detector was used; the Raman spectrometer is configured with a rejection filter and a monochromator. The light source was a diode laser (785.0 nm) and the laser power was kept at less than 3mW at the specimen surface. From 2 to 4 accumulations were performed, with an acquisition time of 10 s.

5.5.6 X-ray Diffraction (XRD)

X-ray diffraction (XRD) is the most used technique for the identification of the structure of crystalline materials. It is based on the concept of diffraction phenomena deriving from the interaction of X-ray and crystalline sample. The basic condition for the diffraction to occur is that the wavelength λ of incident radiation and the distance between planes in the structure are comparable.

In these conditions, when an incident X-ray beam interacts with a material it is scattered by atoms in the structure; if the material presents a regular structure (crystal), the scattered X-ray undergo

to destructive (in the most directions) and constructive (in specific directions) interferences. This phenomenon is known as diffraction and is described by the Bragg's Law:

$$n \lambda = 2d \sin\theta \quad (37)$$

where θ is the angle of incidence of the radiation, λ is the beam wavelength, d is the space between crystal planes and n is any integer.

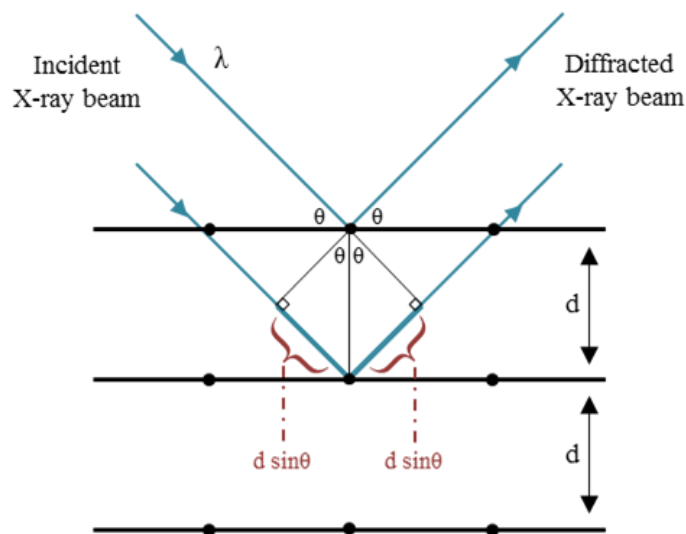


Fig. 44: Graphical representation of Bragg's Law [120]

According to eq. 37, at a specific incident angle, the diffracted X-rays will interact constructively only if the d -spacing between crystal planes is equal to an integer number of λ .

The main components of an X-ray diffractometer (Fig. 45) are:

- ✓ X-ray source
- ✓ Monochromator and filters
- ✓ Sample holder
- ✓ Detector

The most common geometry of current diffractometers is the ' θ - 2θ geometry', in which the radiation source is fixed, the moving sample holder is tilted by an angle θ and the detector by an angle of 2θ (to keep the alignment with the diffracted radiation).

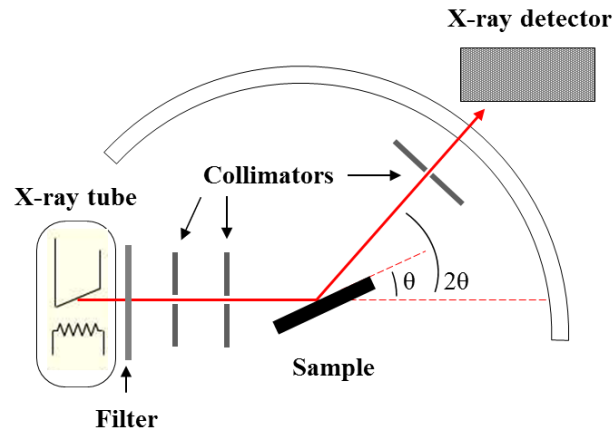


Fig. 45: Scheme of an X-ray diffractometer

X-ray source is represented by a tube containing a tungsten filament (cathode) and a metallic plate (anode). By applying a high voltage to the filament, high energy electrons are emitted, that collide with the anode, producing X-rays; the wavelength of the X-ray beam depends on the nature of the metallic plate, while the penetration in the sample (generally ranging between 10 and 30 μm) depends on the beam power and angle of incidence.

X-rays produced in the source are filtered and collimated over the sample by means of a monochromator and a series of lenses. After the interaction with the sample, the diffracted rays are directed to a detector, usually a scintillator counter or a gas-filled detector, which converts the incoming radiation in electrical signal.

The resulting diffraction spectrum conventionally appears as an intensity vs 2θ graph.

Knowing the operating λ , it is possible to easily calculate the d-spacing value for each θ angle corresponding to an intensity peak in the graph by solution of the Bragg equation.

After determining all the d-spacing values, characteristic for the material examined, a simple comparison with database values allows to definitely identify the unknown sample.

For this work, XRD analysis were carried out with a Bruker AXS diffractometer – D8 Advance, equipped with cobalt X-ray tube and diffracted beam monochromator. Data were collected over 10-80° range, with a step width of 0,03° and an accumulation time of 3 seconds.

5.5.7 Open Circuit Potential (OCP)

As stated in section 2.3, a metal submerged into a solution undergoes a series of electrochemical reactions mainly localised on the metal-solution interface, that generates corrosion. These reactions creates an electrochemical potential known as corrosion potential (E_{corr}) or open circuit potential (OCP).

Voltage measuring instruments cannot directly measure this potential, so it necessary a reference electrode with known potential (i.e. Saturated Calomel Electrode, SCE).

OCP measurements correspond to the observation of the difference of potential between the working electrode (examined metallic surface) and the reference electrode when no external current is applied to the circuit.

Measurements are performed using high impedance voltmeters.

As no external potential is imposed to the system, OCP measurements can be performed during the execution of other experiments, such as accelerated ageing tests.

By monitoring OCP variations over time, it is possible to obtain information about the corrosion process or, more specifically, the passivation grade of the corrosion product patina formed on the material.

Results will be plotted in a E vs time graph, in which higher potentials correspond to lower corrosion.

5.5.8 Mass Loss Determination

Mass loss determination of a metallic specimen allows to determine the corrosion rate after natural or simulated tests.

It is achieved by removing all the corrosion products formed on the sample during the environmental exposure or the laboratory test.

The chemical procedure for mass loss determination for iron and steel, specified by ISO Standard 8407 [114], is quickly described here below:

- ✓ The specimen is weighed on analytical balance and then submerged into a solution of HCl (50%) and hexamethylenetetramine, specifically designed to selectively remove the corrosion products, with minimal dissolution of base metal.
- ✓ The pickling solution containing the sample is kept in ultrasonic bath for 10 minutes.
- ✓ After cleaning, the specimen is rinsed with distilled water and ethanol and dried in oven.
- ✓ Finally, the sample is cooled and weighed again.
- ✓ The procedure is repeated until reaching the weigh stabilization of pickled specimen, to ensure complete removal of the corrosion products; the use of a control specimen (un corroded material), subjected to the same cleaning procedure as the test specimen, is highly recommended.

The corrosion rate r_{corr} arising from the described procedure is expressed as

$$r_{\text{corr}} (\text{g/m}^2 \cdot \text{y}) = \Delta m / A \cdot t \quad (38)$$

where A is the specimen surface (m^2), t is the exposure time (year) and Δm is the mass loss (g).

Alternatively, r_{corr} can also be expressed as the depth of penetration for time unit, according to the equation:

$$r_{\text{corr}} (\mu\text{m/y}) = \Delta m / A \cdot \rho \cdot t \quad (39)$$

where ρ is the density of the material (g/cm^3).

5.6 Data processing

The great number of data collected during the ageing tests and the 4-year field exposure requires a considerable effort for the interpretation of results. In order to facilitate this phase and to make sure that all useful information has been extrapolated from experimental data, multivariate techniques of data exploration were applied.

In the following sections, something about the theory behind the techniques applied in this work will be briefly presented.

5.6.1 Multivariate data analysis

Chemometrics is a relatively young scientific discipline, born in the second part of XX century, when chemistry, especially analytical chemistry, began to turn to statistics to solve more or less complex problems [121].

In 1974 Svante Wold (University of Umeö – Sweden) and Bruce Kowalski (University of Seattle – USA) founded the International Chemometric Society, which proposed, during the following year, the first definition of Chemometrics [122]:

‘Chemometrics is the chemical discipline that uses mathematical and statistical methods, (a) to design or select optimal measurement procedures and experiments; and (b) to provide maximum chemical information by analyzing chemical data.’

In the past few decades this branch has rapidly evolved, as confirmed by the exponential increase of scientific applications and publications [123], mainly driven by the development of new analytical instruments and the advent of high-speed computers and innovative software.

Chemometrics is addressed to the study of complex systems or phenomena, which are characterized by more descriptive variables; biological and pharmacological issues, problems related to industrial processes or environmental studies are typical examples of complex phenomena, driven by multiple factors acting on the system simultaneously.

As a consequence, investigating on these systems means to take in consideration/taking in consideration several information for each sample; therefore, data processing turns from univariate to multivariate level.

As expressed in the definition of the discipline, the interest in extracting the maximum relevant information from a set of experimental data is one of the main goal of chemometric analysis.

By means of the construction of qualitative and quantitative models, this technique allows to highlight possible relationships between the variables that govern a multivariate system and to identify their relevance in solving a specific problem: in this way, it is possible to isolate useful information, minimizing time and costs of analysis.

The tools that will be employed in this work belong to data exploration technique and are briefly described in the following paragraphs.

5.6.1.1 Principal component analysis (PCA)

Principal Component Analysis (PCA) is a data exploration technique designed to evaluate the main properties of a dataset, in order to isolate the relevant information and minimize any possible interference due to instrumental noise or redundant data, thus reducing the dimensionality and the complexity of the examined problem.

PCA is based on the orthogonal transformation of the original variables into a new set of uncorrelated variables, called principal components (PC), which are linear combinations of the observed descriptors. The new variables are defined in such a way that the first component is oriented in the direction of maximum variance, and that the subsequent are oriented in the direction of variance gradually decreasing, so that the information carried by the latest components will be very low and may be excluded.[121]

The procedure for Principal Component calculation is summarized here below [124].

Let's consider a matrix X ($n \times p$) containing the experimental data, in which the n rows correspond to the samples (objects) and the p columns represent the measured variables (descriptors).

The first step consists in the calculation of the covariance matrix S ($p \times p$) and in its diagonalization

$$diag(S) = diag \left[\frac{X_C^T X_C}{n-1} \right] \quad (40)$$

where X_C =centered data matrix, in order to obtain a matrix A ($p \times p$), whose diagonal elements are the eigenvalues λ_m , and a Loading matrix L ($p \times M$), whose column are the eigenvectors I_m of S .

By applying Single Value Decomposition (SVD) technique, it is possible to decompose the covariance matrix in A ($p \times p$) and L ($p \times M$); the determination of these matrices allows to define

a new space, whose axes are oriented in the direction of maximum and gradually decreasing variance.

The matrix \mathbf{X} of original data is translated into the new space and new coordinates of objects are defined in the Score matrix \mathbf{T} ($n \times M$), calculated as

$$\mathbf{T} (n \times M) = \mathbf{X} (n \times p) \cdot \mathbf{L} (p \times M) \quad (41)$$

Since the eigenvalues λ_m of \mathbf{S} matrix represent the explained variance related to each PC, in some cases it is useful to consider only a limited number of components ($M < p$), for example the ones associated with the highest values of variability among data, in order to simplify the problem.

PCA results can be visualized in the form of two bivariate scatter plots, the score and the loading plots, which represent the projections of the of the original objects (samples) and variables (measured quantities) in the new space of principal components, respectively.

5.6.1.2 Three-way principal component analysis (3W-PCA)

The use of PCA offers great advantages over the univariate interpretation, but it is still limited if the original dataset presents an intrinsic three-dimensional structure [125]. Several real phenomena, indeed, may exhibit relationships between more than two dimensions and, therefore, cannot be entirely modelled by ‘conventional’ multivariate techniques.

Just think of the environmental studies involving measurements of a series of pollutants in different sampling sites at several times; in these cases, it can be very useful to define particular trends of behaviour, i.e. spatial or temporal trends, to properly explain the investigated problem.

Three-dimensional dataset can be treated by means of 3W - PCA, a generalization of the ‘conventional’ Two Way - PCA, which can better explain the three-way interactions in the experimental data and allows an easy and complete interpretation of the results.

Tucker3 is one of the most common models for performing three-way PCA [126]–[128]; by generalizing the SVD technique [129], the original data matrix can be decomposed into three Loading matrices (Fig. 46), A (I x P), B (J x Q) and C (K x R), also called modes, and a core matrix G (P x Q x R), so that each element of the three-way dataset X (I x J x K) may satisfy the following relation

$$x_{ijk} = \sum_{p=1}^P \sum_{q=1}^Q \sum_{r=1}^R a_{ip} b_{jq} c_{kr} g_{pqr} + e_{ijk} \quad (42)$$

where a_{ip} , b_{jq} and c_{kr} are the elements of A, B and C, g_{pqr} represents the elements of the core array G, which contains the information about the relationship between elements of A, B and C, and e_{ijk} is the generic element of the residual matrix.

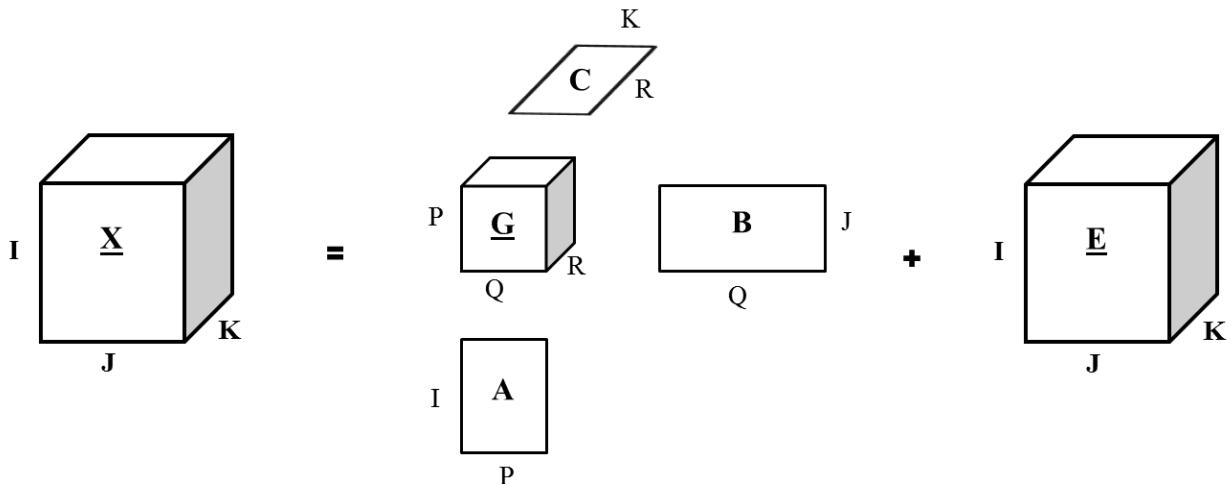


Fig. 46: Scheme of Tucker3 decomposition model

Chapter 6

Results

6.1 Microstructure of CorTen A

The microstructure of Cor-Ten A was observed through a Nikon EPIP- HOT 300 polarized light microscope both in the longitudinal and transversal sections (see section 5.2.1).

Microscopic observation results for the longitudinal and transversal sections at 1000x magnification are shown in Fig. 47 a and b, respectively.

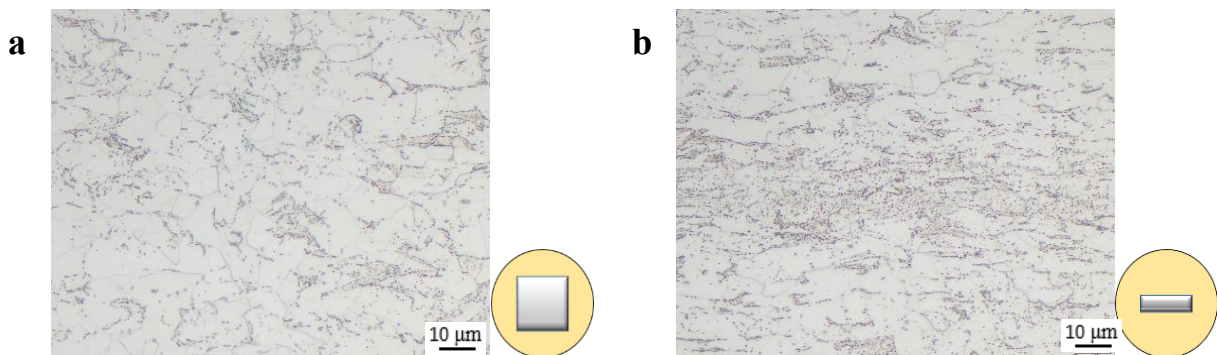


Fig. 47: Microstructure of CorTen A (1000x)

The microstructure of Cor-Ten A appears uniform in both longitudinal and transverse section.

It is characterized by ferrite (brighter areas) and pearlite in very fine particle size (light-brown areas); moreover, the presence of globular pearlite (dotted areas) suggests that the alloy was subjected to particular heat treatments during processing, probably aimed at increasing the toughness and ductility of the material. For more detailed information about ferrite and pearlite see section 3.

6.2 Environmental Exposure

The proper use of weathering steel for outdoor structural or artistic applications requires wide background knowledge of its environmental behaviour.

As seen above (sections 2.4.2, 2.4.3, 3.2.2.2) and reported in various studies [30], under particular conditions, which include the presence of high concentrations of corrosive agents or pollutants or even extreme environmental conditions, the formation of passivation patina, which is the distinctive feature of this material, may be delayed or, in some cases, completely inhibited.

In such situations, the corrosion of material does not slow down and, with the passing of time, can produce both structural damages, seriously affecting costs and safety of the structures, and environmental concerns, mainly related to the release of metals in the environment.

In this context, a 4-year environmental exposure (spring 2011 – spring 2015) of commercial Cor-Ten A was set up and performed. Throughout the test period, development of corrosion products and metal dissolution were constantly monitored. Sections 5.2 and 5.3 offer a complete description of the tested materials, exposure conditions and experimental procedures. Results are presented in this chapter.

6.2.1 Characterization of the exposure site

Bare and pre-treated samples (section 5.2.1) of Cor-Ten A were exposed in the urban coastal site of Rimini, that presents a potentially critical environment for WS, due to the simultaneous presence of chlorides and sulphates from sea spray (Adriatic coastal line is about 1,5 km far from the test site, see Fig. 27) and typical urban pollutants (SO_x , CO, NO_x , Particulate Matter).

The city of Rimini is characterized by high values of relative humidity, with mean values being around 70 % during the test period, and high variability of mean temperature over the year (from about -5°C up to 40 °C).

Moderate amount of annual rainfall with a mean value over the last five years of 750 mm year⁻¹ have been registered. Considering the rainfall trend (Fig. 48) during the test period, the first year of exposure was the driest one, while the last two years were characterized by higher amounts of rain (about twice the rainfall occurred in the first year). The second and third years also presented high variability among different sampling periods and seasons, with winter rainfalls being more prominent than summer ones. On the contrary, the first and the last years of exposure were characterized by rainy summer periods and lower seasonal change in precipitation trend.

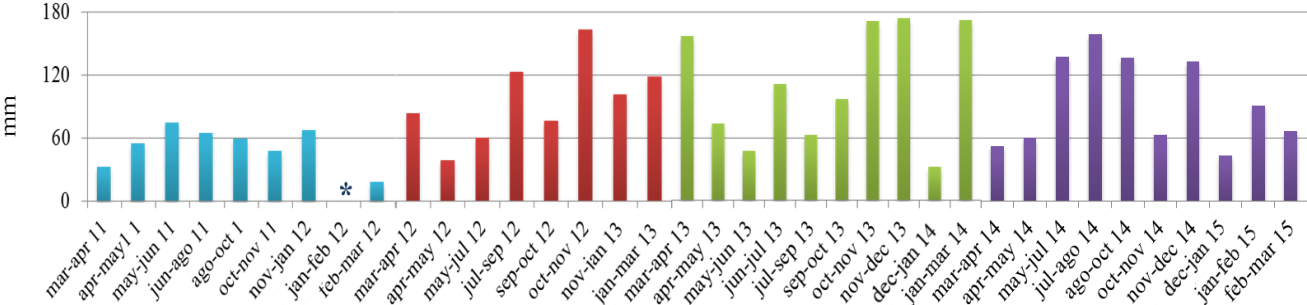


Fig. 48: Rainfall trend during the test period; different colors stand for different year of exposure.

‘*’: in jan-feb 2012 monitoring station was out of order due to heavy snowfalls.

Moving from the first to the last year of exposure, rainfalls have become more frequent and strong: in fact, with the passing of time, the occurrence of heavy precipitations with a mean hourly intensity > 10 mm/h, commonly classified as rainstorms, has been increasing and the mean intensity of these events has passed from 14.5 mm/h of the first year to 22.6 mm/h of the last year of exposure. Such information are reported in Table 13:.

Table 13: Total and seasonal amount of rain during the years of exposure; total and rainstorm events and mean rainfall intensity.

	Annual rainfall (mm)	Summer rainfall (mm)	Winter rainfall (mm)	Total rainfall events	Rainstorm (>10 mm/h) events	Mean rainfall intensity (mm/h)
1° year	422.6	254.8	167.8	104	3	14.47
2° year	765.8	298.2	467.6	189	4	16.74
3° year	1102.6	393.4	709.20	215	5	19.58
4° year	945.20	495.00	450.20	209	7	22.60

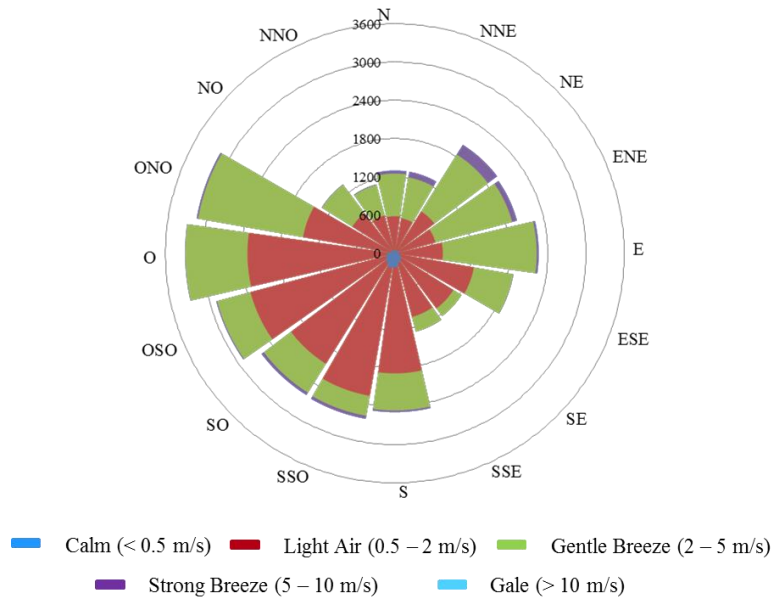
In winter 2012, Rimini was affected by heavy snowfalls (up to 75 cm on the ground [130]) and the specimens remained long time covered with snow. Beside this, another notable meteorological event should be reported, that is flood occurred on February 2015 [131].

During the exposure period, Time of Wetness (TOW) of the specimens (calculated as the length of time during which $RH > 80\%$ and $T > 0\text{ }^{\circ}\text{C}$ [17]) ranged from 1845 to 3204 hours/year, corresponding to 20–36 % of the annual hours of exposure.

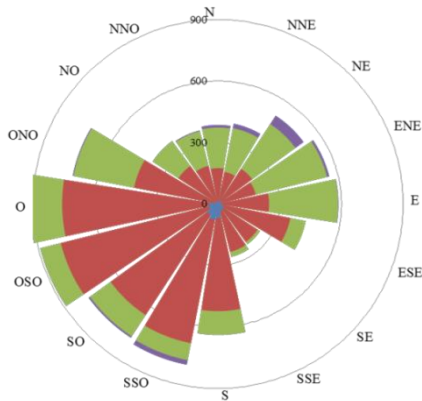
Another important factor to take in consideration is connected to wind direction and intensity: in fact, in addition to mechanical action on material, winds represent the main vector in transporting aggressive substances, i.e. sea spray ions or traffic pollutants, from their sources to the site of exposure. Winds acting on the site were mainly from E - NE and W - SW: the ones from W - SW (land breeze) showed higher frequency, while winds from E - NE (sea breeze) showed greater intensity (a maximum of 96 Km/h was observed in November 2013 [132]).

In Fig. 49 wind roses for each year of exposure and total wind rose are shown.

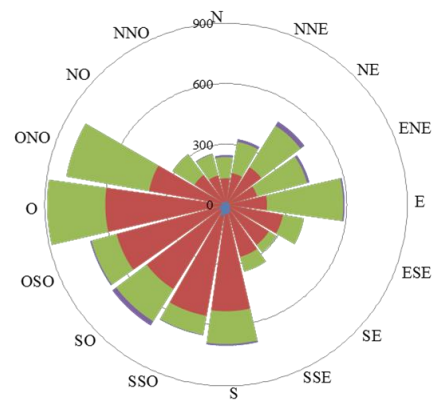
Total period of exposure (09/03/2011 – 13/03/2015)



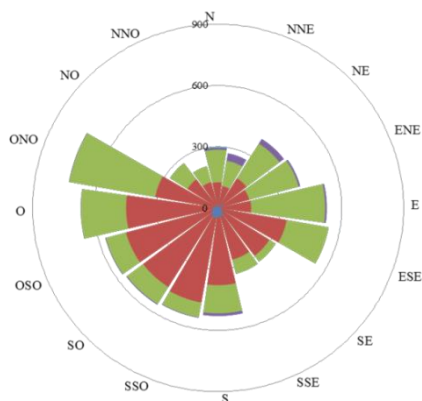
I year (09/03/2011 – 23/03/2012)



II year (23/03/2012 – 05/03/2013)



III year (05/03/2013 – 07/03/2014)



IV year (07/03/2014 – 13/03/2015)

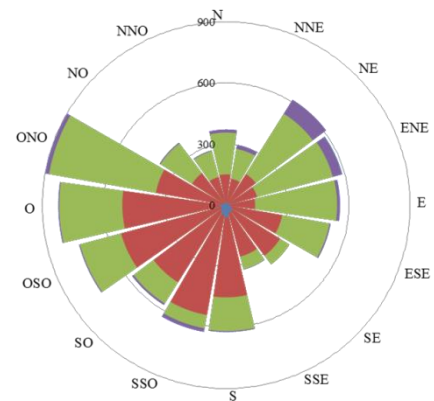


Fig. 49: Intensities and directions of winds acting on the test site during the total period of exposure (on the top) and each year of test. From the inside out, growing wind velocities are plotted.

Monthly average concentrations of O₃, NO₂, PM 2.5 and PM 10 varied, respectively, in the following ranges: 5-94 µg/m³, 13-38 µg/m³, 9-45 µg/m³ and 10-57 µg/m³. Trends of NO₂ and O₃ and particulate matter during the entire period of exposure are presented in Fig. 50 and Fig. 51, respectively.

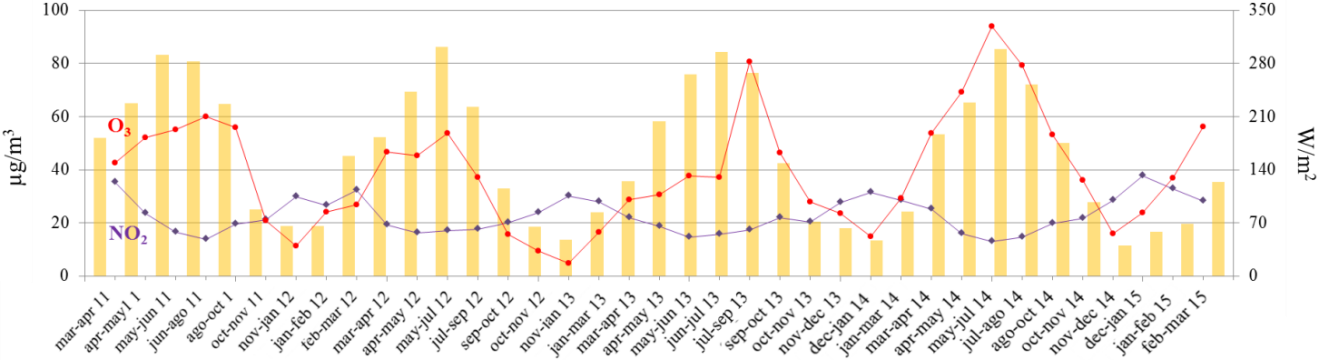


Fig. 50: Monthly average values of NO₂ (violet), O₃ (red) and visible radiation (histogram) during the period of exposure

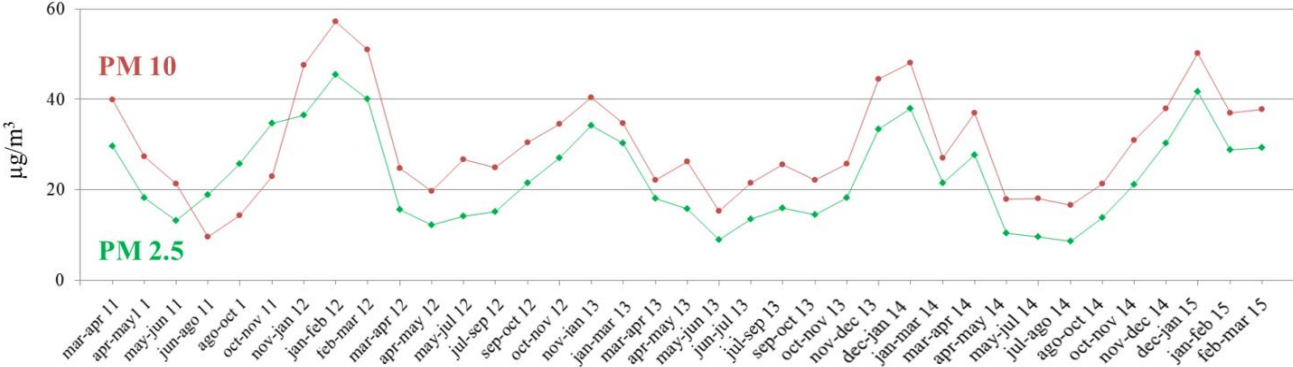
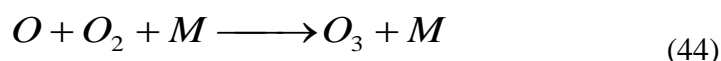


Fig. 51: Monthly average values of PM 2.5 (green) and PM 10 (dark red) during the period of exposure

The intensity of solar radiation follows the normal seasonal pattern, with higher values during summer periods and lower values during winter. In the same way, NO₂ and O₃ concentrations, show seasonal but opposite trends, with ozone increasing during summer, when solar radiation is

higher, and nitrogen dioxide simultaneously decreasing; in fact, solar radiation promotes the reactions of ozone production, among which NO₂ photolysis according to:



where M is any non-reactive species that can take up the energy released in reaction (44) to stabilize O₃.

Seasonal factors also affect the atmospheric amount of particulate matter that, transporting hygroscopic saline particle or acidic compounds, may produce negative effect or accelerate corrosion: both PM_{2.5} and PM₁₀ are generally higher during winter and lower during summer; this is explained by variations in height of the atmospheric boundary level, that is smaller during colder periods and larger during spring-summer periods, providing less or more space for pollutants to disperse and, thus, affecting their concentrations.

Relative humidity (RH), temperature (T), prevalent wind directions, Cl⁻ and SO₄⁼ deposition rate, NO₂, O₃ and PM atmospheric concentrations recorded during each sampling period at the test site are reported in Table 14.

Table 14: Characterization of the exposure site: Relative Humidity (RH), Temperature (T), prevalent wind directions, chloride and sulphate deposition rate, NO₂, O₃ and PM atmospheric concentrations during each sampling period (progressive numbers of sampling periods are reported in bolt).

	Exposure and sampling period	RH % ^a min ÷ max (mean)	T (°C) ^a min ÷ max (mean)	Prevalent Wind Direction	Cl ⁻ deposition ^b (mg/m ² ·d)	SO ₄ ²⁻ deposition ^b (mg/m ² ·d)	NO ₂ mean concentration (µg/m ³)	O ₃ mean concentration (µg/m ³)	PM 2.5 mean concentration (µg/m ³)	PM 10 mean concentration (µg/m ³)
1 st year	Mar-Apr 2011 (1)	26 ÷ 81 (66)	-2 ÷ 22 (11)	E – NE	7.62	4.29	35	43	30	40
	Apr-May 2011 (2)	15 ÷ 83 (64)	7 ÷ 31 (15)	E – NE	22.17	9.05	24	52	18	27
	May-Jun 2011 (3)	21 ÷ 79 (61)	8 ÷ 31 (21)	E – NE	13.71	3.42	17	55	13	21
	Jun-Aug 2011 (4)	15 ÷ 78 (58)	14 ÷ 37 (24)	E – NE	5.27	1.86	14	60	19	10
	Aug-Oct 2011 (5)	10 ÷ 76 (59)	10 ÷ 34 (24)	SW – S	9.29	1.13	19	56	26	14
	Oct-Nov 2011 (6)	30 ÷ 85 (73)	7 ÷ 23 (14)	W – SW	14.62	4.43	21	21	35	23
	Nov-Jan 2012 (7)	22 ÷ 89 (75)	0 ÷ 21 (8)	W – SW	10.49	3.54	30	11	37	48
	Jan-Feb 2012 (8)	25 ÷ 90 (79)	-6 ÷ 12 (2)	W – SW	145.42	33.93	27	24	45	57
2 nd year	Feb-Mar 2012 (9)	28 ÷ 81 (67)	-5 ÷ 20 (8)	S – SE	5.84	3.96	32	27	40	51
	Mar-Apr 2012 (10)	12 ÷ 82 (63)	3 ÷ 26 (13)	SW – S	16.91	7.02	19	47	16	25
	Apr-May 2012 (11)	18 ÷ 83 (63)	7 ÷ 28 (17)	E – NE	20.35	4.92	16	45	12	20
	May-Jul 2012 (12)	10 ÷ 73 (53)	14 ÷ 38 (25)	E – NE	10.66	2.09	17	54	14	27
	Jul-Sep 2012 (13)	18 ÷ 77 (60)	11 ÷ 36 (24)	SW – S	20.57	6.08	18	37	15	25
	Sep-Oct 2012 (14)	31 ÷ 89 (76)	6 ÷ 28 (18)	SW – S	7.80	2.50	20	16	21	30
	Oct-Nov 2012 (15)	29 ÷ 91 (77)	4 ÷ 24 (12)	W – SW	9.45	4.41	24	9	27	34
3 rd year	Nov-Jan 2013 (16)	23 ÷ 98 (85)	-2 ÷ 14 (5)	W – SW	8.67	3.20	30	5	34	40
	Jan-Mar 2013 (17)	24 ÷ 92 (78)	0 ÷ 15 (5)	W – SW	11.73	3.70	28	17	30	35
	Mar-Apr 2013 (18)	23 ÷ 92 (79)	2 ÷ 17 (9)	E – NE	10.57	3.96	22	29	18	22
	Apr-May 2013 (19)	32 ÷ 88 (75)	8 ÷ 23 (16)	E – NE	1.63	2.55	19	31	16	26
	May-Jun 2013 (20)	25 ÷ 80 (61)	9 ÷ 29 (19)	E – NE	3.30	1.84	15	38	9	15
	Jun-Jul 2013 (21)	27 ÷ 74 (58)	14 ÷ 33 (24)	E – NE	5.50	2.69	16	37	13	21
	Jul-Sep 2013 (22)	12 ÷ 72 (57)	16 ÷ 38 (25)	SW – S	11.04	3.75	17	81	16	26
	Sep-Oct 2013 (23)	26 ÷ 87 (73)	10 ÷ 31 (18)	W – SW	12.02	4.66	22	46	14	22
	Oct-Nov 2013 (24)	36 ÷ 94 (81)	9 ÷ 26 (16)	W – SW	129.93	26.32	20	28	18	26
	Nov-Dec 2013 (25)	29 ÷ 86 (74)	1 ÷ 15 (7)	W – SW	19.03	7.12	28	24	33	44
Dec-Jan 2014 (26)	47 ÷ 94 (84)	0 ÷ 17 (8)	S – SE	6.24	4.37	31	15	38	48	
Jan-Mar 2014 (27)	32 ÷ 95 (80)	0 ÷ 19 (9)	W – SW	-	4.29	28	29	21	27	

4 th year	Mar-Apr 2014 (28)	29 ÷ 86 (71)	5 ÷ 23 (13)	E – NE	16.89	9.28	25	54	28	37
	Apr-May 2014 (29)	19 ÷ 84 (66)	8 ÷ 25 (16)	E – NE	10.59	3.37	16	69	10	18
	May-Jul 2014 (30)	26 ÷ 78 (59)	12 ÷ 31 (22)	E – NE	11.27	4.27	13	94	10	18
	Jul-Ago 2014 (31)	28 ÷ 83 (65)	16 ÷ 33 (23)	W – SW	6.26	4.52	15	79	9	17
	Ago-Oct 2014 (32)	28 ÷ 92 (77)	11 ÷ 26 (19)	W – SW	27.32	7.15	20	53	14	21
	Oct-Nov 2014 (33)	24 ÷ 89 (75)	8 ÷ 28 (17)	W – SW	4.38	2.46	22	36	21	31
	Nov-Dec 2014 (34)	42 ÷ 71 (86)	5 ÷ 19 (11)	W – SW	13.90	9.42	28	16	30	38
	Dec-Jan 2015 (35)	22 ÷ 72 (75)	-1 ÷ 18 (6)	W – SW	22.34	5.85	38	24	42	50
	Jan-Feb 2015 (36)	34 ÷ 88 (74)	1 ÷ 18 (7)	W – SW	128.72	26.18	33	37	29	37
	Feb-Mar 2015 (37)	38 ÷ 52 (76)	1 ÷ 17 (8)	W – SW	-	-	28	56	29	38

6.2.2 Characterization of corrosion products

6.2.2.1 Mass variation

A general information about patina growth on each specimen and influence of exposure geometry (sheltered and unsheltered) can be provided by mass variation (MV) values.

In both exposure conditions, all specimens undergo a progressive mass increase (Fig. 52 and Fig. 53), lower, as expected, for the pre-patinated ones, where an artificial patina was already present before the exposure. The addition of a wax covering on pre-patinated WS does not seem to significantly influence MV.

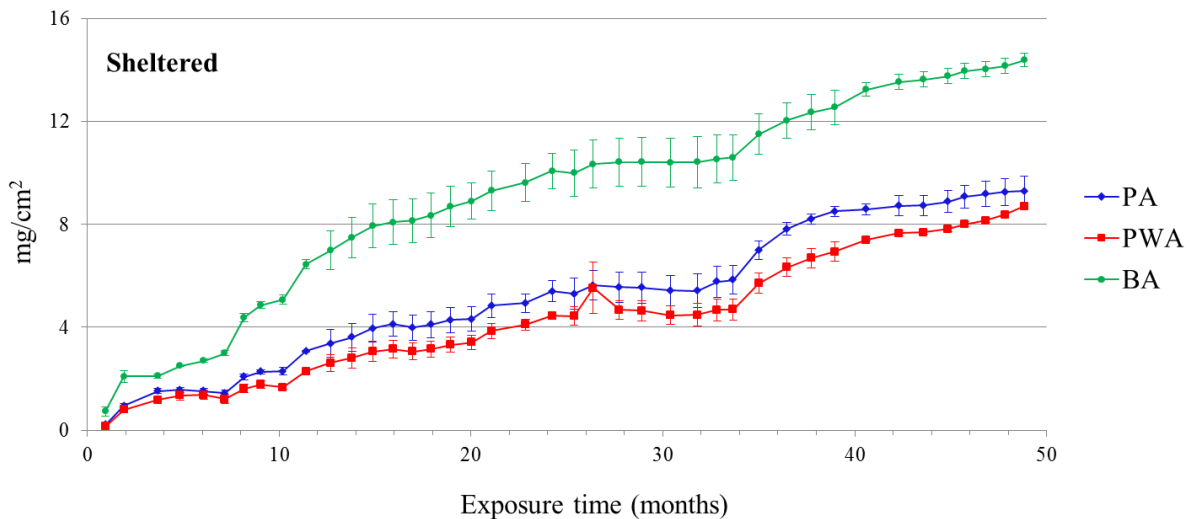


Fig. 52: Mass Variations (mg/cm^2) progressively recorded for bare (BA), pre-patinated (PA) and pre-patinated and waxed (PWA) specimens exposed in sheltered conditions

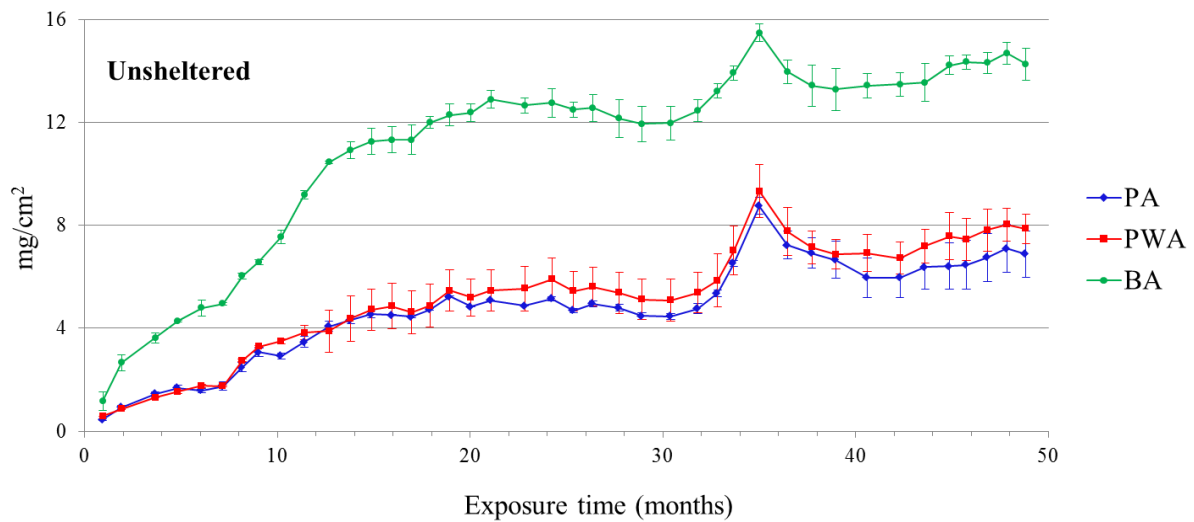


Fig. 53: Mass Variations (mg/cm^2) progressively recorded for bare (BA), pre-patinated (PA) and pre-patinated and waxed (PWA) specimens exposed in unsheltered conditions

Total and annual mass variations are summarized in Table 15; MVs in sheltered and unsheltered conditions are comparable, but, while the geometry of exposure does not have any effect on bare samples, whose total mass variation is $\sim 14 \text{ mg}/\text{cm}^2$ in both cases, it has a greater effect on pre-treated samples. A probable explanation for the different behaviour may be the adhesion and higher residence time of particulate matter on sheltered surfaces, that are protected from the removal action of precipitations. The same behaviour is not observed for bare samples, probably because of differences in physical properties of surfaces with respect to pre-treated specimens.

Table 15 also shows annual mass variations for each finish and condition. First of all, it can be noticed that the difference in mass increase for bare and pre-patinated specimens can be almost completely ascribed to patina growth occurred during the first year of exposure, while, starting from the second year, mass variations become comparable regardless of the surface finish.

Annual MS in Table 15 also suggest that, if on one hand patinas formed on unsheltered specimens have almost reached a steady state condition, in agreement with previous studies [30] that reported that corrosion layers of WS exposed to marine environments takes about 4-6 years to stabilize, on the other hand patinas formed in sheltered conditions are not stabilized yet.

Table 15: Total (4 years) and annual mass variation (mg/cm²) for bare (BA), pre-patinated (PA) and pre-patinated/waxed (PWA) samples exposed in sheltered and unsheltered conditions

	Sheltered (mg/cm ²)	Unsheltered (mg/cm ²)
BA	14.4	14.2
<i>1° year</i>	7.0	10.4
<i>2° year</i>	3.1	2.3
<i>3° year</i>	2.0	1.2
<i>4° year</i>	2.3	0.3
PA	9.3	6.9
<i>1° year</i>	3.4	4.1
<i>2° year</i>	2.0	1.1
<i>3° year</i>	2.4	2.1
<i>4° year</i>	1.5	-0.3
PWA	8.7	7.9
<i>1° year</i>	2.6	3.9
<i>2° year</i>	1.8	2.0
<i>3° year</i>	1.9	1.8
<i>4° year</i>	2.4	0.1

6.2.2.2 Patina composition

In order to study morphological, compositional and structural modifications of corrosion products over time and to better understand the influence of exposure conditions and surface finish on the evolution of the passivation layer, surface investigations during the exposure period were performed.

With regards to the compositional evolution of patinas, EDS analysis (Table 16) performed before the exposure and after 2, 10 and 36 months of natural exposure allows to follow variation in elemental average composition during field test.

Pre-patination treatments result in an initial higher percentage of oxygen on pre-patinated than on bare surfaces (about 40 vs 2.5 wt%) and in a related lower presence of alloying elements. Pre-patination procedures are also responsible for introducing a significant amount of Cl in the artificial patina (1.5-2 wt%).

Since the second month of exposure, the rapid formation of corrosion products on bare WS determines comparable relative percentages of O and Fe (about 40 and 55 wt%, respectively) on all the surfaces.

As the exposure goes on, chlorine is mainly detected on sheltered specimens, while unsheltered samples, that are subjected to the removal action of precipitations, present smaller percentages of Cl on their surfaces. Throughout all the exposure time, crustal elements, such as Al, Si and Ca, can be detected, especially on sheltered specimens.

Finally, alloying elements, such as Cr and Cu, which take part in the stabilization process of the inner part of protective layer (see section 3.2.2.2 and 3.2.2.3), are no longer detectable on the surfaces from the second month on.

Table 16: Elemental composition of bare (BA), pre-patinated (PA) and pre-patinated/waxed (PWA) weathering steel before the exposure and after 2, 10 and 36 months of exposure

	%weight	O	Fe	Si	Cl	Cr	Cu	Al	P	S	Ca	Mn	Ni	K	
t = 0	BA	2.6	94.5	0.7		0.8	0.3		0.1			0.5	0.3		
	PA	41.4	54.5	1.4	1.5	0.2	0.1	0.2		0.1	0.2	0.2	0.1		
	PWA	41.5	54.6	1.1	2.2	0.1				0.1	0.1	0.2			
t = 2 months	BA	She	40.3	57.9	0.5		0.2			0.2		0.6	0.2	0.1	
		Unshe	39.7	59.1	0.2		0.1	0.2		0.2			0.2	0.3	
	PA	She	41.6	54.7	1.4	1.6	0.1	0.1				0.2	0.2	0.1	
		Unshe	41.1	56.2	1.0	0.8		0.2					0.3	0.3	
	PWA	She	43.0	51.0	2.4	1.7	0.1	0.3	0.6	0.1		0.5	0.3		
		Unshe	41.8	55.3	1.0	0.8	0.1		0.4	0.1	0.3			0.1	
t = 10 months	BA	She	41.8	56.0	0.5	0.5			0.2		0.3	0.3	0.3		
		Unshe	41.2	57.6	0.4	0.3					0.2		0.3		
	PA	She	41.0	55.9	1.1	0.9	0.2		0.3		0.3	0.2			
		Unshe	40.9	58.1	0.4						0.2		0.3		
	PWA	She	40.6	54.9	1.6	1.4			0.4		0.3	0.3	0.3		
		Unshe	41.5	57.3	0.4	0.2					0.4	0.2			
t = 36 months	BA	She	42.4	52.6	1.7	0.8			0.6		0.4	1.0	0.2	0.2	
		Unshe	42.4	56.4	0.6				0.3		0.2				
	PA	She	44.1	51.1	1.8	0.9			0.6		0.4	0.9	0.2		
		Unshe	42.5	56.3	0.7				0.2		0.3				
	PWA	She	44.7	51.3	1.5	0.8			0.4		0.4	0.9			
		Unshe	42.3	55.5	0.8				0.4	0.2		0.2	0.4	0.1	

SEM micrographs (Fig. 54) after 36 months of exposure confirm the presence of higher amount of atmospheric deposits on samples exposed in sheltered condition, as already suggested by EDS and mass variation observations (section 6.2.2.1); on the contrary, specimens subjected to the removal action of precipitations appear cleaner but more fractured.

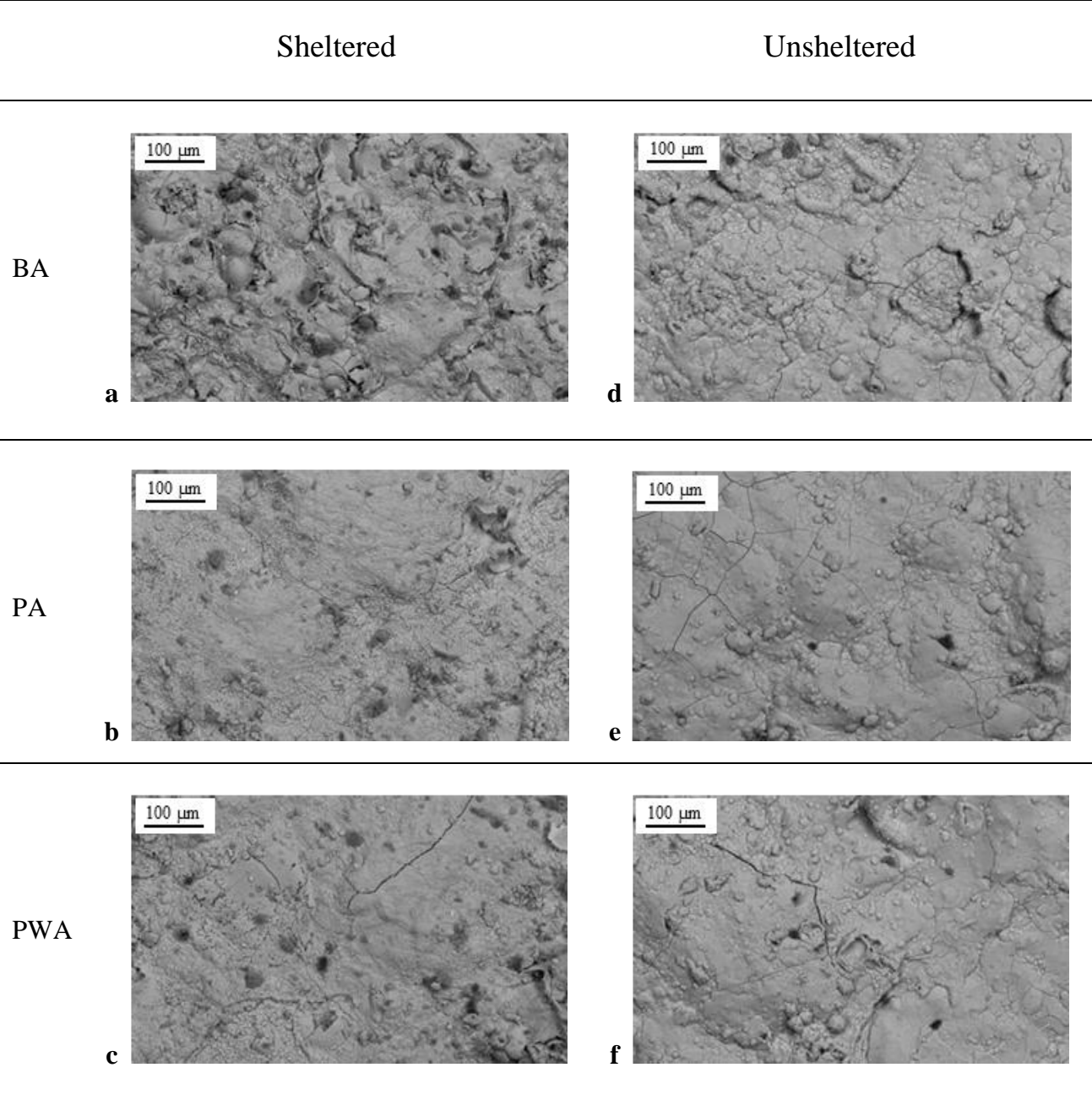


Fig. 54: SEM-QBSD micrographs of bare (a, d), pre-patinated (b, e) and pre-patinated/waxed (c, f) weathering steel exposed in sheltered (on the left) and unsheltered (on the right) conditions after 36 months of environmental exposure in Rimini.

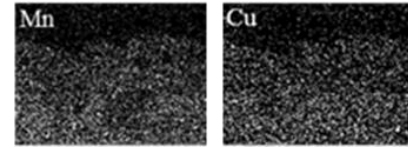
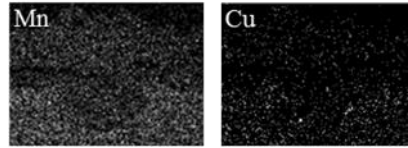
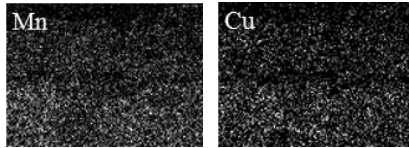
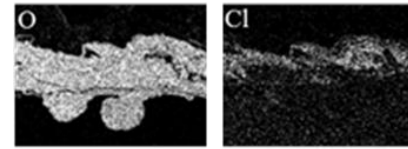
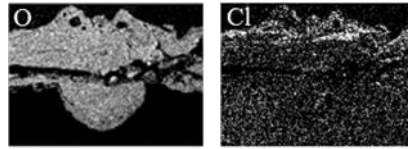
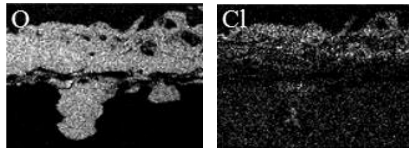
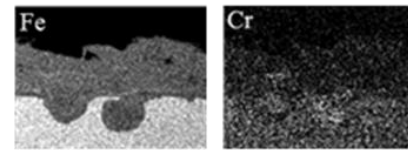
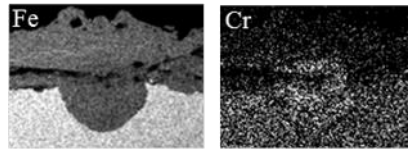
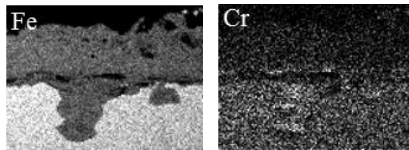
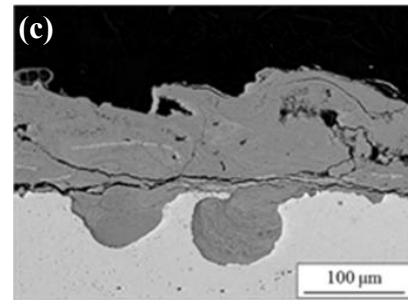
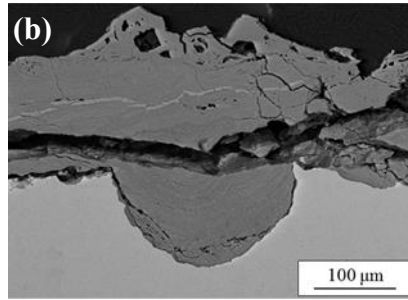
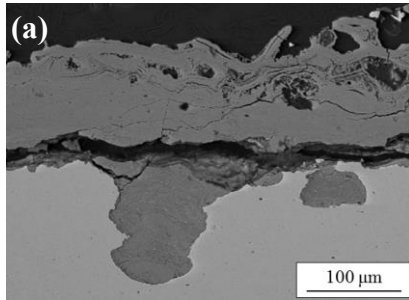
More detailed information about patinas formed were achieved by SEM analysis and EDS elemental mapping on cross sections (Fig. 55). In general, the exposure in unsheltered condition led to the creation of thinner layer; nevertheless, these images do not show any significant dissimilarities in terms of compactness and protectiveness that can be connected to different exposure conditions, especially for pre-patinated samples (with or without the beeswax covering). However, upon closer inspection, some changes due to exposure geometry can be noticed for bare samples: sheltered sample (Fig. 55a) shows an uneven surface and seems to be affected by flaking phenomena; the poor adhesion of the corrosion products is the probable cause of the presence of deep corrosion pits. On the contrary, bare specimen exposed in unsheltered condition (Fig. 55d) presents a much more compact and adherent superficial layer, and, consequently, less pronounced pitting damages.

BA

PA

PWA

Sheltered



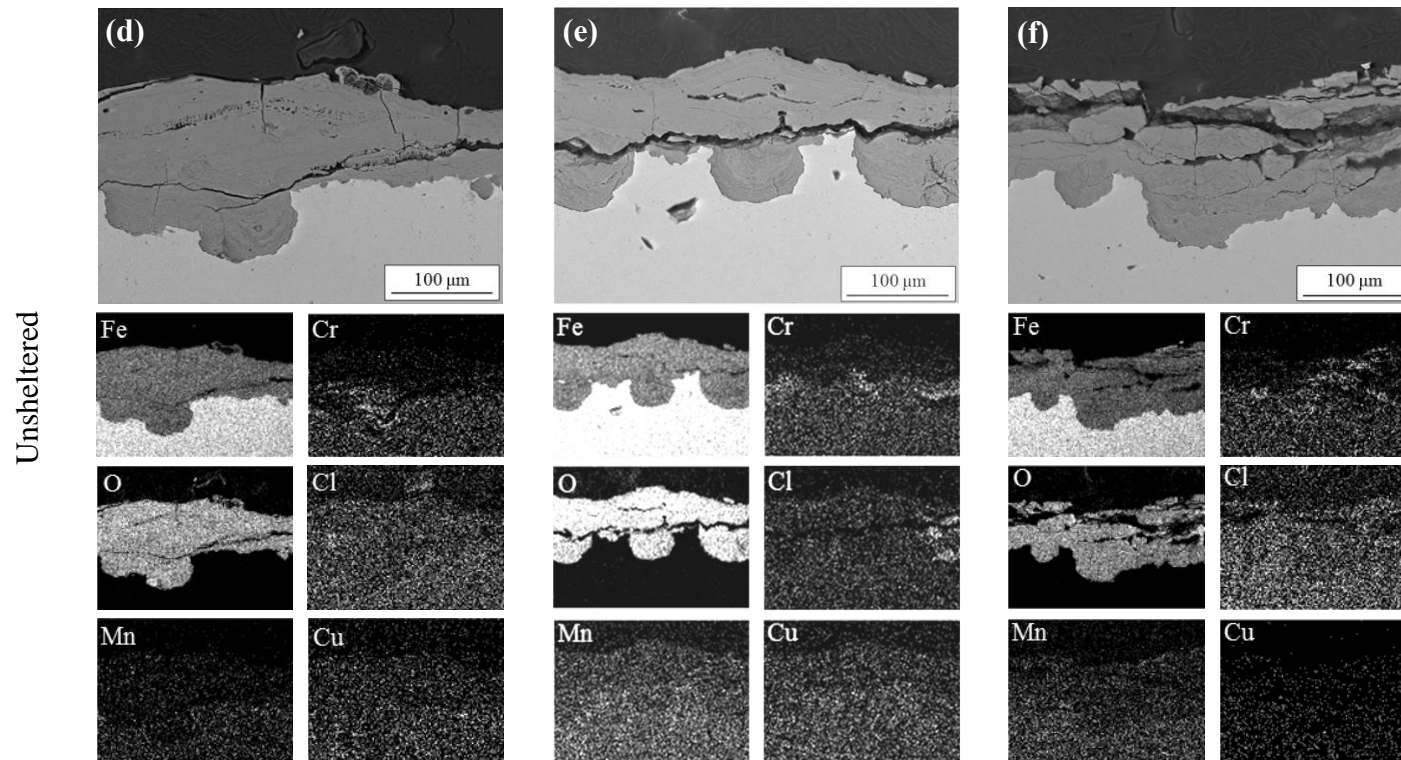


Fig. 55: SEM-SE images and EDS X-Ray maps recorded on cross-section of bare (a, d), pre-patinated (b, e) and pre-patinated/waxed (c, f) weathering steel exposed in sheltered (top) and unsheltered (bottom) conditions after 36 months of environmental exposure in Rimini.

For all finishes and exposure conditions, EDS analyses performed on cross-sections show that Cr mainly concentrates along the metal-patina interface, while Cu and Mn are equally distributed throughout the rust layer, as also shown in previous works [133], [134].

As said before, after three years, Cl deposited on the surfaces or initially present on pre-patinated specimens is not detectable anymore on the surfaces by large-area EDS (Table 16), probably due to the rain action that partly remove and partly facilitates chlorine mobilization and diffusion within the patina (Fig. 55), compromising its stabilization.

The exposure to contaminants and corrosive species, such as chloride, may affect the composition of patina formed and, thus, may negatively act on the corrosion behavior of WS. For this reason, the nature of the corrosion products and their evolution during the exposure period were analyzed by means of Raman spectroscopy.

Raman spectra of sheltered and unsheltered WS specimens after 2, 10 and 36 months of exposure in Rimini are shown in Fig. 56, Fig. 57, Fig. 58, Fig. 59, Fig. 60 and Fig. 61; moreover, results of spectral interpretation, achieved by comparison with the results given in literature [135]–[140] and with RRUFF on-line database, are summarized in Table 17.

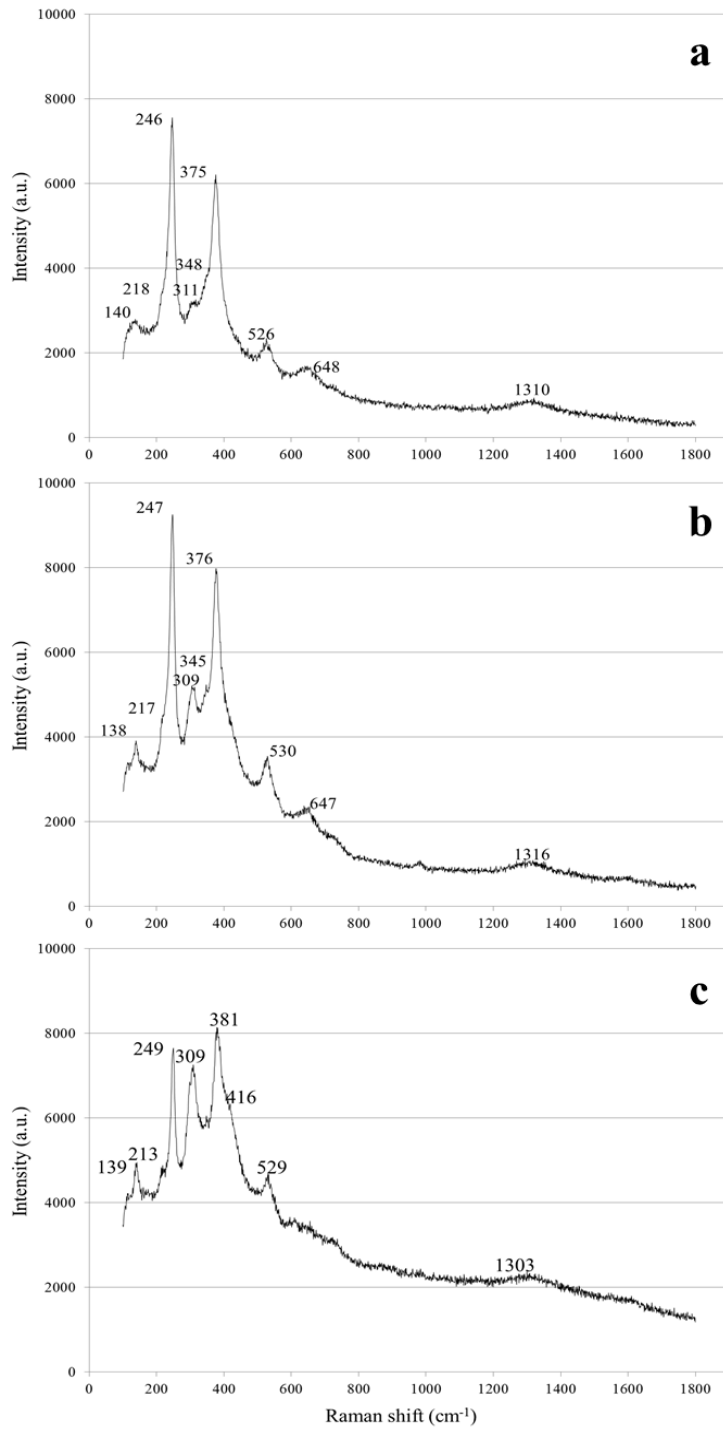


Fig. 56: Raman spectra of Bare (BA) Cor-Ten exposed in sheltered conditions after (a) 2, (b) 10 and (c) 36 months of exposure

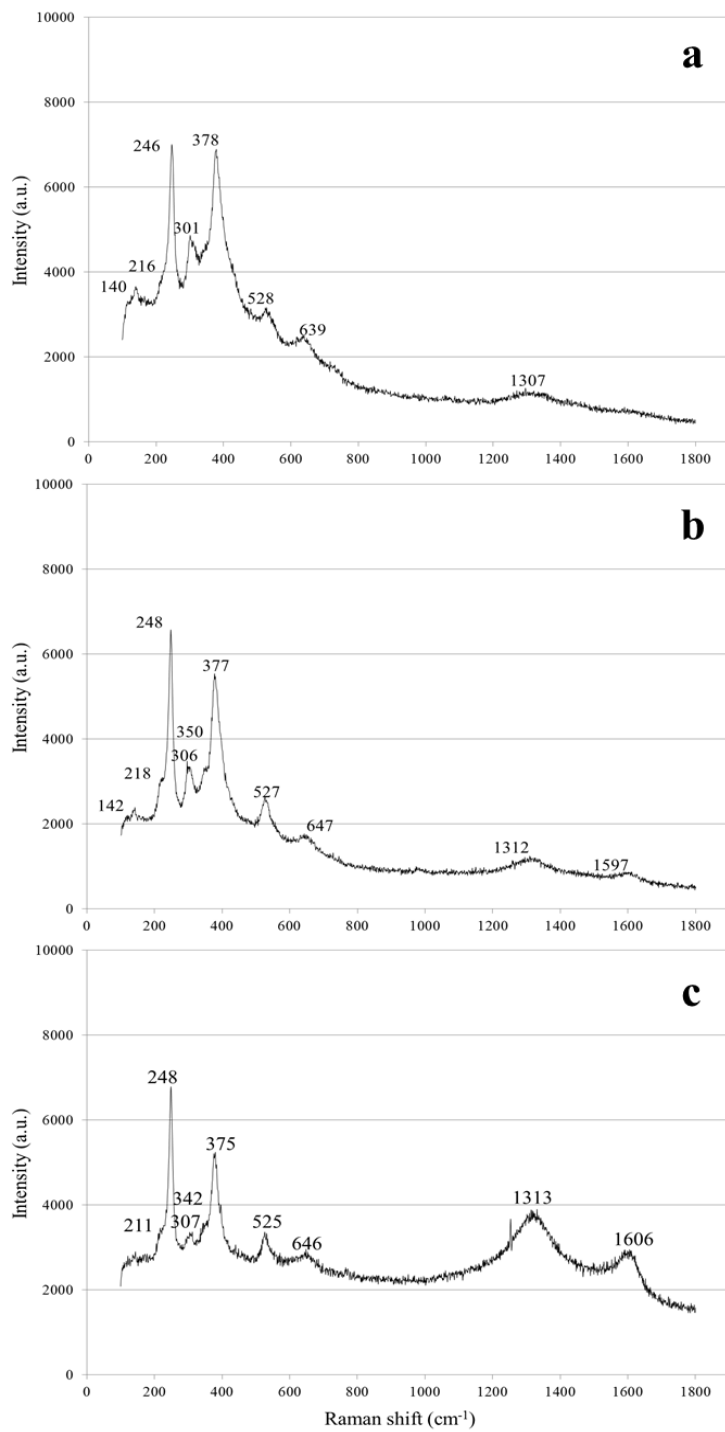


Fig. 57: Raman spectra of Bare (BA) Cor-Ten exposed in unsheltered conditions after (a) 2, (b) 10 and (c) 36 months of exposure

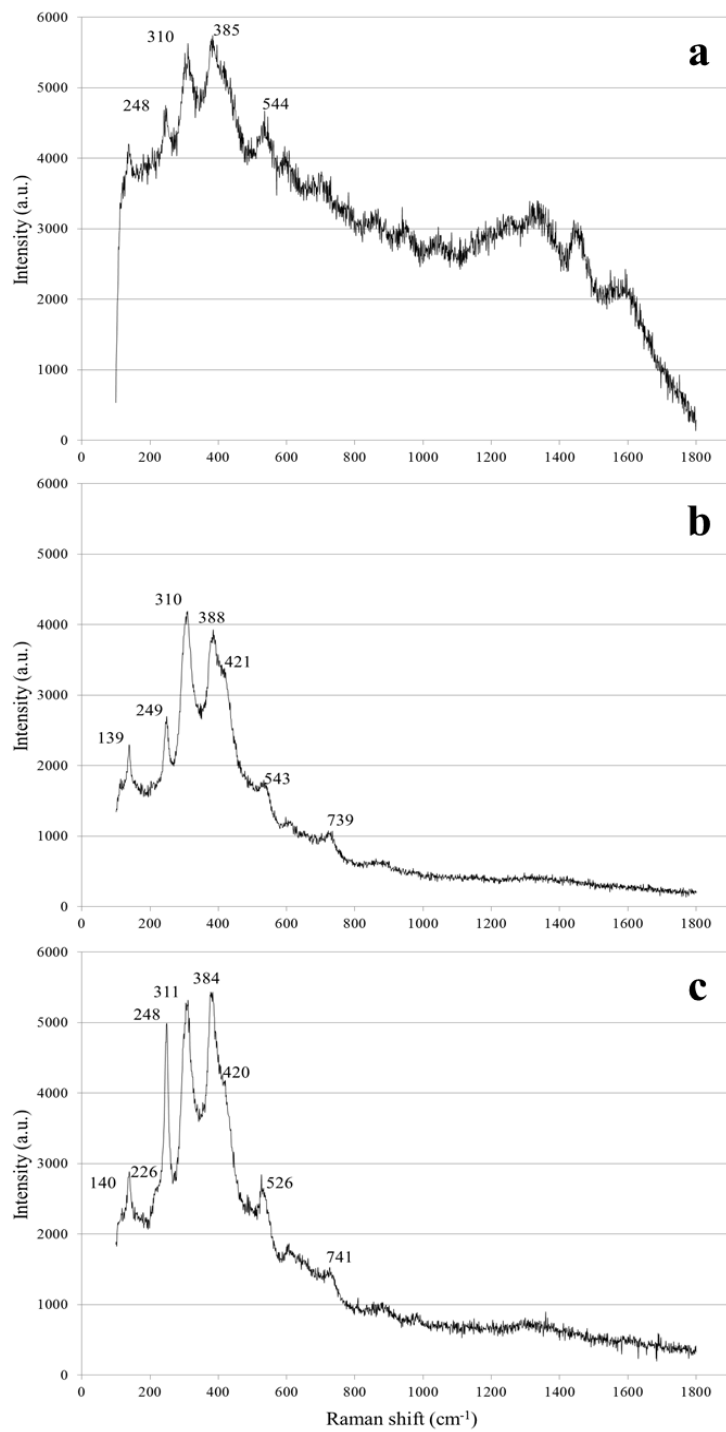


Fig. 58: Raman spectra of Pre-patinated (PA) Cor-Ten exposed in sheltered conditions after (a) 2, (b) 10 and (c) 36 months of exposure

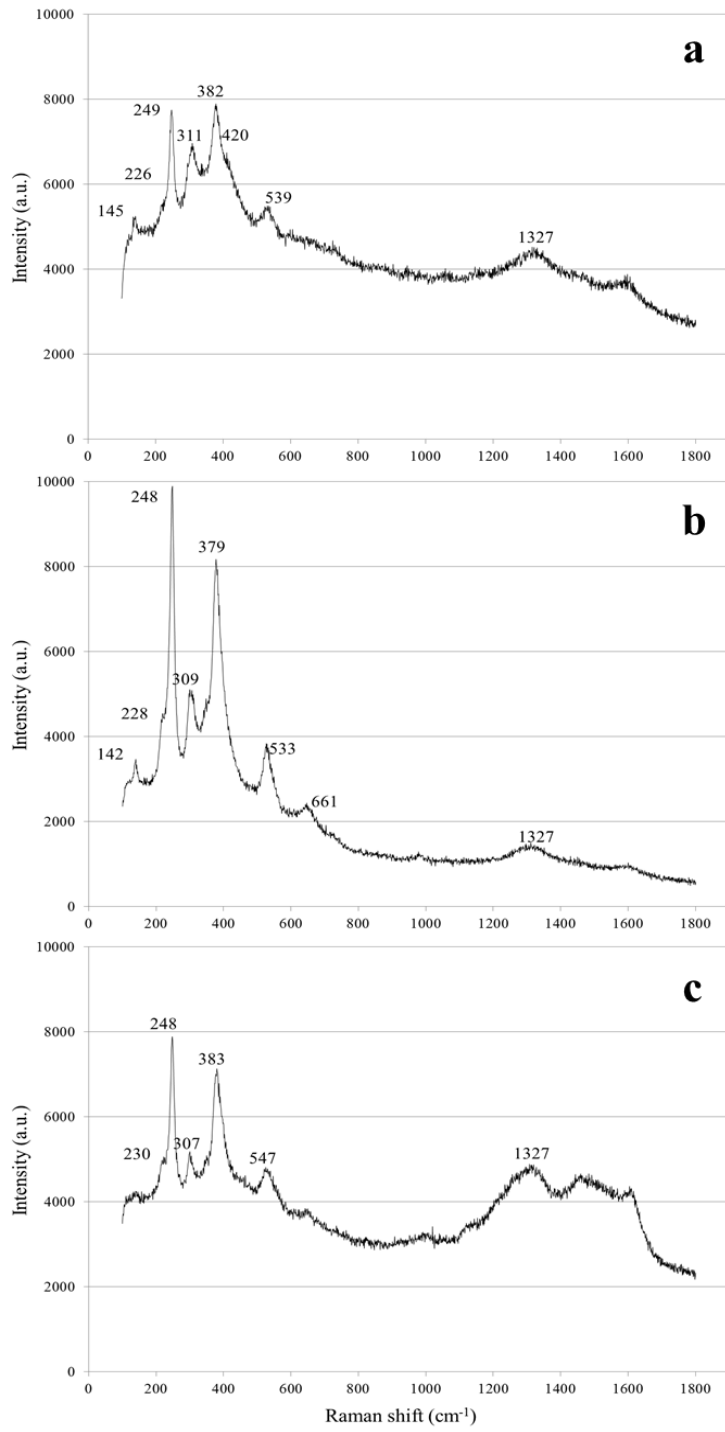


Fig. 59: Raman spectra of Pre-patinated (PA) Cor-Ten exposed in unsheltered conditions after (a) 2, (b) 10 and (c) 36 months of exposure

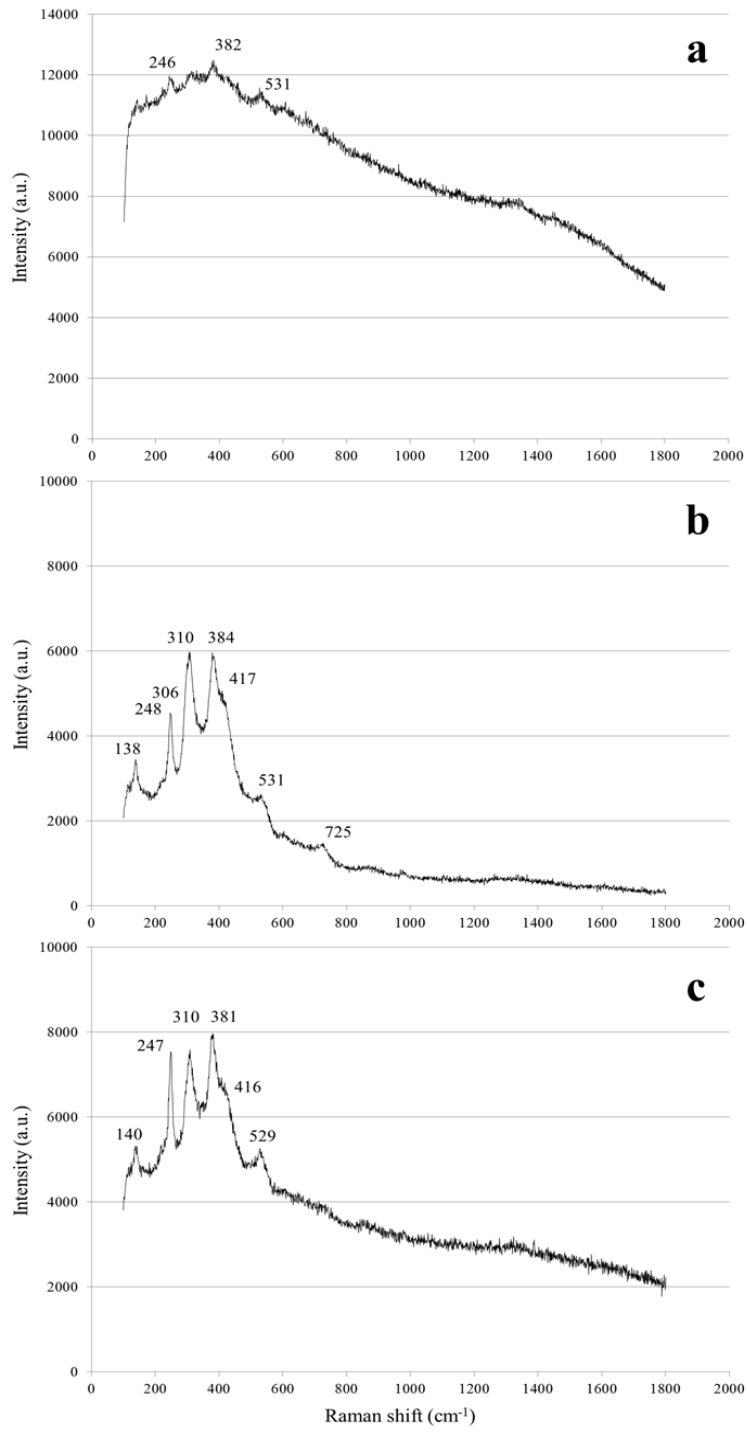


Fig. 60: Raman spectra of Pre-patinated/Waxed (PWA) Cor-Ten exposed in sheltered conditions after (a) 2, (b) 10 and (c) 36 months of exposure

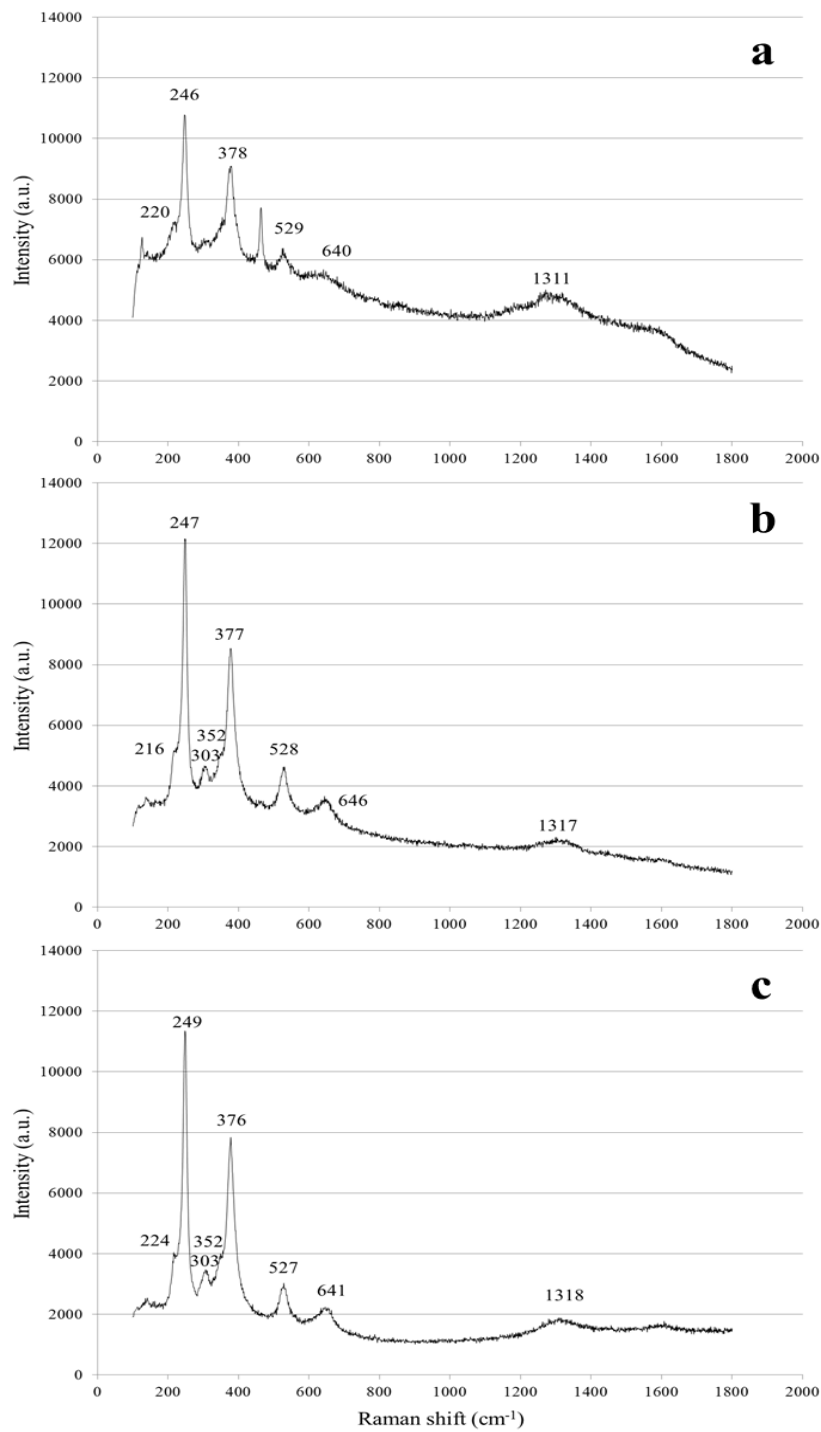


Fig. 61: Raman spectra of Pre-patinated/Waxed (PWA) Cor-Ten exposed in unsheltered conditions after (a) 2, (b) 10 and (c) 36 months of exposure

As reported in literature [38], [39], [135]–[138], [140], [141], in the early stages of exposure (2 months), the main corrosion product is lepidocrocite (γ -FeOOH). As the exposure proceeds, even though Cl is not detectable anymore by large-area EDS (Table 16), localized Raman analysis allowed the detection of traces of Cl-containing species such as akaganeite (β -FeOOH), the typical corrosion product of steels exposed to chlorine-rich environments that compromises patina stabilization. Moreover hematite and magnetite, typically found on outdoor weathering steel samples and sculptures depending on time and condition of exposure [142], [143], were also detected. After 36 months of exposure, akaganeite appear more abundant (qualitative evaluation is made on the basis of relative intensities of characteristic peaks of each phase) on sheltered specimens rather than on unsheltered ones; this may be due to the fact that sheltered samples are not subjected to the chlorine-removal action of precipitation, as confirmed by EDS analysis (Table 16).

On the surface of some sheltered specimens is also identified a second chlorinated product, β -Fe₂(OH)₃Cl (iron hydroxychloride), considered as a direct precursor to the formation of β -FeOOH, containing an higher amount of Cl⁻ (ca. 20%) than Akaganeite (ca. 5-6%) [144]; this evidence supports the idea that it may be considered as an acceptor of Cl⁻ from the atmosphere and, as a consequence, the responsible for the acceleration of corrosion process.

On the contrary, magnetite is mainly found on the surface of unsheltered samples: in fact, this product is usually positioned in the inner part of protective layer, so its detection on unsheltered specimens is an effect of leaching phenomena.

Table 17: Interpretation of Raman spectra of sheltered (She) and unsheltered (Unshe) WS specimens after 2, 10 and 36 months of exposure.

		Raman	
t = 0 months	BA		
	PA		A _(tr) , M _(tr)
	PWA		A _(tr) , H _(tr) , L, M _(tr)
t = 2 months	BA	She	A _(tr) , L, M _(tr)
		Unshe	A _(tr) , L, M _(tr)
	PA	She	L _(tr)
		Unshe	A _(tr) , L, M _(tr)
	PWA	She	L _(tr)
		Unshe	L, M _(tr)
t = 10 months	BA	She	A, L, M _(tr)
		Unshe	A, H _(tr) , L, M
	PA	She	A _(tr) , L
		Unshe	A, H _(tr) , L, M
	PWA	She	A, B _(tr) , H, L
		Unshe	A, H _(tr) , L, M
t = 36 months	BA	She	A, H, L, M
		Unshe	A, H _(tr) , L, M
	PA	She	A, H, L
		Unshe	A, H _(tr) , L, M
	PWA	She	A, B _(tr) , H _(tr) , L
		Unshe	H, L, M

Characteristic Raman peaks:

A = Akaganeite (β -FeOOH): about 310, 378, 530 and 720 cm^{-1} ;

B = Iron hydroxychloride (β -Fe₂(OH)₃Cl) :140 and 420 cm^{-1} ;

H = Hematite (Fe₂O₃): 220, 420 and 1320 cm^{-1} ;

L = Lepidocrocite (γ -FeOOH): about 250 cm^{-1} and 380 cm^{-1} ;

M = Magnetite (Fe₃O₄): 535 and 660 cm^{-1} .

Tr. = corrosion product in trace

6.2.3 Metal dissolution

As described before, WS specimens with different surface finish were exposed in triplicate, both in sheltered and unsheltered conditions (sections 5.2.1 and 5.3.1 and Fig. 29). As suggested by ISO Standard 8565:2011 [102], environmental exposure started in spring (march 2011), when the corrosivity is higher.

Each unsheltered sample was connected to a system for the collection of rainwater impinging on WS surface. Collected rainwaters were filtered and analysed for the determination of metals released in the dissolved, thus soon bioavailable, fraction.

Blank solutions (rainwater impinging only Teflon holders) were also collected in triplicate and subjected to the same procedure as runoff samples; then, the background concentrations of the investigated species, due to natural and anthropogenic atmospheric input, were subtracted in order to isolate only the contribution of WS runoff.

pH of collected samples varied between 4.5 and 7.3, with lower values in winter and higher values in summer, but with no significant differences among samples from blank and WS specimens (ANOVA, $p > 0.5$). Monthly values of pH in blank and runoff solutions are shown in Fig. 62.

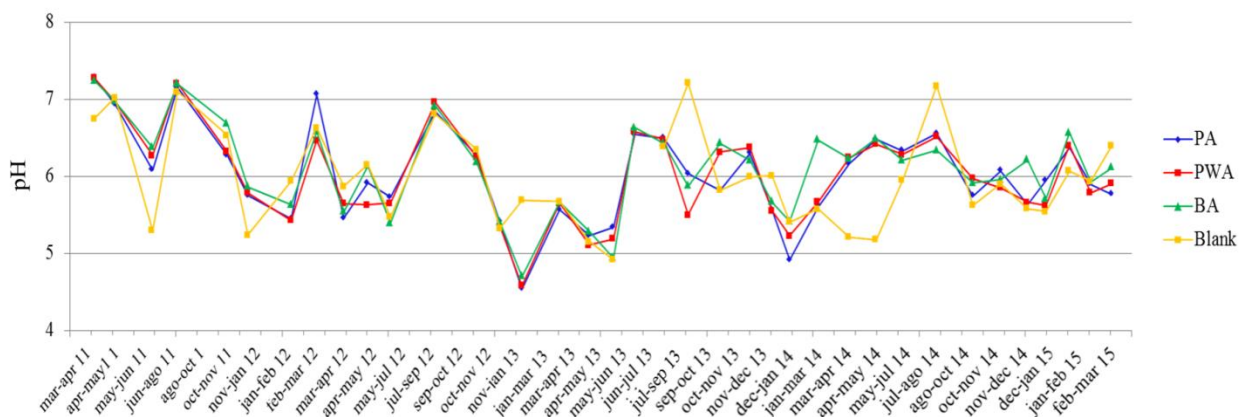


Fig. 62: Monthly values of pH in blank (yellow line) and runoff solutions (Bare: green line; Pre-patinated: blue line; Waxed: red line)

Concentrations of dissolved Cr are always below the LoD ($\text{LoD}_{\text{Cr}} = 0.2 \mu\text{g/L}$), while Cu is always lower than field blanks ($0.02\text{-}0.3 \mu\text{g/cm}^2$). This result supports literature finding [44], [53], [55], [145] based on patina characterization, showing the tendency of these elements to mainly form insoluble products in the patina (see sections 3.2.2.2 and 3.2.2.3) and to be eventually released as non-adherent rust [146].

Annual dissolution of iron, manganese and nickel are shown in

Table 18.

As expected, the total amount of dissolved iron is one or two orders of magnitude higher than that of manganese and nickel; this is not surprising if one consider the initial nominal composition of Cor-Ten A (section 5.2.1) and the fact that, in some environmental conditions, iron oxides formed on weathering steel during the first period of exposure are quite soluble and can be easily dissolved by precipitations [50].

Table 18: Annual dissolution (mg/m^2) of Fe, Mn and Ni from Bare (BA), Pre-patinated (PA) and Pre-patinated/waxed (PWA) weathering steel during four years of exposure

		Fe (mg/m^2)	Mn (mg/m^2)	Ni (mg/m^2)
BA	1° year	194.31	2.25	2.66
	2° year	8.81	0.57	0.67
	3° year	32.87	1.26	1.34
	4° year	35.51	1.78	1.02
PA	1° year	230.86	19.72	5.29
	2° year	14.29	4.35	1.85
	3° year	63.55	11.76	3.07
	4° year	53.26	6.52	1.51
PWA	1° year	127.79	13.67	4.29
	2° year	27.60	9.00	2.70
	3° year	89.78	17.13	3.47
	4° year	81.49	13.47	3.36

Despite these differences, runoff trends for dissolved Fe, Mn and Ni during the entire period of exposure appear similar (Table 19, Table 20 and Table 21) for all finishes.

Dissolution data for each surface finish, expressed as the mean of three values with variability ranging from 10% to 30%, are shown in Fig. 63, Fig. 64, Fig. 65 and Fig. 66.

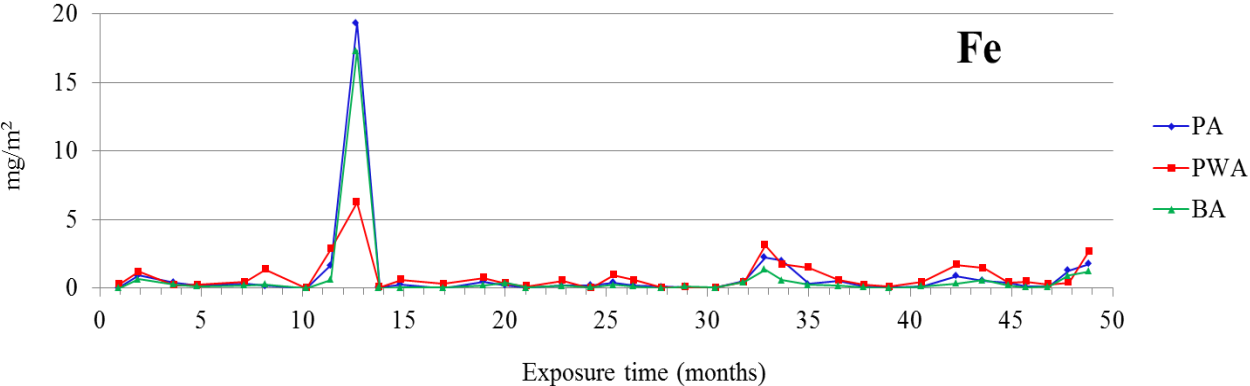


Fig. 63: Monthly dissolution of Fe from bare (BA), pre-patinated (PA) and pre-patinated/waxed (PWA) weathering steel samples during the period of exposure

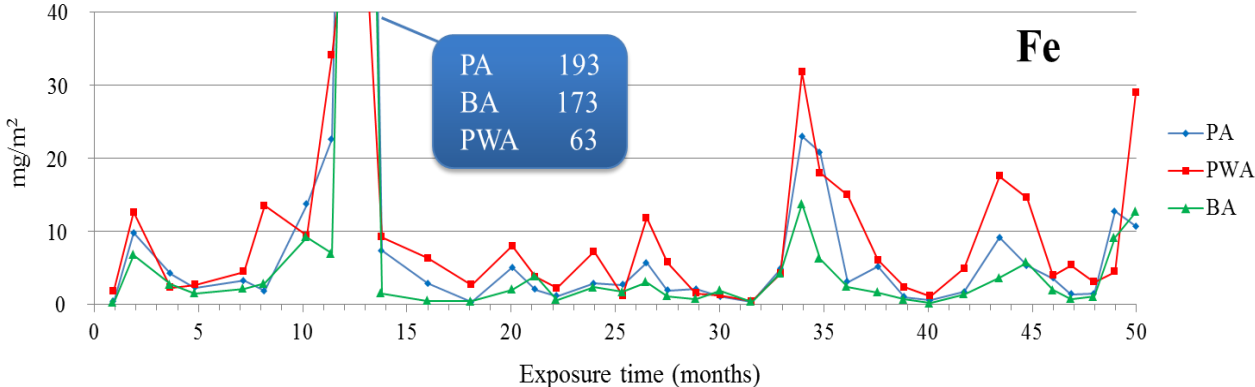


Fig. 64: Detail of Fig. 63

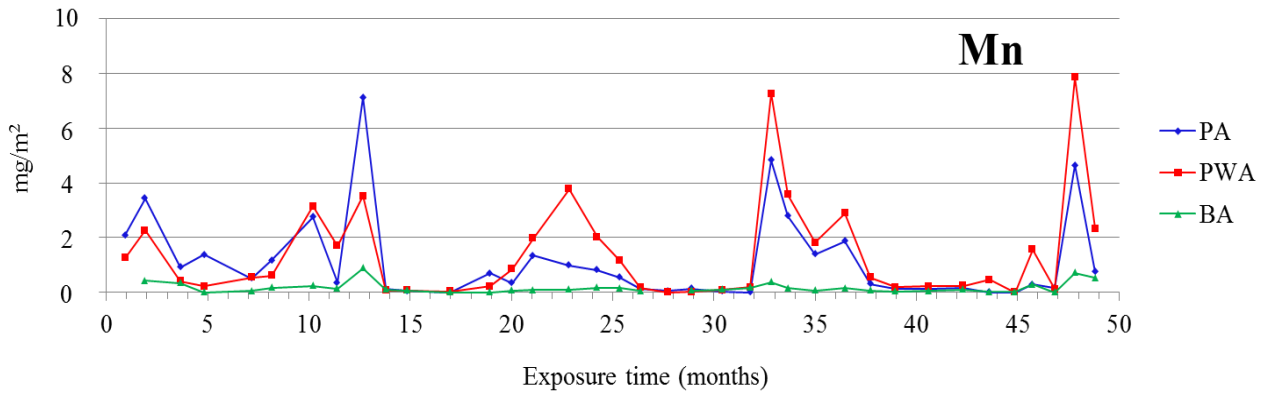


Fig. 65: Monthly dissolution of Mn from bare (BA), pre-patinated (PA) and pre-patinated/waxed (PWA) weathering steel samples during the period of exposure

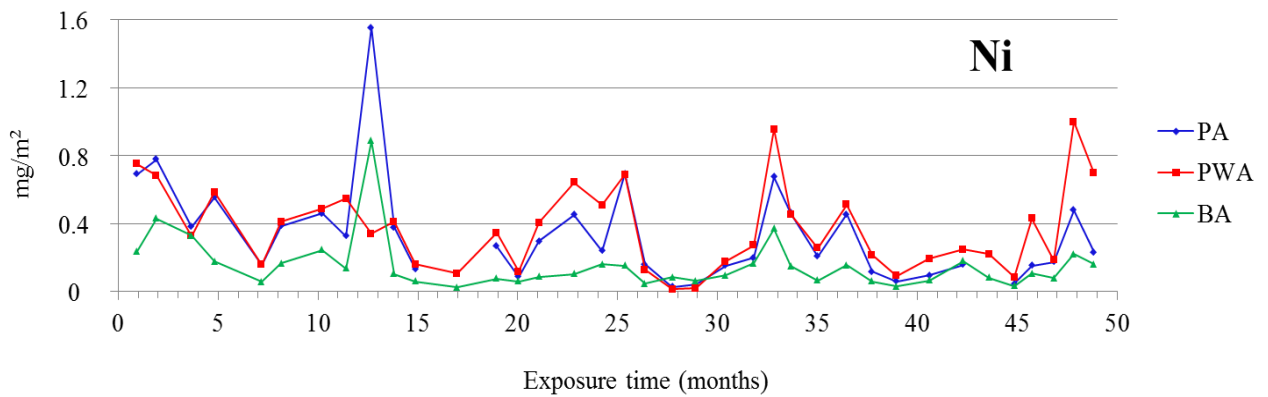


Fig. 66: Monthly dissolution of Ni from bare (BA), pre-patinated (PA) and pre-patinated/waxed (PWA) weathering steel samples during the period of exposure

By comparing these data with rainwater trend (Fig. 48) during each sampling period, significant correlation between amount of dissolved metals and collected rain is not observed, as confirmed by Pearson's Correlation Coefficients (Table 19, Table 20 and Table 21) and previously noticed for different alloys and pure metals [106], [147], [148].

Table 19: Pearson's Correlation Coefficients among dissolved alloying metals, main ions in runoff rainwater, average air pollutant concentrations and rain amount on the specimens. The complete dataset for bare weathering steel is considered (n=37)

	Ni	Mn	Cl	NO ₂ ⁻	NO ₃ ⁻	SO ₄ ⁼	Na ⁺	K ⁺	Ca ²⁺	Mg ²⁺	NH ₄ ⁺	NO ₂	O ₃	PM ₁₀	PM _{2.5}	rain
Fe	0.836 ***	-0.069	0.623 ***	0.0979	0.22	0.383	0.38	0.645 ***	0.195	0.276	0.318	0.264	-0.112	0.337	0.306	-0.236
Ni		0.0483	0.727 ***	0.348 *	0.451 **	0.567 ***	0.516 **	0.694 ***	0.462 **	0.467 **	0.515 **	0.303	-0.0973	0.273	0.264	-0.124
Mn			0.0643	0.0696	-0.131	-0.0326	-0.0298	-0.15	0.0043	0.0723	-0.127	0.516	-0.192	0.531 **	0.539 **	-0.482 **

*** (p<0.001); ** (p<0.01); * (p<0.05)

Table 20: Pearson's Correlation Coefficients among dissolved alloying metals, main ions in runoff rainwater, average air pollutant concentrations and rain amount on the specimens. The complete dataset for pre-patinated weathering steel is considered (n=37)

	Ni	Mn	Cl	NO ₂ ⁻	NO ₃ ⁻	SO ₄ ⁼	Na ⁺	K ⁺	Ca ²⁺	Mg ²⁺	NH ₄ ⁺	NO ₂	O ₃	PM ₁₀	PM _{2.5}	rain
Fe	0.759 ***	0.72 ***	0.438 **	0.104	0.19	0.205	0.259	0.178	0.202	0.224	0.215	0.279	-0.116	0.369 *	0.328	-0.206
Ni		0.847 ***	0.497 **	0.307	0.36 *	0.331	0.343 *	0.295	0.419 *	0.335 *	0.432 *	0.392 *	-0.21	0.309	0.345 *	-0.0522
Mn			0.675 ***	0.501 **	0.288	0.48 **	0.544 ***	0.446 **	0.466 **	0.514 **	0.547 *	0.439 **	-0.247	0.357 *	0.35 *	0.0283

*** (p<0.001); ** (p<0.01); * (p<0.05)

Table 21: Pearson's Correlation Coefficients among dissolved alloying metals, main ions in runoff rainwater, average air pollutant concentrations and rain amount on the specimens. The complete dataset for pre-patinated/waxed weathering steel is considered (n=37)

	Ni	Mn	Cl	NO ₂ ⁻	NO ₃ ⁻	SO ₄ ⁼	Na ⁺	K ⁺	Ca ²⁺	Mg ²⁺	NH ₄ ⁺	NO ₂	O ₃	PM ₁₀	PM _{2.5}	rain
Fe	0.292	0.426 *	0.445 **	0.33	9	0.378 *	0.42 *	***	0.162	0.398 *	0.345 *	0.304	-0.18	**	**	0.0967
Ni		0.769	0.681	0.574			0.596		0.524	0.624	0.529	0.473	-			
		***	***	***	0.213	0.499	***	0.462 **	***	***	***	**	0.256	0.285	0.354 *	0.22
Mn			0.757		0.052	0.608	0.677	0.566		0.692		0.503		0.402	0.387	
			***	0.72 ***	3	***	***	***	0.394 *	***	0.498 **	**	-0.4 *	**	**	0.248

*** (p<0.001); ** (p<0.01); * (p<0.05)

Annual total (Fe + Mn + Ni) metal runoff trend ($1^\circ \gg 4^\circ \sim 3^\circ > 2^\circ$) for all the finishes could not directly be correlated to annual rain quantities ($3^\circ > 4^\circ > 2^\circ > 1^\circ$); thus, factors other than precipitation amounts, such as pH, rain intensity and composition tend to affect more the process.

Seasonal dependence of metal dissolution cannot be either clearly pointed out, while a strong influence of occasional meteorological episodes is evident. The main peaks of release are recorded at 12, 34, 42 and 48 months of exposure. The first increase is connected to the heavy snowfalls occurred in January-February 2012 [130], which led to an increase in TOW of the exposed specimens and caused prolonged contact between surfaces and atmospheric pollutants accumulated in the snow [149]; the second is related to the storm that hit Rimini in November 2013 [132], with strong winds (intensity > 96 km/h) blowing from the north. The third corresponds to the whirlwind of July 2014 [150], that focused on the marine coast and strongly contributed to creation of sea salt aerosol. Finally, the last peak was connected to bad meteorological conditions registered in Rimini during the period January-March 2015 [131], [151], when heavy flood and strong and prolonged winds occurred.

All these events were characterized by medium and strong winds (from 55 km/h to 96 km/h) coming from north/north-east direction, that contribute to the transportation of marine aerosol containing corrosive species (Cl^- , SO_4^{2-}) from the coast to the site of exposure.

During the sampling periods including these events, the highest concentrations of corrosive species, especially Cl^- and SO_4^{2-} deriving from sea spray, were recorded in runoff samples (Fig. 67 and Fig. 68).

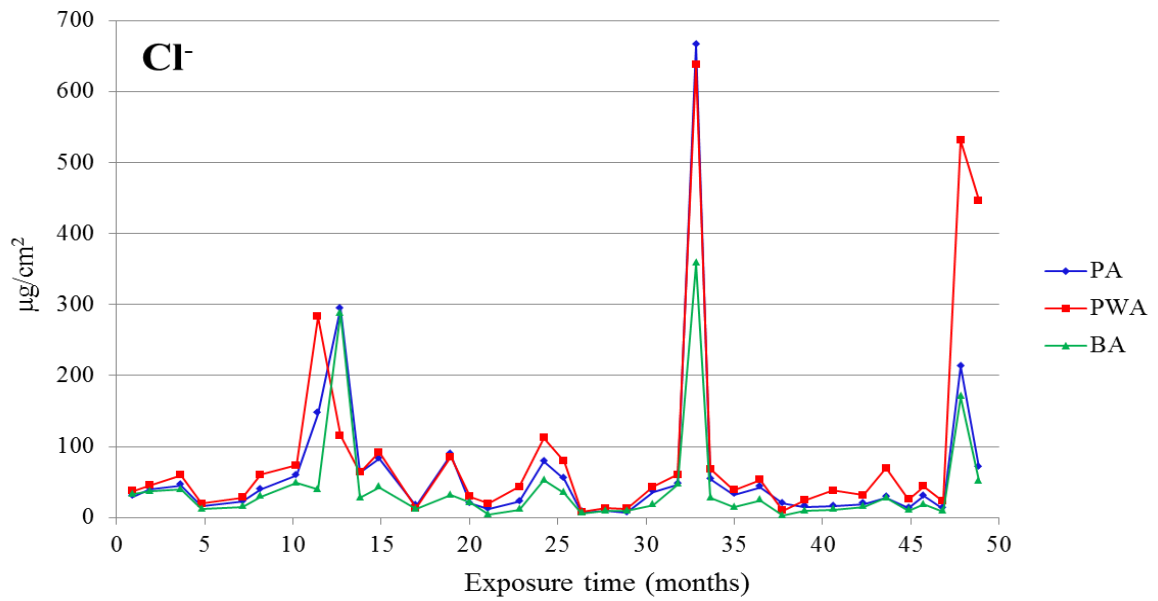


Fig. 67: Chloride concentration ($\mu\text{g}/\text{cm}^2$) in run-off solution from bare (BA), pre-patinated (PA) and pre-patinated/waxed (PWA) samples

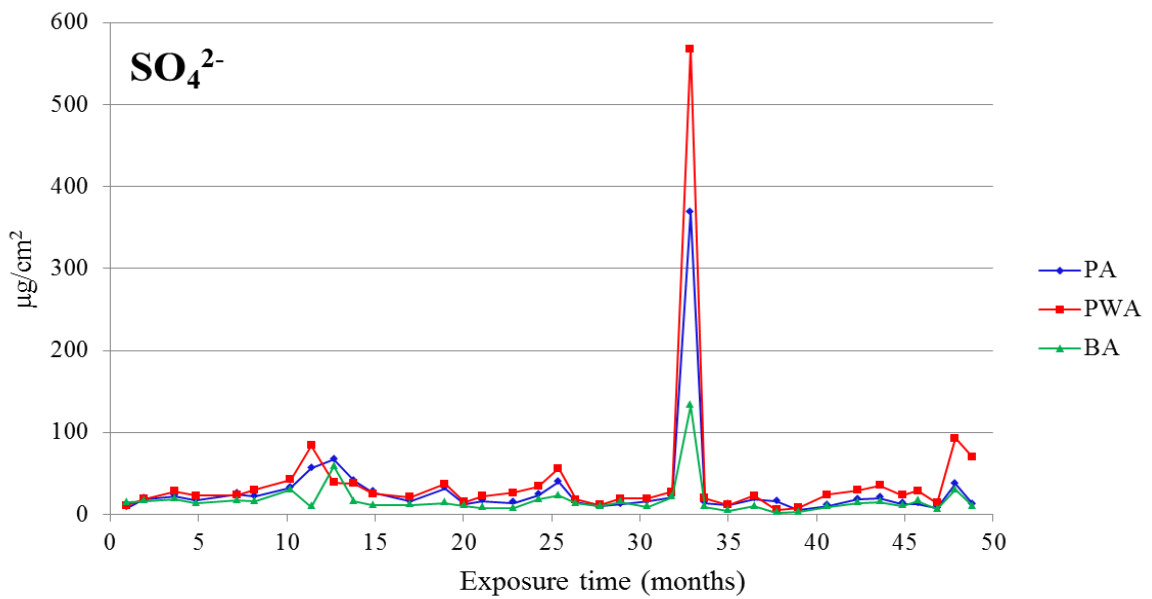


Fig. 68: Sulphate concentration ($\mu\text{g}/\text{cm}^2$) in run-off solution from bare (BA), pre-patinated (PA) and pre-patinated/waxed (PWA) samples

Metal dissolution occurred in the above mentioned sampling periods, in most cases, account for the majority of the annual amounts of runoff metals. This is shown in Table 22, where percentage contributions of each meteorological event are reported.

Table 22: Contribution of extreme meteorological events to the annual metal (Fe + Mn + Ni) runoff for BA, PA and PWA weathering steel

	Year of exposure <i>Meteorological event</i>	mg (Fe + Mn + Ni) / m² (%)	
BA	1° year <i>snowfall</i>	199.2 174.8 (88%)	
	2° year	10.06	
	3° year <i>storm</i>	35.47 14.21 (40%)	
	4° year <i>strong winds - flood</i>	38.31 3.56 (69%)	
	PA	1° year <i>snowfall</i>	255.9 202.2 (79 %)
		2° year	20.49
		3° year <i>storm</i>	78.38 28.07 (36 %)
		4° year <i>strong winds - flood</i>	61.30 8.96 (74 %)
PWA		1° year <i>snowfall</i>	145.75 66.46 (46 %)
	2° year	39.30	
	3° year <i>storm</i>	110.37 39.39 (36 %)	
	4° year <i>strong winds - flood</i>	98.33 60.15 (61 %)	

Snowfalls of winter 2012 represent the event that more affect the annual runoff, especially for bare and pre-patinated samples (88% and 79% of metal dissolution during the first year, respectively).

During the last year of exposure, that was characterized by a flood and several windy days, these events affected total metal runoff for more than 60% for all the finishes (BA: 69%; PA: 74%; PWA: 61%).

This suggest that the relative increase in extreme events worldwide [152] and climate changes could significantly affect the amount of metal dissolved from weathering steel.

For any surface finish, first year total (Fe + Mn + Ni) releases are higher (Table 18), but no decreasing trends are noticeable; actually, even if contributions due to extreme events are excluded, annual dissolution rates follow the order 1 year > 3 year >> 2 year ~ 4 year.

Mass balance calculations based on annual dissolution rates of Fe, Mn and Ni, compared to the bulk alloy composition (Fig. 69), show a high preferential dissolution of Mn and Ni with respect to Fe for all the finishes, especially for pre-treated samples, demonstrating that, also for WS, dissolution rates of single alloying elements cannot be inferred from the initial content in the alloy. Selective dissolution of Mn and Ni is lower during the first year of exposure, strongly influenced by snowfalls and related higher contact times, which acted by raising Fe dissolution with respect to the other metals, especially with respect to Ni.

Actually, if the snowfall sampling period is excluded, first year fractions of each dissolved metal would range, for all the surface finishes, between 70-87% (Fe), 5-7% (Ni) and 6-23% (Mn), more similar to the percentages of following years.

The same behaviour is not observed during the storm occurred on October-November 2013 or during the events of winter 2015, when fractions of dissolved metals are close to those calculated for the rest of the year.

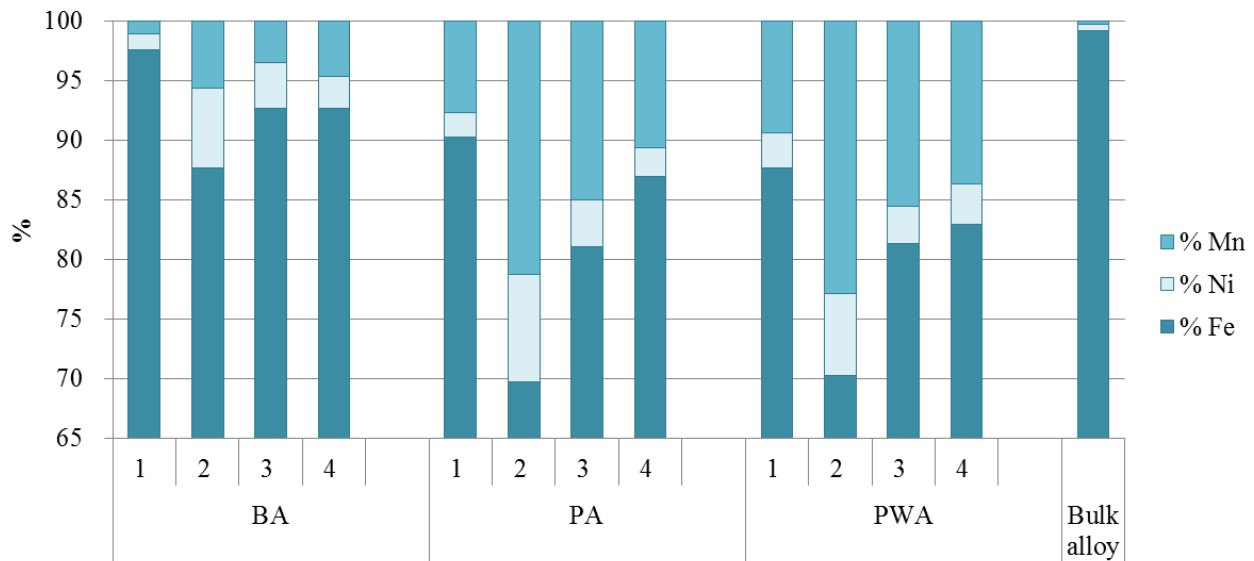


Fig. 69: Fraction of dissolved Fe, Mn and Ni with respect to the sum (Fe + Mn + Ni) for Bare (BA), Pre-patinated (PA) and Pre-patinated/waxed (PWA) weathering steel during each year of exposure, compared with the bulk alloy fractions (about 99% for Fe, 0.3% for Ni and 0.5% for Mn).

Except during the mentioned meteorological events, Fe, Mn and Ni dissolutions tend to be lower for bare than for pre-patinated WS; thus, pre-patination treatments involving the use of Cl^- (section 5.2.1) seem to worsen the performance of weathering steel when exposed outdoor and the wax covering seems to further enhance metal dissolution, confirming preliminary findings of accelerated ageing tests [146].

6.2.4 Multivariate data analysis

The comparative observation of dissolution and environmental data clearly highlight the influence of Cl^- deposition on Fe, Mn and Ni dissolution, while a simple data exploration performed on the global dataset allow to reveal several linear correlations between dissolved metals, atmospheric ions and pollutants (Table 19, Table 20 and Table 21).

However this kind of analysis does not allow to evidence specific temporal trends or to clearly highlight possible different behavior among WS surface finishing. Therefore, a thorough evaluation of the influence of the environment on WS metal dissolution was performed by means of a multivariate approach.

Graphical results of PCA on metal and ion concentrations in runoff waters are shown here below.

Table 23: Exposure and sampling periods (progressive numbers of sampling periods are reported in bold)

	1st year	2nd year	3rd year	4th year
Exposure And Sampling Periods	Mar-Apr 2011 (1)	Mar-Apr 2012 (10)	Mar-Apr 2013 (18)	Mar-Apr 2014 (28)
	Apr-May 2011 (2)	Apr-May 2012 (11)	Apr-May 2013 (19)	Apr-May 2014 (29)
	May-Jun 2011 (3)	May-Jul 2012 (12)	May-Jun 2013 (20)	May-Jul 2014 (30)
	Jun-Aug 2011 (4)	Jul-Sep 2012 (13)	Jun-Jul 2013 (21)	Jul-Ago 2014 (31)
	Aug-Oct 2011 (5)	Sep-Oct 2012 (14)	Jul-Sep 2013 (22)	Aug-Oct 2014 (32)
	Oct-Nov 2011 (6)	Oct-Nov 2012 (15)	Sep-Oct 2013 (23)	Oct-Nov 2014 (33)
	Nov-Jan 2012 (7)	Nov-Jan 2013 (16)	Oct-Nov 2013 (24)	Nov-Dec 2014 (34)
	Jan-Feb 2012 (8)	Jan-Mar 2013 (17)	Nov-Dec 2013 (25)	Dec-Jan 2015 (35)
	Feb-Mar 2012 (9)		Dec-Jan 2014 (26)	Jan-Feb 2015 (36)
			Jan-Mar 2014 (27)	Feb-Mar 2015 (37)

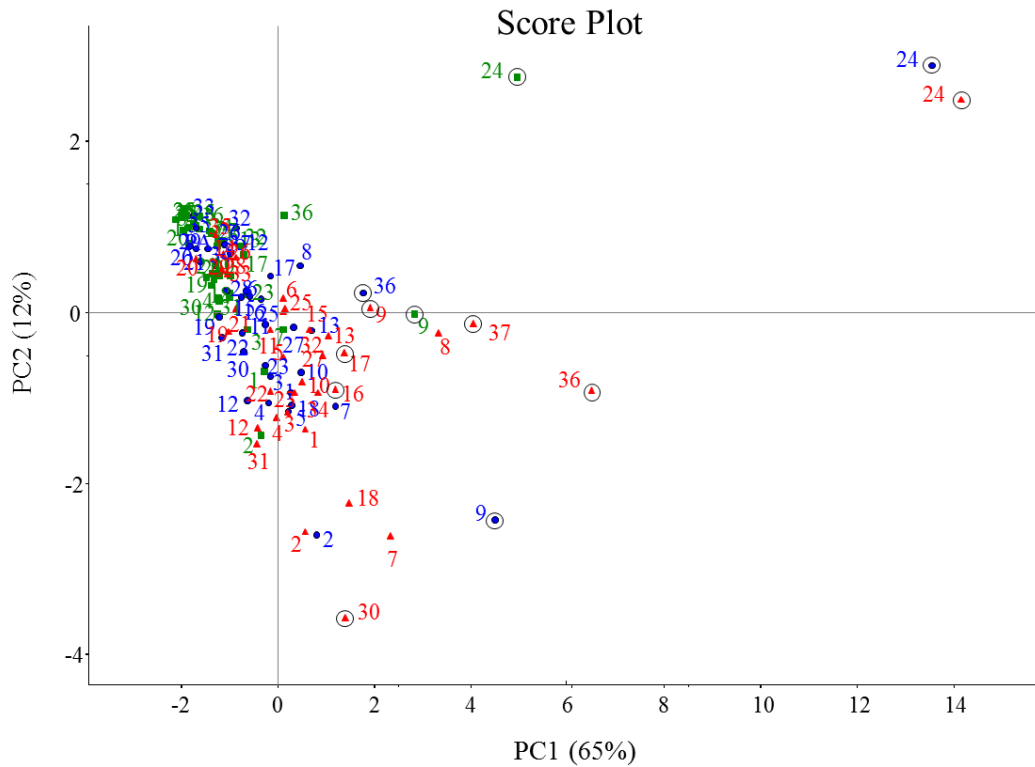


Fig. 70: Score plot for the first component (PC-1, explained variance 65%) and the second component (PC-2, explained variance 12%) of the PCA model. Numbers refer to sampling periods listed in Table 23.

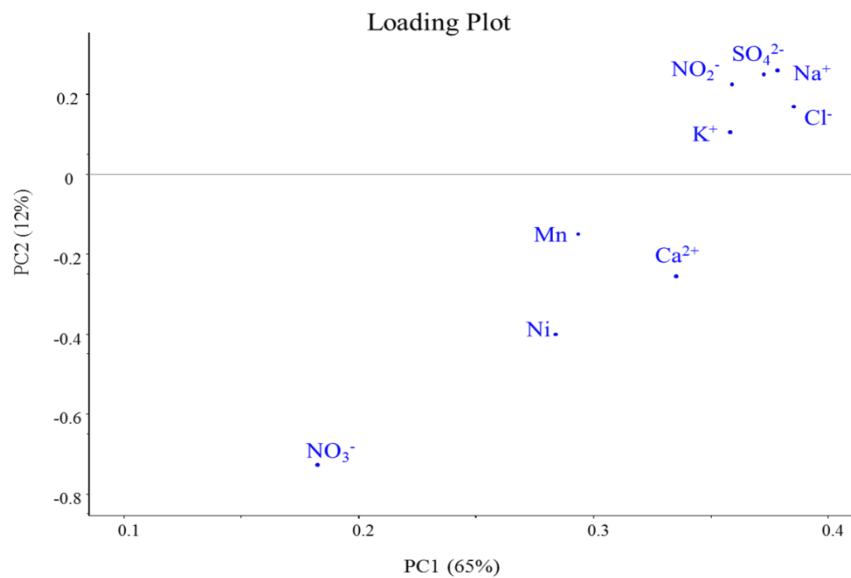


Fig. 71: Loading plot for the first component (PC-1, explained variance 65%) and the second component (PC-2, explained variance 12%) of the PCA model. Experimental variables used for PCA model are Ni, Mn and ions dissolved in run-off water.

Considering the Score Plot (PC1 vs PC2, 77% of explained variance) together with Hotelling's T² Statistics [153], several outliers among samples are observed (circled in Fig. 70); by comparing score and loading plots the unusual behavior of these samples appear mainly affected by aggressive ions, such as NO₃⁻, SO₄⁼ and Cl⁻. Specifically, outliers are placed in the I and IV quadrant of the score plot and mainly refer to the periods characterized by extreme meteorological events (section 6.2.1), pointing out their strong influence on metal dissolution. Even leaving out from computation the identified outliers, the overall results of data exploration do not significantly change; moreover, as in environmental studies also extreme values may add useful information for describing a process or a particular trend, it was decided to include all the outliers in the discussion.

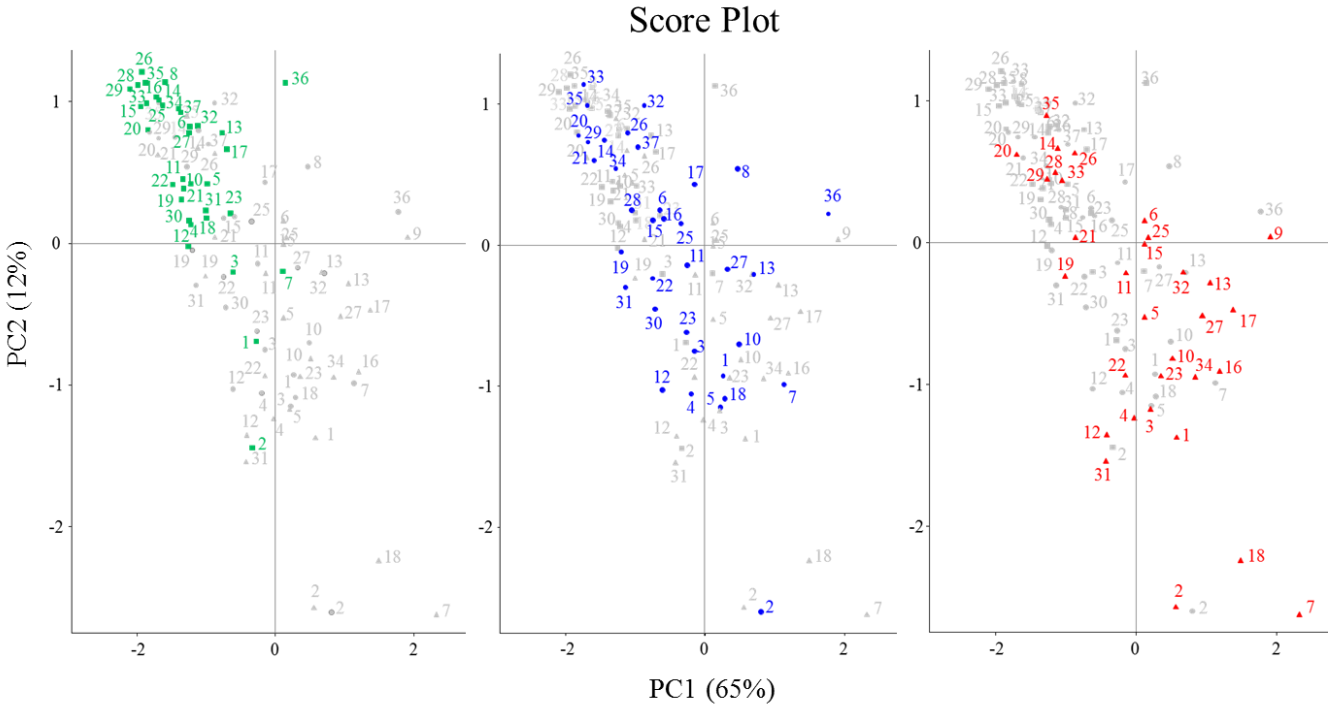


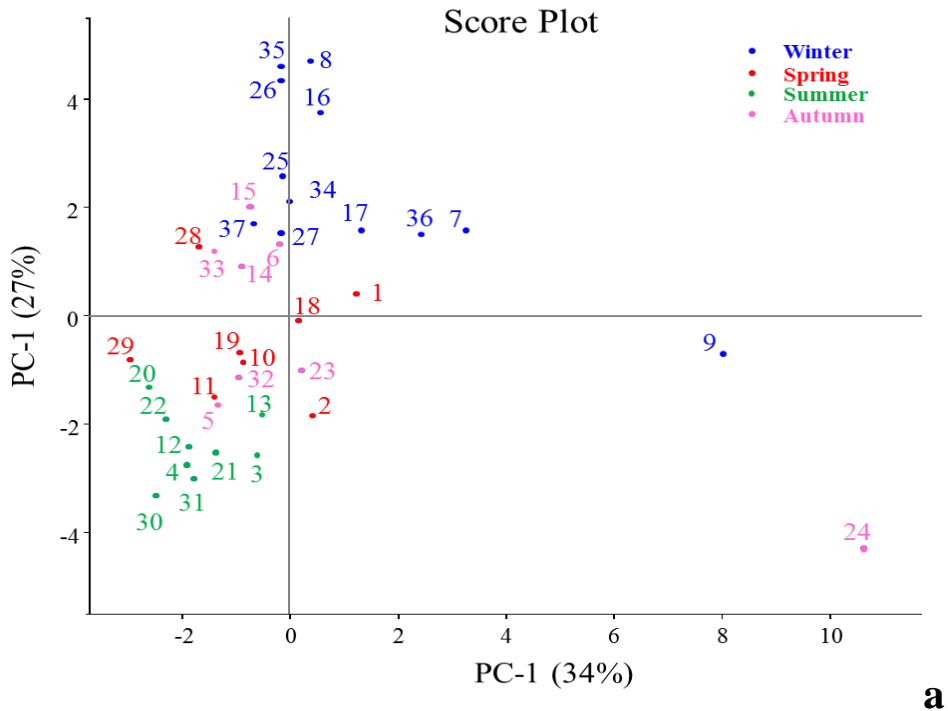
Fig. 72: Score plot for the first (PC-1) and the second component (PC-2) of the PCA model.

Numbers in the score plot refer to sampling periods listed in Table 23 (Summer/Spring: 1-4, 10-13, 18-22, 28-31; Winter/Autumn: 5-9, 14-17, 23-27, 32-37).

Remaining objects in score plot are organized in such a way that bare samples form a compact group in the second quadrant of the graph, whereas pre-patinated samples (with or without wax) are arranged in a less compact way around the axes origin (Fig. 72); this higher dispersion could be related to a lower homogeneity of patinas developed on artificially corroded substrates.

This arrangement confirms the higher variability in the corrosion behavior of WS, due to pre-patination procedures; moreover a slight separation between samples referring to summer and winter periods can be pointed out.

To assess which factors mainly affect this seasonal dependence of metal dissolution, further chemometric investigations were performed for each single finish, including environmental variables in the computation (score and loading plots for bare samples is shown in Fig. 73). Summer samples reveal to be mostly affected by temperature and solar radiation, while winter samples by TOW and atmospheric particulate matter.



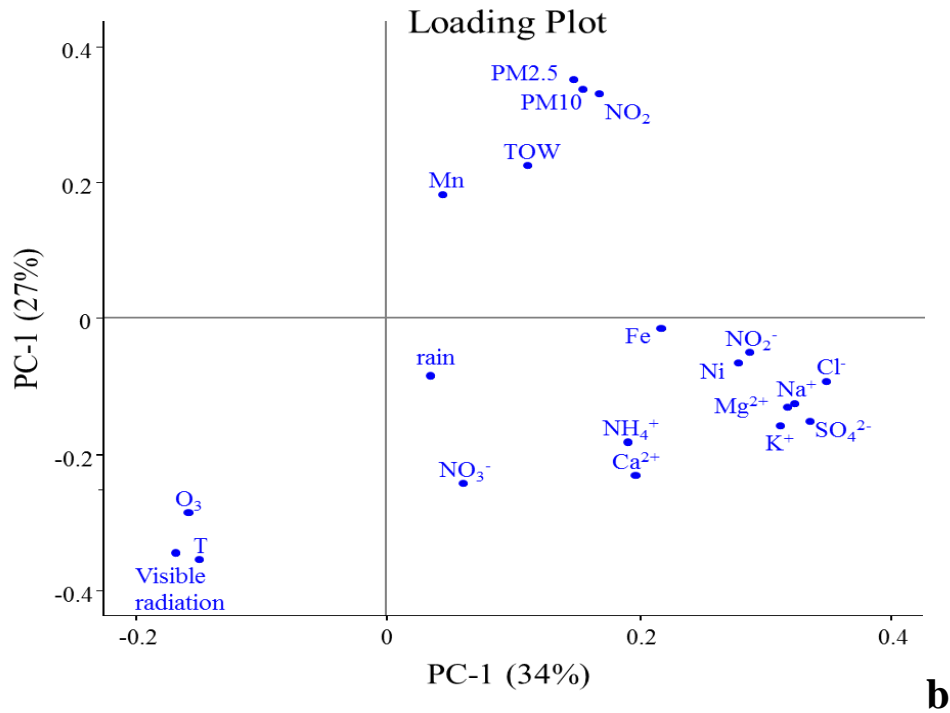


Fig. 73: Score (a) and loading (b) plot for the first (PC-1, explained variance 34%) and the second component (PC-2, explained variance 27%) of the PCA model performed on data referring to bare (BA) samples; the model was run using dissolved Fe, Mn, Ni and ions and environmental data (temperature, visible radiation, wind intensity, rain amount, TOW, PM10, PM2.5, O₃) as experimental variables. Numbers in the score plot refer to sampling periods listed in Table 23 (Summer/Spring: 1-4, 10-13, 18-22, 28-31; Winter/Autumn: 5-9, 14-17, 23-27, 32-37).

3W-PCA (Fig. 74), taking into account the time factor beside samples and measured variables, confirms the separation between bare and pre-patinated samples; moreover, a greater distance between PA and PWA samples is highlighted.

In the plot, the first axis (PC1) is clearly related to the influence of atmospheric ions on WS corrosion, with marine inorganic ions (particularly Cl⁻, Na⁺ and SO₄²⁻) affecting metal dissolution. The action of these ions changes with regard to surface finish, producing an higher metal release from pre-patinated and pre-patinated/waxed samples.

Considering the mode referring to time factor, the separation between summer and winter samples, not very evident from conventional PCA results, is here more marked. This seasonal variation in Fe, Mn and Ni runoff clearly acts on increasing dissimilarities between bare and pre-patinated samples, with a higher influence of the winter season on metal dissolution.

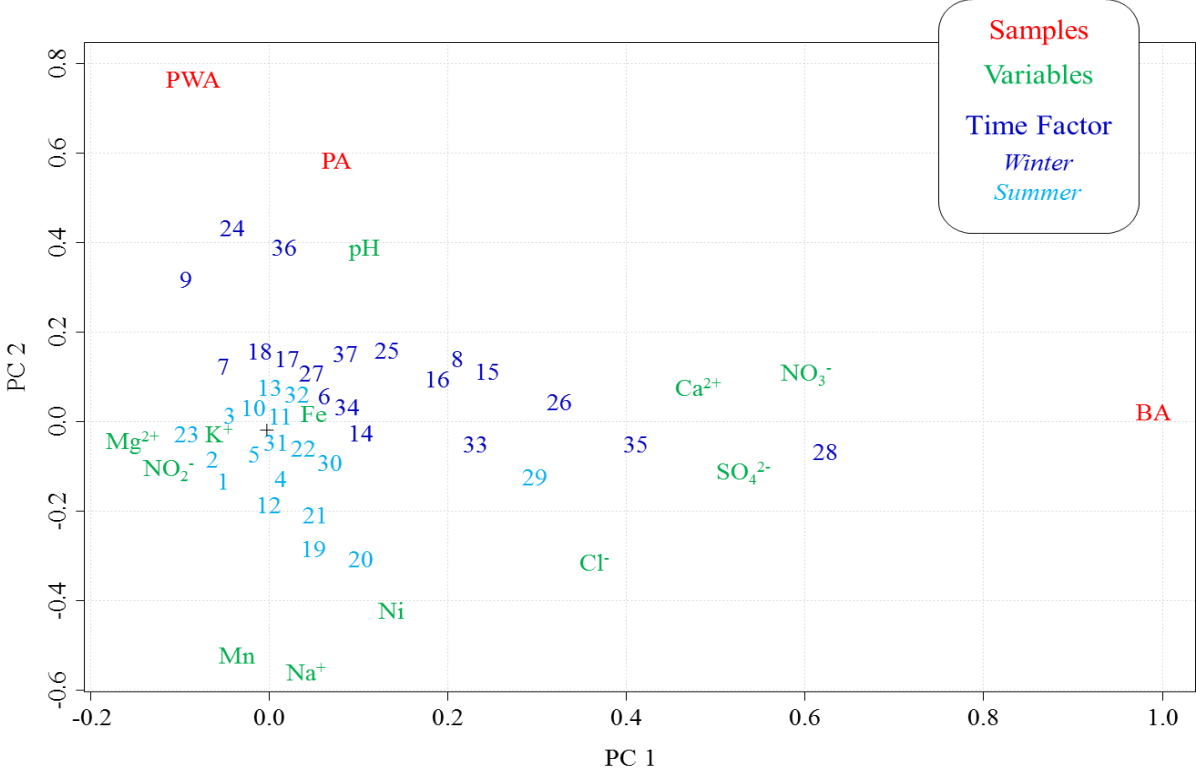


Fig. 74: Triplot for the first and the second component of the 3W-PCA model, showing the results for all three modes (samples, variables and time factor). Numbers refer to sampling periods reported in Table 23 (Summer/Spring: 1-5, 10-13, 19-23, 29-32; Winter/Autumn: 6-9, 14-18, 24-28, 33-37).

6.3 Accelerated ageing test (Cebelcor)

Field exposure of WS in Rimini demonstrated that, beside the action of environmental factors and meteorological events, saline compounds, e.g. chlorides, strongly affect both the features of surface rust and metal runoff.

The action of compounds, such as Cl^- , NO_3^- and SO_4^{2-} , that represent the main ionic constituents of particulate matter formed in coastal and urban areas or in sites where large use of de-icers is made [154], has been evaluated by several authors on materials other than weathering steel [155]–[157]. Even when WS performances were evaluated, the effect of only one of these compounds was considered [158], [159].

Therefore, in the second part of this work, the attention was focused on the evaluation and comparison of possible effects that main saline constituents of PM may have on WS corrosion; this was achieved by means of accelerated ageing test (Cebelcor) and complete characterization of corrosion products and weathering solutions.

The effect of different weathering solutions and concentrations on Cor-Ten A steel was evaluated through corrosion potential measurements, analysis of metal release, mass loss determination and corrosion products characterization; as WS is widely used for art and architecture thanks to its aesthetical aspect, evaluation of aesthetical evolution of samples during test was also performed.

6.3.1 General consideration on patinas

As for morphology and composition, the exposure environment also affects the aesthetical appearance of WS; so, the examination of patina appearance allows evaluating the aggressivity of the medium.

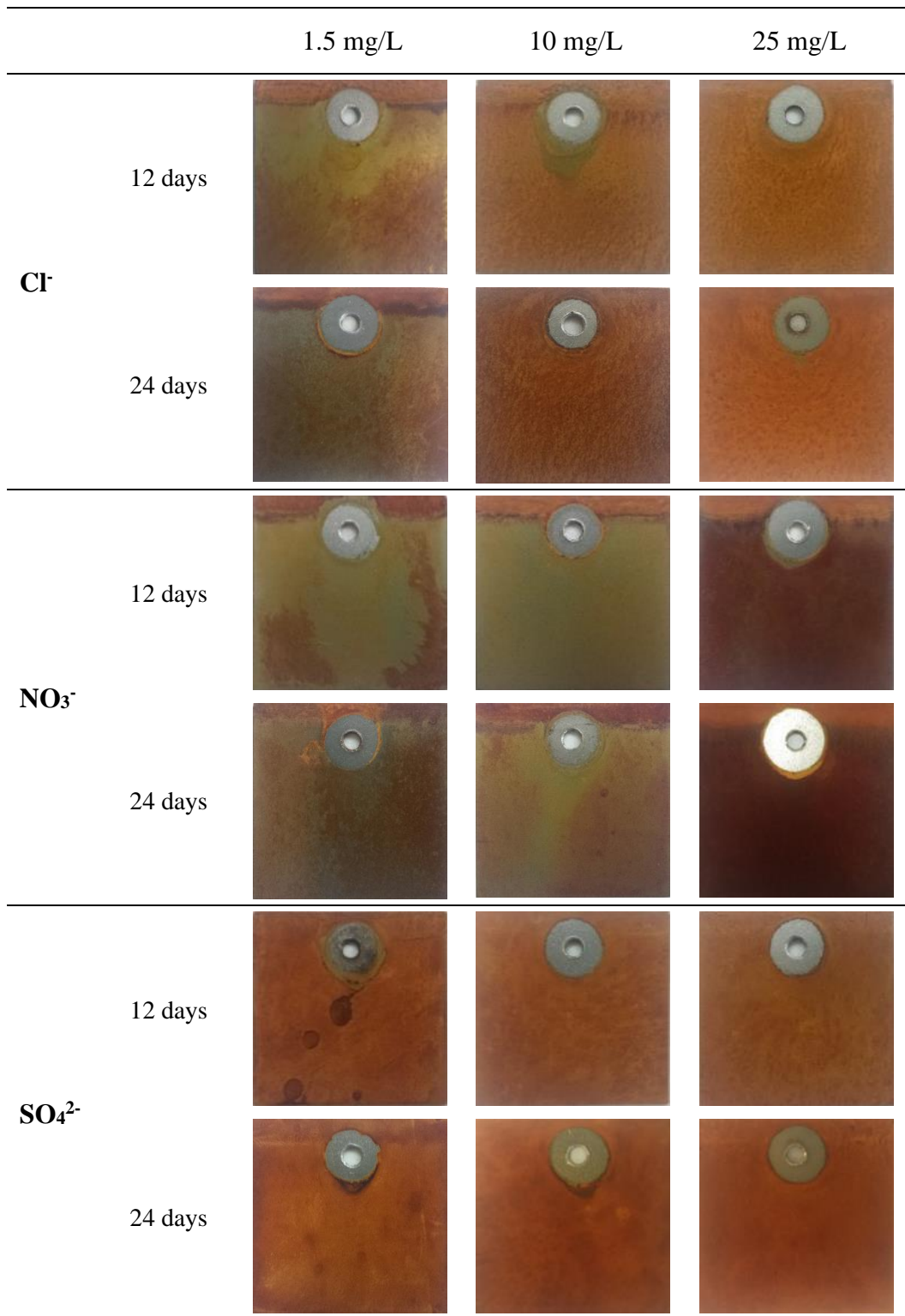


Fig. 75: Aesthetical appearance of WS samples aged in Cl⁻, NO₃⁻ and SO₄²⁻ solution for 12 and 24 days

As shown in Fig. 75, corrosion layers formed on WS after immersion / emersion test appear very different and strongly dependent on testing time and both composition and concentration of

weathering solution. It's easy to see that the corrosive attack of Cl^- and SO_4^{2-} , considered as the most aggressive ionic species for WS, is certainly higher than that of NO_3^- ; almost all specimens aged in nitrate solutions present large non-corroded areas, while corroded parts are mainly localized in the portion where weathering solution accumulates during the drying phase. Only the exposure to high concentration of nitrate ions leads to the creation of a brownish and fairly homogeneous patina.

The effects of chlorides and sulphates are more pronounced even at smaller concentration. Ageing in presence of Cl^- produces patinas gradually more uniform with increasing testing time and solution concentration.

It is a different matter for patinas formed in sulphate solution: in this case, specimens appear completely covered by an orange layer of corrosion products, since the early cycles of immersion / emersion in the solution; the degree of surface covering does not seem to be much affected by concentration of solution.

Further information about the evolution of the color of patinas formed on WS during the test can be obtained through spectrophotometric color measurements (Datacolor D400 spectrophotometer); data recorded were elaborated in the CIE L^* a^* b^* color space, where three parameters are identified:

- the lightness (L^*) is defined as the luminous intensity of a colour, ranging from the darkest black ($L^* = 0$) to the brightest white ($L^* = 100$);
- the a^* and b^* parameters are the chromatic coordinates; particularly, a^* represents the red/green ratio, with positive values indicating red and negative values indicating green, and b^* represents the yellow/blue ratio, with positive values standing for yellow and negative values for blue.

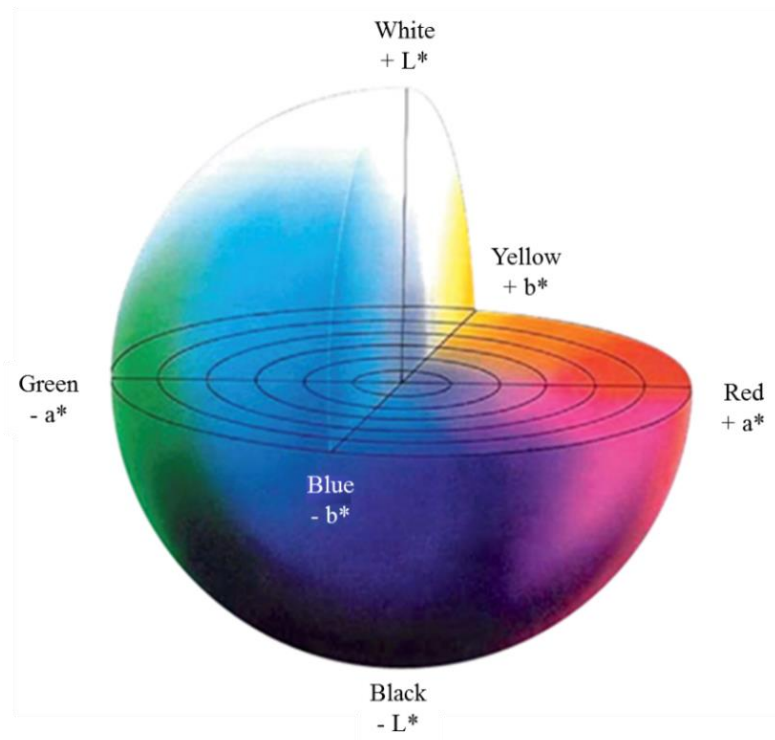


Fig. 76: CIE L* a* b* colour space [160]

The difference between two colours is then expressed as Euclidean distance, according to:

$$\Delta E = \sqrt{(\Delta L^*)^2 + (\Delta a^*)^2 + (\Delta b^*)^2} \quad (45)$$

$\Delta E \leq 3$ can be assumed as a perceptibility threshold for outdoor architecture [161].

Results of color measurements, reported in Table 24, indicate that, with increasing testing time, patinas formed in the presence of Cl^- and SO_4^{2-} tend to increase more in the red (a^*) and in the yellow (b^*) components than patinas formed on samples aged in nitrate solutions, that, on the contrary, become darker (L^* decreases).

Table 24: CIE L* a* b* parameters and ΔE values for Cor-Ten A samples before, during (12 days) and after (24 days) immersion/emersion in SO_4^{2-} , Cl^- and NO_3^- solution. L*, a* and b* represent the lightness, the red/green and the yellow/ blue axis, respectively; ΔE is calculated as

$$\Delta E = \sqrt{(\Delta L^*)^2 + (\Delta a^*)^2 + (\Delta b^*)^2}$$

Solution	L*	a*	b*	ΔE
Bare Cot-Ten A	48.8	0.5	1.7	
SO_4^{2-} 1.5 ppm (12d)	46.1	27.4	36.5	44.0
SO_4^{2-} 1.5 ppm (24d)	43.7	28.2	36.7	44.9
SO_4^{2-} 10 ppm (12d)	45.8	26.7	38.2	45.0
SO_4^{2-} 10 ppm (24d)	41.2	28.1	34.3	43.4
SO_4^{2-} 25 ppm (12d)	45.6	26.9	38.5	45.4
SO_4^{2-} 25 ppm (24d)	43.0	28.0	36.5	44.7
Cl^- 10 ppm (12d)	44.7	20.7	30.6	35.5
Cl^- 10 ppm (24d)	47.8	25.3	38.1	44.0
NO_3^- 1.5 ppm (12d)	48.5	5.4	25.9	24.7
NO_3^- 1.5 ppm (24d)	35.3	10.9	22.8	27.1
NO_3^- 10 ppm (12d)	48.4	3.3	27.4	25.8
NO_3^- 10 ppm (24d)	39.1	15.7	15.5	22.7
NO_3^- 25 ppm (12d)	28.0	16.8	20.8	32.6
NO_3^- 25 ppm (24d)	28.8	17.1	15.0	29.2

6.3.2 Open Circuit Potential (OCP)

Measurements of open circuit corrosion potential allow to follow the evolution and the passivation grade of the corrosion products layer during the entire test. To understand if patina formed on WS shows a protective ability, the Pourbaix diagram (Fig. 77) of Fe/H₂O system has to be considered.

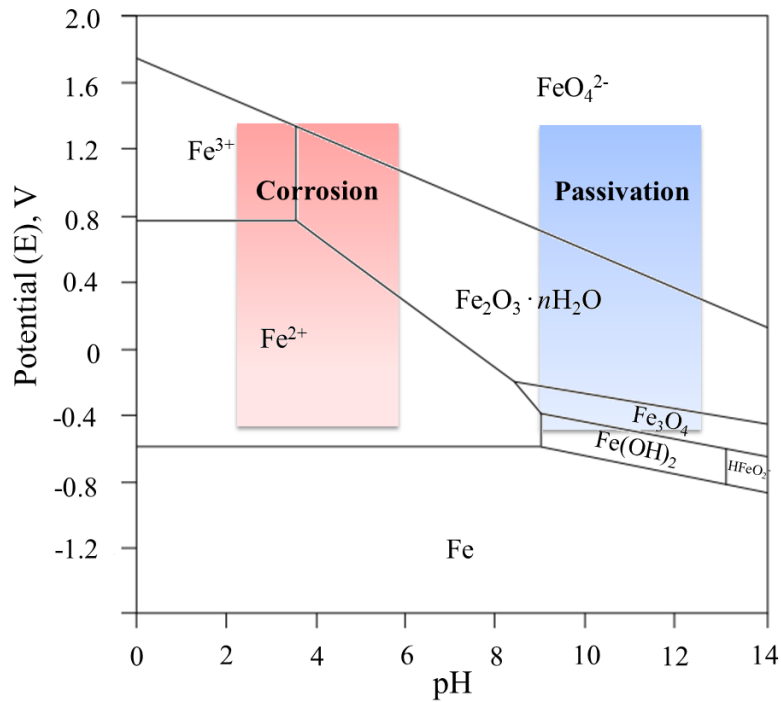


Fig. 77: Pourbaix diagram of Fe/H₂O system at 25 °C, showing the areas of activity and passivation

Pourbaix demonstrated that the passivity range at neutral pH corresponds to the formation of Fe₂O₃ and, on the other hand, that this layer exhibits a real protective ability only if the corrosion potential exceeds the threshold value of 200 mV [162].

Fig. 78 shows open circuit corrosion potential trends of WS in each tested solution; the more the value becomes higher, the more stable and protective the corrosion layer is considered.

The shape of curves strongly depends on the composition and the concentration of the weathering solution. Even though all the samples undergo an anodic polarization (corrosion potential becomes nobler with time), no one of them overcomes the threshold value of 200 mV.

The samples that came closest to it after 24 days of test are the ones aged in NO_3^- solution at very low concentration (showing a linear trend) and in SO_4^{2-} solution at middle-high concentration (asymptotically approaching the threshold value).

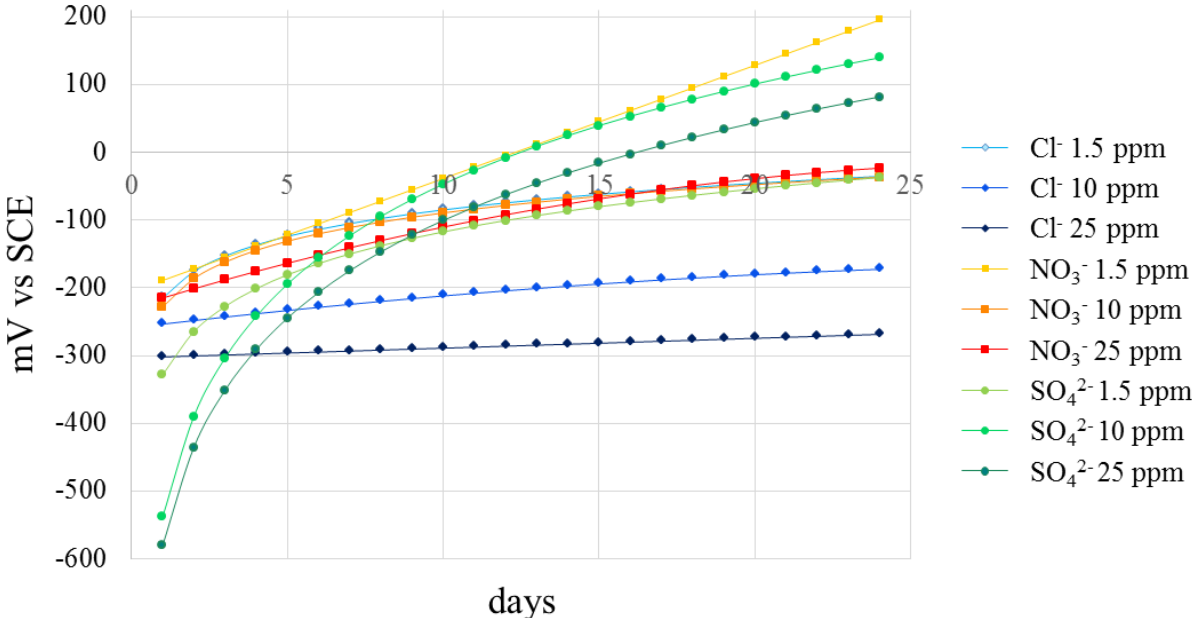


Fig. 78: Evolution of open circuit corrosion potential for WS samples aged in Cl^- (blues), NO_3^- (oranges) and SO_4^{2-} (greens) during the Cebelcor test

The correlation between concentration and protection ability of patinas is particularly clear in the case of Cl^- : with the increase in chloride concentration, the anodic polarization decays sharply and the corrosion potential stabilizes to more negative values, indicating patinas are gradually less protective.

This dependence is no longer observed for NO_3^- and SO_4^{2-} solutions: in fact, specimens aged in nitrate and sulphate solutions at middle-high concentration (10 and 25 ppm) show very similar corrosion potential trends, both in shape and final values. The behaviour of samples aged in the solution of these salts with a lower concentration (1,5 ppm) is quite different: the ones tested

in NO_3^- solution undergo a linear increase in corrosion potential, up to nearly 200 mV; the corrosion potential of samples aged in SO_4^{2-} solution, instead, stabilizes to lower values.

6.3.3 Mass loss determination

Mass loss determination (Fig. 79 - Fig. 80) represents a valid method for evaluating the corrosivity of the exposure environment and to quantify the amount of corroded material.

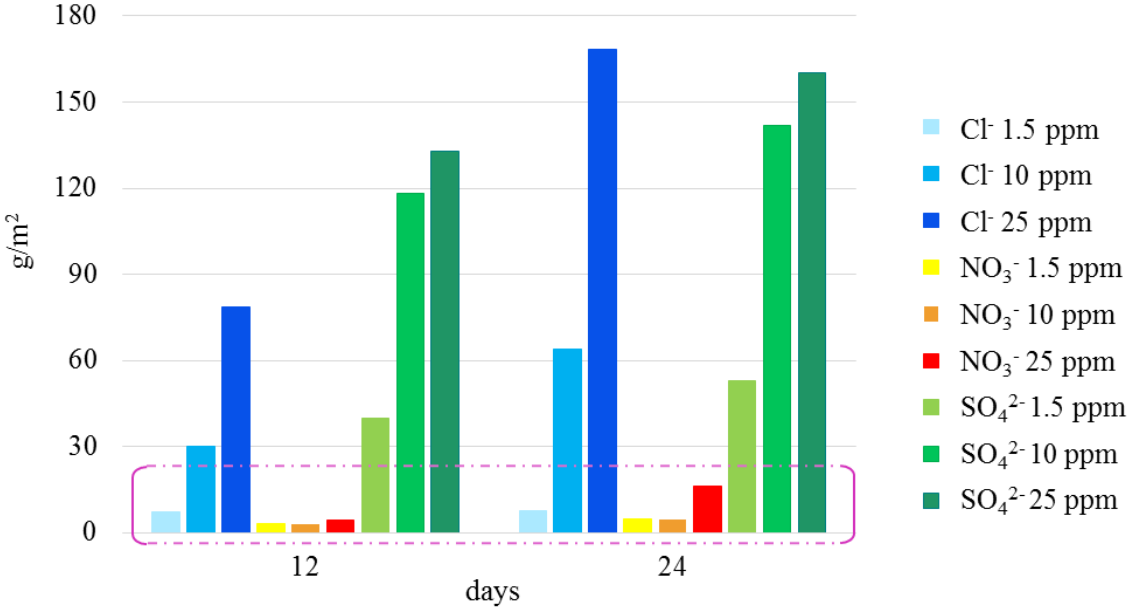


Fig. 79: Mass loss of weathering steel aged in chloride (blues), nitrates (oranges) and sulphates (greens) solution for 12 and 24 days of Cebelcor test

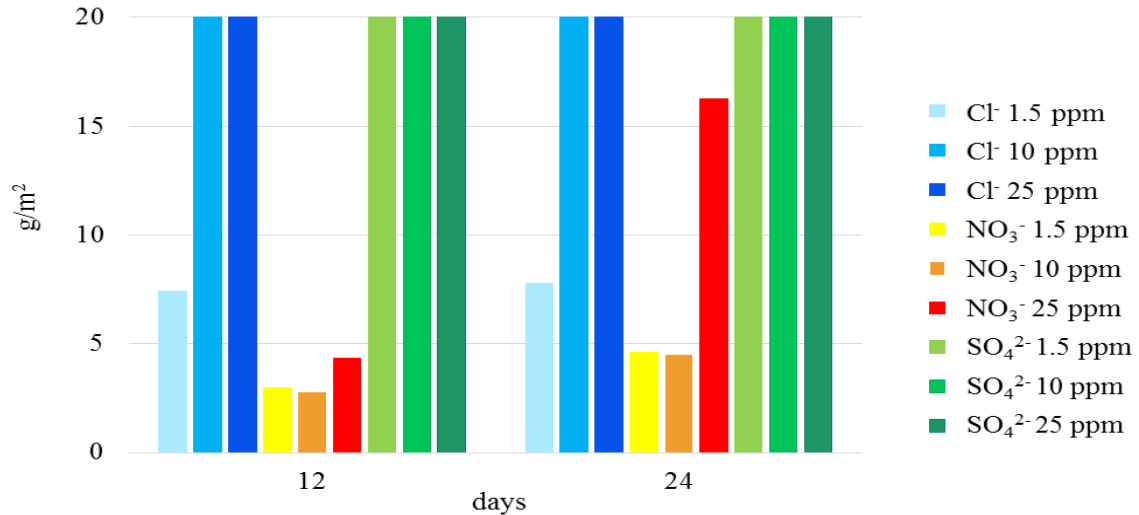


Fig. 80: Detail of Fig. 79

In general terms, specimens aged in NO_3^- solution suffer the lower mass loss, demonstrating its low aggressiveness. Mass loss of samples submerged in 1,5 and 10 ppm solutions appear similar; only by overcoming a threshold value (between 10 and 25 ppm), nitrate ions begin influencing the corrosion process, especially at higher test times.

SO_4^{2-} solutions produce a mass loss that is not particularly affected by TOW (double in testing time promotes only an increment in mass loss of an average value of 20%). Moreover, the mass loss shows a logarithmic growth with increasing concentration.

Samples aged in Cl^- solution, instead, undergo to a mass loss that grows exponentially with increasing concentration and doubles at longer time of wetness. 25-ppm Cl^- solution, as expected, is the most aggressive medium, producing the highest mass loss.

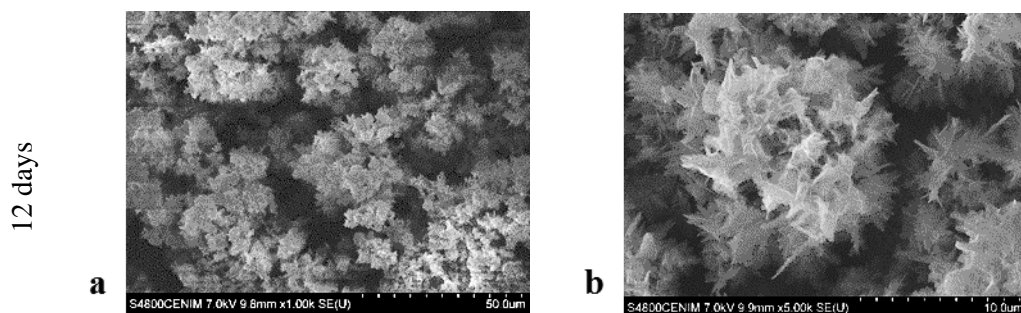
6.3.4 Characterization of corrosion products

Even though monitoring open circuit potential during test gives useful information about the stability of patinas on WS, evaluations on passivation grade and, thus, protective ability of corrosion products cannot be restricted solely to this. That's why a complete characterization of patinas formed on Cor-Ten samples during the test was performed by means of SEM-EDS (sections 5.5.3) and 5.5.4 and XRD (section 5.5.6) analysis.

In the next sections, results of surface investigation will be presented and discussed to better appreciate the influence of different testing times, weathering solutions and concentration on WS corrosion.

6.3.4.1 The effect of Time of Wetness (TOW)

In order to evaluate the effect of time, particularly time of wetness, on the composition and morphology of patinas, SEM-EDS and XRD investigations were performed on WS specimens aged in 25 ppm chloride solution for 12 and 24 days. As shown in Fig. 81 **Errore. L'origine riferimento non è stata trovata.**, both of the samples appear covered by sandy crystals of lepidocrocite, with mean diameter of $\sim 10 - 20 \mu\text{m}$.



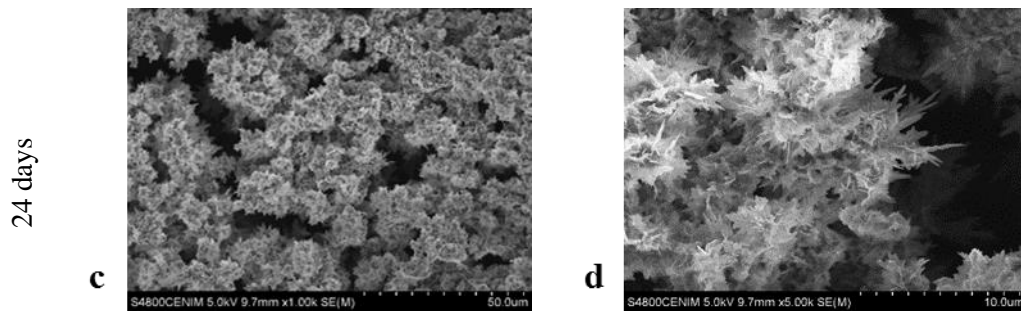


Fig. 81: SEM images of WS samples aged in 25 ppm Cl^- solution for 12 days (a. 1000x and b. 5000x) and 24 days (c. 1000x and d. 5000x).

The increase in time of wetness produces an increase in homogeneity of patina and acts on the degree of coverage of surface.

XRD analysis (Fig. 82) adds other information to the topic: the main components of patinas formed after 12 and 24 days of test are lepidocrocite and hematite; with increasing testing times, lepidocrocite relative percentage diminishes in favor of hematite's.

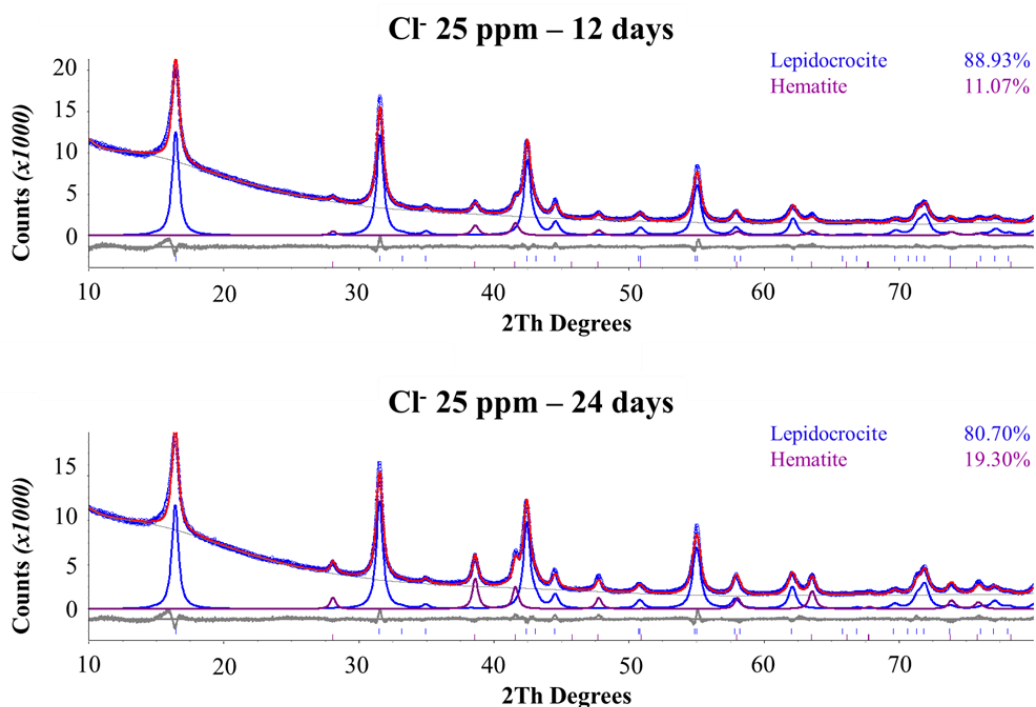


Fig. 82: X-ray diffractogram of corrosion products formed on WS samples aged in 25 ppm Cl^- solution for 12 days (top) and 24 (bottom) days

6.3.4.2 The effect of concentration

In order to evaluate the effect of the concentration of aggressive species on WS, patinas formed on samples aged in differently concentrated chloride solution were analysed.

Fig. 83 shows SEM micrographs of specimens aged in 1.5 ppm (a-b), 10 ppm (c-d) and 25 ppm (e-f) chloride solutions, respectively. In all cases, lepidocrocite is the main corrosion product found. At low concentration of Cl^- , WS surface after 24 days of test appears homogeneously covered by lepidocrocite, which is characterized by small hexagonal crystals (Fig. 83b, 30000X), growing perpendicular to the surface.

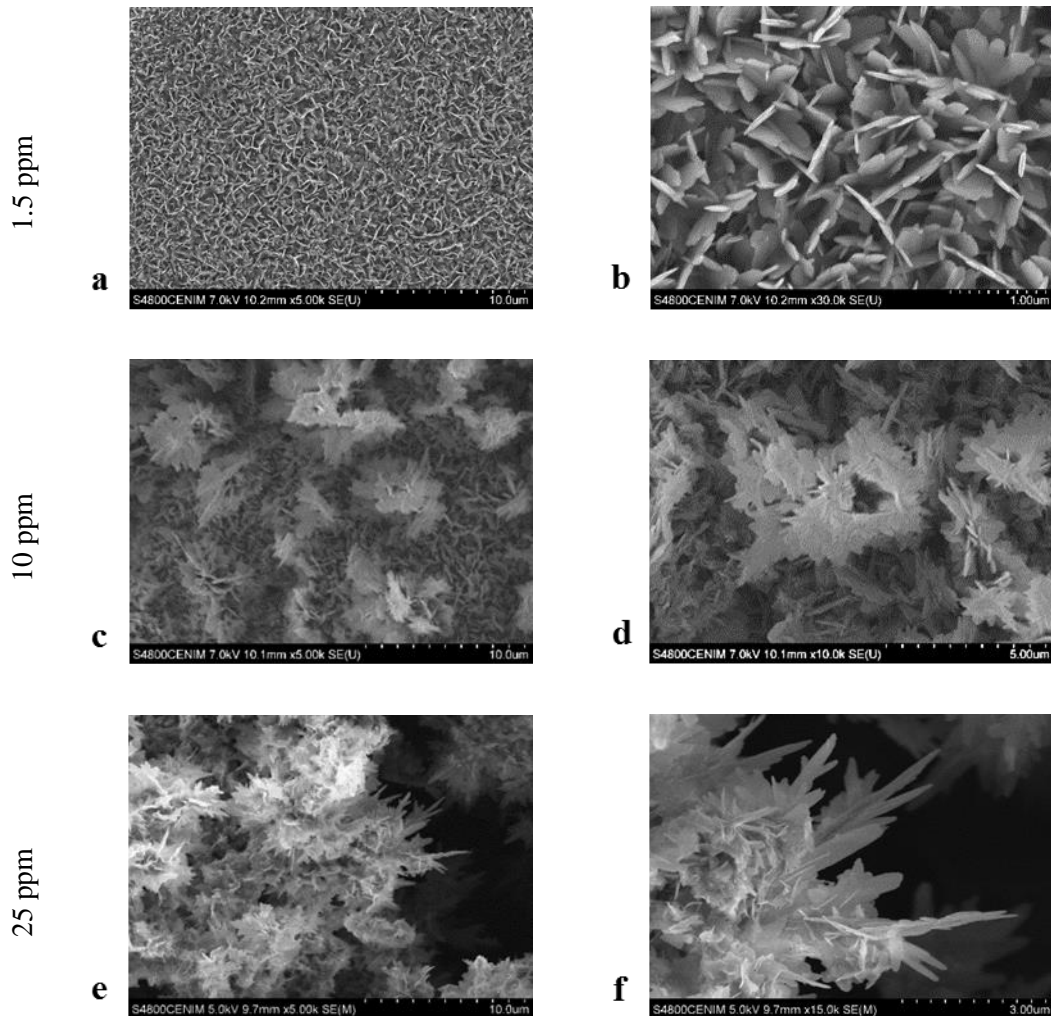


Fig. 83: SEM images of WS samples aged in 1.5 ppm (a-b), 10 ppm (c-d) and 25 ppm (e-f) Cl^- solutions for 24 days.

The increase in concentration acts on the degree of coverage of surfaces, beside affecting the morphology of corrosion products: in medium-concentrated chloride solutions, flowery structures of lepidocrocite (Fig. 83d, 10000X) lay down on the hexagonal crystals ‘carpet’, up to getting predominant at higher concentration (Fig. 83e). Finally, as for time of wetness, concentration also acts on the conversion of lepidocrocite into hematite, as shown in Fig. 84.

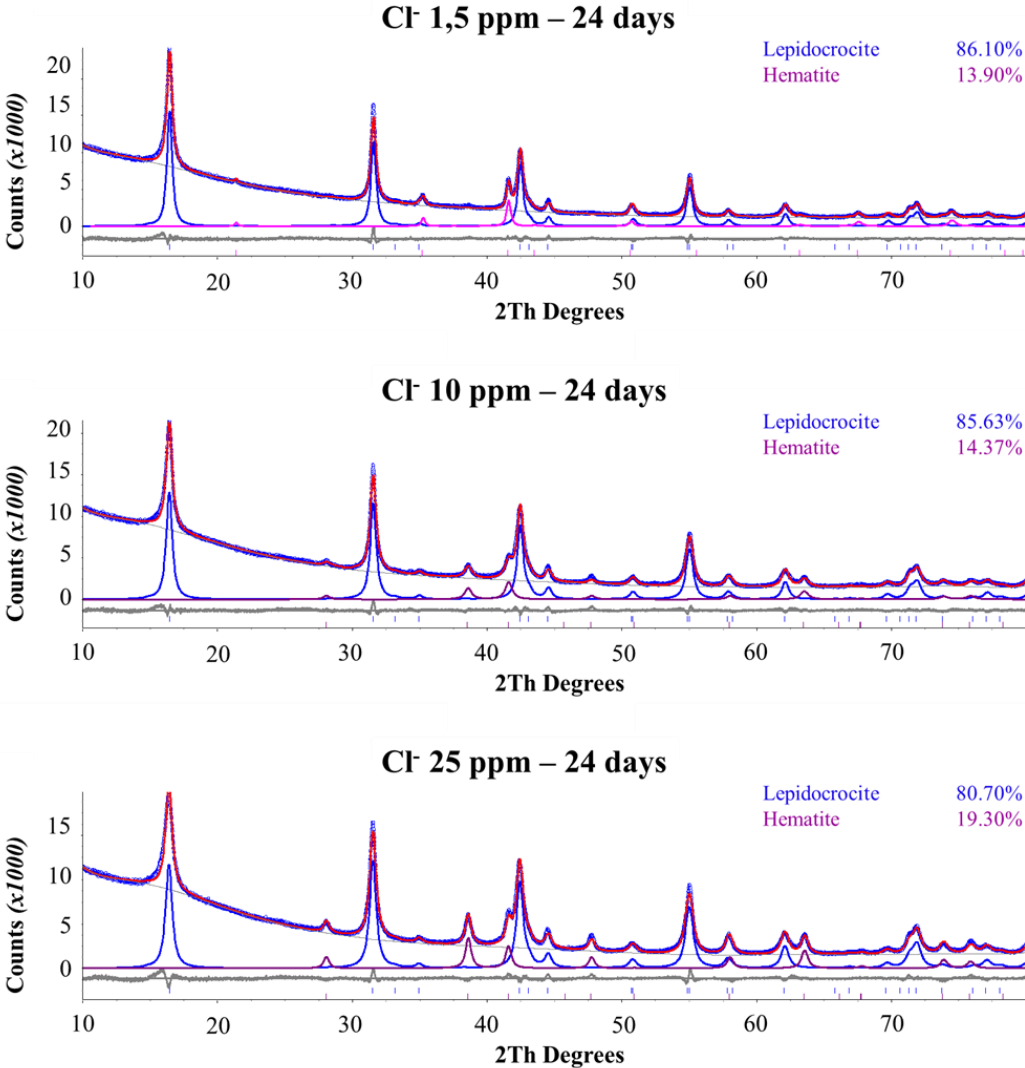
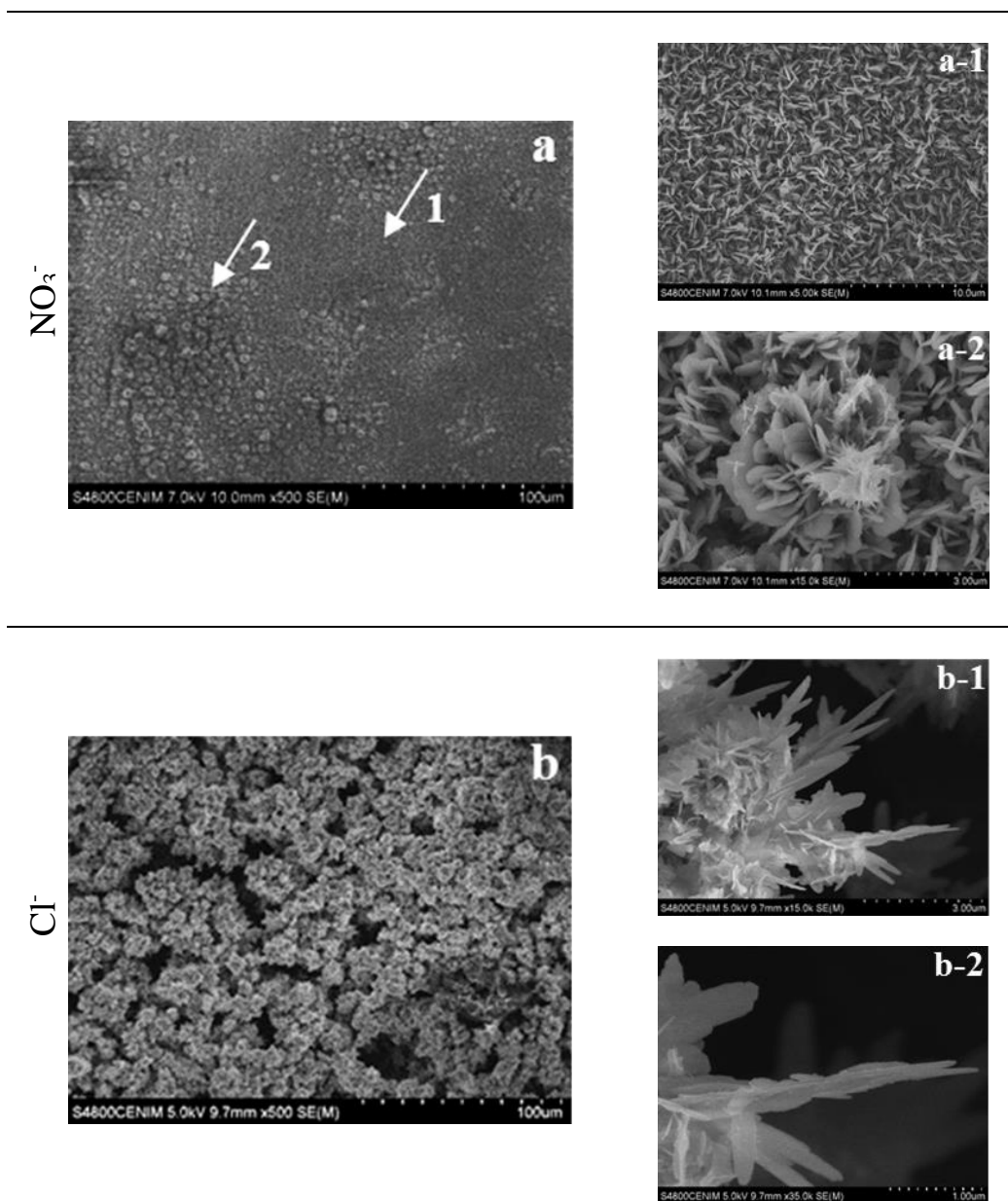


Fig. 84: X-ray diffractogram of corrosion products formed on WS samples aged in 1.5 ppm, 10 ppm and 25 ppm Cl⁻ solutions for 24 days

6.3.4.3 The effect of weathering solution

Finally, SEM analysis were performed on samples aged in concentrated (25 ppm) nitrate, chloride and sulphate solutions, to identify the possible differences in composition and morphology of patinas due to exposure to different weathering solutions; results are shown here below (Fig. 85).



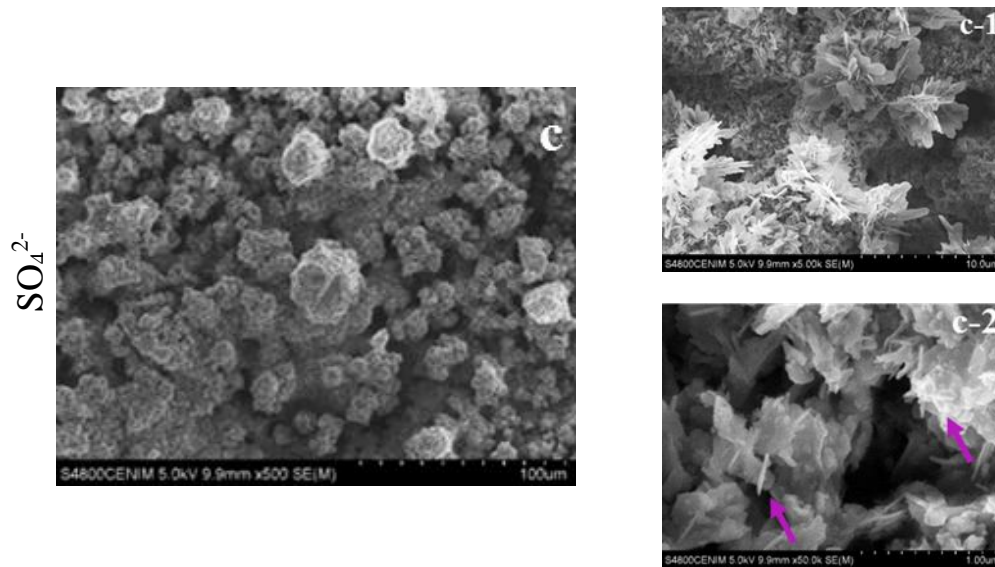


Fig. 85: SEM images of WS samples aged in 25 ppm nitrate (a), chloride (b) and sulphate (c) solutions for 24 days

Once again, nitrate solution results the least aggressive among those tested; even at high concentration (25 ppm), it produces uneven and non-homogeneous patina, where two different areas can be distinguished. The first area (Fig. 85 a-1) is characterized by hexagonal crystals of lepidocrocite, just like patina formed on specimen aged in presence of low Cl^- concentration. The second area (Fig. 85 a-2), instead, appear more complex, presenting flowery crystals of lepidocrocite in addition to hexagonal crystals; moreover, traces of rounded sheets of hematite are also identified, as confirmed by XRD (Fig. 86).

The other weathering solutions appear more aggressive, leading to the formation of more complex and evolved corrosion layers. Surfaces aged in Cl^- (Fig. 85 b) and SO_4^{2-} (Fig. 85 c) solutions are completely covered by sandy and flowery crystals of lepidocrocite.

Crystals growing in presence of sulphates show higher mean diameter (~ 20 μm) compared to those growing in chloride solution and give rise to a more porous patina. On the contrary, chloride promotes the formation of agglomerates of smaller crystals (~ 10 μm) of lepidocrocite, thus reducing porosity of corrosion product layer. WS sample aged in SO₄²⁻ solution is the only one presenting needle-shaped structures of goethite in its corrosion layer, as also confirmed by XRD (Fig. 86); in fact, sulphate ions, if present in relative small amounts, are able to promote and accelerate the transformation of lepidocrocite in goethite [163].

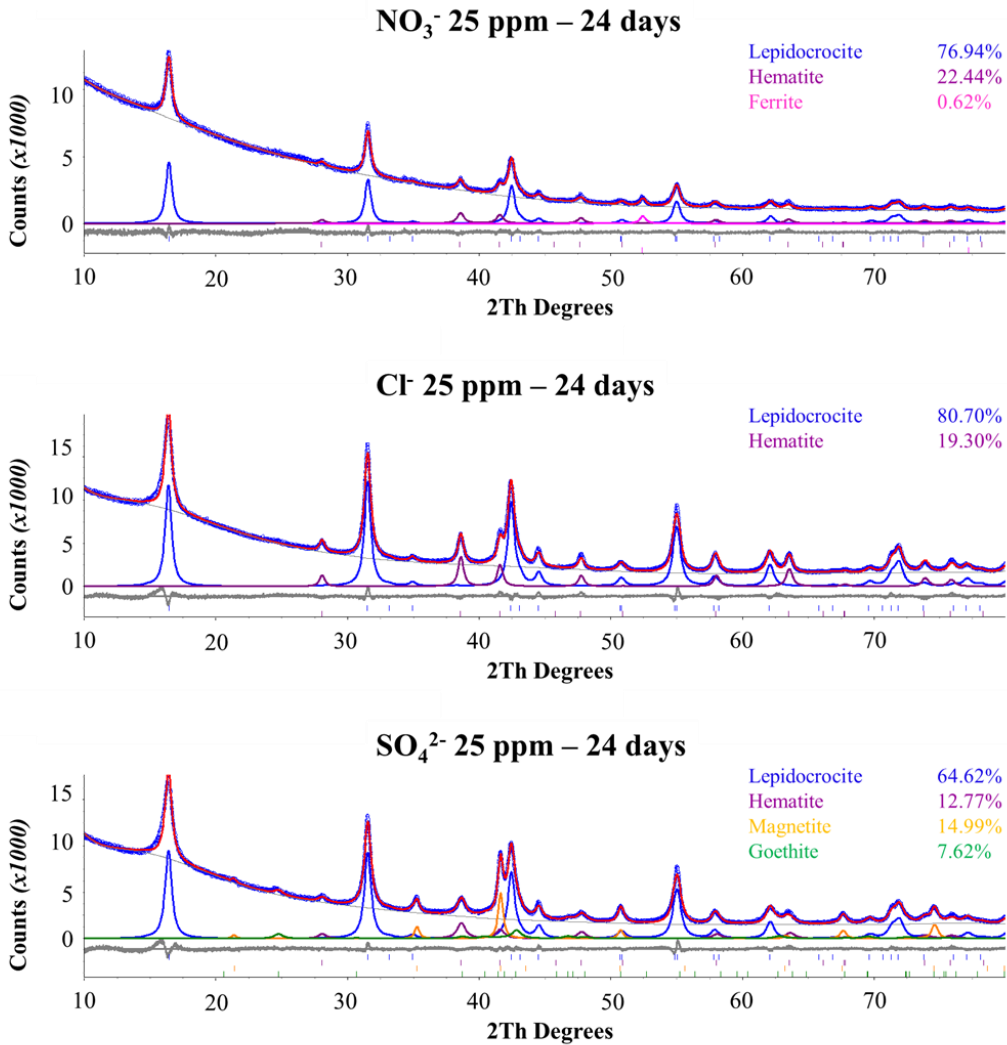


Fig. 86: X-ray diffractogram of corrosion products formed on WS samples aged in 25 ppm nitrate, chloride and sulphate solutions for 24 days

6.3.5 Metal analysis

Further information about the features of patinas formed on WS specimens during the test were obtained by means of analysis of metals released in weathering solutions or retained in corrosion product layers; particularly, three different fractions were analysed:

- dissolved fraction, obtained after the filtration of weathering solutions on 0.45 µm membrane filters;
- Non-Adherent Rust (NAR), or particulate fraction, that is the part of corrosion products that is loosely bound to the metal surface and is lost in weathering solutions during the corrosion process;
- Adherent Rust (AR), that is the part of corrosion products tightly bound to the metal surface.

Results of metal analysis performed on weathering (section 6.3.5.1) and pickling solutions (section 6.3.5.2) will allow to evaluate the effect of different aggressive species on run-off process of alloying metals.

6.3.5.1 Metals release

Metal release was evaluated for each solution and concentration after 6, 12, 18 and 24 days of test. Total and filtered fractions were analysed to assess the amount of main alloying metals (Cr, Cu, Fe, Mn, Ni) in solution and the form in which they are released. Release trends are shown in Fig. 87, Fig. 88, Fig. 89, Fig. 90 and Fig. 91.

Representing the main element of steel, iron, as expected, is the most released metal; aging in aggressive media (Cl^- and SO_4^{2-}) causes comparable release values, but some differences are observed with regard to the influence of time and concentration on the general trend: iron release

appears strongly dependent on the concentration of chloride and only slightly affected by time of wetness; on the contrary, sulphate ions produce an 'immediate' release of iron, then decreasing with the passing of time. As already observed in previous sections, NO_3^- solutions are the least aggressive among the three, causing, at all concentrations tested, iron releases (Fig. 88) that are on average one order of magnitude smaller than those produced during weathering in chloride and sulphate solutions; the general trend of Fe release in nitrate solutions can be described as independent of the concentration and increasing in time. For all solution and concentrations, iron is mainly released in particulate form.

Compared to iron's, manganese and nickel releases, on one hand, and chrome releases, on the other hand, are one and two orders of magnitude smaller, respectively.

Mn and Ni show similar trends of release, strongly affected by weathering solution. Particularly, for samples aged in presence of NO_3^- ions, release is independent of both concentration and testing time; on the contrary, it shows a growing trend with increasing Cl^- concentration, while it slightly decreases with increasing concentration of SO_4^{2-} solution.

With regards to Mn, it is also interesting to note that with increasing concentration of weathering solution the relative percentage of metal released in the dissolved/particulate fraction changes and Mn is mainly released in the dissolved form.

Finally, chrome is almost entirely released as insoluble product, except at high time of test, when it is also found in dissolved fraction but in very low percentage. Cr release trend appears similar for all solutions, while it changes and grows with increasing concentration and weathering time.

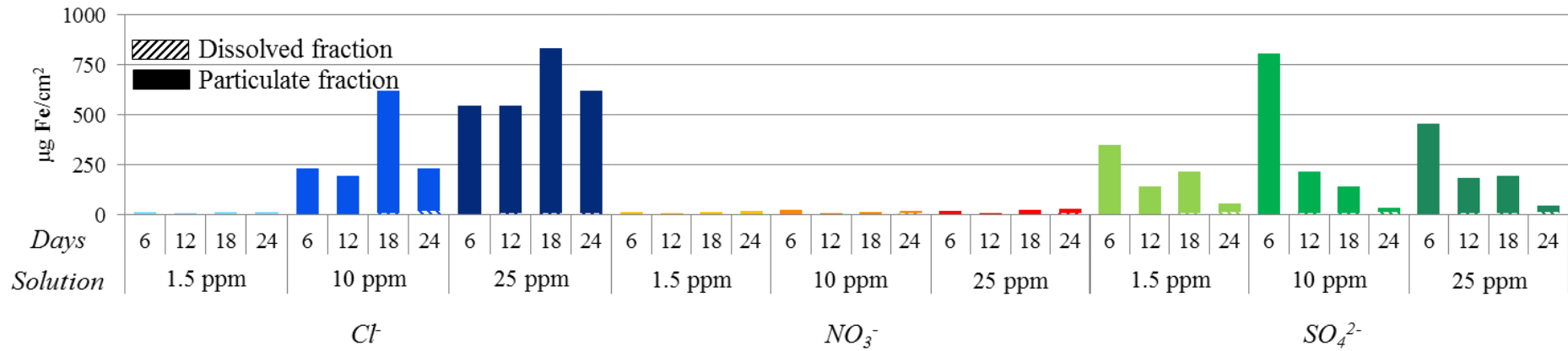


Fig. 87: Fe released by WS aged in chloride (blue), nitrate (orange) and sulphate solutions during immersion/emersion test

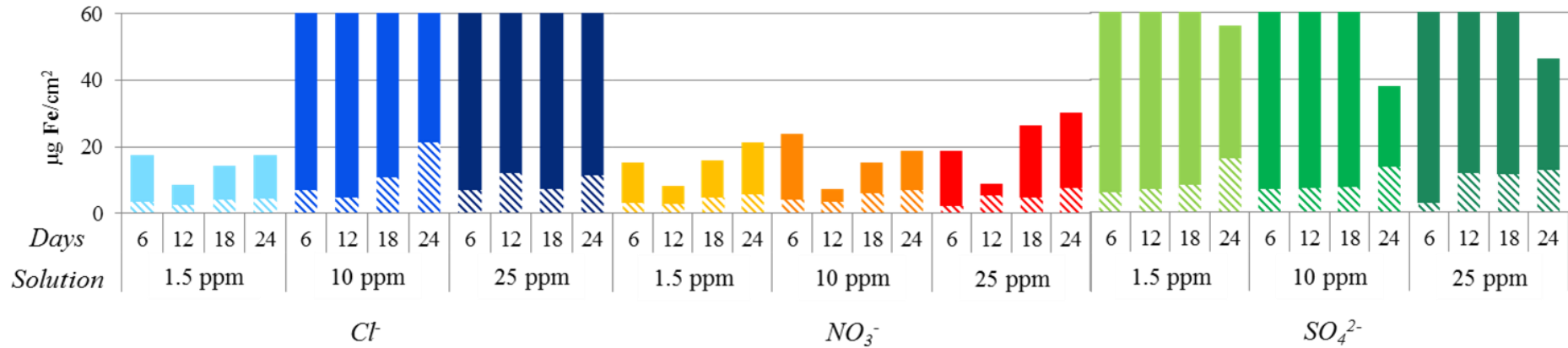


Fig. 88: Detail of Fig. 87 - Fe released by WS aged in chloride (blue), nitrate (orange) and sulphate solutions during immersion/emersion test

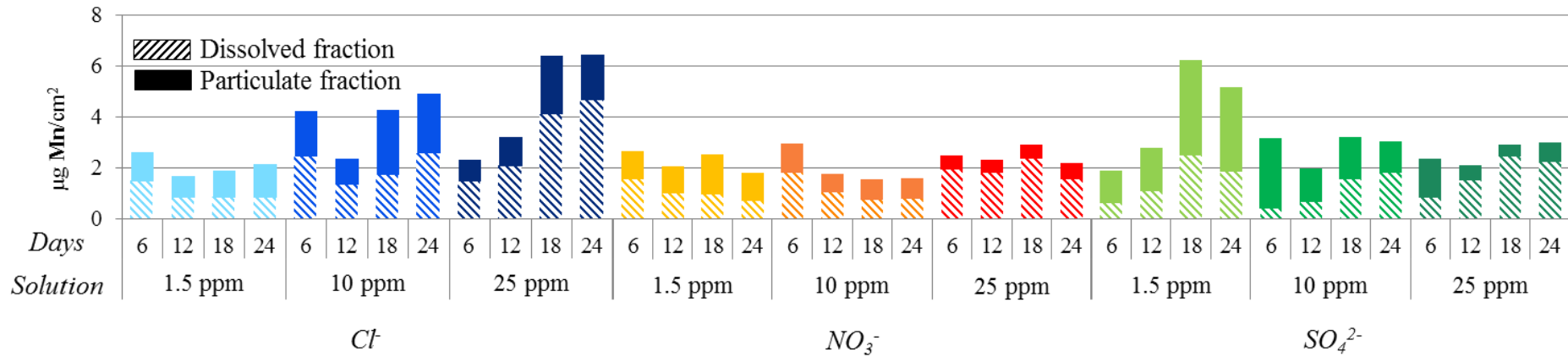
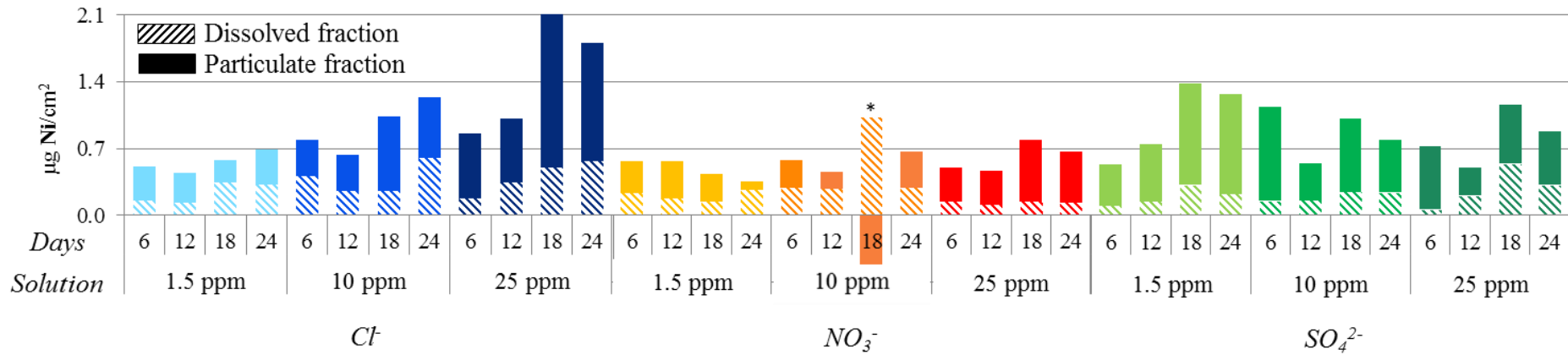


Fig. 89: Mn released by WS aged in chloride (blue), nitrate (orange) and sulphate solutions during immersion/emersion test



* Anomalous value

Fig. 90: Ni released by WS aged in chloride (blue), nitrate (orange) and sulphate solutions during immersion/emersion test

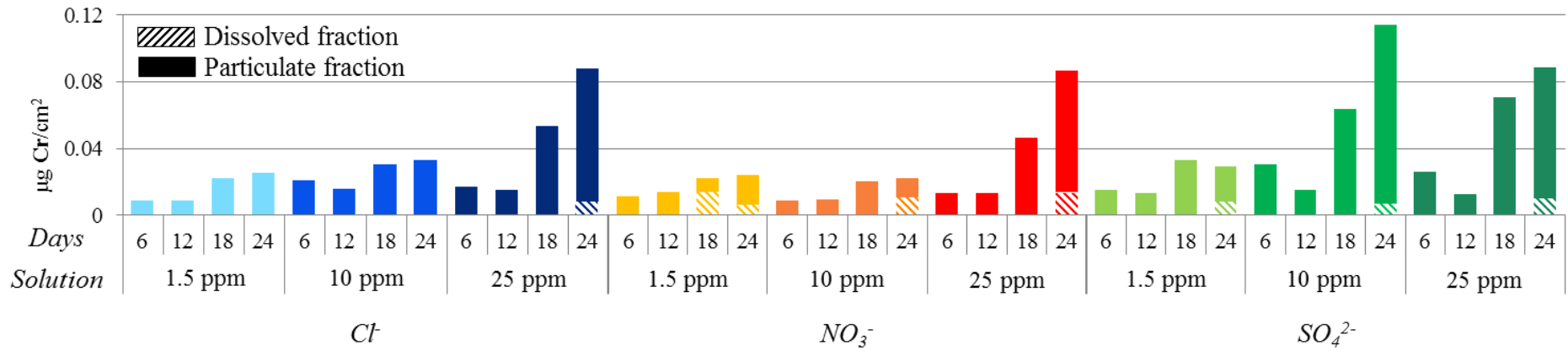


Fig. 91: Cr released by WS aged in chloride (blue), nitrate (orange) and sulphate solutions during immersion/emersion test

6.3.5.2 Metals in patina

In order to complete corrosion product characterization, metals in patinas were also investigated by analysing pickling solutions (section 5.4.1); these analysis allow to identify and quantify metals retained in patinas as adherent rust (AR). Results obtained for WS samples after 12 and 24 days of immersion/emersion test are shown in Fig. 92, Fig. 93, Fig. 94, Fig. 95 and Fig. 96.

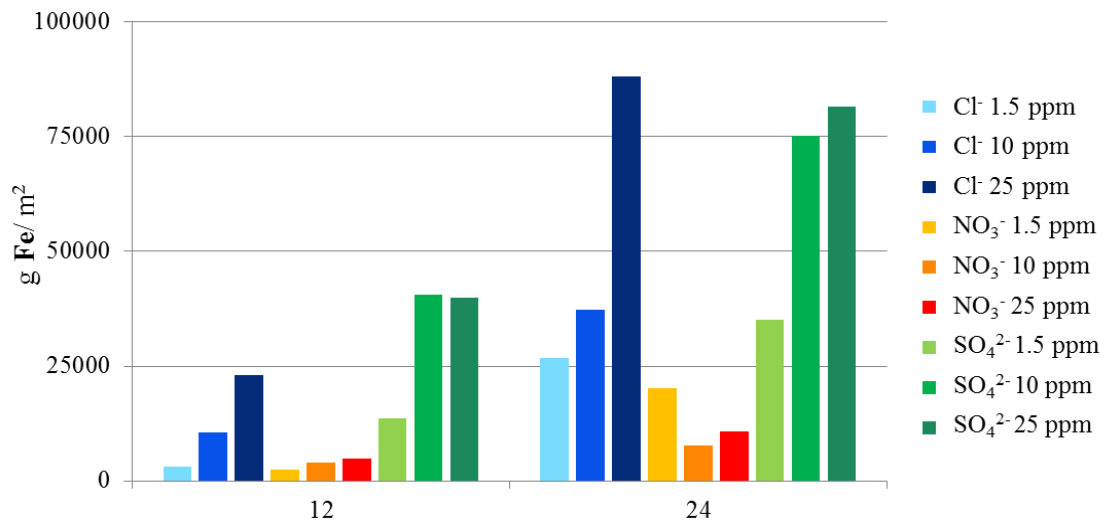


Fig. 92: Fe retained as adherent rust in patinas formed on WS aged in chloride (blue), nitrate (orange) and sulphate solutions during immersion/emersion test

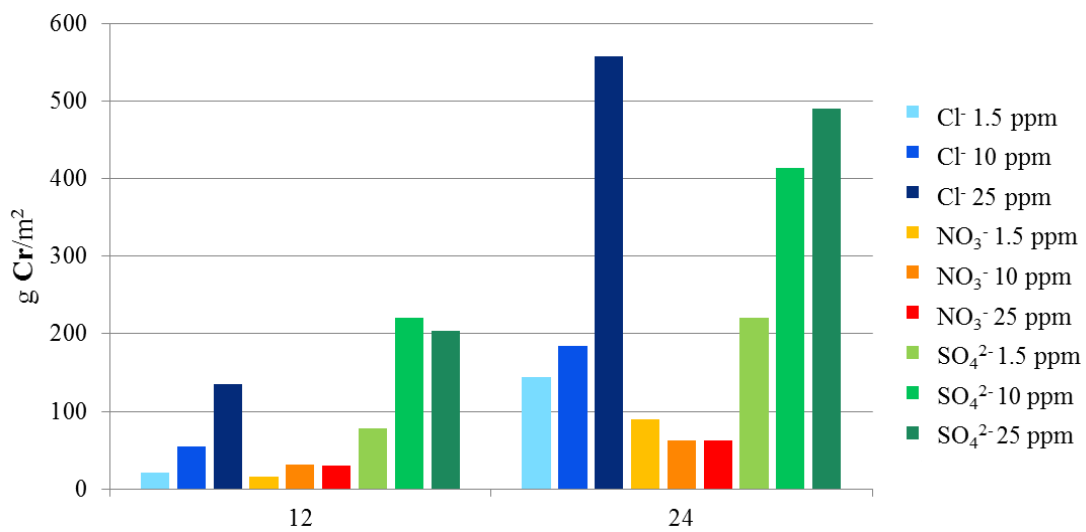


Fig. 93: Cr retained as adherent rust in patinas formed on WS aged in chloride (blue), nitrate (orange) and sulphate solutions during immersion/emersion test

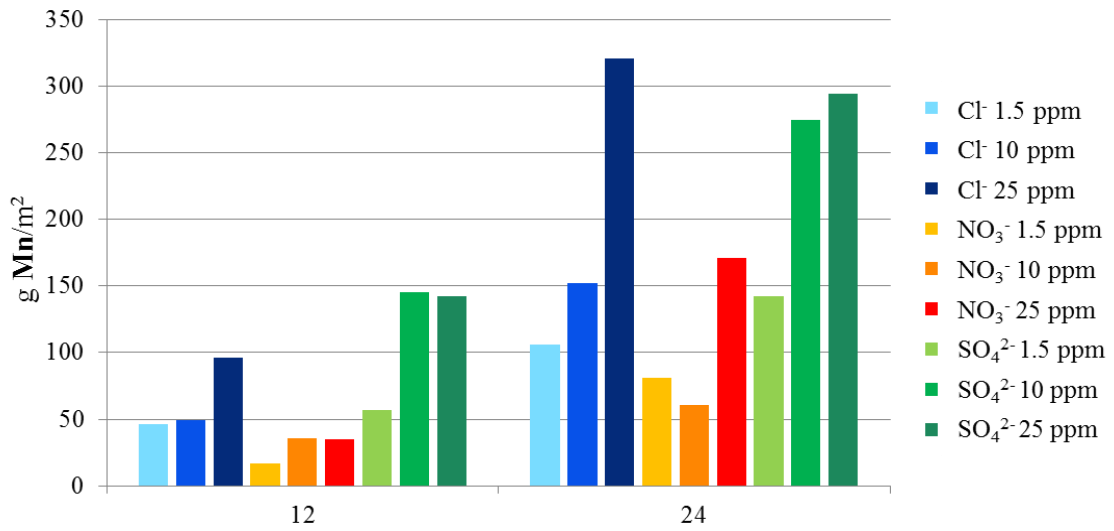


Fig. 94: Mn retained as adherent rust in patinas formed on WS aged in chloride (blue), nitrate (orange) and sulphate solutions during immersion/emersion test

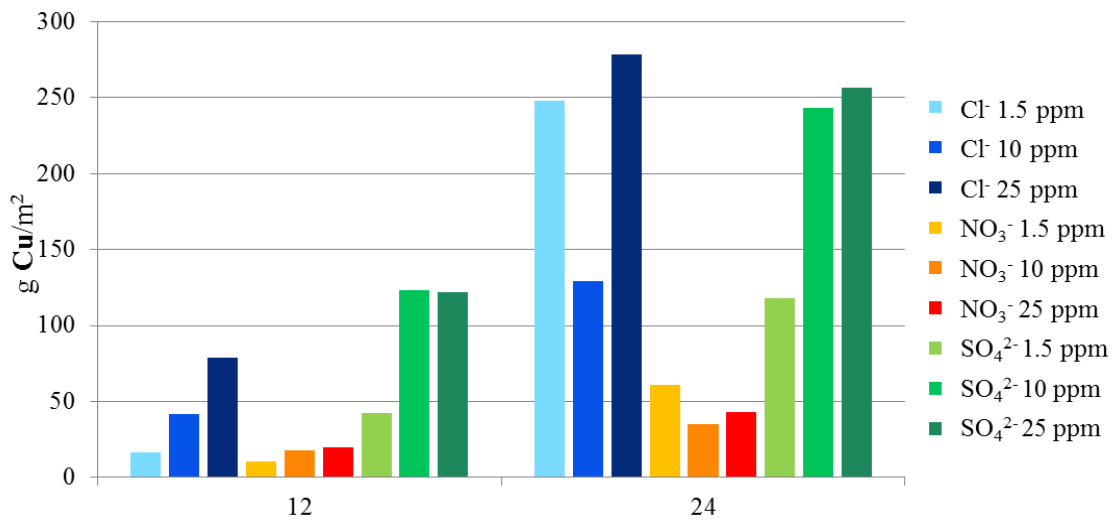


Fig. 95: Cu retained as adherent rust in patinas formed on WS aged in chloride (blue), nitrate (orange) and sulphate solutions during immersion/emersion test

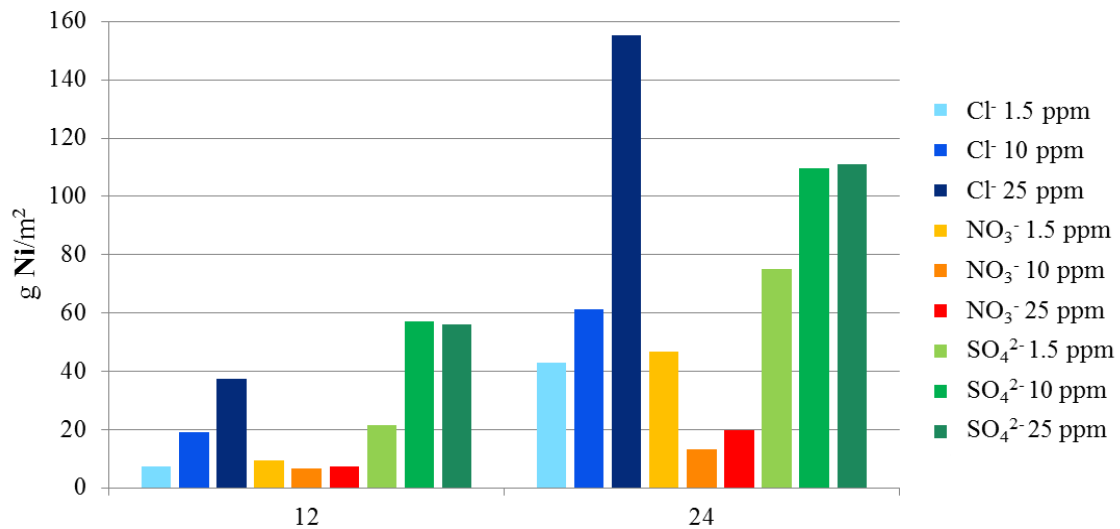


Fig. 96: Ni retained as adherent rust in patinas formed on WS aged in chloride (blue), nitrate (orange) and sulphate solutions during immersion/emersion test

Dissolution of alloying metals to form AR is connected to the corrosivity of weathering medium and affects the amount of corrosion; in general, results show dissolution growing with increasing exposure time.

More specifically, metal dissolution of all metals analyzed grows exponentially with increasing chloride concentration and logarithmically with increasing sulphate concentration in solutions. Once again, this investigation confirms the poor aggressivity of nitrate ions, whose presence becomes relevant in relation to corrosion only at higher weathering times.

6.3.6 Multivariate data analysis

Given all the information obtained, principal component analysis represents a useful tool for better summarizing the effects of weathering conditions on Cor-Ten corrosion. Results are presented in Fig. 97 and Fig. 98.

First of all, the score plot shows a distinction in compactness between samples aged for 12 days (blue) and samples aged for 24 days (red); the former, even though divided into sub-groups, appear more compact, while the latter are spread throughout the graph.

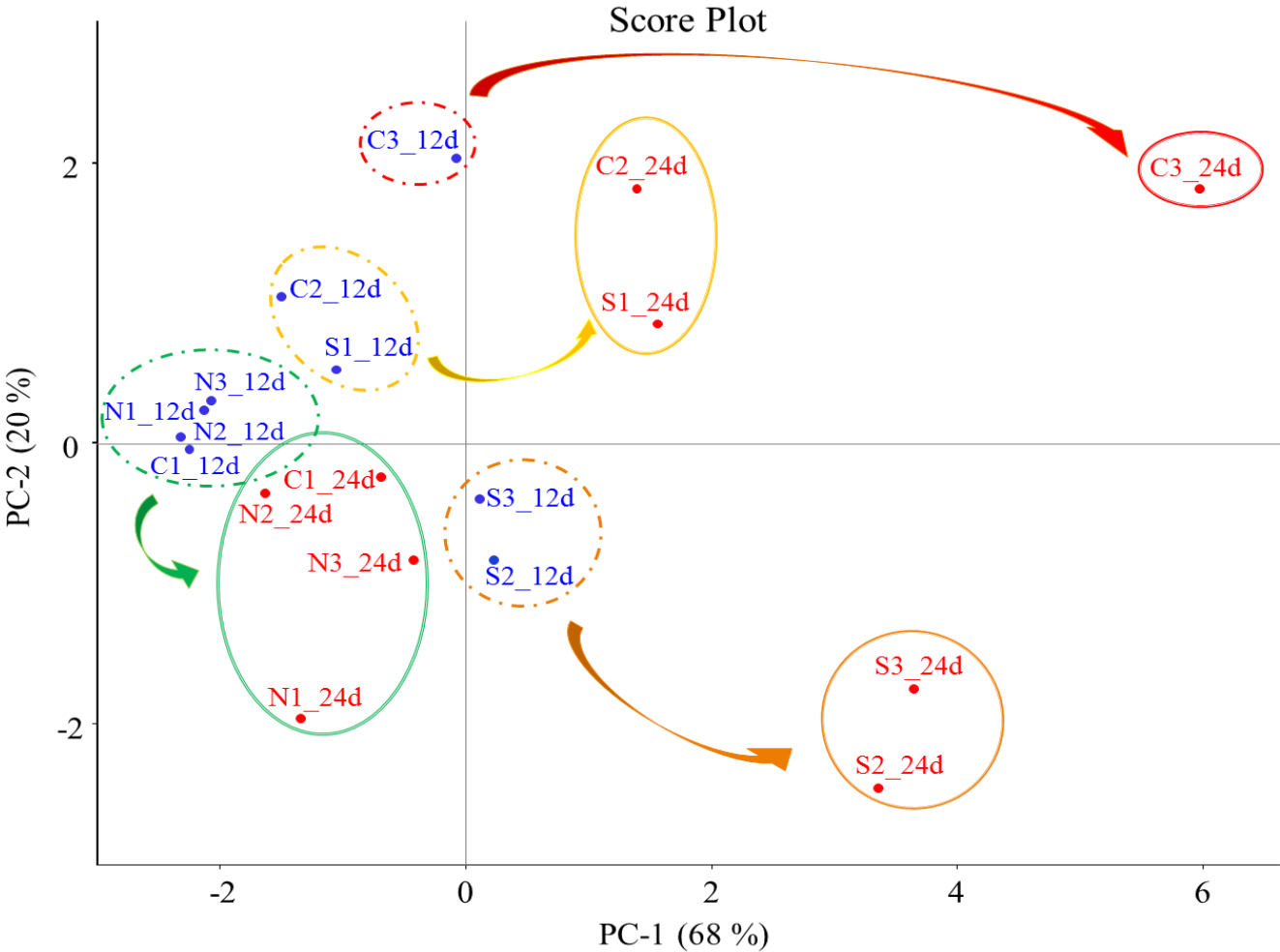


Fig. 97: Score plot for the first component (PC-1, explained variance 68%) and the second component (PC-2, explained variance 20%) of PCA model. In the graph, each sample is labeled with letter, referring to weathering solution (S= sulphate, C= chloride and N= nitrate) and number, referring to concentration (1= 1.5ppm, 2= 10 ppm and 3= 25 ppm)

Among the ‘12-day aged’ samples, four small groups are identified: the first (green) consists of WS samples aged in less aggressive conditions, i.e. all nitrate solutions and low concentrated

chloride solution. Samples aged in 1,5 ppm SO_4^{2-} and 10 ppm chloride solutions and in higher concentrated sulphate solutions form the second (yellow) and third groups (orange), respectively. The last group (red) is formed by an individual object, referring to the sample aged in presence of high amounts of chlorides.

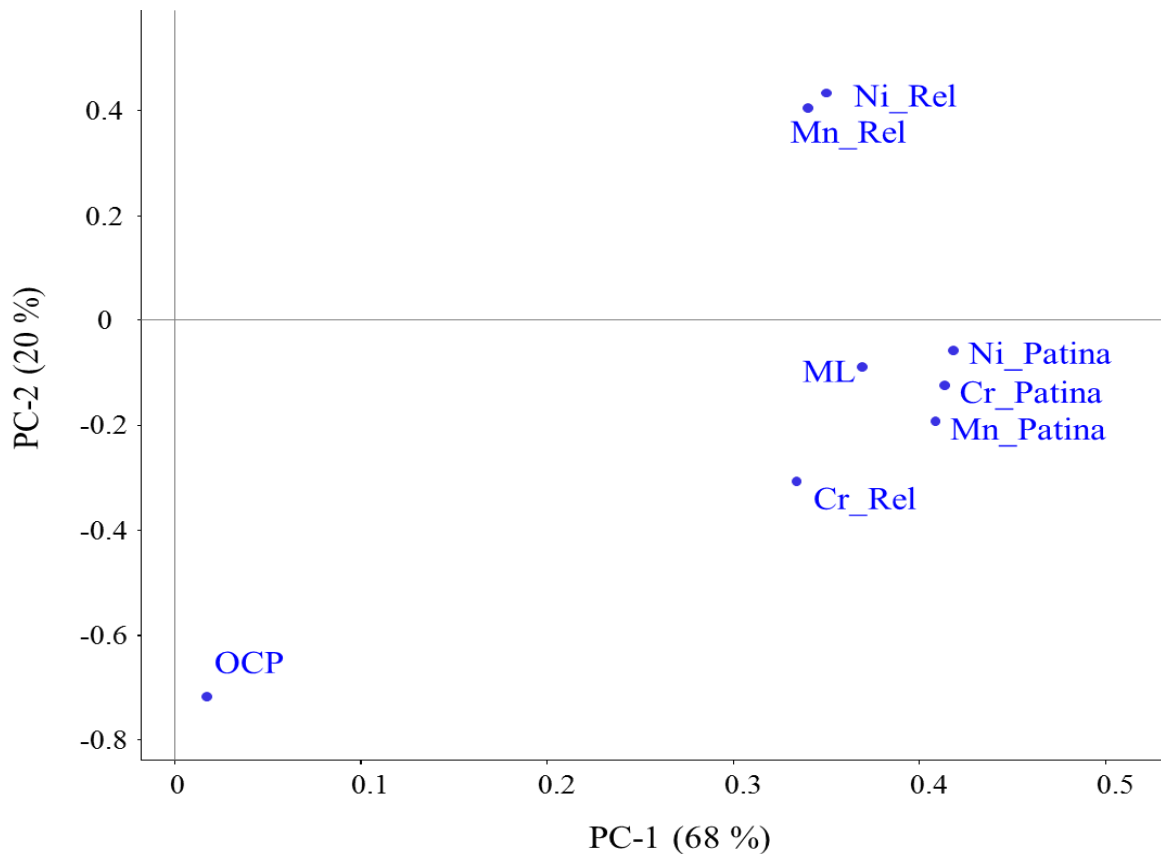


Fig. 98: Loading plot for the first component (PC-1, explained variance 66%) and the second component (PC-2, explained variance 16%) of PCA model. Variables used for the calculation are: corrosion potential (OCP), mass loss (ML), metals released in solution ('Rel') and metals retained in patinas ('Patina')

The separation into groups is preserved and accentuated at higher weathering times; each subgroup belonging to '24-days' samples, is positioned in a different area of the score plot, far from the other samples.

The 'green' group slightly move over and arrange in less compact way in the third quadrant of the plot; corrosion potential registered on these samples seems to be an important factor for determining their behavior, especially for WS specimen aged in 1,5 ppm NO_3^- solution, the only one to get very close to the passivity threshold value of 200 mV (section 6.3.2).

Going forward, after 24 days of test, 'yellow' and 'orange' groups are positioned in the first and the fourth quadrant, respectively. By comparing score and loading plots, it appears clear that these samples are more vulnerable to metal release and, more specifically, that samples aged in presence of small-medium concentration of Cl^- and SO_4^{2-} mainly release metals such as Mn and Ni, while the ageing of samples in concentrated sulphate solutions acts on the stability of patinas, affecting the release of Cr, considered the alloying element responsible for the growth and stabilization of the passivation film on weathering steels.

Finally, the 'red' group is the one suffering the greatest displacement from the original position, thus showing a marked dependence on weathering time of WS corrosion in concentrated Cl^- solution.

Chapter 7

Discussion of results

7.1 Influence of the geometry of exposure

Weathering steel, as said before, is widely used in architectural and artistic applications, where it appears, both for structural and conceptual reasons, in various arrangements.

This kind of structures consists of areas with different inclinations, more or less exposed to atmospheric factors, or completely sheltered.

The different geometry of exposure can lead the material to be more or less susceptible to the action of solar radiation, rain and winds or can produce water accumulation and stagnation on the surface; as a consequence, uneven and not homogeneous patinas form, making it even more difficult to assess the environmental corrosion behavior of weathering steel.

The exposure of weathering steel specimens both in sheltered and unsheltered conditions analyzed in the first part of this work allowed to deep this topic and study how the geometry of exposure can affect the stability of patinas during the first years of exposure in a moderate marine environment [164].

Morphological and compositional dissimilarities between sheltered and unsheltered samples were pointed out; in general, specimens not subjected to precipitations showed thicker patinas, also due to the deposition and the adsorption of particulate matter from the atmosphere, as confirmed by EDS results.

Speaking about particulate matter, chlorides and sulphates deriving from salt spray resulted the main corrosive species affecting weathering steel corrosion with regards to patina composition: akaganeite (β -FeOOH), that is the typical corrosion product of steel exposed to marine atmosphere, is the main component of patinas formed on sheltered samples, where chloride ions deposit and dissolved in the electrolyte film present on sample or simply accumulate on the surface. Beside it, another Cl-containing compound is found on some sheltered specimens, that is iron hydroxychloride (β -Fe₂(OH)₃Cl), which contains higher amounts of Cl⁻ than akaganeite (about 20% vs 5-6%) and it is supposed to be its direct precursor [144].

The continuous deposit of exogenous particles together with the lack of removal by precipitation leads to formation of patinas generally unstable, especially if the exposure occurs in corrosive environments.

However, unsheltered specimens, more subjected to removal of pollutants than the sheltered ones, are not exempt from the attack of corrosive species: in fact, micrographs in cross section (Fig. 55) clearly demonstrate that precipitations promote the entry and convey the diffusion of chloride ions throughout the entire corrosion layer [165].

On the other hand, the lower amount of Cl-containing products on these samples shows that while favoring their entrance, rainwater locally keeps Cl⁻ ions concentration down and reduces their corrosive action: as reported in literature, in fact, chlorinated compounds only form under conditions of relatively high concentration of Cl⁻ [166].

To further assess the importance of chloride concentration on patina composition, patinas formed on Cor-Ten specimens exposed in the urban-coastal site of Rimini for 36 months were compared to those formed on a real Cor-Ten structure, the Gate of the Jewish Cemetery, located in the urban site of Bologna [164] after 24 months of exposure. Raman spectra referring to Rimini (a, b) and Bologna (c, d) samples are reported in Fig. 99.

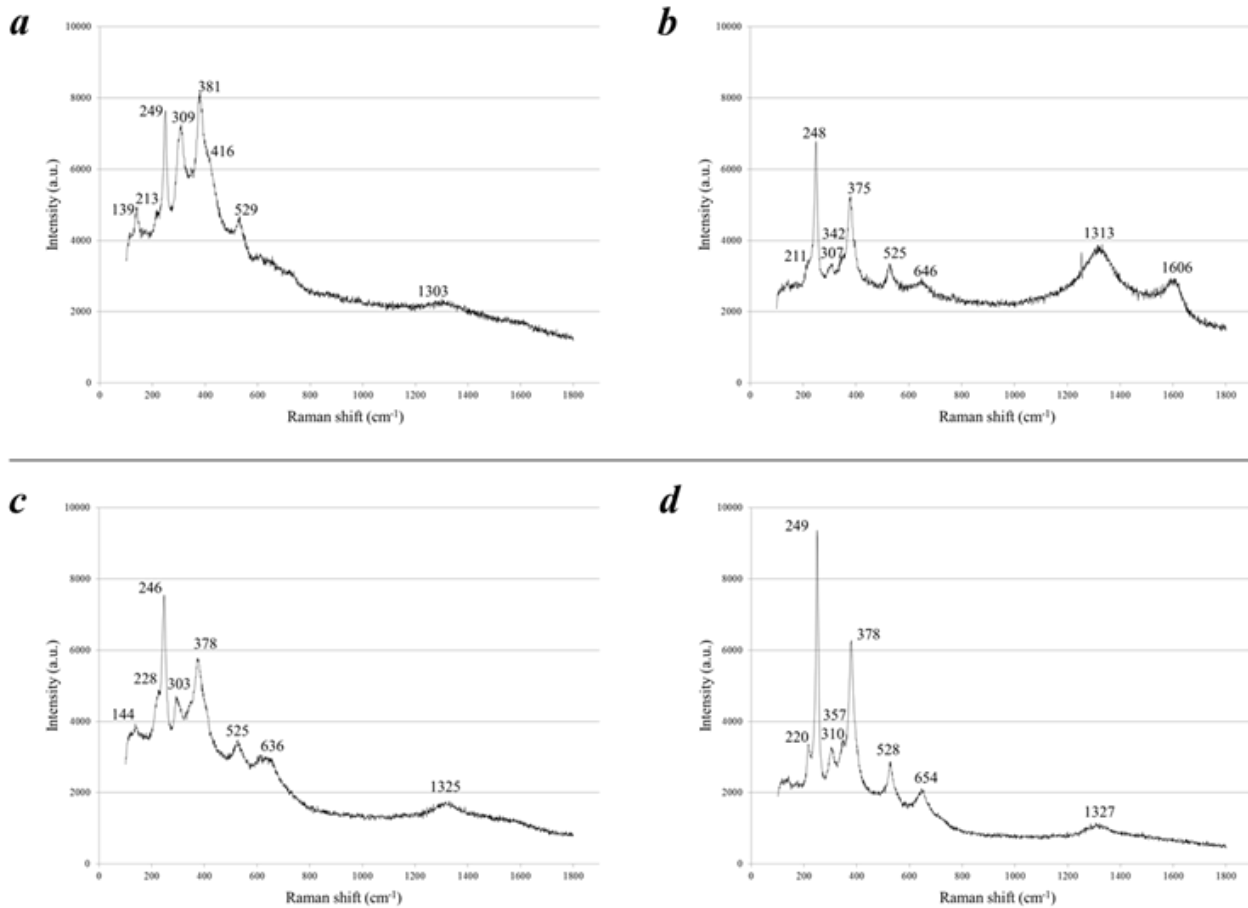


Fig. 99: On the top, Raman spectra of bare Cor-Ten exposed in Rimini in a) sheltered and b) unsheltered conditions. On the bottom, Raman spectra on c) sheltered and d) unsheltered areas of the Gate of the Jewish Cemetery in Bologna.

The comparison of Raman spectra makes it clear that, in general terms, the corrosion products on WS are the same in the two sites, mainly lepidocrocite, akaganeite, hematite and magnetite. However, as Bologna atmosphere presents lower concentration of chlorides ions, akaganeite was only detected in very low amount on the surface of sheltered areas of Cor-ten gate.

7.2 Influence of surface finish

Weathering steel arose from the necessity of developing a versatile material that doesn't need to be covered with protective paintings or corrosion inhibitors when exposed to atmosphere, with the aim of reducing costs of raw materials and maintenance procedures.

Prepatination and waxing processes do not correspond to common procedures of application of protective paintings, but rather to techniques of material preparation performed to accelerate the formation of the characteristic and aesthetically attractive surface patina or to defend from the attack of atmospheric pollutants.

However, such procedures are usually not recommended for outdoor applications, as they modify the natural process of creation and passivation of patinas and, in some cases, introduce corrosive chemicals on steel surface. Despite this, during the last decades time-saving and/or aesthetical reasons led several artists and architects to patinate or to use commercial WS artificially rusted, even for exposure in corrosive environments [167].

Although their large use for outdoor applications, to our knowledge, no studies are present in literature about corrosion behaviour of patinated WS. The research group I've worked with conducted a preliminary study in simulated laboratory conditions [146], during which WS specimens with different surface finishes were exposed to runoff, in order to evaluate their behavior in unsheltered conditions. Metal release from pre-treated samples appeared lower than from bare steel, but rather significant, starting to reveal a poor protection of artificial patinas towards alloy dissolution, even in controlled laboratory conditions.

When exposed to quite aggressive real environment [165], instead, dissolution from bare samples was generally lower than that from pre-patinated samples; the greater complexity and variability found in field exposure represent the discriminating factor, causing a worse corrosion behavior of artificial patinas.

First of all, even if no evident compositional differences have been detected between bare and treated samples after four years of exposure, a more brittle structure and numerous cracks characterize the pre-patinated and pre-patinated/waxed WS (section 6.2.2.2), especially in unsheltered conditions.

The main reason for this may be ascribed to the process of prepatination of samples that, beside introducing a certain amount of chlorides on WS, which cause destabilization and a continuous risk for the material, also produces artificial patinas, characterized by different mechanical features and lower adhesion with the substrate with respect to patinas naturally developed on bare WS. Moreover, especially during the first phases of environmental exposure, the different chemical-physical properties of bare and pre-treated surfaces may be responsible for a different interaction with atmospheric pollutants, such as particulate matter. In fact, smoother surfaces usually suffer less deposition, while the presence of irregularities or pores, like pre-treated samples of this study, increases the probability of particles diffusion and reduces the possibility of their resuspension [168].

Beside acting on the stability of patinas, surface finish also affects the dispersion of metals from the alloy. This aspect will be deepened in next section.

7.3 Atmospheric factors affecting corrosion and metal dissolution

Results presented in sections 6.2.3 and 6.2.4 point out the influence of atmosphere composition and meteorological factors on corrosion from WS samples.

Metal dissolution exhibits a clear seasonal trend and, as revealed by multivariate analysis (section 6.2.4), solar radiation, time of wetness, winds and precipitations are the main factors causing it.

Radiation and TOW affect corrosion in opposite ways: higher irradiation promotes the drying of surfaces, reducing the time in which samples are covered by the electrolyte film as well as its thickness, thus slowing down corrosion rate. During the entire exposure period, in fact, it was precisely the prolonged wetting of surfaces that had caused the worst effects with regards to metal dissolution: suffice it to say that, during the snowfall of 2012, that turned out to be the meteorological event with the greatest effect on dissolution (Table 22, section 6.2.3), specimens underwent to an extreme condition of stagnation; also due to the presence of pollutants included in snow and put in contact with surfaces, this situation created the ideal conditions for the increase of corrosion and metal dissolution.

The other meteorological events having negative effects on metal dissolution presented a common feature, that was the simultaneous occurrence of heavy rainfalls and intense winds from the sea direction: this combination allowed corrosive species, such as chlorides and sulphates, not only to be transported at the test site but also to be easily introduced in WS patinas.

Particularly, chlorides turned out to be the most aggressive species and, by affecting corrosion phenomena occurring at the interface between metal and patina (section 6.2.2), enhanced runoff processes occurring at the interface between patina and atmosphere (section 6.2.3 and 6.2.4).

The present work demonstrated how, during these extreme meteorological events, the material is exposed to a greater risk from the point of view of corrosion and the release of alloying metals increases to the point that just one of these events could be responsible for almost all the annual metal release in the environment [165].

During the 4-year exposure in Rimini, the frequency of such events has increased over the years; furthermore, as stated by increasing studies on the subject of climate change, the number of extreme events is inevitably destined to grow [152], [169]–[172]. So in this light, on the basis of

obtained results, it is good to start evaluating what could be the possible impacts of the material on the environment.

Table 25 offers an interesting comparison between concentrations of metals (Fe, Mn and Ni) released by bare, pre-patinated and pre-patinated/waxed weathering steels exposed in Rimini and examples of metals in urban and highway run-off reported in literature [173], [174]: it is clear that WS runoff can significantly contribute to urban dissolved metal loading at local level, especially as regards Mn and Ni; moreover a not negligible contribution also to dissolved Fe loading could be given close to motorways, along which WS is widely employed as noise-barrier.

In order to give a first indication about direct adverse effects of WS runoff waters on sensible receptors, available law or guideline limits for health or environment protection are also provided.

Obviously, it has to be reminded that release data recorded in standard conditions should not be directly used to predict environmental effects, as metal runoff depends also on the surfaces inclination and orientation, and, during environmental entry, metals can undergo different phenomena (e.g. dilution, retention on solid surface or change in their chemical speciation [148], [178]); so this discussion must be considered as a general information about the possible environmental impact of this material.

Table 25: Dissolved alloying metal concentrations in runoff rainwater from bare, pre-patinated and pre-patinated/waxed weathering steel, compared with literature ranges for dissolved metal concentrations in urban runoff waters and law limits for drinking and irrigation waters. Minimum/maximum concentration values recorded during single sampling periods and average concentrations are reported. For weathering steel, average concentrations were calculated by considering annual metal releases ($\text{mg m}^{-2} \text{yr}^{-1}$) and annual rain amount fall on the specimens

		Fe ($\mu\text{g L}^{-1}$) min - max (avg)	Mn ($\mu\text{g L}^{-1}$) min - max (avg)	Ni ($\mu\text{g L}^{-1}$) min - max (avg)
BA	1 st year	2.0 – 3640 (460)	4.8 – 157 (5)	1.3 – 19 (6.3)
	2 nd year	15.4 – 112 (27)	0.4 – 16 (1)	1.3 – 4.0 (2.0)
	3 rd year	5.2 – 137 (36)	0.3 – 26 (1.4)	0.7 – 4.3 (1.5)
	4 th year	4.4 – 282 (38)	0.3 – 17 (2)	0.7 – 4.5 (1.1)
PA	1 st year	9.6 – 5100 (546)	4.6 – 183 (47)	2.3 – 40 (12.5)
	2 nd year	0.13 – 52 (19)	1.0 – 19 (6)	1.7 – 6.5 (2.4)
	3 rd year	1.6 – 290 (70)	0.5 – 41 (13)	0.6 – 6.8 (3.4)
	4 th year	8.7 – 321 (56)	0.1 – 60 (7)	0.8 – 6.4 (1.6)
PWA	1 st year	21 – 1051 (302)	2.6 – 68 (32)	1.7 – 17 (10)
	2 nd year	8.7 – 122 (36)	0.6 – 39 (12)	1.4 – 6.8 (3.5)
	3 rd year	2 – 353 (99)	0.2 – 42 (19)	0.4 – 5.9 (3.8)
	4 th year	15 – 165 (86)	0.04 – 48 (14)	1.0 – 6.1 (3.6)
Urban runoff – residential sites ^a	<i>21.64-347.92</i> (133.2)	<i>nd-21.06</i> (1.44)	<i>0.99-5.71</i> (2.89)	
Urban runoff – industrial sites ^a	<i>24.04-4104</i> (521.42)	<i>0.83-175.5</i> (32.54)	<i>1.85-16.77</i> (4.71)	
Highway Runoff ^b	<i>9.76-57.83</i>	<i>12.01-150.46</i>	<i>2.74-5.06</i>	
Italian limits for drinking water ^c	200 [#]	50 [#]	20	
Italian limits for irrigation water ^d and urban waste water discharging on the ground ^e	2000	200	200	

[#] recommended values

^a [174]; ^b [173] ^c[175]; ^d [176]; ^e [177]

In general, concentrations of metals dissolved from WS in the first four years of exposure result far below the limits for metal concentrations in waters for agricultural use and human consumption; however, during the first year, characterized by the most critical environmental

conditions, average Fe and maximum Mn concentrations for all the finishes exceeded the suggested acceptable level for drinking waters, while maximum Ni concentrations from pre-patinated samples were close or exceeded the Italian limit [175]. During the same period, maximum Fe concentrations (recorded during snowfall) exceeded also Italian limit for irrigation water and urban waste water discharging on the ground [176], [177].

In order to provide a conservative evaluation to estimate possible WS long-term release, data of metal flows were processed using moving-averages on six-monthly subsets, to reduce variability among sampling periods. The obtained minimum and maximum monthly values were used to calculate the ranges of annual dissolved metal flows (Table 26).

Table 26: Esteemed conservative ranges of annual dissolved metal ($\text{mg m}^{-2} \text{y}^{-1}$) for Bare (BA), Pre-patinated (PA) and Pre-patinated/ waxed (PWA) weathering steel in the test conditions

	Fe ($\text{mg m}^{-2} \text{y}^{-1}$)	Ni ($\text{mg m}^{-2} \text{y}^{-1}$)	Mn ($\text{mg m}^{-2} \text{y}^{-1}$)
BA	14 – 552	0.8 – 3.3	0.5 – 3.7
PA	20 – 640	1.1 – 6.9	1.6 – 27
PWA	40 – 267	2.1 – 5.8	3.2 – 32.5

According to these results, one squared meter of the most common bare WS, during an hypothetical exposure of 10 years in the test conditions, could locally release dissolved metals in the following order of magnitudes: from 0.1 up to 5 g of Fe, from 5 up to 50 mg of Mn and from 10 to 35 mg of Ni. Therefore, if the EC limit values for annual addition of Ni to agricultural land is assumed as a reference (300 mg/m^2 of soil, based on a 10-year average (86/278/EEC, 1986)), Ni release could become significant for wide structures standing on a small area.

7.4 Influence of saline compounds on corrosion

The application of a specific accelerated aging test (namely, immersion/emersion Cebelcor test) allowed to point out some interesting conclusions about the influence of main saline compounds (Cl^- , NO_3^- and SO_4^{2-}) of particulate matter, and atmospheric depositions in general, on WS corrosion behavior.

The weathering solutions, each presenting a specific corrosive agent, act on weathering steel with different mechanisms and kinetics; in barely aggressive solutions, the corrosive attack on the metal surface is initially inhibited, while in the presence of more aggressive ions or higher concentrations, the surface is immediately subjected to browning and formation of an homogeneous patina of oxides (sections 6.3.1 and 6.3.4).

The increase in exposure time simply widens this gap, as illustrated by multivariate data analysis (Fig. 97), where time action is clearly highlighted and corresponds to higher or lower dislocations of sample groups in the graph.

Referring to patina composition, the main product was lepidocrocite, the iron oxide that usually characterized the first steps of WS corrosion; beside it, hematite was also detected; relative percentages of these compounds change with regards to weathering solution and time of wetness, with hematite amounts ranging from 10% to 25% of corrosion layer composition.

The presence of relatively large amounts of hematite is not commonly cited in literature and, when it is detected, it mainly refers to exposure at industrial sites [179], [180]; in this case, the fact that hematite is found on all samples tested, lets us consider that its formation is strongly promoted by water stagnation on surfaces.

Moreover, according to what reported in literature [50], hematite is not generated through direct transformation of lepidocrocite; on the contrary, we might think about a competitive formation during the mechanism of dissolution-riprecipitation of lepidocrocite.

On the other hand, goethite, one of the main responsible of the stabilization of patinas on WS, is detected in low amounts on the specimens aged in concentrated (25 ppm) sulphate solution, proving the beneficial action that S-containing compounds may have on the passivation of corrosion layers [163]. Considering data of mass loss and cumulative metal release, a series of equations describing the evolution of runoff and corrosion processes have been obtained (Table 27). Keeping in mind that these two processes can proceed independently, a comparison between the two trends may offer more information about the behavior of Cor-ten steel in analyzed conditions.

The first thing to note is that the presence of SO_4^{2-} allows both corrosion and runoff rates to decrease over time; this confirms that, even though the corrosive attack of sulphate solutions is the one showing the highest kinetic, patinas formed in these conditions turn out to be the only ones that show a tendency to passivation and stabilization, thanks to the formation of goethite (section 6.3.4.3).

This effect is even more evident when compared with weathering in presence of chlorides, when both runoff and corrosion rate tend to grow over time, without signs of stabilization.

WS aged in nitrate solutions shows a different behavior: in fact, there seems to be a threshold value of NO_3^- concentration (ranging from 10 to 25 ppm), beyond which the rate of corrosion undergoes rapid acceleration.

Table 27: Functions approximating time evolution of mass loss and total (Fe + Mn + Ni + Cr) metal release for each solution tested

Solution	mg/L	Mass Loss Trend	Metal Release Trend
Cl ⁻	1.5	$y = - 0.024 x^2 + 0.9 x$	$y = 14 e^{0.07x}$
	10	$y = 2.6 x$	$y = 64 x - 194$
	25	$y = 6.9 x$	$y = 115 x - 190$
NO ₃ ⁻	1.5	$y = - 0.005 x^2 + 0.3 x$	$y = 12 e^{0.08x}$
	10	$y = 0.004 x^2 + 0.3 x$	$y = 19 e^{0.006x}$
	25	$y = 0.026 x^2 + 0.04x$	$y = 13 e^{0.08x}$
SO ₄ ²⁻	1.5	$y = - 0.093 x^2 + 4.43 x$	$y = 330 \ln (x) - 262$
	10	$y = - 0.33 x^2 + 13.8 x$	$y = 307 \ln (x) + 268$
	25	$y = - 0.37 x^2 + 15.5 x$	$y = 330 \ln (x) - 143$

Relative percentages of Fe, Cr, Mn and Ni found in adherent and non-adherent rust were then compared to the initial bulk alloy composition (Fig. 100), to point out possible trends of preferential metal dissolution after 12 and 24 days of test.

Results show that non-adherent rust deriving from specimens aged in less aggressive solutions (NO₃⁻ and 1.5 ppm - Cl⁻ solutions) appear enriched in Mn and Ni with respect to bulk composition; then, this behavior becomes less pronounced with increasing testing time, especially in nitrate

solutions. In contrast, in sulphate solutions the preferential dissolution of Mn and Ni increases with time.

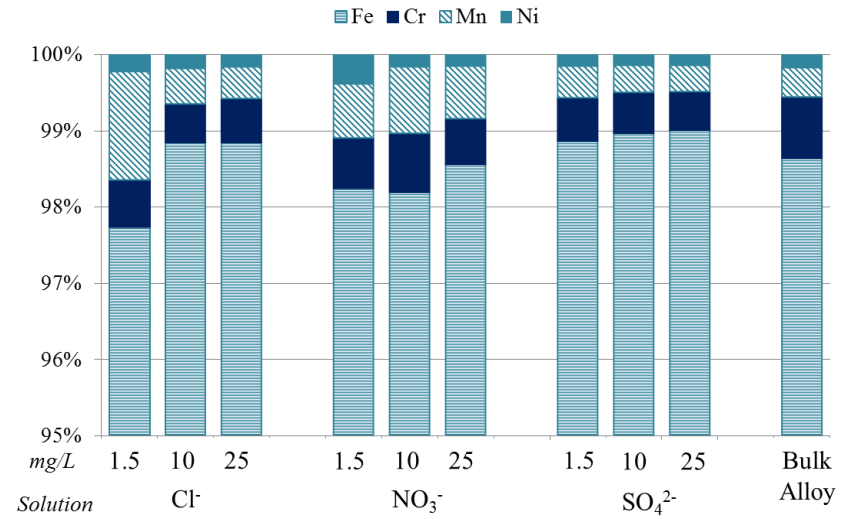
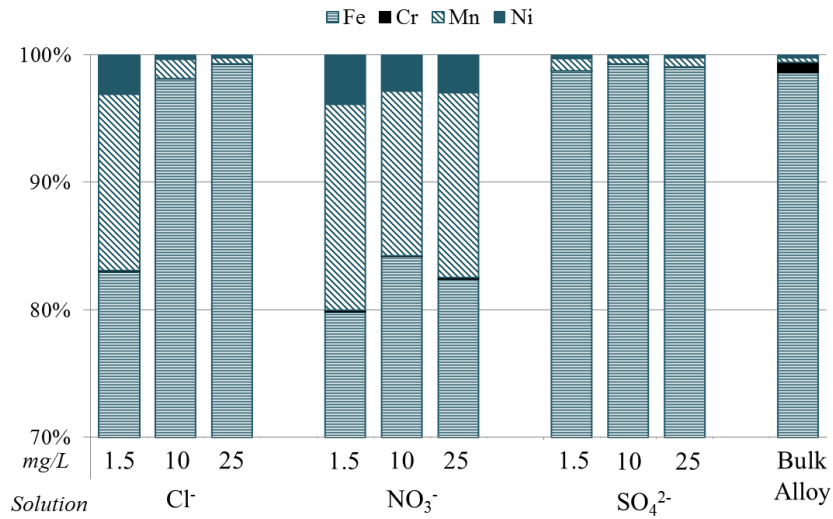
Finally, it's interesting to note that Cr is released in solution in lower percentage compared to its amount in bulk alloy; on the contrary, its presence in adherent rust is perfectly consistent with the amount in bulk alloy.

In general, adherent rust composition reliably reflects the initial alloy composition, with a few exceptions which concern NO_3^- and 1.5 ppm - Cl^- solutions during the first part of test and 10 and 25 ppm nitrate solutions at higher testing times, all producing, also in this case, preferential dissolution of Mn and Ni.

Non-adherent rust (NAR)

Adherent rust (AR)

12 days



24 days

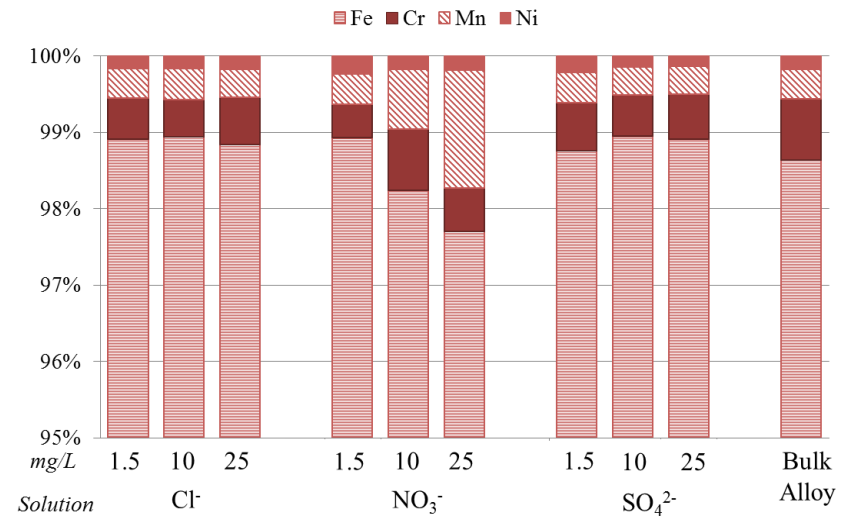
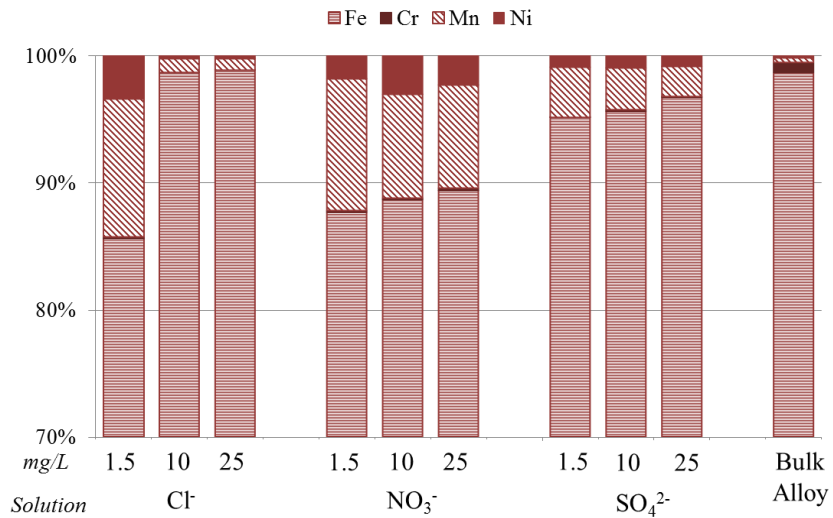


Fig. 100: Relative percentage amount of Fe, Cr, Mn and Ni in adherent (right) and non-adherent (left) rust with respect to the sum (Fe + Cr + Mn + Ni) for weathering steel samples aged in Cl^- , NO_3^- and SO_4^{2-} solutions compared to the bulk alloy fractions (about 98% for Fe, 0.8 for Cr, 0.2% for Ni and 0.4% for Mn), during the first (12 days) and the second (24 days) phase of immersion/emersion test.

By analyzing all data collected during the test, including corrosion potential measurements, weekly metal release, information about patina characterization and taking into account additional information obtained from multivariate data analysis, a scale of corrosivity for weathering solution tested is proposed here below.

12 days:		NO ₃ ⁻ 1.5 ppm				
		NO ₃ ⁻ 10 ppm	<	SO ₄ ²⁻ 1.5 ppm	<	Cl ⁻ 25 ppm
		NO ₃ ⁻ 25 ppm		Cl ⁻ 10 ppm	<	SO ₄ ²⁻ 10 ppm
		Cl ⁻ 1.5 ppm				SO ₄ ²⁻ 25 ppm

24 days:						
		NO ₃ ⁻ 1.5 ppm	<	NO ₃ ⁻ 10 ppm	<<	SO ₄ ²⁻ 1.5 ppm
				NO ₃ ⁻ 25 ppm		Cl ⁻ 10 ppm
			Cl ⁻ 1.5 ppm			SO ₄ ²⁻ 10 ppm
						SO ₄ ²⁻ 25 ppm
						Cl ⁻ 25 ppm

Chapter 8

Conclusions

In the present PhD work, the issue of atmospheric corrosion of weathering steel was extensively investigated by means of natural field exposure and laboratory ageing tests, in order to evaluate and quantify the effects that surface treatments, geometry of exposure, environmental factors and main atmospheric contaminants may have on the corrosion behavior of weathering steel [165].

Specifically, the characterization of the composition and morphology of corrosion products formed on weathering steel was usefully combined with an innovative approach, as regards this material, that is the study and quantification of corrosion-induced metal release and dissolution during the early years of exposure, when the environmental impact could be greater.

A specific focus was made on a particular aspect of atmospheric corrosion of weathering steel, that is the interaction of the material with the main aggressive saline ions contained in particulate matter.

Conclusion achieved are summarized here below.

Results of four-year field exposure in the marine atmosphere of Rimini show that weathering steel release of Fe, Mn and Ni in the immediate dissolved, thus soon bioaccessible, fraction may significantly contribute to the urban metal loading at local level, especially with regards to Mn and Ni.

During the test period, annual release did not show a decreasing trend with time; annual total dissolution rate (sum of all dissolved metals) varied between 10 - 255 mg m⁻² y⁻¹ depending on environmental conditions and surface finishing.

Actually, metal dissolution was mainly affected by the occurrence of extreme meteorological events, such as snowfall, storm and heavy and prolonged precipitations, when high concentrations of ionic corrosive species were also observed. Patinas developed in this slight marine environment seems to be very sensitive to chlorides, as they rapidly react to short-term Cl⁻ variations.

The initial exposure condition, that includes both geometry of exposure and surface finish, had a marked influence on the subsequent corrosion behavior, particularly with regards to metal runoff. Surface pre-treatment, usually performed to ensure an aesthetically-pleasing and uniform appearance to the material for outdoor applications, worsened WS performances in terms of metal dissolution and determined a more inhomogeneous behavior of patinas along time.

The application of multivariate analyses to the experimental data showed that two-way and three-way PCA can provide useful and complementary information in the study of atmospheric corrosion, enabling to point out a seasonal dependence of WS dissolution, with summer samples mainly affected by temperature and solar radiation and winter samples by TOW and atmospheric particulate matter.

A broad overview of the effects of the main saline compounds of particulate matter (Cl⁻, NO₃⁻ and SO₄²⁻) and of their concentration on WS corrosion with regards to the stability of corrosion layers and to metal release was obtained by means of immersion / emersion ageing test (Cebelcor) and complete characterization of corrosion products and weathering solutions.

Results showed that both the composition of patinas and metal release were strongly affected by nature and concentration of the investigated compounds.

In general, nitrate ions appeared the least aggressive among the compounds tested, causing a poor corrosion attack and non-homogeneous patinas and inducing a total metal release that was, on average, one or two orders of magnitude smaller than that produced in presence of chlorides or sulphates.

Chlorides and sulphates were more aggressive and acted on weathering steel with different mechanisms and kinetics. Particularly, the evaluation of runoff and corrosion rates pointed out that ageing in presence of SO_4^{2-} ions induced the rapid formation of homogenous patinas that showed a passivation tendency, even though a complete stabilization was not appreciated during the relatively short test period.

On the contrary, the presence of chloride ions, despite with slower kinetic, produces poorly protective patinas and induces both corrosion and runoff to continuously grow over time.

Considering these findings in view of the ongoing climate changes, that will be responsible, among other effects, for rising global temperature, for increasing the frequencies of extreme events and, in general, for drier summer and wetter winter [169], [170], it appears essential to plan and perform long-term monitoring of the performance, the durability and the possible environmental impact of weathering steel. Moreover, as particulate matter (both composition and concentration) is strongly correlated with meteorological parameters [181] and, thus, climate change is supposed to have a substantial influence on it, it is also fundamental to continue evaluating both the effect of single component and the simultaneous action of more constituents of PM on weathering steel corrosion, in order to fully understand the mechanisms of action and to lay the fundamentals for proper prevention and maintenance programs.

References

- [1] P. Pedferri, *Corrosione e protezione dei materiali metallici*. Ed. Polipress, 2007.
- [2] V. Cicek and B. Al-Numan, *Corrosion Chemistry*. Wiley, 2011.
- [3] G. H. Koch, M. P. H. Bronger, N. G. Thompson, Y. P. Virmani, and J. H. Payer, "Corrosion Costs and Preventive Strategies in the United States, Supplement to Materials Performance," *NACE Int.*, p. 12, 2002.
- [4] Committee on Cost of Corrosion in Japan, "Survey of Corrosion Cost in Japan," 2003.
- [5] M. J. Lieser and J. Xu, "Preventing a legacy of costly corrosion with modern materials," 2010.
- [6] G. Schmitt, M. Schütze, G. F. Hays, W. Burns, E. Han, A. Pourbaix, and G. Jacobson, "Global Needs for Knowledge Development in Materials Deterioration and Corrosion Control," *world Corros. Organ.*, 2009.
- [7] P. Maass, P. Peissker, and C. Anher, "Corrosion and Corrosion Protection," in *Handbook of Hot-dip Galvanization*, 2011.
- [8] L. Lazzari, "Corrosione," *Enciclopedia della scienza e della tecnica*. Treccani, 2008.
- [9] W. Revie and H. H. Uhling, *Corrosion and corrosion control: an introduction to corrosion science and engineering*, 4th editio. John Wiley & Sons, Inc., 2008.
- [10] G. Hinds and from the original work of J G N Thomas, "The elctrochemistry of corrosion." 2008.
- [11] V. Cicek, *Corrosion Engineering*. Wiley, 2014.
- [12] C. Casalino, "Online lecture note - Elettrochimica," 2010. .
- [13] P. Marcus, *Corrosion Mechanisms in Theory and Practice*. 2002.
- [14] C. Leygraf and T. E. Graedel, *Atmospheric Corrosion*. New York: John Wiley & Sons, 2000.
- [15] E. Bardal, *Corrosion and Protection*. Springer, 2004.
- [16] P. A. Schweitzer, *Fundamentals of metallic corrosion: atmospheric and media corrosion of metals*. Taylor and Francis Group, LLC, 2006.

- [17] “International Standard ISO 9223 - Corrosion of metals and alloys - Corrosivity of atmospheres - Classification.” 1992.
- [18] F. T. Mackenzie and J. A. Mackenzie, *Our changing planet: an introduction to earth system science and global environmental change*. Prentice-Hall, 1995.
- [19] “US EPA Definition of Particulate Matter.” .
- [20] J. R. Davis, “High-Strength Low-Alloy Steels,” in *Alloying: Understanding the Basics*, J. R. Davis and D. & Associates, Eds. 2001.
- [21] W. D. Callister and D. G. Rethwisch, *Material science and engineering: an introduction*, 9th Editio. Wiley.
- [22] H. K. D. H. Bhadeshia, “Martensite in Steels,” *Mater. Sci. Metall.*, pp. 1–12, 2002.
- [23] N. Nutal, C. J. Gommès, S. Blacher, P. Pouteau, J.-P. Pirard, F. Boschini, K. Traina, and R. Cloots, “Image analysis of paerlite spheroidization based on the morphological characterization of cementite particles,” *Imaga Anal Stereol*, vol. 29, pp. 91–98, 2010.
- [24] “Italian Standard UNI EN 10020 - Definizione e classificazione dei tipi di acciaio.” 2005.
- [25] M. Morcillo, D. De la Fuente, I. Díaz, and H. Cano, “Atmospheric corrosion of mild steel,” *Rev. Metal.*, vol. 47, no. 5, pp. 426–444, Dec. 2011.
- [26] M. Stratmann and H. Streckel, “On the atmospheric corrosion of metals which are covered with thin electrolyte layers—II. Experimental results,” *Corros. Sci.*, vol. 30, no. 6–7, pp. 697–714, Jan. 1990.
- [27] L. Pezzato, “Effetto del trattamento con plasma atmosferico sullo strato di ossidi di leghe di alluminio e acciai inossidabili,” Padova, 2012.
- [28] M. De Sanctis, “Online lecture note - Appunti di corrosione.” .
- [29] R. Mallett, “Corrosion of iron and steel,” *Civ. Eng. Archit. J.*, vol. 6.
- [30] M. Morcillo, B. Chico, I. Díaz, H. Cano, and D. de la Fuente, “Atmospheric corrosion data of weathering steels. A review,” *Corros. Sci.*, vol. 77, pp. 6–24, 2013.
- [31] Siderservizi, “Cor-Ten.” [Online]. Available: <http://www.siderservizi.com/corten.htm>.
- [32] ASTM Standard A690, “High-Strength Low-Alloy Nickel, Copper, Phosphorus Steel H-Piles and Sheet Piling with Atmospheric Corrosion Resistance for Use in Marine Environments.” pp. 1–3, 2006.
- [33] ASTM Standard A242, “High-Strength Low-Alloy Structural Steel.” pp. 6–11, 2001.

- [34] ASTM International A588, “High-Strength Low-Alloy Structural Steel, up to 50 ksi [345 MPa] Minimum Yield Point, with Atmospheric Corrosion Resistance.” pp. 1–3, 2001.
- [35] ASTM Standard A606, “Steel, Sheet and Strip, High-Strength, Low-Alloy, Hot-Rolled and Cold-Rolled, with Improved Atmospheric Corrosion Resistance,” pp. 1–4, 2009.
- [36] ASTM Standard A633, “Normalized High-Strength Low-Alloy Structural Steel Plates.” pp. 1–3, 2006.
- [37] “Hokkaido 100 years memorial tower, Sapporo” [Online]. Available: <http://www.nssmc.com/en/product/plate/COR-TEN.html>.
- [38] M. Yamashita, H. Miyuki, Y. Matsuda, H. Nagano, and T. Misawa, “Long term growth of the protective rust layer formed on weathering steel by atmospheric corrosion during a quarter of a century,” *Corros. Sci.*, vol. 36, no. 2, pp. 283–299, 1994.
- [39] K. Asami and M. Kikuchi, “In-depth distribution of rusts on a plain carbon steel and weathering steels exposed to coastal–industrial atmosphere for 17 years,” *Corros. Sci.*, vol. 45, no. 11, pp. 2671–2688, 2003.
- [40] M. Kimura, T. Suzuki, G. Shigesato, H. Kihira, and S. Suzuki, “Characterization of Nanostructure of Rusts Formed on Weathering Steel,” *ISIJ Int.*, vol. 42, no. 12, pp. 1534–1540, 2002.
- [41] M. Morcillo, I. Díaz, B. Chico, H. Cano, and D. De Fuente, “Weathering steels: from empirical development to scientific design. A Review,” *Corros. Sci.*, vol. 83, pp. 6–31, 2014.
- [42] H. Townsend, “Effects of alloying elements on the corrosion of steel in industrial atmospheres,” *Corrosion*, vol. 57, no. 6, p. 497, 2001.
- [43] M. Kimura, “Nanoscopic Mechanism of Protective Rust Formation on Weathering Steel Surfaces,” *Nippon Steel Tech. Rep.*, no. 91, pp. 86–90, 2005.
- [44] M. Yamashita, H. Konishi, J. Mizuki, and H. Uchida, “Nanostructure of Protective Rust Layer on Weathering Steel Examined Using Synchrotron Radiation X-rays,” *Mater. Trans.*, vol. 45, no. 6, pp. 1920–1924, 2004.
- [45] D. C. Cook, S. J. Oh, R. Balasubramanian, and M. Yamashita, “The role of goethite in the formation of the protective corrosion layer on steels,” *Hyperfine Interact.*, vol. 122, pp. 59–70, 1999.
- [46] T. Misawa and H. Miyuki, “Long-term exposure rust transformation and ion selectivity of Cr-substituted goethite consisting final protective rust-layer on a weathering steel,” *Electrochem. Soc. Proc. Ser.*, vol. 99 (27), no. 104, pp. 122–131, 1999.
- [47] M. Yamashita, H. Miyuki, H. Nagano, and T. Misawa, “Compositional gradient and ion

selectivity in Cr substituted goethite consisting the final stable protective rust layer on a weathering steel,” in *Proc. 13th International Corrosion Congress*, 1996.

- [48] T. Kamimura, S. Hara, H. Miyuki, M. Yamashita, and H. Uchida, “Composition and protective ability of rust layer formed on weathering steel exposed to various environments,” *Corros. Sci.*, vol. 48, no. 9, pp. 2799–2812, 2006.
- [49] I. Díaz, H. Cano, B. Chico, D. de la Fuente, and M. Morcillo, “Some Clarifications Regarding Literature on Atmospheric Corrosion of Weathering Steels,” *Int. J. Corros.*, vol. 2012, no. i, pp. 1–9, 2012.
- [50] R. M. Cornell and U. Schwertmann, *The Iron Oxides: Structure, Properties, Reactions, Occurrences and Uses*. Wiley-VCH, 2003.
- [51] Y. Ma, Y. Li, and F. Wang, “Corrosion of low carbon steel in atmospheric environments of different chloride content,” *Corros. Sci.*, vol. 51, no. 5, pp. 997–1006, 2009.
- [52] J. Wang, Z. Y. Wang, and W. Ke, “A study of the evolution of rust on weathering steel submitted to the Qinghai salt lake atmospheric corrosion,” *Mater. Chem. Phys.*, vol. 139, no. 1, pp. 225–232, 2013.
- [53] I. C. Guedes, I. V. Aoki, M. . Carnezim, M. F. Montemor, M. G. S. Ferreira, and M. Da Cunha Belo, “The influence of copper and chromium on the semiconducting behaviour of passive films formed on weathering steels,” *Thin Solid Films*, vol. 515, no. 4, pp. 2167–2172, 2006.
- [54] T. Kamimura and M. Stratmann, “The influence of chromium on the atmospheric corrosion of steel,” *Corros. Sci.*, vol. 43, pp. 429–447, 2001.
- [55] Y. H. Qian, D. Niu, J. J. Xu, and M. S. Li, “The influence of chromium content on the electrochemical behavior of weathering steels,” *Corros. Sci.*, vol. 71, pp. 72–77, 2013.
- [56] I. Diaz, H. Cano, D. de la Fuente, B. Chico, J. M. Vega, and M. Morcillo, “Atmospheric corrosion of Ni-advanced weathering steels in marine atmospheres of moderate salinity,” *Corros. Sci.*, vol. 76, pp. 348–360, 2013.
- [57] M. Kimura and H. Kihira, “Nanoscopic Mechanism of Protective Rust Formation on Weathering Steel Surfaces,” *Nippon STEEL Tech. Rep.*, no. 91, pp. 86–90, 2005.
- [58] “Old Flour Store, Tallin” [Online]. Available: <http://www.solness.ee/maja/?mid=112&id=441>.
- [59] “Museum of Monteagudo, Bolivia” [Online]. Available: <http://www.zeroundicipiu.it/2012/05/07/museo-de-monteagudo/>.
- [60] “Caixa Forum, Madrid” [Online]. Available: http://www.constructalia.com/portugues_br/galeria_de_projetos/espanha/caixaforum_mad

rid#.VuFtWX3hDIU.

- [61] “House in New Leyden, Netherlands” [Online]. Available: <http://www.contemporist.com/2011/04/12/urban-housing-in-nieuw-leyden-by-24h-architects/>.
- [62] “Museum of Tadeusz Kantor and Cricoteka, Krakow,” [Online]. Available: http://www.archdaily.com/602238/cricoteka-museum-of-tadeusz-kantor-wizja-sp-z-o-omoonstudio/54ed2492e58ece5dcd00004e_cricoteka-museum-of-tadeusz-kantor-wizja-nsmoonstudio_wk_cricoteka_0035-jpg.
- [63] “Piazza Duomo '08, Racconigi” [Online]. Available: <http://1995-2015.undo.net/Pressrelease/foto/1275646312b.jpg>.
- [64] “Cerchio imperfetto, Parco Archeologico Scolacium” [Online]. Available: <https://s-media-cache-ak0.pinimg.com/736x/53/1f/f3/531ff344c271c0d51d6cdd0d16d1b200.jpg>.
- [65] “Da sinistra a destra, Parco Archeologico Scolacium” [Online]. Available: http://www.culturaitalia.it/opencms/export/sites/culturaitalia/thumbs/250x220/images/Mauro_Staccioli_x_da_sinistra_a_destra_.jpg.
- [66] “Vortex, Modern Art Museum of Forth Worth, USA” [Online]. Available: <https://s-media-cache-ak0.pinimg.com/736x/d3/c6/20/d3c620f15f7f5420ff183171181091a4.jpg>.
- [67] “Te Tuhirangi Contour, Gibbs Farm, New Zeland” [Online]. Available: <http://www.gibbsfarm.org.nz/serra.php>.
- [68] “Blade Runners, USA” [Online]. Available: <https://s-media-cache-ak0.pinimg.com/736x/32/4f/40/324f4082e623e8ee5257cee3ad1f5530.jpg>.
- [69] “219.5° Arc x 28, Hong Kong” [Online]. Available: <http://desarthe.com/exhibitions/bernar-venet-hong-kong-cultural-centre-museum-of-art-piazas-2/>.
- [70] “Three indeterminate lines, Michigan” [Online]. Available: http://artdaily.com/index.asp?int_sec=2&int_new=58613&b=galerie#.VscnH7ThDIU.
- [71] “85.8° Arc x 16, Versailles” [Online]. Available: <http://smaury.tumblr.com/>.
- [72] “Xavier Font Projects” [Online]. Available: www.bierot.net/completed.htm.
- [73] “New River Gorge Bridge, USA” [Online]. Available: http://www.highestbridges.com/wiki/index.php?title=New_River_Gorge_Bridge.
- [74] S. E. Manahan, *Toxicological Chemistry and Biochemistry - Third Edition*. 2006.
- [75] National Geographic, “The Biosphere.” [Online]. Available:

<http://education.nationalgeographic.org/encyclopedia/biosphere/>.

- [76] R. Bhat and V. M. Gómez-lópez, “Heavy metal contamination as a global problem and the need for prevention/reduction measurements,” in *Practical food safety: contemporary issues and future directions*, I., John Wiley and sons, 2014.
- [77] S. Costantini, L. Bodano, R. Giordano, and S. D. Ilio, “Rapporto ISTISAN 04/28. Contaminazione ambientale da metalli pesanti connessa con attività mineraria dismessa in Sardegna,” 2004.
- [78] P. Hooda, *Trace elements in soils*. Wiley-Blackwell, 2010.
- [79] L. Järup, “Hazards of heavy metal contamination,” *Br. Med. Bull.*, vol. 68, pp. 167–182, 2003.
- [80] A. Violante, P. M. Huang, and G. M. Gadd, *Biophysico-chemical processes of heavy metals and metalloids in soil environment*. Wiley, 2008.
- [81] M. Deville and F. Deville, *Gli oligoelementi: catalizzatori della nostra salute*. Mediterranea, 2003.
- [82] V. V Goncharuk, N. M. Soboleva, and A. A. Nosonovich, “Physicochemical Aspects of the Contamination of Soil and Hydrosphere with Heavy Metals,” vol. 11, pp. 787–801, 2003.
- [83] G. M. Naja, V. Murphy, and B. Volesky, “Biosorption of metals,” *Encyclopedia of Industrial Biotechnology: Bioprocess, Bioseparation, and Cell Technology*. John Wiley & Sons, Inc., 2010.
- [84] R. P. Mason, *Trace metals in aquatic system*. Wiley-Blackwell, 2013.
- [85] P. Muller, “Definition of Chemical Species in Glossary of terms used in physical organic chemistry (IUPAC Recommendations),” *Pure Appl. Chem.*, vol. 66, no. 5, pp. 1077–1184, 1994.
- [86] M. Nordberg, J. H. Duffus, and D. M. Templeton, “Definition of Speciation in Glossary of terms used in toxicokinetics (IUPAC Recommendations),” *Pure Appl. Chem.*, vol. 76, no. 5, pp. 1033–1082, 2004.
- [87] T. P. Flaten and E. Steinnes, “Soil and Fresh Water,” *Gen. Appl. Toxicol.*, 2011.
- [88] R. Cornelis, J. Caruso, H. Crews, and K. Heumann, *Handbook of elemental speciation: techniques and methodology*. John Wiley & Sons, Inc., 2004.
- [89] A. M. Ure and C. M. Davidson, *Chemical speciation in the Environment*, 2nd edition. Blackwell Science Ltd, 2007.

- [90] Agency for Toxic Substances and Disease Registry, "Toxicological profile for chromium," 2012.
- [91] R. Cornelis, J. Caruso, H. Crews, and K. Heumann, *Handbook of elemental speciation II: species in the environment, food, medicine and occupational health*. John Wiley & Sons, Inc., 2005.
- [92] E. Merian, M. Anke, M. Inhat, and M. Stoepler, *Elements and their compound in the environment: occurrence, analysis and biological relevance*, 2nd edition. Wiley-VCH, 2008.
- [93] International Agency for Research on Cancer (IARC), "Monographs on the Evaluation of Carcinogenic risk to humans - Chromium, Nickel and Welding," 1990.
- [94] Agency for Toxic Substances and Disease Registry, "Toxicological profile for copper," 2004.
- [95] J. Marx, "Possible role for environmental copper in Alzheimer's disease," *Science*, vol. 301, no. 5635, p. 905, 2003.
- [96] J. Albretsen, "Toxicology brief. The toxicity of iron: an essential element," *Vet. Med.*, 2006.
- [97] Agency for Toxic Substances and Disease Registry, "Toxicological profile for manganese," 2000.
- [98] A. Sirko and R. Brodzik, "Plant ureases: Roles and regulation," *Acta Biochim. Pol.*, vol. 47, no. 4, pp. 1189–1195, 2000.
- [99] C. Chen, D. Huang, and J. Liu, "Functions and toxicity of nickel in plants: recent advances and future prospects," *Clean*, vol. 37, no. 4–5, pp. 304–313, 2009.
- [100] US-EPA 1994, "Method 200.7/rev 4.4 - Determination of metals and trace elements in water and wastes by Inductively Coupled Plasma-Atomic Spectrometry." .
- [101] "Map data © 2016 Google." [Online]. Available: <https://www.google.it/maps/place/Via+Domenico+Angher%C3%A0,+47921+Rimini+RN/@44.0620492,12.5524832,14z/data=!4m2!3m1!1s0x132cc3a1e2b8c6a7:0x11e4c75a8ddf9fb7>.
- [102] "EN ISO 8565:2011; Metals and alloys - Atmospheric corrosion testing - General requirements for field tests." 2011.
- [103] "EN ISO 9226:2012; Corrosion of metals and alloys - Corrosivity of atmospheres - Determination of corrosion rate of standard specimens for the evaluation of corrosivity." 2012.

- [104] ARPA E-R, "Rete di monitoraggio della qualità dell'aria della Provincia di Rimini – Report 2007," 2007.
- [105] "EN ISO 17752:2012; Corrosion of metals and alloys - Procedures to determine and estimate runoff rates of metals from materials as a result of atmospheric corrosion." 2012.
- [106] S. Goidanich, J. Brunk, G. Herting, M. A. Arenas, and I. Odnevall Wallinder, "Atmospheric corrosion of brass in outdoor applications. Patina evolution, metal release and aesthetic appearance at urban exposure conditions," *Sci. Total Environ.*, vol. 412–413, pp. 46–57, 2011.
- [107] R. Huston, Y. C. Chan, H. Chapman, T. Gardner, and G. Shaw, "Source apportionment of heavy metals and ionic contaminants in rainwater tanks in a subtropical urban area in Australia," *Water Res.*, vol. 46, no. 4, pp. 1121–1132, 2012.
- [108] J. Herrera, S. Rodriguez Roman, and A. P. Baéz, "Chemical composition of bulk precipitation in the metropolitan area of Costa Rica, Central America," *Atmos. Res.*, vol. 94, no. 2, pp. 151–160, 2009.
- [109] H. Sakihama, M. Ishiki, and A. Tokuyama, "Chemical characteristics of precipitation in Okinawa Island, Japan," *Atmos. Environ.*, vol. 42, no. 10, pp. 2320–2335, 2008.
- [110] Y. S. Hedberg, S. Goidanich, G. Herting, and I. Odnevall Wallinder, "Surface–rain interactions: Differences in copper runoff for copper sheet of different inclination, orientation, and atmospheric exposure conditions," *Environ. Pollut.*, vol. 196, pp. 363–370, 2015.
- [111] I. F. Al-Momani, "Wet and dry deposition fluxes of inorganic chemical species at a rural site in northern Jordan," *Arch. Env. Contam Toxicol.*, vol. 55, no. 4, pp. 558–565, 2008.
- [112] A. Avila and M. Alarcon, "Relationship between precipitation chemistry and meteorological situations at a rural site in NE Spain," *Atmos. Environ.*, vol. 33, no. 11, pp. 1663–1677, 1999.
- [113] P. Montoya, I. Diaz, N. Granizo, D. De la Fuente, and M. Morcillo, "A study on accelerated corrosion testing of weathering steel," *Mater. Chem. Phys.*, vol. 142, pp. 220–228, 2013.
- [114] "EN ISO 8407:2009; Corrosion of metals and alloys - Removal of corrosion products from corrosion test specimens." 2009.
- [115] D. A. Skoog, *Fundamentals of Analytical Chemistry*. Thomson-Brooks/Cole, 2004.
- [116] "Signals produced in SEM." [Online]. Available: <http://www.texample.net/tikz/examples/scanning-electron-microscopy/>.
- [117] M. T. Postek, K. S. Howard, A. H. Johnson, and K. L. McMichael, *Scanning Electron*

Microscopy: a student's handbook. 1980.

- [118] "Energy-Dispersive X-ray Spectroscopy" [Online]. Available: http://serc.carleton.edu/research_education/geochemsheets/eds.html.
- [119] B. Schrader, *Infrared and Raman Spectroscopy. Methods and Applications*. VCH Publishers Inc, 1995.
- [120] "Graphical representation of Bragg's Law." [Online]. Available: http://serc.carleton.edu/research_education/geochemsheets/BraggsLaw.html.
- [121] R. Todeschini, *Introduzione alla Chemiometria*. EdiSES, 1998.
- [122] D. L. Massart, B. G. M. Vandeginste, and L. M. C. Buydens, *Handbook of Chemometrics and Qualimetrics*. Elsevier Science, 1998.
- [123] O. Y. Rodionova and a L. Pomerantsev, "Chemometrics: achievements and prospects," *Russ. Chem. Rev.*, vol. 75, no. 4, pp. 271–287, 2007.
- [124] J. Shlens, "A tutorial on principal component analysis. Derivation, Discussion and Singular Value Decomposition," 2005.
- [125] R. Pardo, B. A. Helena, C. Cazorro, C. M. Guerra, L. Debán, and M. Vega, "Application of two- and three-way principal component analysis to the interpretation of chemical fractionation results obtained by the use of the B.C.R. procedure," *Anal. Chim. Acta*, vol. 523, no. 1, pp. 125–132, 2004.
- [126] B. Giussani, D. Monticelli, R. Gambillara, A. Pozzi, and C. Dossi, "Three-way principal component analysis of chemical data from Lake Como watershed," *Microchem. J.*, vol. 88, pp. 160–166, 2008.
- [127] C. B. Cordella, T. Tekye, D. N. Rutledge, and R. Leardi, "A multiway chemometric and kinetic study for evaluating the thermal stability of edible oils by (1)H NMR analysis: comparison of methods," *Talanta*, vol. 88, pp. 358–368, 2012.
- [128] R. Leardi, C. Armanino, S. Lanteri, and L. Alberotanza, "Three-mode principal component analysis of monitoring data from Venice lagoon," *J. Chemom.*, vol. 14, pp. 187–195, 2000.
- [129] H. Fanaee-t, M. Oliveira, J. Gama, S. Malinowski, and R. Morla, "Event and Anomaly Detection Using Tucker3 Decomposition," pp. 1–11, 2014.
- [130] ARPA E-R, "Rapporto dell'evento meteorologico da 7 al 12 febbraio 2012," 2012.
- [131] ARPA E-R, "Rapporto dell'evento meteorologico del 5 e 6 febbraio 2015," 2015.
- [132] ARPA E-R, "Rapporto dell'evento idrologico e meteo-marino del 10-12 novembre 2013,"

2013.

- [133] H. Cano, D. Neff, M. Morcillo, P. Dillmann, I. Diaz, and D. de la Fuente, "Characterization of corrosion products formed on Ni 2.4wt%–Cu 0.5wt%–Cr 0.5wt% weathering steel exposed in marine atmospheres," *Corros. Sci.*, vol. 87, pp. 438–451, 2014.
- [134] Q. X. Li, Z. Y. Wang, W. Han, and E. H. Han, "Characterization of the rust formed on weathering steel exposed to Qinghai salt lake atmosphere," *Corros. Sci.*, vol. 50, no. 2, pp. 365–371, 2008.
- [135] L. Bellot-Gurlet, D. Neff, S. Réguer, J. Monnier, M. Saheb, and P. Dillmann, "Raman Studies of Corrosion Layers Formed on Archaeological Irons in Various Media," *Journal of Nano Research*, vol. 8, pp. 147–156, 2009.
- [136] S. Das and M. J. Hendry, "Application of Raman spectroscopy to identify iron minerals commonly found in mine wastes," *Chem. Geol.*, vol. 290, pp. 101–108, 2011.
- [137] M. Hanesch, "Raman spectroscopy of iron oxides and (oxy)hydroxides at low laser power and possible applications in environmental magnetic studies," *Geophys. J. Int.*, vol. 177, pp. 941–948, 2009.
- [138] M. K. Nieuwoudt, J. D. Comins, and I. Cukrowski, "The growth of the passive film on iron in 0.05 M NaOH studied in situ by Raman microspectroscopy and electrochemical polarization. Part II: In situ Raman spectra of the passive film surface during growth by electrochemical polarization," *J. Raman Spectrosc.*, vol. 42, no. 6, pp. 1353–1365, 2011.
- [139] S. J. Oh, D. C. Cook, and H. E. Townsend, "Characterization of iron oxides commonly formed as corrosion products on steel," *Hyperfine Interactions*, vol. 112, no. 1–4, pp. 59–66, 1998.
- [140] C. Rémazeilles and P. Refait, "On the formation of β -FeOOH (akaganéite) in chloride-containing environments," *Corros. Sci.*, vol. 49, no. 2, pp. 844–857, 2007.
- [141] S. J. Oh, D. C. Cook, and H. E. Townsend, "Characterization of iron oxides commonly formed as corrosion products on steel," *Hyperfine Interact.*, vol. 112, pp. 59–66, 1998.
- [142] J. Aramendia, L. Gomez-Nubla, K. Castro, I. Martinez-Arkarazo, D. Vega, a. Sanz López de Heredia, a. García Ibáñez de Opakua, and J. M. Madariaga, "Portable Raman study on the conservation state of four CorTen steel-based sculptures by Eduardo Chillida impacted by urban atmospheres," *J. Raman Spectrosc.*, vol. 43, no. 8, pp. 1111–1117, 2012.
- [143] J.-R. Park and K. Y. Kim, "Passivities of Steels Weathered for Nine Years," *Corrosion*, vol. 64, no. 1, pp. 4–14, 2008.
- [144] S. Réguer, D. Neff, L. Bellot-gurlet, and P. Dillmann, "Deterioration of iron archaeological artefacts : micro-Raman investigation on Cl-containing corrosion products," *J. Raman Spectrosc.*, vol. 38, pp. 389–397, 2007.

- [145] T. Kamimura and M. Stratmann, "The influence of chromium on the atmospheric corrosion of steel," vol. 43, pp. 429–447, 2001.
- [146] C. Chiavari, E. Bernardi, C. Martini, F. Passarini, A. Motori, and M. C. Bignozzi, "Atmospheric corrosion of Cor-Ten steel with different surface finish : Accelerated ageing and metal release," *Mater. Chem. Phys.*, vol. 136, no. 2–3, pp. 477–486, 2012.
- [147] J. Sandberg, I. Odnevall Wallinder, C. Leygraf, and N. Le Bozec, "Corrosion-induced copper runoff from naturally and pre-patinated copper in a marine environment," *Corros. Sci.*, vol. 48, no. 12, pp. 4316–4338, Dec. 2006.
- [148] I. O. Wallinder, S. Bertling, D. B. Kleja, and C. Leygraf, "Corrosion-induced release and environmental interaction of chromium, nickel and iron from stainless steel," *Water. Air. Soil Pollut.*, vol. 170, pp. 17–35, 2006.
- [149] S. Oesch and P. Heimgartner, "Environmental effects on metallic materials – Results of an Outdoor exposure programme running in Switzerland. Materials and Corrosion," *Mater. Corros.*, vol. 47, no. 8, pp. 425–438, 1996.
- [150] ARPA E-R, "Rapporto dell'evento meteorologico dal 29 al 30 luglio 2014," 2014.
- [151] ARPA E-R, "Rapporto dell'evento meteorologico del 4 e 5 marzo 2015," 2015.
- [152] S. C. Herring, M. P. Hoerling, T. C. Peterson, and P. a. Stott, "Explaining Extreme Events of 2013 from a Climate Perspective," *Bull. Amer. Meteor. Soc.*, vol. 95, no. 9, pp. S1–S96, 2014.
- [153] J. D. Williams, W. H. Woodall, J. B. Birch, and J. H. Sullivan, "Distribution of Hotelling's T2 Statistic Based on the Successive Differences Estimator," *J. Qual. Technol.*, vol. 38, no. 3, pp. 217–229, 2006.
- [154] N. Ghedini, I. Ozga, A. Bonazza, M. Dilillo, H. Cachier, and C. Sabbioni, "Atmospheric aerosol monitoring as a strategy for the preventive conservation of urban monumental heritage: The Florence Baptistery," *Atmos. Environ.*, vol. 45, no. 33, pp. 5979–5987, 2011.
- [155] N. T. Lau, C. K. Chan, L. I. Chan, and M. Fang, "A microscopic study of the effects of particle size and composition of atmospheric aerosols on the corrosion of mild steel," *Corros. Sci.*, vol. 50, no. 10, pp. 2927–2933, 2008.
- [156] V. Padilla and A. Alfantazi, "Corrosion film breakdown of galvanized steel in sulphate–chloride solutions," *Constr. Build. Mater.*, vol. 66, pp. 447–457, 2014.
- [157] F. R. Perez, C. A. B. Meneses, and O. Arnache, "Structural properties of iron phases formed on low alloy steels immersed in sodium chloride-rich solutions," *Phys. B Condens. Matter*, vol. 404, no. 8–11, pp. 1347–1353, 2009.

- [158] Y. S. Choi and J. G. Kim, "Aqueous Corrosion Behavior of Weathering Steel and Carbon Steel in Acid-Chloride Environments," *Corrosion*, vol. 56, no. 12, pp. 1202–1210, 2000.
- [159] F. R. Perez, C. A. B. Meneses, A. R. High Walker, and K. Nomura, "Effects of chloride concentration, immersion time and steel composition on the spinel phase formation," *Mater. Chem. Phys.*, vol. 117, no. 1, pp. 214–223, 2009.
- [160] "Representation of CIE L*a*b* colour space." [Online]. Available: http://www.inkjetfineart.it/pagina.phtml?_id_articolo=29-Cosa-sono-le-Coordinate-Colore-Lab-CIELab.html.
- [161] C. Chiavari, A. Balbo, E. Bernardi, C. Martini, M. C. Bignozzi, M. Abbottoni, and C. Monticelli, "Protective silane treatment for patinated bronze exposed to simulated natural environments," *Mater. Chem. Phys.*, vol. 141, no. 1, pp. 502–511, 2013.
- [162] I. Diaz, "Corrosion Atmosferica de Aceros Patinables de nueva generacion," Universidad Complutense de Madrid, 2012.
- [163] T. Misawa, T. Kyuno, W. Suëtaka, and S. Shimodaira, "The mechanism of atmospheric rusting and the effect of Cu and P on the rust formation of low alloy steels," *Corros. Sci.*, vol. 11, no. 1, pp. 35–48, 1971.
- [164] E. Bernardi, S. Raffo, C. Chiavari, C. Martini, L. Nobili, M. C. Bignozzi, and I. Vassura, "Cor-Ten in a marine atmosphere: the influence of the environment on corrosion," in *Metalli in Architettura. Conoscenza, conservazione, innovazione*, 2015, pp. 113–122.
- [165] S. Raffo, I. Vassura, C. Chiavari, C. Martini, M. C. Bignozzi, F. Passarini, and E. Bernardi, "Weathering steel as a potential source for metal contamination: metal dissolution during 3-years of field exposure in a urban coastal site," *Environ. Pollut.*, vol. 213, pp. 571–584, 2016; doi: 10.1016/j.envpol.2016.03.001.
- [166] P. Refait, M. Abdelmoula, and J.-M. R. Genin, "Mechanisms of formation and structure of green rust one in aqueous corrosion of iron in the presence of chloride ions," *Corros. Sci.*, vol. 40, no. 9, pp. 1547–1560, 1998.
- [167] W. P. Gallagher, "The performance of weathering steel in sculpture," *Mater. Perform.*, vol. 40, no. 7, pp. 58–61, 2001.
- [168] L. Morawska and T. Salthammer, *Indoor environment: airborne particles and settled dust*. Wiley-VCH, 2003.
- [169] P. Kumar and B. Imam, "Footprints of air pollution and changing environment on the sustainability of built infrastructure," *Sci. Total Environ.*, vol. 444, pp. 85–101, 2013.
- [170] L. A. M. B. Metz, O.R. Davidson, P.R. Bosch, R. Dave, "Climate change 2007: mitigation of climate change. IPCC Fourth Assessment Report (AR4)," 2007.

- [171] C. A. Booth, F. N. Hammond, J. Lamond, and D. G. Proverbs, *Solutions for Climate Change Challenges in the built Environment*. Wiley-Blackwell, 2012.
- [172] S. Solomon, D. Qin, M. Manning, Z. Chen, M. Marquis, K. B. Averyt, M. Tignor, and H. L. Miller, "Climate Change 2007: the physical science basis. IPCC Fourth Assessment Report (AR4)," 2007.
- [173] M. Hallberg, G. Renman, and T. Lundbom, "Seasonal Variations of Ten Metals in Highway Runoff and their Partition between Dissolved and Particulate Matter," *Water. Air. Soil Pollut.*, vol. 181, no. 1–4, pp. 183–191, 2007.
- [174] U. M. Joshi and R. Balasubramanian, "Characteristics and environmental mobility of trace elements in urban runoff," *Chemosphere*, vol. 80, no. 3, pp. 310–8, Jun. 2010.
- [175] D.Lgs 31/2001, *Italian Legislative Decree "Attuazione della direttiva 98/83/CE relativa alla qualità delle acque destinate al consumo umano."* 2001.
- [176] D.M. 185/2003, "Italian Ministerial Decree 'Regolamento recante norme tecniche per il riutilizzo delle acque reflue in attuazione dell'articolo 26, comma 2, del D.Lgs. 11 maggio 1999, n. 152,' " 2003.
- [177] D.Lgs 152/2006, "Italian Legislative Decree 'Norme in materia ambientale,'" 2006.
- [178] Y. S. Hedberg, S. Goidanich, G. Herting, and I. Odnevall Wallinder, "Surface–rain interactions: Differences in copper runoff for copper sheet of different inclination, orientation, and atmospheric exposure conditions," *Environ. Pollut.*, vol. 196, pp. 363–370, 2015.
- [179] D. de la Fuente, I. Díaz, J. Simancas, B. Chico, and M. Morcillo, "Long-term atmospheric corrosion of mild steel," *Corros. Sci.*, vol. 53, no. 2, pp. 604–617, 2011.
- [180] R. A. Antunes, I. Costa, and D. L. A. De Faria, "Characterization of corrosion products formed on steels in the first months of atmospheric exposure," *Mater. Res.*, vol. 6, no. 3, pp. 403–408, 2003.
- [181] D. J. Jacob and D. A. Winner, "Effect of climate change on air quality," *Atmos. Environ.*, vol. 43, pp. 51–63, 2009.
- [182] A. Krätschmer, I. Odnevall Wallinder, and C. Leygraf, "The evolution of outdoor copper patina," *Corros. Sci.*, vol. 44, no. 3, pp. 425–450, 2002.
- [183] E. Bernardi, C. Chiavari, B. Lenza, C. Martini, L. Morselli, F. Ospitali, and L. Robbiola, "The atmospheric corrosion of quaternary bronzes: The leaching action of acid rain," *Corros. Sci.*, vol. 51, no. 1, pp. 159–170, 2009.
- [184] C. Chiavari, K. Rahmouni, H. Takenouti, S. Joiret, P. Vermaut, and L. Robbiola, "Composition and electrochemical properties of natural patinas of outdoor bronze

- monuments,” *Electrochim. Acta*, vol. 52, no. 27, pp. 7760–7769, 2007.
- [185] C. Chiavari, E. Bernardi, A. Balbo, C. Monticelli, S. Raffo, M. C. Bignozzi, and C. Martini, “Atmospheric corrosion of fire-gilded bronze: Corrosion and corrosion protection during accelerated ageing tests,” *Corros. Sci.*, vol. 100, pp. 435–447, 2015.
- [186] E. Mello, “The gilding of Lorenzo Ghiberti’s ‘Doors of Paradise,’” *Gold Bull.*, vol. 19, no. 4, pp. 123–126, 1986.
- [187] M. Finsgar and I. Milosev, “Inhibition of copper corrosion by 1,2,3-benzotriazole: A review,” *Corros. Sci.*, vol. 52, no. 9, pp. 2737–2749, 2010.
- [188] A. Galtayries, A. Mongiatti, P. Marcus, and C. Chiavari, “Surface characterisation of corrosion inhibitors on bronzes for artistic casting,” in *Corrosion of Heritage Artefacts*, P. Dillmann, P. Piccardo, H. Matthiesen, and G. Beranger, Eds. European Federation of Corrosion, 2006, pp. 335–350.
- [189] Health Council of the Netherlands: Dutch expert committee on Occupational Standards and (DECOS), “1,2,3-Benzotriazole, The Hague: Health Council of the Netherlands,” 2000.
- [190] D. A. Pillard, J. S. Cornell, D. L. Dufresne, and M. T. Hernandez, “Toxicity of benzotriazole and benzotriazole derivatives to three aquatic species,” *Water Res.*, vol. 35, pp. 557–560, 2001.
- [191] M. A. Chen, X. Bin Lu, L. H. Guo, and R. Huang, “Influence of hydrolysis time on the structure and corrosion protective performance of (3-mercaptopropyl)triethoxysilane film on copper,” *Corros. Sci.*, vol. 53, pp. 2793–2802, 2011.
- [192] A. Balbo, C. Chiavari, C. Martini, and C. Monticelli, “Effectiveness of corrosion inhibitor films for the conservation of bronzes and gilded bronzes,” *Corros. Sci.*, vol. 59, pp. 204–212, 2012.
- [193] F. Zucchi, A. Frignani, V. Grassi, G. Trabaneli, and M. Dal Colle, “The formation of a protective layer of 3-mercapto-propyl-trimethoxy-silane on copper,” *Corros. Sci.*, vol. 49, pp. 1570–1583, 2007.
- [194] Y. S. Li, W. Lu, Y. Wang, and T. Tran, “Studies of (3-mercaptopropyl)trimethoxysilane and bis(trimethoxysilyl)ethane sol-gel coating on copper and aluminum,” *Spectrochim. Acta - Part A Mol. Biomol. Spectrosc.*, vol. 73, pp. 922–928., 2009.
- [195] W. J. van Ooij, D. Zhu, M. Stacy, A. Seth, T. Mugada, and J. Gandhi, “Corrosion Protection Properties of Organofunctional Silanes—An Overview,” *Tsinghua Sci. Technol.*, vol. 10, pp. 639–664, 2005.
- [196] Y. F. Xing, S. F. Y. Li, A. K. H. Lau, and S. J. O’Shea, “Electrochemical impedance spectroscopy study of mixed thiol monolayers on gold,” *J. Electroanal. Chem.*, vol. 583, pp. 124–132, 2005.

- [197] M. M. Antonijevic and M. B. Petrovic, "Copper Corrosion Inhibitors. A review," *Int. J. Electrochem. Sci.*, vol. 3, pp. 1–28, 2008.
- [198] G. Masi, C. Chiavari, J. Avila, J. Esvan, S. Raffo, M. C. Bignozzi, M. C. Asensio, L. Robbiola, and C. Martini, "Corrosion investigation of fire-gilded bronze involving high surface resolution spectroscopic imaging," *Appl. Surf. Sci.*, vol. 366, pp. 317–327, 2016.
- [199] E. Bernardi, C. Chiavari, C. Martini, and L. Morselli, "The atmospheric corrosion of quaternary bronzes: An evaluation of the dissolution rate of the alloying elements," *Appl. Phys. A*, vol. 92, no. 1, pp. 83–89, 2008.
- [200] C. Chiavari, E. Bernardi, C. Martini, F. Passarini, F. Ospitali, and L. Robbiola, "The atmospheric corrosion of quaternary bronzes: The action of stagnant rain water," *Corros. Sci.*, vol. 52, no. 9, pp. 3002–3010, 2010.

Figure Captions

Fig. 1: Scheme of the electrochemical mechanism of corrosion [1].....	7
Fig. 2: Iron-carbon equilibrium phase diagram.....	23
Fig. 3: Anodic polarization curve of passivating material [28].....	30
Fig. 4: Corrosion trends vs exposure time for weathering steels (WS) and carbon steel (CS) exposed in rural atmosphere and polluted areas [31]	34
Fig. 5: Hokkaido 100 years memorial tower, Sapporo [38].....	35
Fig. 6: Mechanism of formation of the passive layer on weathering steel [43].....	36
Fig. 7: Corrosion trends vs exposure time for weathering steels (Cor-Ten A) exposed in rural, industrial and marine atmospheres [31].....	39
Fig. 8: Corrosion trends vs exposure time for weathering steels (Cor-Ten B) exposed in rural, industrial and marine atmospheres [31].....	39
Fig. 9: Old Flour Store, Tallin [59] © Martin Siplane	41
Fig. 10: Museum of Montegudo, Bolivia [60] ©David Frutos	41
Fig. 11: Caixa Forum, Madrid (Spain) [61] ©Pierre Engel	42
Fig. 12: House in Nieuw Leyden, Netherlands [62] © Boris Zeisser	42
Fig. 13: Museum of Tadeusz Kantor and Cricoteka, Kraków, Poland [63] © Wojciech Kryński	43
Fig. 14: Piazza Duomo '08, Mauro Staccioli, Racconigi (CN) [64] © Enzo Isaia	43
Fig. 15: Cerchio Imperfetto, Mauro Staccioli, Parco Archeologico Scolacium (CZ) [65] © Marco Gronchi	43
Fig. 16: Da sinistra a destra, Mauro Staccioli, Parco Archeologico Scolacium (CZ) [66] © Cultura Italia	44

Fig. 17: Vortex, Richard Serra, Modern Art Museum of Fort Worth, Texas, USA [67] © Dallas Photoworks	44
Fig. 18: Te Tuhirangi Contour, Richard Serra, Gibbs Farm, New Zeland [68] © Gibbs Farm 2013	45
Fig. 19: Blade Runners, Richard Serra, Florida, USA [69] © Martina Muller.....	45
Fig. 20: Bernar Venet, 219.5° Arc x 28, 2011. Temporary exhibition along the Hong Kong bay, November 2015 – February 2016 [70]	46
Fig. 21: Bernar Venet, Three indeterminate lines. Permanent exhibition at Frederik Meijer Gardens & Sculpture Park, Michigan [71].....	46
Fig. 22: Bernar Venet, 85.8° Arc x 16, 2011. Temporary exhibition at Place d’Armes in Versailles, June 2011 – November 2011 [72].....	47
Fig. 23: Footbridge in Granollers (Spain) [73] © Xavier Font	47
Fig. 24: Restoration of a Middle Ages bridge in Sant Celoni (Spain) [73] © Xavier Font	48
Fig. 25: New River Gorge Bridge (USA) [74] © N. Mueller	48
Fig. 26: Commercial sample of a) bare, b) pre-patinated and c) pre-patinated/waxed CorTen A	63
Fig. 27: Site of exposure (Rimini, Italy) [102].....	64
Fig. 28: Scheme of Bare (BA), Pre-patinated (PA) and Pre-patinated/Waxed (PWA) Cor-Ten A specimens exposed in sheltered conditions	65
Fig. 29: Scheme of Bare (BA), Pre-patinated (PA) and Pre-patinated/Waxed (PWA) Cor-Ten A specimens exposed in unsheltered conditions	65
Fig. 30: Assembling of WS specimens	68
Fig. 31: CEBELCOR chamber in the wet (a) and dry (b) positions	69
Fig. 32: Working plan for Cebelcor test.....	71
Fig. 33: PinAAcle 900T Atomic Absorption Spectrometer (Perkin Elmer)	73

Fig. 34: Scheme of Atomic Absorption Spectrometer	73
Fig. 35: Hollow Cathode Lamp emission process.....	74
Fig. 36: Scheme of an electrothermal atomizer [116]	77
Fig. 37: Representation of graphite tube with platform [116].....	77
Fig. 38: Laminar flow burner head (left) and flame regions (right) [116]	78
Fig. 39: Ion-chromatography equipment for anion determination; the equipment for cation quantification does not include the suppressor.	82
Fig. 40: Kinds of signal produced in SEM [117]	84
Fig. 41: Diagram of scanning electron microscope.....	85
Fig. 42: Scheme of radiation scattering and Raman spectrum.....	90
Fig. 43: Scheme of a Raman equipment	92
Fig. 44: Graphical representation of Bragg's Law [121]	93
Fig. 45: Scheme of an X-ray diffractometer	94
Fig. 46: Scheme of Tucker3 decomposition model.....	101
Fig. 47: Microstructure of CorTen A (1000x).....	102
Fig. 48: Rainfall trend during the test period; different colors stand for different year of exposure. “*”: in jan-feb 2012 monitoring station was out of order due to heavy snowfalls.....	104
Fig. 49: Intensities and directions of winds acting on the test site during the total period of exposure (on the top) and each year of test. From the inside out, growing wind velocities are plotted.	106
Fig. 50: Monthly average values of NO ₂ (violet), O ₃ (red) and visible radiation (histogram) during the period of exposure.....	107
Fig. 51: Monthly average values of PM 2.5 (green) and PM 10 (dark red) during the period of exposure	107

Fig. 52: Mass Variations (mg/cm^2) progressively recorded for bare (BA), pre-patinated (PA) and pre-patinated and waxed (PWA) specimens exposed in sheltered conditions.....	111
Fig. 53: Mass Variations (mg/cm^2) progressively recorded for bare (BA), pre-patinated (PA) and pre-patinated and waxed (PWA) specimens exposed in unsheltered conditions.....	112
Fig. 54: SEM-QBSD micrographs of bare (a, d), pre-patinated (b, e) and pre-patinated/waxed (c, f) weathering steel exposed in sheltered (on the left) and unsheltered (on the right) conditions after 36 months of environmental exposure in Rimini.....	116
Fig. 55: SEM-SE images and EDS X-Ray maps recorded on cross-section of bare (a, d), pre-patinated (b, e) and pre-patinated/waxed (c, f) weathering steel exposed in sheltered (top) and unsheltered (bottom) conditions after 36 months of environmental exposure in Rimini.	119
Fig. 56: Raman spectra of Bare (BA) Cor-Ten exposed in sheltered conditions after (a) 2, (b) 10 and (c) 36 months of exposure.....	121
Fig. 57: Raman spectra of Bare (BA) Cor-Ten exposed in unsheltered conditions after (a) 2, (b) 10 and (c) 36 months of exposure.....	122
Fig. 58: Raman spectra of Pre-patinated (PA) Cor-Ten exposed in sheltered conditions after (a) 2, (b) 10 and (c) 36 months of exposure	123
Fig. 59: Raman spectra of Pre-patinated (PA) Cor-Ten exposed in unsheltered conditions after (a) 2, (b) 10 and (c) 36 months of exposure	124
Fig. 60: Raman spectra of Pre-patinated/Waxed (PWA) Cor-Ten exposed in sheltered conditions after (a) 2, (b) 10 and (c) 36 months of exposure	125
Fig. 61: Raman spectra of Pre-patinated/Waxed (PWA) Cor-Ten exposed in unsheltered conditions after (a) 2, (b) 10 and (c) 36 months of exposure	126
Fig. 62: Monthly values of pH in blank (yellow line) and runoff solutions (Bare: green line; Pre-patinated: blue line; Waxed: red line).....	129
Fig. 63: Monthly dissolution of Fe from bare (BA), pre-patinated (PA) and pre-patinated/waxed (PWA) weathering steel samples during the period of exposure.....	131

Fig. 64: Detail of Fig. 63	131
Fig. 65: Monthly dissolution of Mn from bare (BA), pre-patinated (PA) and pre-patinated/waxed (PWA) weathering steel samples during the period of exposure.....	132
Fig. 66: Monthly dissolution of Ni from bare (BA), pre-patinated (PA) and pre-patinated/waxed (PWA) weathering steel samples during the period of exposure.....	132
Fig. 67: Chloride concentration ($\mu\text{g}/\text{cm}^2$) in run-off solution from bare (BA), pre-patinated (PA) and pre-patinated/waxed (PWA) samples.....	136
Fig. 68: Sulphate concentration ($\mu\text{g}/\text{cm}^2$) in run-off solution from bare (BA), pre-patinated (PA) and pre-patinated/waxed (PWA) samples.....	136
Fig. 69: Fraction of dissolved Fe, Mn and Ni with respect to the sum (Fe + Mn + Ni) for Bare (BA), Pre-patinated (PA) and Pre-patinated/waxed (PWA) weathering steel during each year of exposure, compared with the bulk alloy fractions (about 99% for Fe, 0.3% for Ni and 0.5% for Mn).....	139
Fig. 70: Score plot for the first component (PC-1, explained variance 65%) and the second component (PC-2, explained variance 12%) of the PCA model. Numbers refer to sampling periods listed in Table 23.....	141
Fig. 71: Loading plot for the first component (PC-1, explained variance 65%) and the second component (PC-2, explained variance 12%) of the PCA model. Experimental variables used for PCA model are Ni, Mn and ions in run-off water.....	141
Fig. 72: Score plot for the first (PC-1) and the second component (PC-2) of the PCA model. Numbers in the score plot refer to sampling periods listed in Table 23 (Summer/Spring: 1-4, 10-13, 18-22, 28-31; Winter/Autumn: 5-9, 14-17, 23-27, 32-37).	142
Fig. 73: Score (a) and loading (b) plot for the first (PC-1, explained variance 34%) and the second component (PC-2, explained variance 27%) of the PCA model performed on data referring to bare (BA) samples; the model was run using dissolved Fe, Mn, Ni and ions and environmental data (temperature, visible radiation, wind intensity, rain amount, TOW, PM10, PM2.5, O ₃) as experimental variables. Numbers in the score plot refer to sampling periods listed in Table 23 (Summer/Spring: 1-4, 10-13, 18-22, 28-31; Winter/Autumn: 5-9, 14-17, 23-27, 32-37).	144

Fig. 74: Triplot for the first and the second component of the 3W-PCA model, showing the results for all three modes (samples, variables and time factor). Numbers refer to sampling periods reported in Table 23 (Summer/Spring: 1-5, 10-13, 19-23, 29-32; Winter/Autumn: 6-9, 14-18, 24-28, 33-37).	145
Fig. 75: Aesthetical appearance of WS samples aged in Cl^- , NO_3^- and SO_4^{2-} solution for 12 and 24 days	147
Fig. 76: CIE $L^* a^* b^*$ colour space [161]	149
Fig. 77: Pourbaix diagram of Fe/ H_2O system at 25 °C, showing the areas of activity and passivation	151
Fig. 78: Evolution of open circuit corrosion potential for WS samples aged in Cl^- (blues), NO_3^- (oranges) and SO_4^{2-} (greens) during the Cebelcor test	152
Fig. 79: Mass loss of weathering steel aged in chloride (blues), nitrates (oranges) and sulphates (greens) solution for 12 and 24 days of Cebelcor test	153
Fig. 80: Detail of Fig. 79	154
Fig. 81: SEM images of WS samples aged in 25 ppm Cl^- solution for 12 days (a. 1000x and b. 5000x) and 24 days (c. 1000x and d. 5000x).....	156
Fig. 82: X-ray diffractogram of corrosion products formed on WS samples aged in 25 ppm Cl^- solution for 12 days (top) and 24 (bottom) days.....	156
Fig. 83: SEM images of WS samples aged in 1.5 ppm (a-b), 10 ppm (c-d) and 25 ppm (e-f) Cl^- solutions for 24 days.....	157
Fig. 84: X-ray diffractogram of corrosion products formed on WS samples aged in 1.5 ppm, 10 ppm and 25 ppm Cl^- solutions for 24 days	158
Fig. 85: SEM images of WS samples aged in 25 ppm nitrate (a), chloride (b) and sulphate (c) solutions for 24 days	160
Fig. 86: X-ray diffractogram of corrosion products formed on WS samples aged in 25 ppm nitrate, chloride and sulphate solutions for 24 days.....	161

Fig. 87: Fe released by WS aged in chloride (blue), nitrate (orange) and sulphate solutions during immersion/emersion test	164
Fig. 88: Detail of Fig. 87 - Fe released by WS aged in chloride (blue), nitrate (orange) and sulphate solutions during immersion/emersion test	164
Fig. 89: Mn released by WS aged in chloride (blue), nitrate (orange) and sulphate solutions during immersion/emersion test	165
Fig. 90: Ni released by WS aged in chloride (blue), nitrate (orange) and sulphate solutions during immersion/emersion test	165
Fig. 91: Cr released by WS aged in chloride (blue), nitrate (orange) and sulphate solutions during immersion/emersion test	166
Fig. 92: Fe retained as adherent rust in patinas formed on WS aged in chloride (blue), nitrate (orange) and sulphate solutions during immersion/emersion test	167
Fig. 93: Cr retained as adherent rust in patinas formed on WS aged in chloride (blue), nitrate (orange) and sulphate solutions during immersion/emersion test	167
Fig. 94: Mn retained as adherent rust in patinas formed on WS aged in chloride (blue), nitrate (orange) and sulphate solutions during immersion/emersion test	168
Fig. 95: Cu retained as adherent rust in patinas formed on WS aged in chloride (blue), nitrate (orange) and sulphate solutions during immersion/emersion test	168
Fig. 96: Ni retained as adherent rust in patinas formed on WS aged in chloride (blue), nitrate (orange) and sulphate solutions during immersion/emersion test	169
Fig. 97: Score plot for the first component (PC-1, explained variance 68%) and the second component (PC-2, explained variance 20%) of PCA model. In the graph, each sample is labeled with letter, referring to weathering solution (S= sulphate, C= chloride and N= nitrate) and number, referring to concentration (1= 1.5ppm, 2= 10 ppm and 3= 25 ppm)	170
Fig. 98: Loading plot for the first component (PC-1, explained variance 66%) and the second component (PC-2, explained variance 16%) of PCA model. Variables used for the calculation are: corrosion potential (OCP), mass loss (ML), metals released in solution ('Rel') and metals retained in patinas ('Patina')	171

Fig. 99: On the top, Raman spectra of bare Cor-Ten exposed in Rimini in a) sheltered and b) unsheltered conditions. On the bottom, Raman spectra on c) sheltered and d) unsheltered areas of the Gate of the Jewish Cemetery in Bologna.	175
Fig. 100: Relative percentage amount of Fe, Cr, Mn and Ni in adherent (right) and non-adherent (left) rust with respect to the sum (Fe + Cr + Mn + Ni) for weathering steel samples aged in Cl ⁻ , NO ₃ ⁻ and SO ₄ ²⁻ solutions compared to the bulk alloy fractions (about 98% for Fe, 0.8 for Cr, 0.2% for Ni and 0.4% for Mn), during the first (12 days) and the second (24 days) phase of immersion/emersion test.....	187
Fig. 98: Evolution of corrosion products on bronze during atmospheric exposure [183]	220
Fig. 99: Cu cumulative release (µg/cm ²) from bare and gilded bronze during dropping test.....	226
Fig. 100: Pb cumulative release (µg/cm ²) from bare and gilded bronze during dropping test ...	226
Fig. 101: Cu cumulative release (µg/cm ²) from gilded and coated gilded bronze during dropping test.....	227
Fig. 102: Pb cumulative release (µg/cm ²) from gilded and coated gilded bronze during dropping test.....	227

Table Captions

Table 1: Average composition of atmosphere (dry air) [18].....	14
Table 2: Corrosivity levels based on Cl ⁻ and SO ₂ depositions and TOW values.....	20
Table 3: Corrosion rates for the first year of exposure of carbon steel for the different corrosivity categories.....	21
Table 4: Elemental composition (% by weight) of commercial Cor-Ten	33
Table 5: Alloy composition (weight %) determined on CorTen A sample by Optical Emission Spectroscopy.	62
Table 6: Weathering solution for the Cebelcor ageing test	70
Table 7: Operating conditions for Cr.	79
Table 8: Operating conditions for Cu.....	80
Table 9: Operating conditions for Fe.	80
Table 10: Operating conditions for Mn.....	80
Table 11: Operating conditions for Ni.	80
Table 12: Limits of quantification (LoQ) for soluble ions.....	83
Table 13: Total and seasonal amount of rain during the years of exposure; total and rainstorm events and mean rainfall intensity.....	105
Table 14: Characterization of the exposure site: Relative Humidity (RH), Temperature (T), prevalent wind directions, chloride and sulphate deposition rate, NO ₂ , O ₃ and PM atmospheric concentrations during each sampling period (progressive numbers of sampling periods are reported in bolt).....	108
Table 15: Total (4 years) and annual mass variation (mg/cm ²) for bare (BA), pre-patinated (PA) and pre-patinated/waxed (PWA) samples exposed in sheltered and unsheltered conditions	113

Table 16: Elemental composition of bare (BA), pre-patinated (PA) and pre-patinated/waxed (PWA) weathering steel before the exposure and after 2, 10 and 36 months of exposure ..	115
Table 17: Interpretation of Raman spectra of sheltered (She) and unsheltered (Unshe) WS specimens after 2, 10 and 36 months of exposure.	128
Table 18: Annual dissolution (mg/m ²) of Fe, Mn and Ni from Bare (BA), Pre-patinated (PA) and Pre-patinated/waxed (PWA) weathering steel during four years of exposure	130
Table 19: Pearson's Correlation Coefficients among dissolved alloying metals, main ions in runoff rainwater, average air pollutant concentrations and rain amount on the specimens. The complete dataset for bare weathering steel is considered (n=37)	133
Table 20: Pearson's Correlation Coefficients among dissolved alloying metals, main ions in runoff rainwater, average air pollutant concentrations and rain amount on the specimens. The complete dataset for pre-patinated weathering steel is considered (n=37)	133
Table 21: Pearson's Correlation Coefficients among dissolved alloying metals, main ions in runoff rainwater, average air pollutant concentrations and rain amount on the specimens. The complete dataset for pre-patinated/waxed weathering steel is considered (n=37).....	134
Table 22: Contribution of extreme meteorological events to the annual metal (Fe + Mn + Ni) runoff for BA, PA and PWA weathering steel.....	137
Table 23: Exposure and sampling periods (progressive numbers of sampling periods are reported in bolt).....	140
Table 24: CIE L* a* b* parameters and ΔE values for Cor-Ten A samples before, during (12 days) and after (24 days) immersion/emersion in SO ₄ ²⁻ , Cl ⁻ and NO ₃ ⁻ solution. L*, a* and b* represent the lightness, the red/green and the yellow/ blue axis, respectively; ΔE is calculated as $\Delta E = \sqrt{(\Delta L^*)^2 + (\Delta a^*)^2 + (\Delta b^*)^2}$	150
Table 25: Dissolved alloying metal concentrations in runoff rainwater from bare, pre-patinated and pre-patinated/waxed weathering steel, compared with literature ranges for dissolved metal concentrations in urban runoff waters and law limits for drinking and irrigation waters. Minimum/maximum concentration values recorded during single sampling periods and average concentrations are reported. For weathering steel, average concentrations were	

calculated by considering annual metal releases ($\text{mg m}^{-2} \text{ yr}^{-1}$) and annual rain amount fall on the specimens	180
Table 26: Esteemed conservative ranges of annual dissolved metal ($\text{mg m}^{-2} \text{ y}^{-1}$) for Bare (BA), Pre-patinated (PA) and Pre-patinated/ waxed (PWA) weathering steel in the test conditions...	181
Table 27: Functions approximating mass loss and total (Fe + Mn + Ni + Cr) metal release for each solution tested.....	184
Table 28: Metal release ($\mu\text{g}/\text{cm}^2$) from bare bronze and gilded bronze during short-term (TOW=10 d) wet & dry and dropping tests [179].	225

APPENDIX A – Atmospheric corrosion of Bronze

A1. Introduction

As for steel, atmospheric corrosion also affects other metallic materials exposed to the environment. Among these, bronzes and gilded bronzes have always been very recurrent materials in ancient works of art and in modern installations, thanks to mechanical workability and good corrosion resistance [9]. Obviously, also in the case of bronzes, the conditions and the environment of exposure play a key role in the corrosion behavior of the material and in the state of preservation of the bronze artifact.

For this reason, also relating to the increase in the aggressiveness of atmosphere occurred in the last century, patinas formed in the environment are now more porous and vulnerable and dissolution of alloying metals increased significantly. As a consequence, the study of the corrosion behavior of these materials aimed at the identification of proper strategies for conservation has become a topic of pressing interest.

Therefore, a part of PhD work was dedicated to the investigation on bronze behavior and, particularly, to the evaluation of the effectiveness of corrosion inhibitors in relation to the stability of corrosion product layer and the dissolution of metals from the alloy.

A1.1 Bronzes

Bronzes are basically copper-tin alloys with ratio between the two metals varying from 90-10% to 80-20%. The presence of tin in the composition is known to provide enhanced mechanical and resistance properties [9].

However, as in the case of alloyed steels, researchers and industries have intensively studied the possibility of adding other elements to Cu-Sn alloy, in order to achieve a bronze with enhanced mechanical and resistance performances. This research led to the formulation of new groups of bronzes which contain, beside Cu and Sn, appropriate concentrations of elements such as Pb, Al, Zn, Be, Ni, that are capable to improve toughness, hardness, workability and resistance to atmospheric corrosion.

In general, bronzes exposed to the atmosphere undergo various reactions which lead to the formation of a series of corrosion products; the composition of this patina is extremely complex and appears highly affected by the nominal composition of the alloy and the features of the environment of exposure (e.g. rural, industrial, marine) [14].

The mechanism of patina formation can be summarized as follows:

- ✓ Formation of oxides. Cuprite (Cu_2O) is the first product which forms when the metal is exposed to the atmosphere, according to the reaction



Beside cuprite, environmental exposure also leads to the formation of insoluble Sn oxide ($\text{SnO}_x(\text{OH})_y$), Pb oxide (PbO) and Zn oxide and hydroxide (ZnO , $\text{Zn}(\text{OH})_2$).

- ✓ Conversion of oxides into salts. As the exposure goes on, Cu^+ , present in the form of cuprite, is further oxidized, according to



leading to the formation of copper salts that vary depending on the composition of the exposure atmosphere.

In urban environments, in fact, where S-containing compounds prevail, basic copper sulfates form, according to



Brochantite (3,5 < pH < 6.5)



Antlerite (2,8 < pH < 3,5)

In environments with high concentration of chlorides, other compounds form, which are responsible of pitting corrosion on bronzes [182]:



Atacamite/Paratakamite

As for Cu_2O , zinc and lead oxides also convert into the respective salts, poorly soluble the ones of Pb, more soluble the ones of Zn [14].

Above the layers of oxides (inner) and salts (outer), a deposit of particulate matter deriving from the atmosphere is usually found.

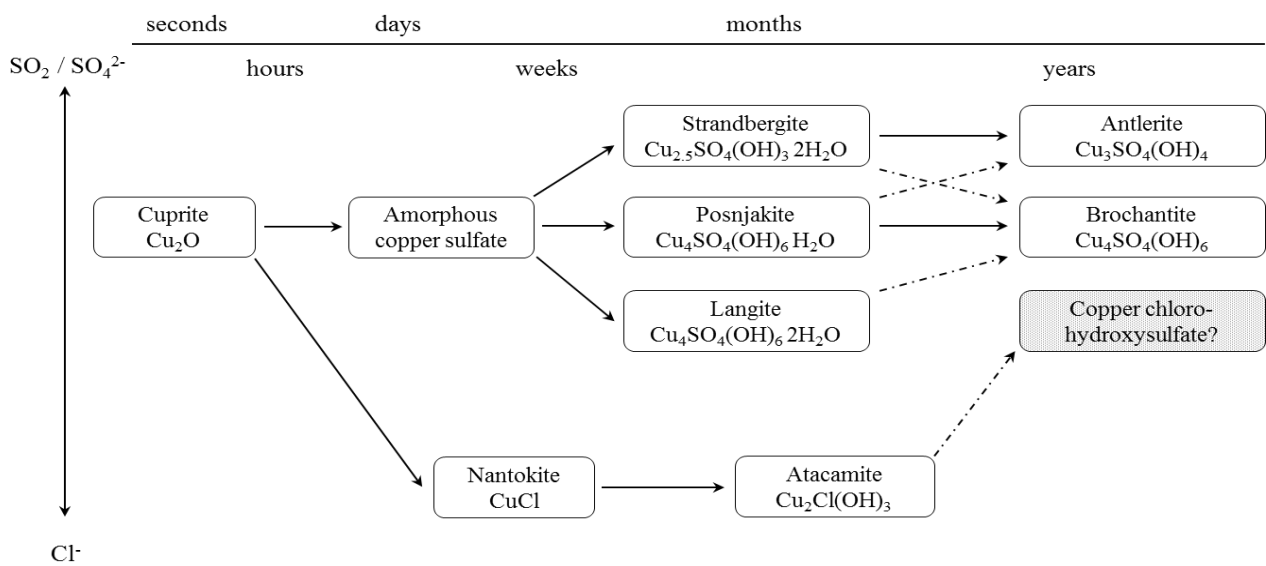


Fig. 101: Evolution of corrosion products on bronze during atmospheric exposure [182]

In fairly aggressive environments, where the concentrations of corrosive species, such as Cl^- and $\text{SO}_2/\text{SO}_4^{2-}$ are high and a general acidification of precipitation is also recorded, the deterioration of exposed surfaces results in serious phenomena of dissolution, mainly concerning copper and zinc (decuprification and dezincation [9]), resulting in surface enrichment in Sn [183], [184].

Nowadays, the application of protective coatings and/or corrosion inhibitors has thus become crucial to contrast the premature deterioration of bronze surfaces and reduce the effects of atmospheric corrosion.

A1.2 Gilded Bronzes

Another material widely used in architecture and in historical works of art is gilded bronze. The gilding techniques have always been exploited to make precious a series of objects, including bronzes. Among the methodologies applied since ancient times, fire gilding with mercury amalgam is one of the most important: it consists in applying a $\text{Au}_2\text{Hg}/\text{Hg}$ amalgam on cleaned substrate, then heating to remove the excess of Hg and to produce the golden coating (2-10 μm); the process is then completed by means of burnishing, which allows to reduce the porosity and the opacity of the gold layer [185].

The atmospheric degradation of fire-gilded bronzes is connected to two fundamental aspects: the presence of porosity and imperfections in the gold layer and the galvanic coupling of Cu and Au.

Defects in the coating derive from the process of gold deposition and cause the interaction between the bronze substrate and the atmosphere; as a consequence, the formation of corrosion products at the interface bronze/gold occurs, according to the mechanisms analyzed in the previous section (section A2); this, in the long term, may lead to blistering or break-up and loss of the gold layer [186].

Therefore, also in the case of gilded-bronzes, preventive and conservative actions to slow the atmospheric corrosion process and to protect the integrity of the gilding are of enormous importance in the field of cultural heritage.

A1.3 Methods for preventing bronze corrosion

Given these considerations, the application of protective coatings and/or corrosion inhibitors appears necessary to safeguard the life of bronze artifacts exposed to the environment.

Historically, Benzotriazole (BTA) and its derivatives have always been the main inhibitors against copper corrosion, capable to slow down both the anodic reaction of copper oxidation and the cathodic reaction of oxygen reduction [187]. However, due to the reduced inhibiting efficiency of these compounds towards bronze compared to pure copper [188], as well as problems related to the toxicity for humans [189] and the environment [190], researches aimed at identifying alternative coatings/inhibitors have significantly increased.

Among tested inhibitors and protective compounds, organosilane coatings [191], and, particularly, 3-mercaptopropyl-trimethoxy-silane (PropS-SH) [161], [192]–[194], have shown very promising results on both bare and exposed surfaces, reducing mass loss and alloying metal release.

The action of this inhibitor on bronze surfaces consists of various phases [193], [195]:

- ✓ Formation of silanol (Si-OH) groups on the surface, after silane hydrolysis.
- ✓ Chemisorption of PropS-SH through the formation of metal-thiolate (Me-S-C) and metal-siloxane (Me-O-Si) bonds.
- ✓ Reticulation to form a dense network acting as protective barrier.

As PropS-SH also showed a high affinity with Au [196], [197], the gilding of surface does not modify the mechanism of action, leading this compound to be an excellent candidate as an inhibitor also for gilded-bronze corrosion.

Therefore, the principal aims of this work were: (i) to study and compare the corrosion behavior of bronzes and gilded bronzes after simulated exposure to runoff conditions (dropping test) and water stagnation (W&D test); (ii) to evaluate the inhibiting efficiency of PropS-SH on gilded bronze after simulated exposure in runoff conditions.

These topic was investigated through a complete characterization of corrosion product layer and the quantification of metal runoff.

This work was performed in collaboration with the Department of Industrial Engineering and the Interdepartmental Center for Industrial Research (CIRI), Advanced Applications in Mechanical Engineering and Materials Technology. In this Appendix, only the results of metal dissolution will be discussed; a complete overview of all the results can be found in [185], [198].

A2. Experimental

In this study, bronze and fire-gilded bronze were considered. The main elements in the tested alloy are (weight %): Cu (91.9 %), Zn (2.9 %), Sn (2.4 %), Pb (1,0 %) and Sb (0,8 %). A complete compositional and microstructural characterization is given in [185].

The gilding was carried out by applying a Au-Hg (1:8) amalgam on the polished bronze surface, then heating with a free flame and, finally, burnishing to reduce layer porosity.

The inhibitor tested was 3-mercaptopropyl-trimethoxy-silane (PropS-SH), the best performing silane coating resulted from a previous work [192].

The corrosion behavior of bare and gilded bronze was evaluated by means of two different accelerated ageing tests, the wet & dry and the dropping test.

The Wet & Dry test simulates the exposure in stagnant conditions by means of continuous cycles of immersion and emersion in a weathering solution miming the composition of natural acid rain collected in Bologna [199]. The duration of each cycle was 1 hour, alternating 20 minutes of immersion and 40 minutes of emersion; for each cycle, a total time of wetness (TOW) of 40 minutes was estimated [200].

On the other hand, the dropping test simulates the exposure in runoff conditions; cycles of 2-day dropping / 1-day drying / 3-day dropping / 1-day drying were applied.

At first, short-term (10 days of TOW) wet & dry and dropping tests were performed in order to compare the corrosion behavior of bare and gilded-bronze. Secondly, long-term (30 days of TOW) dropping test was applied to study the inhibiting efficiency of PropS-SH on gilded-bronzes.

In both cases, weathering solutions were collected and analyzed by AAS (section 5.5.1), to quantify metal (Cu and Pb) dissolution.

A3. Results

In order to assess the corrosion behavior of bare and gilded bronze in different exposure conditions, the extent of metal release in synthetic rain during wet & dry and dropping test was quantified (Table 28).

Table 28: Metal release ($\mu\text{g}/\text{cm}^2$) from bare bronze and gilded bronze during short-term (TOW=10 d) wet & dry and dropping tests [179].

		Cu	Pb
Wet & Dry	Bare bronze	52 ± 4	12 ± 2
	Gilded bronze	30 ± 12	0.38 ± 0.01
Dropping	Bare bronze	1774 ± 266	67 ± 13
	Gilded bronze	288 ± 150	9 ± 5

Results clearly show that the exposure to runoff conditions is more severe than water stagnation for both bare and gilded bronzes; in fact, the cumulative release of copper and lead is one order of magnitude higher during dropping test, confirming the significant phenomenon of metal dissolution that occurs when the material is exposed to the action of pouring rain, as already reported in literature [183].

The lower release from gilded bronze, which suggests that the gold layer acts as a barrier contrasting O_2 diffusion to the substrate and thus corrosion phenomena, is also confirmed after long-term (30 days of TOW) dropping test (Fig. 102 and Fig. 103). The release of Cu and Pb from bare bronze aged in aggressive conditions shows a linear and increasing trend up to cumulative values of about $5000 \mu\text{g}/\text{cm}^2$ and $140 \mu\text{g}/\text{cm}^2$, respectively [185]. The cumulative metal release from gilded bronze was significantly lower than that from bare samples, reaching $\sim 1000 \mu\text{g}/\text{cm}^2$ for Cu and $20 \mu\text{g}/\text{cm}^2$ for Pb.

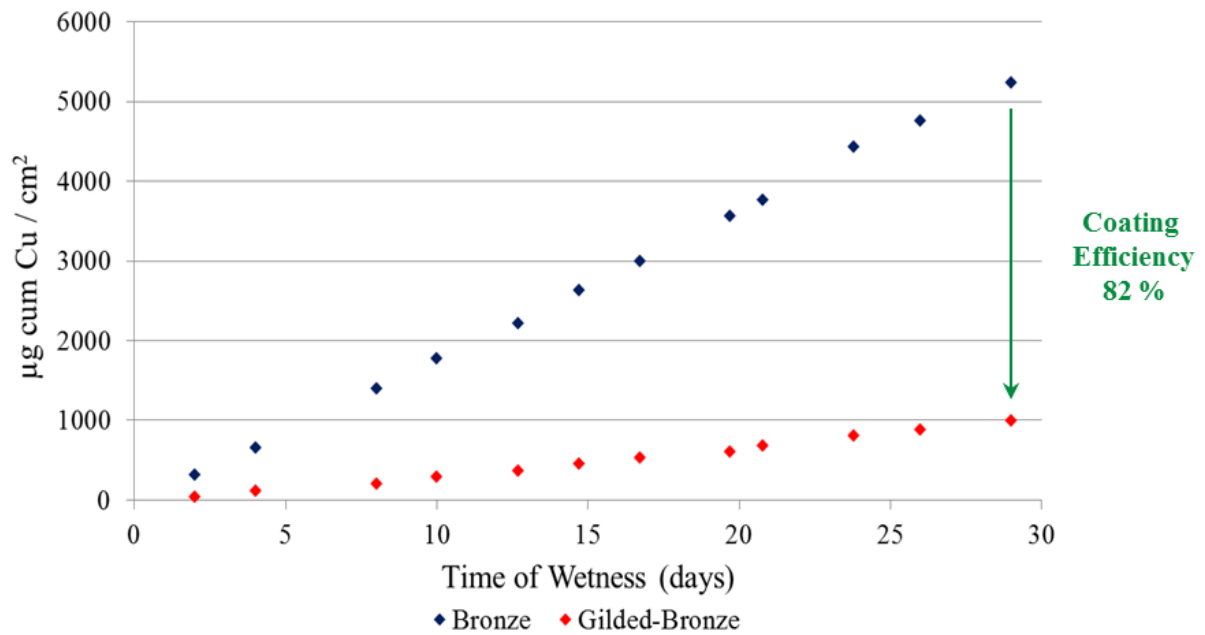


Fig. 102: Cu cumulative release ($\mu\text{g}/\text{cm}^2$) from bare and gilded bronze during dropping test

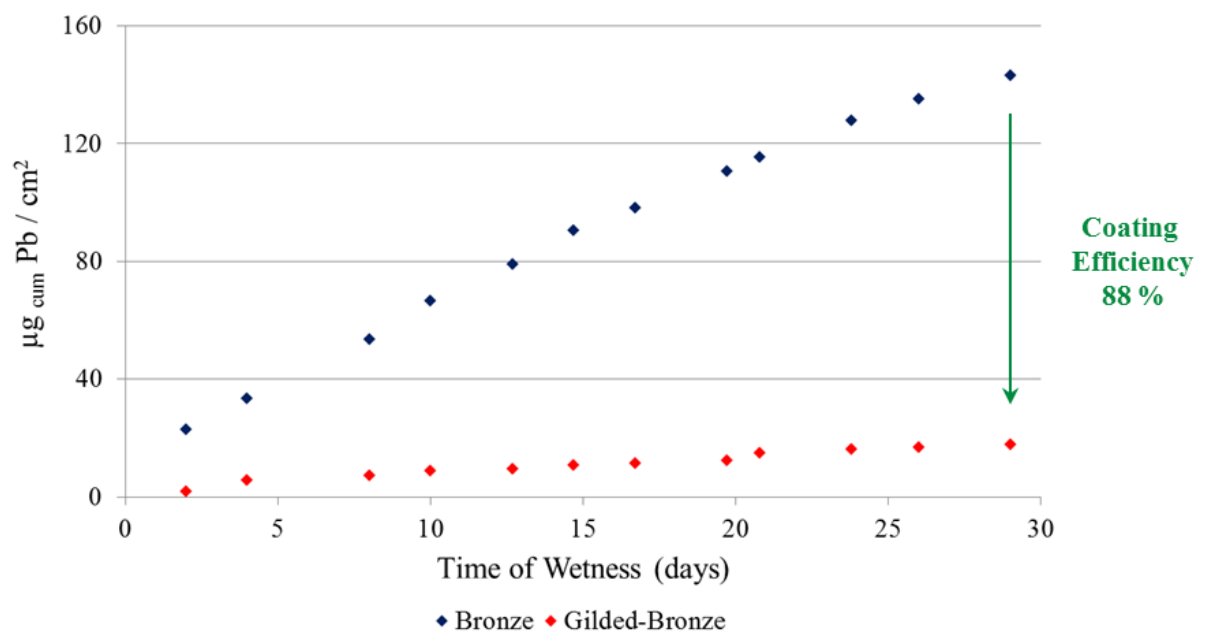


Fig. 103: Pb cumulative release ($\mu\text{g}/\text{cm}^2$) from bare and gilded bronze during dropping test

Once assessed that ageing in runoff conditions produces higher corrosion, it was also chosen for the evaluation of PropS-SH performances as corrosion inhibitor for gilded bronze during long-term exposure.

Cumulative Cu and Pb release from gilded and coated gilded bronzes are summarized in Fig. 104 and Fig. 105.

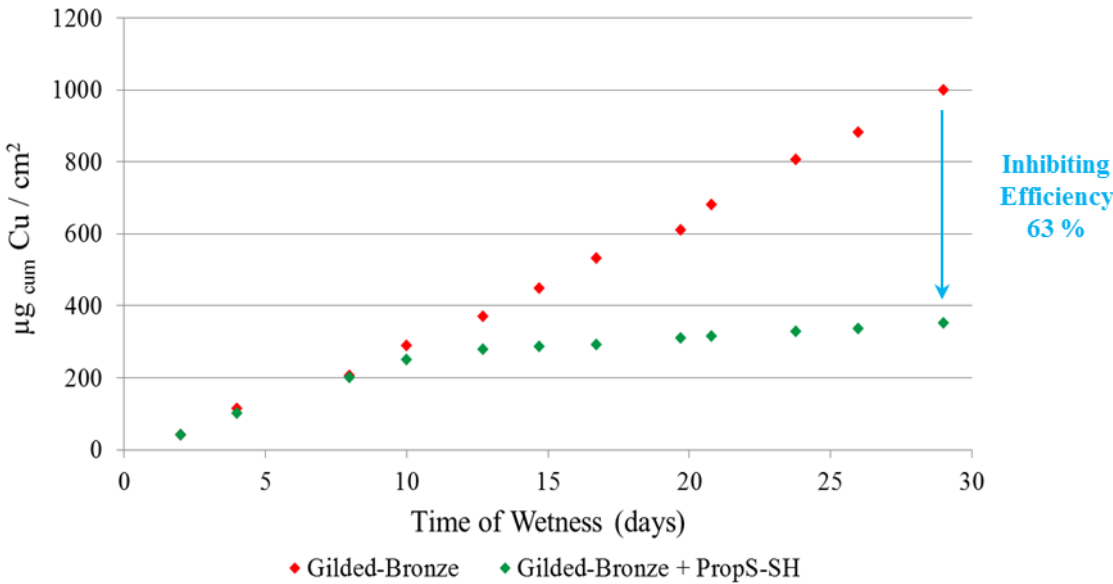


Fig. 104: Cu cumulative release ($\mu\text{g}/\text{cm}^2$) from gilded and coated gilded bronze during dropping test

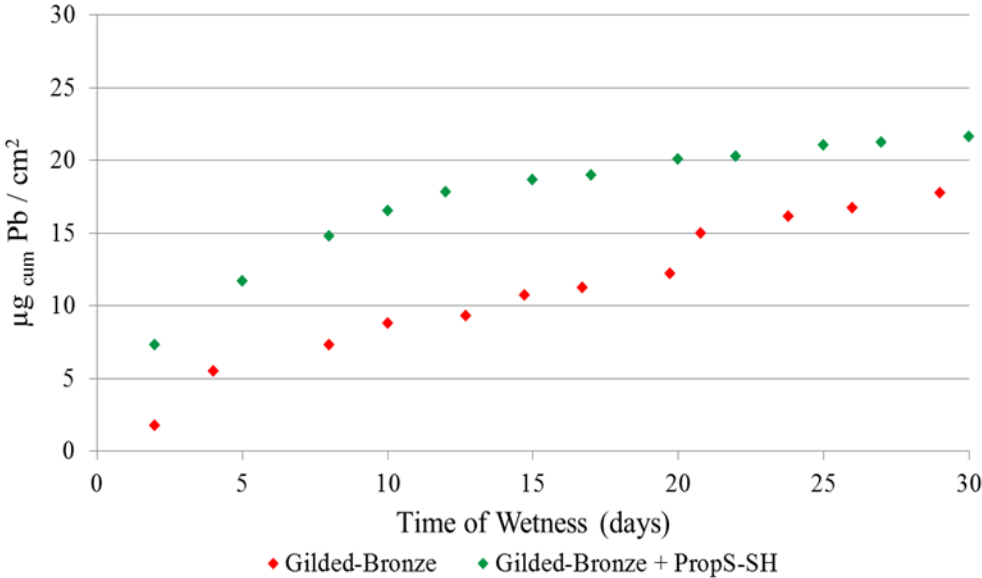


Fig. 105: Pb cumulative release ($\mu\text{g}/\text{cm}^2$) from gilded and coated gilded bronze during dropping test

The application of PropS-SH on gilded bronze produces significant advantages with regards to copper dissolution, but it does not produce beneficial effects on Pb release [185]. This selective action on metal dissolution during runoff test was already reported for non-gilded bronze [161].

Given that the gold coating on bronze surface slows down the phenomenon of copper dissolution, the application of silane inhibitor on gilded bronze further increases the protective ability up to 93%.

A4. Conclusion

In this work the corrosion behavior of bronzes and gilded bronzes during accelerated ageing tests was studied in relation to corrosion-induced metal release; moreover, the suitability and the inhibiting efficiency of PropS-SH on gilded bronze after simulated exposure in runoff conditions were also evaluated.

Results showed that simulated exposure in runoff conditions produced the most severe corrosion damages, which reflect in higher metal release.

The gold layer on bronze surface acts like a barrier that inhibits the diffusion of O₂ to the substrate and, as a consequence, reduces corrosion rate.

Finally, the inhibiting efficiency of PropS-SH coating on gilded bronze was evaluated: results showed that the coating is well performing in reducing copper release (~ 90%), but it does not produce any benefits with regards to Pb dissolution.

APPENDIX B – Papers and Contributions

Weathering steel as a potential source for metal contamination: metal dissolution during 3- year of field exposure in a urban coastal site

Simona Raffo^a, Ivano Vassura^{a,b}, Cristina Chiavari^c, Carla Martini^d, Maria C. Bignozzi^e, Fabrizio Passarini^{a,b}, Elena Bernardi^{a,b}

^a Dipartimento di Chimica Industriale “Toso Montanari”, Università di Bologna, Via Risorgimento 4, 40136 Bologna (Italy)

^b Centro Interdipartimentale di Ricerca Industriale (CIRI) Energia e Ambiente, Università di Bologna, Via Angherà 22, 47900 Rimini (Italy)

^c Centro Interdipartimentale di Ricerca Industriale (CIRI) Meccanica Avanzata e Materiali, Università di Bologna, Via Risorgimento 2, 40136 Bologna (Italy)

^d Dipartimento di Ingegneria Industriale, Università di Bologna, Via Risorgimento 4, 40136 Bologna (Italy)

^e Dipartimento di Ingegneria Civile, Chimica, Ambientale e dei Materiali, Università di Bologna, Via Terracini 28, 40131 Bologna (Italy)

Journal: ENVIRONMENTAL POLLUTION, 213 (2016), pp. 571-584

10.1016/j.envpol.2016.03.001

Abstract

Surface and building runoff can significantly contribute to the total metal loading in urban runoff waters, with potential adverse effects on the receiving ecosystems. The present paper analyses the corrosion-induced metal dissolution (Fe, Mn, Cr, Ni, Cu) from weathering steel (Cor-Ten A) with or without artificial patinas, exposed for 3 years in unsheltered conditions at a marine urban site (Rimini, Italy). The influence of environmental parameters, atmospheric pollutants and surface

finish on the release of dissolved metals in rain was evaluated, also by means of multivariate analysis (two-way and three-way Principal Component Analysis). In addition, surface and cross-section investigations were performed so as to monitor the patina evolution. The contribution provided by weathering steel runoff to the dissolved Fe, Mn and Ni loading at local level is not negligible and pre-patination treatments seem to worsen the performance of weathering steel in term of metal release. Metal dissolution is strongly affected by extreme events and shows seasonal variations, with different influence of seasonal parameters on the behaviour of bare or artificially patinated steel, suggesting that climate changes could significantly influence metal release from this alloy. Therefore, it is essential to perform a long-term monitoring of the performance, the durability and the environmental impact of weathering steel.

Capsule. Runoff-induced metal dissolution from weathering steel is influenced by seasonal variation and extreme events, and can significantly contribute to Fe, Mn, Ni urban loading.

Keywords. Urban runoff; Atmospheric corrosion; Cor-Ten; Marine environment; Chlorides deposition; PCA.

Cor-ten in marine atmosphere: the influence of the environment on corrosion

E. Bernardi¹, S. Raffo¹, C. Chiavari², C. Martini³, L. Nobili¹, M.C. Bignozzi⁴, I. Vassura¹

¹ Department of Industrial Chemistry - University of Bologna, Viale Risorgimento 4, Bologna, elena.bernardi@unibo.it; simona.raffo2@unibo.it; lara.nobili3@unibo.it; ivano.vassura@unibo.it

² Interdepartmental Center for Industrial Research “Advanced Applications in Mechanical Engineering and Materials Technology”, Viale Risorgimento 2, Bologna, cristina.chiavari@unibo.it

³ Department of Industrial Engineering – University of Bologna, Viale Risorgimento 4, Bologna, carla.martini@unibo.it

⁴ Department of Civil, Chemical, Environmental, and Materials Engineering – University of Bologna, Via Terracini 28, Bologna, maria.bignozzi@unibo.it

Conference Proceedings: *Metalli in architettura. Conoscenza, conservazione, innovazione. Scienza e Beni Culturali*, Arcadia Ricerche s.r.l., 2015, pp. 113 - 122

Abstract

Architectural and artistic heritage exposed to environment undergoes spontaneous degradation. Thanks to its atmospheric corrosion resistance and pleasant aesthetical features, Cor-Ten (Weathering Steel) has been increasingly employed for outdoor applications. However, the exposure to aggressive atmosphere (e.g. marine or polluted sites) can significantly influence Cor-Ten performances.

In this work, the behaviour of three kinds of commercial Cor-Ten (untreated, patinated, patinated and waxed) exposed to a coastal environment, in sheltered and unsheltered conditions, is examined. SEM/EDS and Raman investigations were performed on Cor-Ten surfaces and cross-

sections to identify the main corrosion products and to study the evolution of the passivation layer. The corrosion-induced release of alloying metals (Cu, Cr, Fe, Ni, Mn) in runoff waters was also analysed. Chemometrical techniques were applied for the interpretation of experimental data in relation to the different surface finishes and to the environmental conditions. Results highlight the great influence the site and the geometry of exposure have on the composition of corrosion layer. Runoff process, on the other hand, result not related to rain amount but strongly affected by seasonal variations and atypical meteorological events.

Key-words:

Weathering Steel, Marine/Urban Environment, SEM/EDS, Raman, Metal runoff.

Corrosion investigation of fire-gilded bronze involving high surface resolution spectroscopic imaging

G. Masi ^{a,*}, C. Chiavari ^{a,b}, J. Avila ^c, J. Esvan ^d, S. Raffo ^e, M.C. Bignozzi ^a, M.C. Asensio ^c, L. Robbiola ^f, C. Martini ^g

^a Dipartimento di Ingegneria Civile, Chimica, Ambientale e dei Materiali, Università di Bologna, via Terracini 28, 40131 Bologna, Italy

^b C.I.R.I. (Centro Interdipartimentale Ricerca Industriale) Meccanica Avanzata e Materiali, Università di Bologna, Bologna, via Terracini 28, 40131 Bologna, Italy

^c Synchrotron SOLEIL, L'Orme des Merisiers, 91190 Saint-Aubin, France ^d Centre Interuniversitaire de Recherche et d'Ingénierie des Matériaux, Université de Toulouse, 4 allée Emile Monso, 31030 Toulouse, France

^e Dipartimento di Chimica Industriale "Toso Montanari", Università di Bologna, viale Risorgimento 4, 40136 Bologna, Italy

^f TRACES Lab (CNRS UMR5608), Université Toulouse Jean-Jaurès, 5, allées Antonio-Machado, 31058 Toulouse, France

^g Dipartimento di Ingegneria Industriale, Università di Bologna, viale Risorgimento 4, 40136 Bologna, Italy

Journal: APPLIED SURFACE SCIENCE, 366 (2016), pp. 317–327

10.1016/j.apsusc.2016.01.101

Abstract

Gilded bronzes are often affected by severe corrosion, due to defects in the Au layer and Au/Cu alloy galvanic coupling, stimulated by large cathodic area of the gilded layer. Galvanic corrosion, triggered by gilding defects, leads to products growth at the Au/bronze interface, inducing blistering or break-up of the Au layer. In this context, fire-gilded bronze replicas prepared by ancient methods (use of spreadable Au–Hg paste) was specifically characterised by compiling complementary spectroscopic and imaging information before/after accelerated ageing with

synthetic rain. Fire-gilded bronze samples were chemically imaged in cross-section at nano-metric scale (<200 nm) using high energy and lateral resolution synchrotron radiation photoemission (HR-SRPES) of core levels and valence band after conventional characterisation of the samples by Glow Discharge optical Emission Spectroscopy (GD-OES) and conventional X-ray photoelectron spectroscopy (XPS). We have found a net surface enrichment in Zn and Sn after fire-gilding and presence of metallic Hg, Pb and Cu within the Au layer. Moreover, the composition distribution of the elements together with their oxidation has been determined. It was also revealed that metallic phases including Hg and Pb remain in the gilding after corrosion. Moreover, selective dissolution of Zn and Cu occurs in the crater due to galvanic coupling, which locally induces relative Sn species enrichment (decuprification). The feasibility advantages and disadvantages of chemical imaging using HR-SRPES to study artworks have been investigated on representative replicas.

Keywords. Fire gilded bronze; Corrosion; Chemical imaging; Synchrotron radiation; Photoemission; Artworks; XPS; Decuprification.

Atmospheric corrosion of fire-gilded bronze: Corrosion and corrosion protection during accelerated ageing tests

C. Chiavari ^a, E. Bernardi ^b, A. Balbo ^c, C. Monticelli ^c, S. Raffo ^b, M.C. Bignozzi ^d, C. Martini ^{*}

^a C.I.R.I (Centro Interdipartimentale di Ricerca Industriale) Meccanica Avanzata e Materiali, Università di Bologna, Via Risorgimento 2, 40136 Bologna, Italy

^b Dipartimento di Chimica Industriale “Toso Montanari”, Università di Bologna, Via Risorgimento 4, 40136 Bologna, Italy

^c Centro di Studi sulla Corrosione e Metallurgia “A. Daccò”, University of Ferrara, Via Saragat 1, 44122 Ferrara, Italy

^d Dipartimento di Ingegneria Civile, Chimica, Ambientale e dei Materiali, Università di Bologna, Via Terracini 28, 40131 Bologna, Italy

^{*} Dipartimento di Ingegneria Industriale, Università di Bologna, Via Risorgimento 4, 40136 Bologna, Italy

Journal: CORROSION SCIENCE, 100 (2015), pp. 435-447

10.1016/j.corsci.2015.08.013

Abstract

Fire-gilded bronze (replicating the materials of Lorenzo Ghiberti’s Paradise Door (Baptistry of Florence, 1452)) was aged in runoff/stagnant conditions by accelerated exposure tests in synthetic acid rain. After preliminary electrochemical investigations, a detailed characterization of gilded bronze samples before and after artificial ageing tests followed. Surface and cross-sections analyses were performed by FIB/FEG-SEM, SEM/EDS and micro-Raman spectroscopy. The protective efficiency of a coating based on 3-mercaptopropyl-trimethoxy-silane was also quantitatively assessed by GF-AAS through analysis of metal release, while the aesthetical appearance of coated and uncoated gilded bronze before and after ageing was evaluated by color

measurements.

Highlights

- ✓ Fire-gilded bronze (analogous to Lorenzo Ghiberti's Paradise Door, Florence, 1452)
- ✓ Corrosion rate decreases with time in electrochemical tests during wet & dry exposure
- ✓ Accelerated ageing in runoff/stagnant conditions (synthetic acid rain) induces corrosion at the gold/bronze interface
- ✓ Severe corrosion in runoff conditions, with morphology comparable to reference historical fire-gilded bronzes
- ✓ Organosilane coating on gilded bronze limits mass decrease and Cu release

Keywords. Copper; Organic coatings; Polarization; Raman spectroscopy; SEM; Atmospheric corrosion.

Conference Contributions

- 1) E. Bernardi, S. Raffo, C. Chiavari, C. Martini, L. Nobili, M.C. Bignozzi, I. Vassura, **“Cor-Ten in marine atmosphere: the influence of the environment on corrosion”**, 31° Congress on Science and Cultural Heritage – Metalli in Architettura: conoscenza, conservazione e innovazione, Bressanone, 2015 [Conference Proceedings - Oral communication]
- 2) L. Nobili, E. Bernardi, I. Vassura, S. Raffo, M. Casati, L. Ferrero, G. Sangiorgi, G. Perrone, E. Bolzacchini, **“Particolato atmosferico e degrado dei materiali: sviluppo di una metodica per l’analisi SEM/EDS di depositi atmosferici campionati tramite “Deposition Box”**, XV National Congress of Chemistry for Environment and Cultural Heritage, Bergamo 2015 [Conference Proceedings - Poster communication]
- 3) C. Chiavari, G. Masi, J. Avila, J. Esvan, S. Raffo, M.C. Bignozzi, M.C. Asensio, L. Robbiola, C. Martini, **“Fire-gilded bronze: investigation of the corrosion mechanism by synchrotron radiation (nanoscale XRF and XPS)”**, E-MRS Spring Meeting and Exhibit 2015, Lille (France) 2015 [Conference Proceedings - Oral communication]
- 4) C. Chiavari, C. Martini, E. Bernardi, S. Raffo, A. Balbo, M. Abbottoni, M.C. Bignozzi, C. Monticelli, **“Atmospheric corrosion of fire-gilded bronze: accelerated ageing in runoff conditions”**, European Corrosion Congress EUROCORR 2014, Pisa 2014 [Conference Proceedings - Oral communication]
- 5) Raffo S., Vassura I, Chiavari C., Martini C., Bignozzi M.C., Bernardi E., **“Corrosione atmosferica del Cor-Ten in ambiente urbano costiero”**, XXV National Conference of Italian Chemical Society, Arcavacata di Rende 2014 [Conference Proceedings - Oral communication]
- 6) Raffo S., Vassura I, Chiavari C., Martini C., Bignozzi M.C., Bernardi E., **“Atmospheric Corrosion of Weathering Steel: a Chemometric Approach”**, III International Congress of Chemistry for Cultural Heritage, Vienna (2014) [Conference Proceedings - Oral communication]
- 7) E. Venturini, I. Vassura, S. Raffo, L. Ferroni, E. Bernardi, F. Passarini, **“Un nuovo approccio per identificare e localizzare le sorgenti di PM_{2.5}”**, VI National Conference on Atmospheric Particulate, Genova (2014) [Conference Proceedings - Oral communication]
- 8) Raffo S., Bernardi E., Vassura I., **“Multivariate Data Analysis applied to the study of**

corrosion", XXIV Conference of Analytical Chemistry, Sestri Levante 2013 [Conference Proceedings - Poster communication]

- 9) Raffo S., Bernardi E., Vassura I., Chiavari C., Martini C., Bignozzi M.C., Morselli L., **"Cor-Ten exposed to a urban-coastal environment: preliminary study on metal release"**, 14th EuCheMS International Conference on Chemistry and the Environment, Barcellona (Spain) 2013 [Conference Proceedings - Poster communication]
- 10) Raffo S., Bernardi E., Vassura I., Chiavari C., Martini C., Bignozzi M.C., Morselli L., XIV National Congress of Chemistry for Environment and Cultural Heritage, Rimini 2013 [Conference Proceedings - Poster communication]